HEAT TREATMENT AND CORROSION BEHAVIOUR OF 2101 DUPLEX STAINLESS STEEL CATHODICALLY MODIFIED WITH RUTHENIUM

Olaseinde Oluwatoyin Adenike

A thesis submitted to the Faculty of Engineering, University of the Witwatersrand, in fulfilment of the requirements for the degree of Doctor of Philosophy in Engineering.

July 2014

DECLARATION

I, Oluwatoyin Adenike OLASEINDE, declare that this thesis is my own work, unless where otherwise acknowledged. It is being submitted for the degree of Doctor of Philosophy in Engineering at the University of the Witwatersrand, Johannesburg. It has not been submitted before for any degree or examination in any other University.

---------- ---------- day of ----------, 2014

Signature

ABSTRACT

The objective of this study was to improve the overall corrosion ressitance of 2101 by cathodic modification with ruthenium. Initially, the corrosion behaviour of 2101, 316, 2205 and 2507 was studied by potentiodynamic tests.

Samples of 2101 with different amounts of ruthenium up to 10wt% were manufactured using arc melting. All as-received samples were analysed by spark emission spectroscopy. Samples were characterised with optical and scanning electron microscopy with EDX analyses, and the phases were confirmed with XRD. The volume fractions of the phases were also measured. Hardness measurements were done to check that the ruthenium additions were not detrimental to the mechanical properties.

Thermo-Calc was used to deduce the expected phases, check for any low temperature phase and to deduce the temperatures at which the ferrite:austenite ratio was 50:50. The dual phase threshold (1080°C) was then used for the heat treatment. The actual heat treatment time was determined experimentally. Thermo-Calc showed that ruthenium additions of up to 0.2wt% Ru did not give a significant change to the phase proportion diagram, thereby retaining the duplex structure, whereas above 2.5wt% Ru, the phases were different. The calculation with up to ~10% Ru gave ferrite and hcp. The temperature at which the liquid disappeared in 2101-10 wt% Ru was 1280°C, which was lower than the other 2101 alloys with less ruthenium. The results of Thermo-Calc agreed with the experimental results.

The effects of ruthenium additions to 2101 lean duplex stainless steel on corrosion were studied in sulphuric acid, sulphuric acid with chloride, hydrochloric acid and sodium chloride solutions, and compared to 316, 2205 and 2507 stainless steels using potentiodynamic measurements. Ruthenium was beneficial at both the cathodic and anodic regions of the curves by modification of the cathodic and anodic behaviour. The increase in ruthenium addition increased the corrosion resistance in all the solutions. Increasing temperature and concentration of the corrosive media increased the corrosion rates, passive current densities and critical current densities of the alloys investigated. The optimum ruthenium addition was 1wt% Ru.

DEDICATION

To God Almighty,

To my Lord and Saviour Jesus Christ

To the Holy Spirit who has been my helper

To my Darling husband (Ibukun) and my two daughters (Joy Oyinde and Emmanuella Ipoola)

ACKNOWLEDGEMENTS

I would like to acknowledge first and foremost my Lord and Saviour Jesus Christ for saving me.

I would like to acknowledge my supervisors Prof. Lesley Cornish for her thorough and good supervision, Dr Josias Van der Merwe and Dr Peter Olubambi.

I would like to thank Dr Jones Papo and all staff of Physical Metallurgy at Mintek, Magdaline Morufula of Element Six, Brayner Nelwani.

I specifically want to appreciate all staff of the DST/NRF Centre of Excellence in Strong Materials: Mrs Casey Sparkes, Mrs Moira Messenger and Mrs Marina Labauschagne.

I would also like to acknowledge my parents Alhaji Y.O Sanni and Mrs Theresa Ebun Sanni for giving me a solid foundation in life, especially my mum, for her love, dedication and endurance.

I would like to appreciate Prof. B.O. Adewuyi for believing in me. Thank you sir.

I sincerely want to acknowledge the Late Prof. Adepoju, former Dean of the School of Engineering and Engineering Technology, FUTA, Nigeria, for introducing me to Metallurgical Engineering.

I appreciate my siblings Dr & Mrs Sanni, Mr & Mrs Udoye, Mr & Mrs Adeniyi Sanni, Mr & Mrs Kunle Sanni for their support during the programme.

Finally, I would like to appreciate my sweetheart Pastor Ibukunoluwa Olaseinde for your love and endurance even going across the nations to make sure that I am able to finish this work and for encouraging me when I felt like giving up. Thank you so much. I love you.

I would like to appreciate my daughters Joy Oyinde and Emmanuela Ipoola for being good girls even when mummy had to travel and leave you.

I would also like to appreciate AMSEN for funding the project.

Federal University of Technology Akure, Ondo-State, Nigeria for granting me study leave.

I appreciated everybody in our research group.

Table of Contents

List Of Figures

List of Tables

CHAPTER 1

INTRODUCTION

1.1 Overview

Duplex stainless steels are a special class of steels that are used in many industrial environments. They can be employed in a variety of applications in the oil and gas industries [1982Her, 1986Ros, 1986Gus, 1997Tys, 2005Hus, 2008Pot] where carbon dioxide corrosion easily causes the failure of steel pipelines [2006Cui]. Other applications include pulp and paper plants [1997Ben], chloride-containing process fluids and ammonium carbonate solutions, mining and minerals processing industries, phosphatic and urea-based fertilizer plants [1999Fra]. By having both austenite and ferrite in the microstructure, duplex stainless steels have properties of both classes of stainless steel [1979Suu, 1980Suu, 1981Ber]. According to Khoshnaw and Gardi [1983Sol, 2006Kho], duplex stainless steels offer a combination of properties, such as particularly good corrosion resistance in hot corrosive environments containing-chloride ions, mechanical strength and ductility, abrasion resistance and weldability.

The most prominent types of duplex stainless steels include 2507 and 2205. They are so named due to their respective compositions of 25wt% chromium, 7wt% nickel and 22wt% chromium and 5wt% nickel [2008Alv]. Grades 2205 and 2507 are highly resistant to uniform corrosion in many industrial environments [2008Inv]. The nickel in the austenite phase increases the ability of duplex stainless steel to passivate in many environments. However, at nickel contents greater than 10%, this passivation effect is overshadowed by the fact that nickel raises the passivation potential, the rest potential and the critical corrosion potential. Lower nickel contents in duplex stainless steels could thus result in an improvement of its resistance to stress corrosion cracking when compared with the conventional austenitic stainless steels [2007Ezu]. Super-duplex stainless steels, which have high chromium and molybdenum contents, have been observed to be more sensitive to sigma formation which reduces their corrosion resistance [1989Cha]. Also, super-duplex stainless steels are costly since they contain relatively high nickel contents (4-7 wt%). As a result of these reasons, super-duplex stainless steels are only used in selective

environments, normally chosen when the increased performance justifies the additional cost [1989Cha, 1999Fra].

The 2101 duplex stainless steel is a newly-developed lean stainless steel which has lower chromium and nickel contents [2006Inv]. The lower nickel content provides a lower cost when compared with the other types of super-duplex stainless steels, while the comparatively lower chromium content gives it a comparatively reduced susceptibility to the formation of sigma phase, as the sigma phase formation increases with the chromium content in duplex stainless steels [URLBss]. Although 2101 is inferior to the conventional duplex stainless steels in terms of its corrosion resistance; it was developed as an alternative stainless steel to the more expensive 304 and 316 austenitic stainless steels. However, the corrosion and heat treatment behaviour of 2101 are not fully known. Therefore, the corrosion integrity of 2101 over 304 and 316 has to be determined in greater detail.

1.2 Background and Motivation

Studies on the corrosion behaviour of 2101 duplex stainless steel compared to 316 and 304 stainless steels in certain environments have been done by Iversen, Olson and Zhang [2006Ive, 2007Ols, 2008Zha]. Owing to the rationale of effectiveness and cost of 2101 in replacing 316 and 304, studies have shown that 2101 has a better corrosion resistance than 304, but has not been able to effectively surpass that of 316. According to Olson *et al.* [2007Ols] and Zhang *et al.* [2008Zha], 2101 has an improved pitting and crevice corrosion resistance, which is superior to that of 304L and similar to 316L.

Studies [2008Zha, 2009Zha1] on the corrosion behaviour of 2101 were mostly concentrated only on a few aspects of corrosion and in a limited number of environments. The overall corrosion behaviour of 2101 in many environments, especially in acidic and acid chloride/chloride media where 316 and 304 are mostly applied, is therefore yet to be fully investigated. As heat treatment is a major metallurgical factor in improving the corrosion resistance properties of duplex stainless steel, it is also observed that there are virtually no reported studies on the heat treatment behaviour of 2101 compared with the many reported studies on the conventional 2205 and 2507 duplex stainless steels.

Cathodic modification of stainless steel with minor alloying additions of noble metals has proved to be an effective approach to improving their corrosion resistance in many reducing environments, and a number of studies on the addition of noble metals on stainless steel and other alloys have already been done by several authors [1959Ste, 1960Hoa, 1961Gre, 1964Tom, 1970Tom, 1974Tom, 1974Str, 1975Tom, 1977Str, 1981Che, 1984Dup, 1989Hig 1990Tjo, 1990Pot, 1991Pot, 1993Pot, 1998Wol, 2008Olu]. The ability of this group of metals in improving corrosion resistance of stainless steel results from their comparatively larger exchange current density and low overpotential for hydrogen evolution, which can easily facilitate the cathodic reaction. As a means of improving the corrosion resistance of 2101 over that of 316, 2101 can be cathodically modified with minor additions of noble metals and platinum group metals (PGMs).

While aiming at improving the corrosion resistance of 2101 over 316, without compromising its cost, alloying it with minor ruthenium additions could be the best alternative. This could be attributed to the fact that ruthenium is the cheapest of the known PGMs [1977Str, 1984Tom, 1990Pot, 1990Tjo, 2001Van], although the price fluctuates. Ruthenium has been proved to be one of the most effective of all the PGMs in the cathodic modification process [1961Gre, 1977Str, 1993Pot, 1998Wol]. Although there have been many studies on the means by which ruthenium additions improves the corrosion resistance of stainless steel [1990Pot, 1991Pot, 1992Pot, 2008Olu], no work has been reported on its cathodic modification effects on corrosion and hardness on type 2101. This study was focused on improving the overall corrosion resistance of 2101 by cathodically modifying it with minor ruthenium additions, but without compromising the mechanical properties.

1.3 Hyphothesis

Cathodic modification of stainless steels with minor alloying additions of noble metals has proved to be an effective approach to improving their corrosion resistance in many reducing environments [1959Ste, 1960Hoa, 1961Gre, 1964Tom, 1970Tom, 1974Tom,1974Str, 1975Tom, 1977Str, 1981Che, 1984Dup, 1989Hig 1990Tjo, 1990Pot, 1991Pot, 1993Pot, 1998Wol 2008Olu]. Thus, it is expected that the addition of ruthenium to 2101 duplex stainless steel should improve its corrosion resistance.

1.4 Specific Objectives of this Study

The aim of the study was to improve the overall corrosion resistance of 2101 duplex stainless steel through cathodic modification with minor ruthenium additions.

The specific objectives are:

i. Calculation of phase proportions of 2101 with varying additions of ruthenium and determination of the optimum heat treatment temperature.
ii. Investigation of any microstructural change of 2101 with varying compositions of ruthenium additions.
iii. Investigation on the effect of heat treatment on the calculated optimum heat treatment temperature, and at a slightly higher temperature, to verify that the optimum was correct.
iv. Investigation of the effect of ruthenium additions on the hardness of 2101 to ensure that the mechanical properties were not compromised.
v. Comparative investigations on the corrosion behaviour (corrosion rate, passivity, pitting) of 2101 lean duplex stainless steel compared to 316, 2205 and 2507.
vi. Assessment of the improvements of varying compositions of minor ruthenium additions on the corrosion resistance of 2101.

CHAPTER 2

LITERATURE REVIEW

2.1 Stainless steel

Stainless steels are considered to be stainless when they do not stain, corrode, or rust as easily as ordinary steel. Passivation of iron is achieved by dissolving sufficient chromium in the iron, which produces a consistent, adherent, insulating and regenerating chromium oxide protective film on the surface [1950Pug, 1986Ros]. Therefore, it is not surprising that stainless steels found application in the harsh environments of the chemical, oil production and power generation industries, and in utility goods such as furniture, automotive trims and cutlery, as well as food processing equipment and medical equipment where aesthetic appearance and corrosion resistance are important.

The passivation of iron occurs when the concentration of chromium exceeds ~12 wt% [1981Ber]. However, this is not adequate to resist corrosion in acids such as HCl or H_2SO_4; higher chromium concentrations and the judicious use of other solutes such as molybdenum, nickel and nitrogen is then needed to ensure a robust material [2003Sou]. About 200,000 tons of nickel-containing stainless steel is used each year by the food processing industry in North America. It is used in a variety of food handling, storing, cooking and serving equipment. Beverages such as milk, wine, beer, soft drinks and fruit juice are processed in stainless steel equipment, thus some resistance to corrosion in organic acids (e.g. lactic, oxalic, citric and acetic acids) is required. Stainless steel is also used in commercial cookers, pasteurizers, transfer bins, and other specialized equipment. Advantages include easy cleaning, good corrosion resistance, durability, food flavour protection and sanitary design. According to a U.S. Department of Commerce report [1995Usi, 2008Rev], in 1992 shipments of all stainless steel totalled 1,514,222 tons per year increased to 1,533,800 tons per year in 1993. The ratio of imports to consumption of stainless steel increased from 24% in 1992 to 31.9% in 1993, shipments to the automotive industry accounted for much of the increase. In 1989 47.9% of stainless steel mill product exported were sheet and strip, while in 1993 sheet and strip was 57.7%.

2.1.1 Classes of stainless steels

Stainless steels come in several types, depending on their chemical composition and microstructure. Generally, stainless steels can be categorised as austenitic, ferritic, martensitic and duplex. Austenitic stainless steels are much more widely used than ferritic stainless steels [1982Her]. About 75% of all stainless steel used worldwide is austenitic and about 25% is ferritic. The other families, martensitic, duplex and precipitation hardenable stainless steels, each represent less than 1% of the total market. The main components of the stainless steel production are dominated by China. The growth rate of stainless steel scrap markets slowed down from approximately 8% in the past to around 5% in the short to medium term future. There was 5.2% increase in crude stainless steel melting globally between 2009 and 2011 [2012Par].

Austenitic steels are non-magnetic, and have a face centred cubic (fcc) structure. They contain at least 16 wt% chromium, 6wt% nickel, and are commonly used in incessant and irregular high temperature services. The most common types of austenitic stainless steels include 304 and 316. Type 304 austenitic stainless steel is widely used; it accounts for about 50% of all stainless steel production [URLSou]. Other standard grades have different preferred applications; for example, Type 316 which contains up to 3 wt% Mo, has an improved general and pitting corrosion resistance, and is widely used in marine applications and coastal environments and is often called marine grade stainless steel.

Chromium's main role is to expand the passivity range of iron [1961Gre, 1974Str, 1993Des]. Nickel is a very commonly used alloying element of these steels. The adjustment of the nickel content of austenitic stainless steel caters for the various chemical compositions of the different types of austenitic stainless steels. For example, a minimum of 7wt% Ni is needed for 17wt% Cr to keep it austenitic as chromium is a ferrite stabilizer. Manganese can be used to replace nickel, because its atoms are substitutional austenite stabilizers which take the place of Fe atoms in the crystal structure. Manganese has large atoms which diffuse slowly in Fe and stabilise the austenitic crystal structure down to temperatures below which the atoms have sufficient mobility for a crystal structure change to occur. Molybdenum is added to austenite to increase its corrosion resistance, but being a ferrite stabiliser, the Ni content has to be increased. Some specialised austenitic stainless steels are made up to 0.4 wt% nitrogen when prepared at ambient

pressure, and about 1 wt% nitrogen when using high-pressure melting techniques [1989Ree]. Nitrogen is a very effective solid-solution strengthener, and can increase the resistance to localised corrosion (pitting and crevice) in acid-chloride solutions. The Copson curve (Figure 2.1 [URLSpe]) is often used to compare resistance to stress cracking in chloride-containing environments. Alloys with higher nickel contents are normally found to be more resistant to stress corrosion than those with less nickel [URLSpe]. The test has shown that alloys containing more than about 45% nickel are resistant to chloride stress cracking.

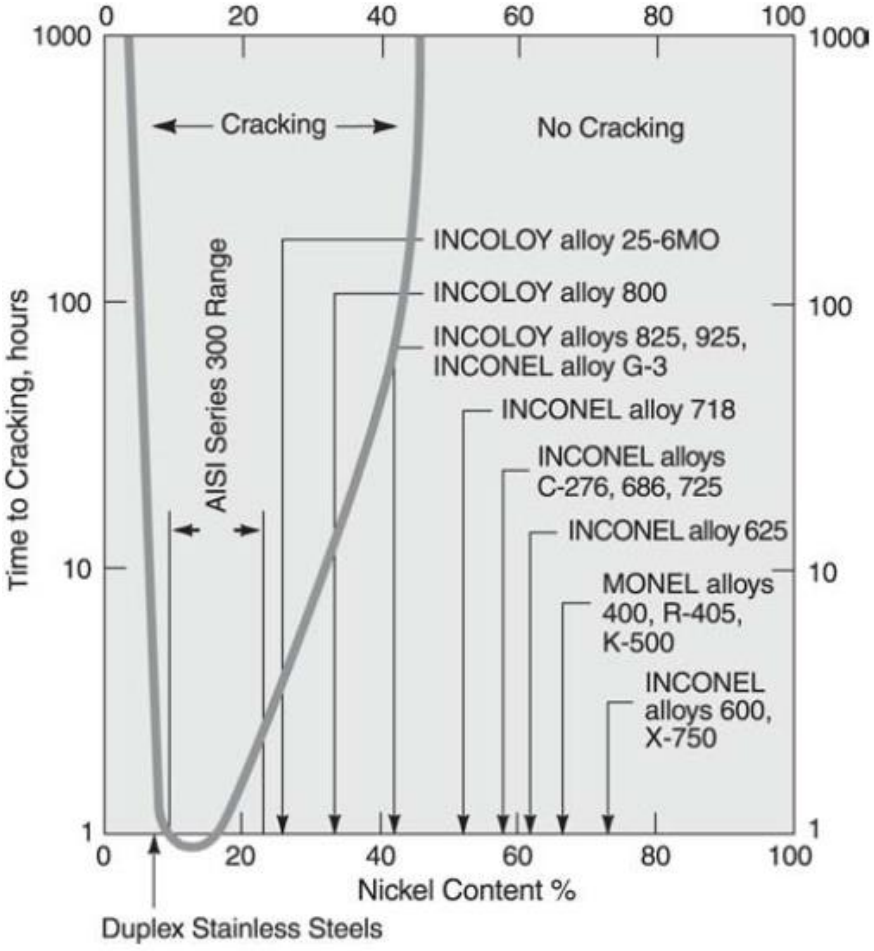

Figure 2.1 Copson's curve showing susceptibility of alloys to chloride-ion stress corrosion cracking in the boiling 42% magnesium chloride test [URLSpe].

Austenitic stainless steels can be hardened by cold work. Heat treatments of these steels in the 450–850°C range promotes intense chromium carbide precipitation in the grain boundaries

[1965Lew, 1999Tri, 2008Yae, 2009Tav]. When heated for small periods and/or to low temperatures (450°C) in this temperature range, the steel becomes sensitized and susceptible to intergranular corrosion attack, due to chromium carbide formation and depletion of chromium near the grain boundaries [1979Sed, 1997May].

Ferritic stainless steels contain between 12wt% and 30wt% chromium, with very little nickel content [URLOut]. The cheapest stainless steels are found in this type. They have a body-centred cubic (bcc) structure, and their corrosion resistance is comparable to that of the austenitic grades in certain applications. Ferritic stainless steels have excellent resistance to chlorides; they are highly corrosion-resistant, but less durable than austenitic grades. These steels have better resistance to stress corrosion cracking (SCC) than austenitic stainless steels. Typical applications include appliances, automotive and architectural. These grades are frequently considered for thermal transfer applications. The thermal conductivity is about half that of carbon steels. Ferritic stainless steels are magnetic, with generally good ductility and they can be welded or fabricated easily, but only in thin sections. They cannot be hardened by heat treatment, but can be hardened by cold rolling, although not as much as the austenitic alloys. Ductility and formability are less than the austenitic grades, because of the bcc structures.

The compositions of martensitic stainless steels are about 12 to 18 wt% Cr and 0.1 to 1.2 wt% C [1993Des]. Martensitic stainless steels contain martensite, with a lath or needle-like structure. The austenite in these steels is able to transform into martensite, which allows control on the mechanical properties by exploiting the phase change. Typical heat treatments consist of austenitisation at a temperature high enough to dissolve the carbides, followed by quenching to obtain martensite. Given the high hardenability inherent in such alloys, the quench rates required to achieve martensite is not high; oil quenching is used when dealing with thick sections. As with all martensitic steels, a balance must be sought between hardness and toughness. An untempered martensitic structure is typically strong, but it lacks toughness and ductility, which depend on the carbon concentration. As a consequence, the martensite is in many cases tempered between 600°C and 750°C to optimise the mechanical properties and for the carbon atoms to diffuse and react to form Fe_3C in a ferrite matrix. Large numbers of alloyed martensitic stainless steels have been developed for moderately high temperature applications. The most common additions include Mo, V and Nb [1965Bri], which lead to increased hardenability. The 12Cr-Mo-V-Nb

steels are used in the power generation industry, for steam turbine blades operating at temperatures around 600°C.

2.1.2 Duplex stainless steel

Duplex stainless steels (DSSs) are also referred to as ferritic-austenitic steels, which have the beneficial properties of both ferritic and austenitic steels [URLOut]. They contain high contents of chromium and nitrogen and sometimes molybdenum. They have good resistance to pitting and uniform corrosion. The microstructure of the duplex stainless steels contributes to the high strength and high resistance to stress corrosion cracking. The well-known duplex stainless steels are 2304, 2205 and 2507. Their chemical composition varies slightly between different national standards. Some of the applications of duplex stainless steels are heat exchangers, water heaters, pressure vessels, tanks, rotors, impellers, shaft flue–gas cleaning and hydrocarbon process piping systems.

After melting, duplex stainless steels solidify from the liquid phase to a completely ferritic structure. As the materials cool, about half the ferritic grains transform to austenitic grains. In the annealed condition (at about 1000^{o}C [2009Imo]), duplex stainless steels consist of approximately equal amounts of ferrite and austenite. Decomposition of the ferritic phase may lead to higher hardness, yield stress and ultimate tensile strength, although this decreases ductility and toughness. The chemical composition of each phase may vary as the annealing temperature varies. The contents of Cr and Mo may change slightly in the ferrite phase because they are ferrite formers and partition more to that phase. The nitrogen concentration in the austenite phase may decrease with temperature as the volume fraction of austenite increases. This could lead to increasing pitting corrosion resistance of duplex stainless steel. Lardon [1988Lar] found that Cr and Mo enrichment can occur in the ferrite phase, while Ni and N may concentrate in austenite.

The commercial production of duplex stainless steels started in about 1937 [1993Des]. Duplex stainless steels are called “duplex” because they have two-phase microstru ctures of grains of ferritic and austenitic stainless steel. Duplex stainless steel is about twice as strong as regular austenitic or ferritic stainless steels. However, they are more susceptible than austenitic stainless steels to precipitation of phases, causing embrittlement. They have better toughness and ductility than ferritic grades, although they do not reach the high values of austenitic grades.

The corrosion resistance of duplex stainless steel depends mostly on the composition [2009Imo]. For chloride pitting and crevice corrosion resistance, their chromium, molybdenum and nitrogen contents are most important. Duplex stainless steel grades have a range of corrosion resistance, similar to the range for austenitic stainless steels. Duplex stainless steels have lower nickel and molybdenum contents than their austenitic counterparts of similar corrosion resistance. Compared to austenitic stainless steel, duplex stainless steels can be less expensive, which is usually because of the lower nickel contents. It may often be possible to reduce the section thickness of duplex stainless steel, compared to austenitic stainless steel, because of its higher yield strength. The combination of lower nickel content and reduction of thickness of duplex stainless steel can lead to significant cost and weight savings compared to austenitic stainless steels.

Duplex stainless steels have higher yield strength and higher toughness than austenitic stainless steel, possibly due to their good ductility [1982Her, 2009Shr, 2009Mul]. They have lower coefficients of thermal expansion and higher thermal conductivities than austenitic stainless steels. Plastic deformation tends to be concentrated in the more ductile austenite grains. However, duplex stainless steel possess low fatigue properties, and their room temperature impact energy of duplex stainless steels may decrease gradually with ageing temperature [2009Zha1].

Sigma formation, which is the formation of a brittle, non-magnetic intermetallic phase, can occur in duplex stainless steels at temperature range of 600^{o}C-950^{o}C, while embrittlement or reformation of ferrite can occur in the range of 350^{o}C-525^{o}C (475^{o}C-embrittlement) [1983Sol]. Also, ageing in duplex stainless steel may cause the precipitation of Cr_2N, which could lead to a decrease in their impact energies [1978Sol, 1983Sol, 2000Tav, 2008Zha]. Although duplex stainless steels are regarded as high-potential industrial materials, they are susceptible to spinodal decomposition, which is a mechanism by which the ferrite phase decomposes into a Cr-rich phase and an Fe-rich phase when exposed to temperatures between 300 and 500ºC.

2.1.3 Effect of elements on duplex stainless steel

2.1.3.1 Chromium

Chromium is a key alloying element used in stainless steel to stabilize the ferritic phase. It can form a resistant passive oxide film on the surface [1983Sol]. However, it cannot be used alone because of brittleness. When alloyed with other metals, especially nickel, chromium easily enhances passivity 1992Jon]. There is a limit to the level of chromium that can be added to duplex steel, as it enhances the precipitation of intermetallic phases, such as sigma, which lead to reduction in ductility, toughness and corrosion resistance [2008Alv].

2.1.3.2 Nickel

Nickel is an important alloying element of duplex stainless steel. The addition of nickel to duplex stainless steels can play an important role in maintaining an austenite/ferrite balance, because nickel is an austenite promoter and improver of pitting resistance [1990Cor, 2001Tav]. Nickel additions considerably improve the pitting resistance (pitting potentials) of the duplex stainless steels. Increasing nickel contents lowered the depassivation pH of duplex stainless steels in acidic media [1988Yau, 2004Azu]. Olubambi *et al.* [2008Olu] studied the influence of nickel additions on the corrosion behaviour of low nitrogen 22% Cr series duplex stainless steels and found that increasing nickel content helped in improving its corrosion resistance in sodium chloride and sulphuric acid media.

2.1.3.3 Nitrogen

The addition of nitrogen is an alternative to nickel, which is due to its effective nickel-substituting potential for austenite formation. Nitrogen increases strength, and improves the resistance of duplex stainless steel to crevice and pitting corrosion in chloride environments. There is a limit to which nitrogen addition can be used to substitute nickel, which is the solubility limit of nitrogen in the steel melt (which approaches ≈ 0.3wt% at 1460-1500°C [2006Ban]). Its solubility can be increased by the addition of manganese and molybdenum. Hänninen *et al.* [2001Hän] reported that higher chromium and nitrogen with low nickel super-duplex stainless steels were very difficult to manufacture through traditional metal working practices, because

they are prone to hot cracking in forging and macro-segregation in casting. Increasing nitrogen additions can also cause chromium nitride precipitation, especially in the heat-affected zone in welded joints [1987Wri, 1990Cor]. Chromium nitride decreases the corrosion resistance, as it could cause a chromium-depleted zone, which could result in localized corrosion attack. An increase in nitrogen content decreases the degree of chromium partitioning.

2.1.3.5 Manganese

Manganese is used in lean duplex stainless steels (which are alloys containing reduced nickel content) for effective ferrite-austenite phase balancing, while allowing a reduction in nickel content 1983Cha, 2009Imo]. Manganese is an austenite stabilizer. Its additions to the DSS increase abrasion and wear resistance and tensile properties, without loss of ductility. It also increases the solid solubility of nitrogen, and thus allows for increased nitrogen contents to eliminate the risk of out-gassing.

2.1.3.4 Molybdenum

Molybdenum is a ferrite former which is used in several types of stainless steel to improve corrosion resistance, particularly pitting and crevice corrosion resistance in chloride-containing solutions It has atomic weight of 42, which is close to ruthenium (44), and so should share some characteristics [1978Sol, 2001Imo]. Molybdenum-containing steels are used in applications that are more corrosive, such as chemical processing plants or in marine applications. High molybdenum contents can lead to the formation of δ-ferrite and R-phase (rhombohedral phase) which decrease toughness and corrosion resistance. The best grade for a given application is selected based on the corrosivity of the service environment. As a large atom, molybdenum increases the elevated temperature strength of stainless steels through solid solution hardening. This effect is used in heat exchangers and other elevated temperature equipment such as in automotive exhaust systems.

2.1.3.6 Ruthenium

The platinum group metals (PGMs) are six metallic elements clustered together in the periodic table. The elements are ruthenium, rhodium, palladium, osmium, iridium and platinum. They have similar physical and chemical properties and are likely to be present in the same mineral deposits [1971Eng, 1978Sat, 1989Sav, 1991Har, 1995Ver]. The PGMs are highly resistant to wear, tarnish and chemical attack. They have excellent high temperature performance and stable electrical properties. They are silver-white and refractory, and are refered to as noble metals because of their attractive appearance and high chemical stability. Ruthenium is the most versatile of the platinum group metals and is readily available in South Africa. Ruthenium is a hard white metal which does not tarnish under normal temperatures. It has an atomic number of 44, atomic weight of 101.07g.mol^{-1}, density at room temperature of 12.45g.cm^{-3} and liquid density of 10.65 g.cm^{-3}. It has thus the smallest atomic weight of the platinum group metals, hence this makes it more comparable to the usual alloying elements for duplex stainless steels. The application of ruthenium is found in film chip resistors, jewellery, high temperature superalloys used as turbine blades in jet engines, radiotherapy (particularly eye tumours) [1995Ver]. Ruthenium is also obtained as a by-product from copper and nickel processing.

2.2 Cathodic Modification

2.2.1 Mechanism of cathodic modification

Cathodic modification is an electrochemical means of improving the corrosion resistance of alloys, particularly of stainless steels and titanium-based alloys in non-oxidizing acid media. Cathodic modification is the addition of an element exhibiting high exchange current density for the reduction of H^+ ($2H^+ + 2e^- \rightarrow H_2$) to raise the corrosion potential (E_{corr}) of the matrix. Tomashov [1967Tom] indicated that there are four possible ways in which corrosion resistant alloys can be produced and the resistance of alloys against electrochemical attack increased:

(a) an increase in the degree of thermodynamic stability,

(b) retardation of the kinetics of the cathodic processes (Figure 2.2),

(c) retardation of the kinetics of the anodic processes, and

(d) production of stable passivating oxide layers.

The cathodic polarization curves can be changed by the retarded cathodic reactions, as shown in Figure 2.2 [1990Pot]. It can be retarded by eliminating the active cathodic impurities such as iron or copper in zinc (Figure 2.2a), and by increase of the overvoltage of the cathodic process, such as alloying of manganese or zinc to magnesium alloys (Figure 2.2b).

The a nodic reaction can be regarded as the result of an increase in the ability of the alloy to be passivated. Passivity is a condition of corrosion resistance due to formation of thin surface films under oxidising conditions with high anodic polarization [1975Eva, 1992Jon]. This can be done in various ways, including the alloying of iron, nickel and ferronickel steels with chromium, or the introduction of active cathodes into the alloy. The technique of alloying stainless steels and titanium with active cathodes, e.g. the PGMs, is known as cathodic modification.

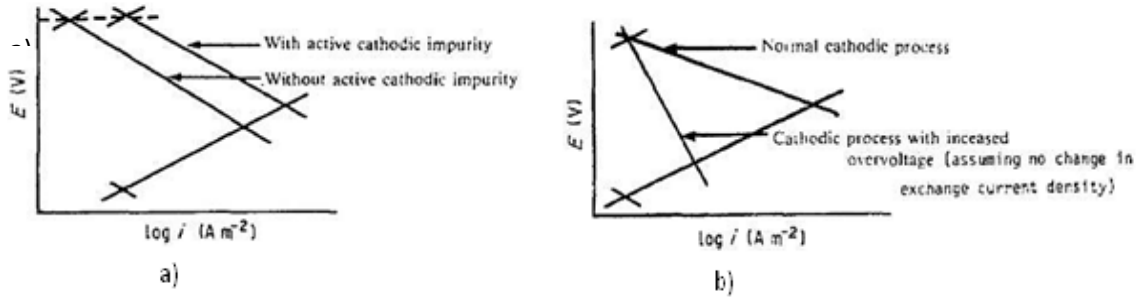

Figure 2.2. Schematic representation showing ways in which cathodic reactions can be retarded [1990Pot].

As early as 1911, Monartz [1911Mon] reported that the rapid corrosion of iron–chromium alloys in certain acids could be prevented by the winding of a platinum wire around the sample used in the corrosion test, or by alloying of the steel with platinum. Hoar [1960Hor] reported that for titanium; platinum, palladium, rhodium, and ruthenium gave the best results; osmium and iridium appeared to be slightly less effective. Greene *et al.* [1961Gre] reported that passivity can be induced in a base metal or an alloy by the addition of a noble metal (one of the PGMs, gold or silver) having a high cathodic exchange current density, provided that the passive region of the base alloys extends to potentials that are more negative than the redox potentials of the environments. This is schematically represented in Figure 2.3 [1990Pot]. Line A represents the

cathodic polarization curve for the metal, and line B is that for the cathodically modified alloy. Hence, for metals that exhibit stable passivity at potentials sufficiently more negative than the existing hydrogen potential in the system, spontaneous passivation will be possible in the absence of any substance or compound more oxidizing than hydrogen ions, i.e. where hydrogen ion reduction remains the dominant cathodic reaction.

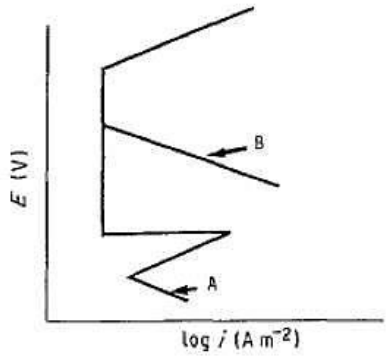

Figure 2.3. Schematic illustration of cathodic modification, Line A represents the cathodic polarization curve for the metal, and line B is the same for the cathodically modified alloy [1990Pot].

The schematic diagram of different active-passive states in alloy system is presented in Figure 2.4 [1967Tom]. The different states are active, passive, passive-active and transpassive [1967Tom, 1990Pot]. The active state is where the rate of the cathodic process is relatively low. The alloy undergoes active dissolution at a potential of E_{co} at i_{co} and the conditions $E_o^A < E_p < E_o^C$ and i_{cath} $(E_p) < i_{cr}$; if the system is moved temporarily to a passive potential range, the active state will be spontaneously re-established.

The passive-active state is at intermediate rate of cathodic process, which has three conditions and are given at three points A, B and C at which the cathodic line and anodic curves intersect (Figure 2.4b) [1967Tom]. Anodic dissolution of the metals occurs at a high corrosion rate at potential C. At B the system is in an unstable state rarely observed in practise, while the potential is in passive state at point A.

In the passive state (Figure 2.4c), the anodic curves intersect at only one point in the passive range, and the rate of alloy dissolution is very low because of the passive state [1967Tom]. This kind of system is typical of cathodically modified chromium, stainless steel and titanium alloys

in non-oxidising acid environments. The transpassive system has a very high rate of the cathodic process, as shown by the solid line of the cathodic process in Figure 2.4d; the metal or alloy will have a higher rate of dissolution than in the passive range and considerable corrosion can take place.

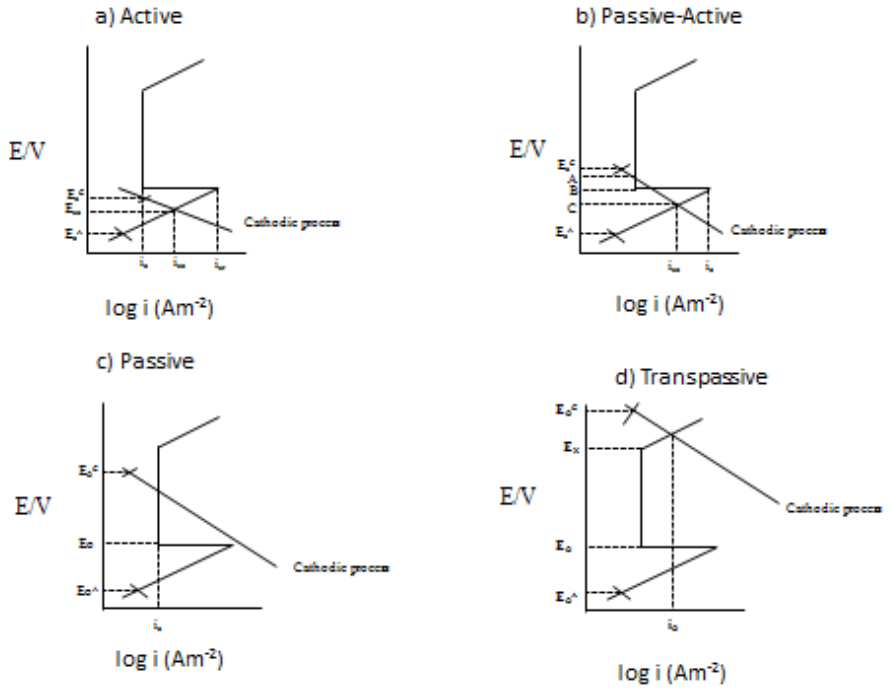

Figure 2.4. Different active-passive states in alloy system: a) Active, b) Passive-active, c) Passive, and d) Transpassive [1967Tom].

The effect of cathodic modification should therefore be most pronounced in non-oxidizing acid environments, for example, de-aerated hydrochloric and sulphuric acids. Addition of PGMs to chromium in non-oxidizing acids improved its corrosion resistance, although they had a detrimental effect in oxidizing acid (nitric acid). Stern and Wissenberg [1959Ste] reported that various PGMs and other noble metals caused the spontaneous passivation of titanium in boiling dilute sulphuric and hydrochloric acid. The increase in corrosion resistance of the titanium depended on the concentration of the PGMs added and also alloying additions of as little as 0.1wt% resulted in a pronounced improvement in corrosion resistance.

The effect of the various alloying elements in improving the corrosion resistance of an alloy is shown in Table 2.1, and was found to be generally decreasing in the order [1961Gre]:

Ir > Rh > Ru > Pt > Pd > Os > Au > Re > Cu > Ag.

The order of the hydrogen overpotential behaviours of these metals was almost the same [1961Gre]. Elements with low hydrogen over voltages (e.g iridium, rhodium, platinum and palladium) are very effective, while those with high over voltages (e.g gold, silver and copper) are not. The critical anodic currents are also listed by Greene *et al.* [1961Gre] in order of decreasing effect, as shown in Table 2.1. These are Ir > Pd> Rh > Pt > Os > Re > Ag > Au.

The detrimental effect of noble metal alloying in HNO_3 is shown in Tables 2.1 [1961Gre]. Most of the alloying metals increased corrosion in the medium, the effects being more pronounced with increasing alloy content. Platinum, ruthenium and gold were more detrimental in HNO_3, and this was attributed to the transpassive region exhibited by the chromium. The corrrosion potential of the chromium in 65% HNO_3 was close to the beginnig of the transpassive region. Alloying Cr with noble metals moves it to its tranpassive region, resulting in increased dissolution rates. This is presented schematically in Figure 2.5 [1961Gre], where E_o is the redox potential and $i_{a,m}$ and $i_{o,a}$ are the exchange current densities of the pure metal and noble metal alloy respectively.

If the alloying metal is not attacked and has exchange current densities greater than the base, and the mixed potential of the pure metal is close to the transpassive region, the corrosion rate is increased. In Figure 2.5 [1961Gre], the pure metal corrodes at potential M at a rate i_{corr} (m), while the alloy corrodes at A with a rate i_{corr} (A). It was discovered that all the PGMs, apart from rhodium, are detrimental in HNO_3 which was probably due to the small exchange current density for HNO_3 reduction.

Table 2.1. Effects of alloying additions on the corrosion resistance of chromium (mils/year) [1961Gre].

Nominal composition	Boiling H_2SO_4 (%)											Boiling HCl (%)			Boiling 85% NHO_3
	5	10	20	30	40	50	60	70	80	90	Conc	5	10	15	
Cr	D	D*	D	D	D	D	D	D	D	2400	300	D#	D	D	3
Cr +0.5%Ir	-	1	2	13 (49)	43	100	D	-	-	-	-	<1	2 (20)	D	34
Cr+0.5%Rh	-	-	3	16 (23)	68	66	970	-	-	-	-	<1 11	3 (45)	D	5
Cr+0.5%Ru	-	2	11	17 (48)	83	7100	-	-	-	-	-	<1 (11)	<1 (D)	D	110
Cr +0.5%Pt	<1	3	12 (16)	28	175	120	36	D	D	D	185	<1	8 (25)	D	200
Cr + 0.5%Pd	-	2	8 (14)	22	180	1500	1300	-	-	-	-	<1 (56)	D	D	15
Cr + 0.5%Os	<1	1 (18)	67	560	-	-	-	-	-	-	-	5 (2800)	D	D	8
Cr+ 0.5%Au	<1 (300)	600	1900	-	-	-	-	-	-	-	-	D	-	-	120
Cr + 0.5%Re	<1 (D)	D	D	-	-	-	-	-	-	-	-	D	-	-	5
Cr + 2% Cu	780	2700	D	D	D	-	-	-	-	-	-	D	D	D	70
Cr + 0.5%Ag	2600	-	D	-	-	-	-	-	-	-	-	D	-	-	4
Cr + 0.1% Pt	2	1	5 (11)	22	100	840	D	D	-	-	-	<1	9 (1400)	D	9
Cr + 0.5% Pt	<1	3	12 (16)	28	175	120	36	D	-	-	-	<1	8 (25)	D	200
Cr + 1.0% Pt	-	-	6 (3)	22	210	68	21	1260	-	-	-	<1 (5)	140	D	500
Cr + 2.0% Pt	-	-	6 (18)	18	130	28	9	56	-	-	-	<1	3 (51)	D	300
Cr + 5.0% Pt	-	-	1 (4)	18	51	12	-	55	-	-	-	<1 (1)	170 (280)	D	490
Cr + 0.05% Pd	-	-	0-22 (56)	57	-	D	D	-	-	-	-	D	D	-	6
Cr + 0.1% d	-	2	0-20 (20)	31	130	1600	D	-	-	-	-	0-40 (915)	D	-	5
Cr + 0.2%Pd	-	-	0-13 (13)	23	150	1400	D	-	-	-	-	0-38 (94)	D	-	7
Cr + 0.3%Pd			1-12 (13)	21	370	1400	300	-	-	-	-	<1 (48)	D	-	5
Cr + 0.5%Pd			8 (14)	22	180	1500	1300	-	-	-	-	<1 (56)	D	D	15
Cr + 1.0%Pd	-	-	2 (16)	56	2800	725	400	-	-	-	-	2 (12)	D	D	23

D Dissolved during test
( ) sample activated with an iron wire for at least 1 min.
* Corrosion rate - 100,000 mpy (0.5 hr test).
# Corrosion rate -240,000 mpy (0.5 hr test).

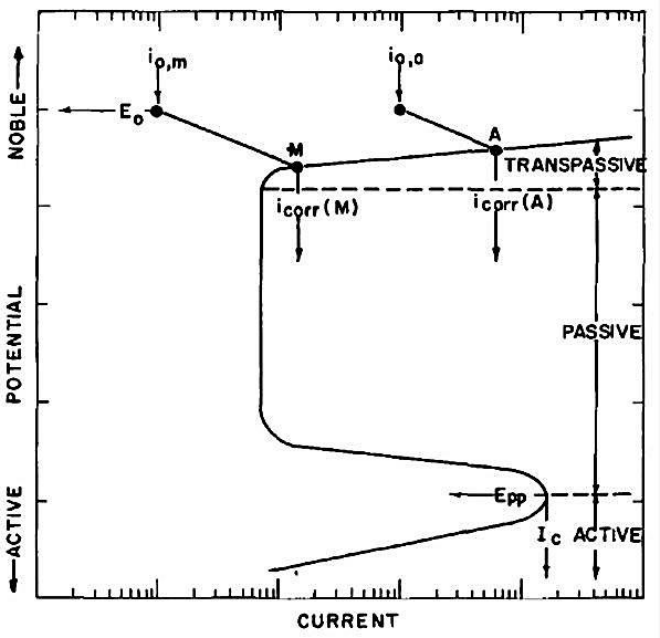

Figure 2.5. Schematic diagram showing the effect of exchange current density on corrosion behaviour in transpassive region [1961Gre].

Greene *et al.* [1961Gre] concluded that the noble metal alloy additions can affect both anodic and cathodic reaction kinetics. The additions simultaneously increased cathodic and anodic current density when alloyed with a metal, and these changes increased the passivation tendency.

Streicher [1974Str] noticed a beneficial synergistic effect between nickel and ruthenium. Lower concentrations of ruthenium (0.1 wt%) and Ni (0.1 wt%) were needed to passivate Fe-28%Cr-4%Mo in a 10% solution of boiling sulphuric acid than the concentration of either 0.2 wt% ruthenium or 0.25 wt% nickel that were needed when they were used alone. This became a motivation for Tullmin's work on the development of experimental ferritic stainless steels containing 40 percent chromium [1992Tul].

Streicher [1977Str] tested Pd, Ir, Os, Rh and Ru as cathodic additives to ferritic stainless steels (Fe-28%Cr-4%Mo) and reported that ruthenium additions (0.2 wt%) produced better corrosion resistance, than did palladium additions (0.2 wt%). All the platinum metals were used to produce passivity in boiling 10% sulphuric acid; small amounts of the six platinum metals were added as alloying elements. Some of the results are reported in Table 2.3 [1977Str].

The rate of corrosion of the ferritic alloy Fe-28.5Cr-4Mo was over 52,000 mm/year, the six platinum group metals were added in excess of minimum concentrations which varied from 0.005 to 0.2 wt%, depending on the noble metal [1977Str]. This was independent of the atomic weight; the determining factors are probably differences in electrochemical properties of the six platinum metals such as electrode potential, hydrogen overvoltage and exchange current of cathodic reactions taking place on the surfaces in the solution.

Fe-28.5Cr-4Mo required 0.5 wt% Ru addition to make it self repassivating; that is passivity was recovered when the specimen was activated with an iron rod [1977Str]. Streicher discovered that none of the noble metal additions to Fe-28.5Cr-4Mo alloy affected its excellent resistance to stress corrosion cracking in boiling magnesium chloride except for 0.5 wt% Ru. There was no cracking observed for 0.5 wt% addition in sodium chloride environment up to 200°C (Table 2.2 [1977Str]).

Table 2.2. Effect of noble metal additions on the corrosion resistance of Fe - 28.5 wt% Cr - 4.0 wt% Mo alloy [1977Str].

Noble metals additions		**Boiling 10 per cent Sulphuric acid**		**Pitting Corrosion (a)**		**Stress corrosion (b)**
		State	**Corrosion rate, in mils/year (c)**	**$KMnO_4$-NaCl**	**$FeCl_3$**	**$MgCl_2$**
None	t	Active	52,180	R	R	R
Platinum	0.005	Active	58,000	R	R	-
	0.006	Passive	48	-	R	-
	0.200	Passive	1	-	-	R
Palladium	0.010	Active	74,000	-	F	-
	0.020	Passive	4	-	F	-
	0.200	Passive	1	F	F	R
Iridium	0.010	Passive	112	R	R	-
	0.100	Passive	13	R	R	R
Rhodium	0.005	Passive	14	R	F	-
Osmium	0.015	Active	76,600	R	R	-
	0.020	Passive	36	-	R	-
Ruthenium	0.015	Active	62,200	-	-	-
	0.017	Active	-	-	-	-
	0.020	Passive	60	R	R	R
	0.200	Passive	9	-	R	R
	0.300	Passive	2	R	R	R
	0.500	Passive*	3	-	R	Cracked in 17 h (d)

* Self-repassivating, R- Resistance, F- Fail, R- no cracking after 2400 h exposure.

(a) 2 per cent $KMnO_4$, 2 per cent NaCl at 90°C, simple immersion, 10 per cent Ferric Chloride, $FeCl_3.6H_2O$ at 50°C with crevices. (b) boiling (155°C) 45 per cent $MgCl_2$ U-bend specimen. (c) thousandths of an inch per year. (d) no cracking in 26 per cent NaCl at 200°C

Streicher [1977Str] tested AISI 316, Carpenter 20Cb-3, Hastealloy C, Titanium, Fe-35Cr and Fe-28%Cr-4%Mo in permanganate chloride at 90°C, ferric chloride at 50°C, bromine–bromide at room temperature and sodium hypochlorite at room temperature (Table 2.3 [1977Str]). The best alloy was Fe-28%Cr-4%Mo-0.3Ru, which was resistant in the solutions.

Additions of iridium, osmium and ruthenium were without effect in the pitting and crevice corrosion resistance Fe-28Cr-4Mo [1977Str]. Iridium, osmium and ruthenium are the only PGMs that can be used to produce passivity of stainless steels in sulphuric acid without impairing resistance to pitting and crevice corrosion in oxidising, chloride environments. Ruthenium, because of its lower cost, was the preferred metal for addition to stainless steel for production of alloy resistance to acid corrosion [1977Str].

Table 2.3. Comparison of pitting resistance in halide media at different temperatures [1977Str].

Alloy	**Permanganate chloride at 90°C (a)**	**Ferric chloride at 50°C (b)**	**Bromine bromide at room temperature (c)**	**Sodium hypochlorite at room Temperature (d)**
AISI 316	F	F	F	F
Carpenter 20 Cb-3	F	F	F	F
Hastelloy C	R	R	F	F
Titanium	R	R	R	R
Fe-35%Cr	F	F	F	F
Fe-28%Cr-4%Mo	R	R	R	R
Fe-28%Cr-4%Mo+Pd	F	F	F	-
Fe-28%Cr-4%Mo+ Rh	R	F	F	-
Fe-28%Cr-4%Mo+Pt	R	R	F	-
Fe-28%Cr-4%Mo+Ir	R	R	R	-
Fe-28%Cr-4%Mo+Os	R	R	R	-
Fe-28%Cr-4%Mo+Ru	R	R	R	R

R- Resistant; F- Fails.

(a) 2 per cent $KMnO_4$- 2percent NaCl. (b) 2 per cent $FeCl_3.6H_2O$ with crevices.

(c) 54.5 per cent Br_2 + 20.6 percent $ZnBr_2$ (d) 0.1 per cent NaClO with Teflon ® crevices.

Du Plessis [1984Dup], in an otherwise unpublished MSc dissertation, reported that the performance of 3CR12-0.2Ru alloy and 3CR12-0.25Pt alloy was better than the rest of the alloys in a reducing corrosive environment. The passivation potential (E_{pp}) leveled off at 0.1 wt% ruthenium. Additions in excess of 0.1% ruthenium resulted in a constant critical current density (i_c) minimum of 0.6mA/cm^2. He concluded that a 0.2% ruthenium alloying addition would be the optimum amount for a reduced corrosion rate (Figure 2.6 [1984Dup]). However, the graph showed the optimum to be at 0.1% Ru, not the 0.2% Ru as specified by Du Plessis [1984Dup].

No errors were given. It was interesting that with Pt and Ru additions below 0.1wt%, there was an increase in the corrosion rate.

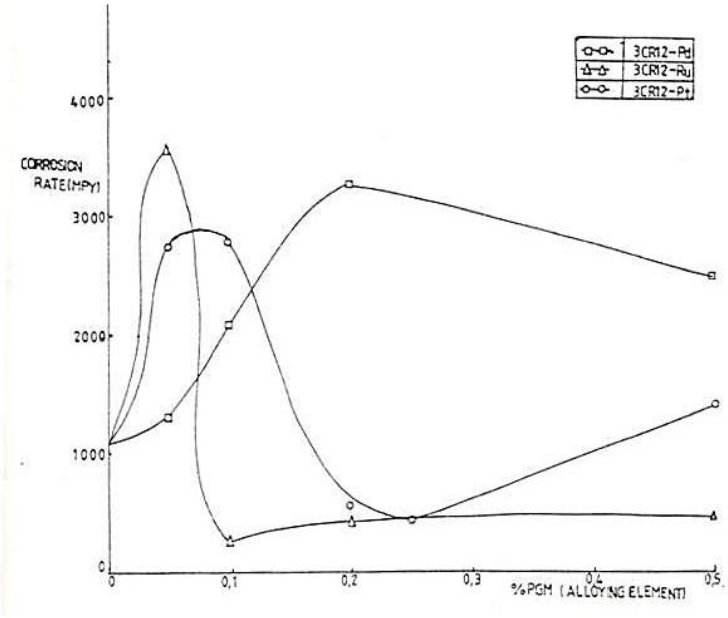

Figure 2.6. Corrosion rate of 3Cr12 steels alloyed with platinum group metal additions in 1N H_2SO_4 at 30°C [1984Dup].

Higginson [1984Hig] confirmed that ruthenium improved corrosion resistance in ferritic stainless steels more than palladium. Potgieter *et al.* [1990Pot] showed that cathodic modification can increase corrosion resistance of materials in non-oxidizing acids, by increasing the potential to a value that is in the passive potential range. It was found that during anodic dissolution, noble metal atoms were redistributed on the surface alloy, possibly by a surface diffusion mechanism.

The corrosion of ductile chromium alloyed with ruthenium, osmium, iridium, platinum, palladium or rhenium in solutions of 5 to 60% sulphuric acid at various temperatures (shown as stability areas under the curve) was described by Tomashov *et al.* [1979Tom, 1980Tom1, 1980Tom2, 1980Tom3, 1984Tom]. The effect of different alloying additions on the corrosion stability of ductile chromium in acids of different concentrations and temperatures is given in Figure 2.7 [1980Tom1].

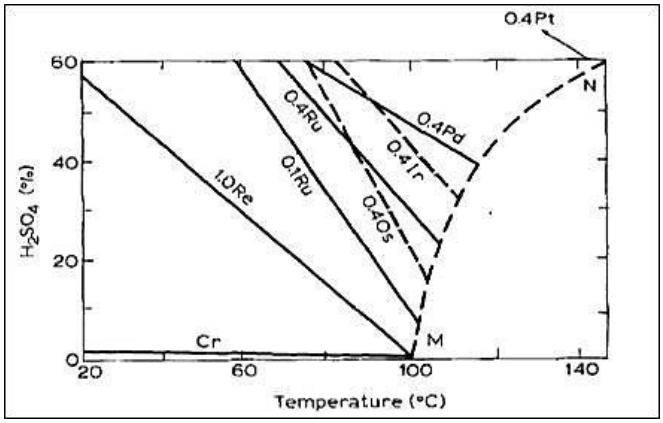

Figure 2.7. Effect of modification of ductile chromium by the addition of 1 wt% Re and 0.4 wt% Os, Ru, Ir, Pd and Pt on its passivation and corrosion stability as functions of the concentration and temperature of sulphuric acid [1980Tom1].

The lower the concentration of the PGM addition to the alloy, the lower and more to the left the line shifts for the alloy in Figure 2.7 (e.g. the Cr-0.1 wt% Ru and Cr-0.4 wt% Ru lines on the graph) [1980Tom1]. The dotted curve MN represents the boiling points of the sulphuric acid solutions versus their concentrations. Figure 2.7 clearly shows that chromium without cathodic modification corrodes at a high rate, while cathodically modified alloys self-passivated easily. Higginson [1987Hig] found that an improvement was obtained in the corrosion rate of 1×10^{-4} to 5×10^{-4} for Fe - 40%Cr -0.2%Ru alloys compared with Fe - 40%Cr in a boiling solution of 10% sulphuric acid, and the alloy containing ruthenium was more resistant than the alloy containing palladium. The greater effect of the ruthenium was explained on the basis that it is a more effective cathode for the evolution of hydrogen than palladium. Howarth [1987How] found no improvement in corrosion resistance with platinum over ruthenium. The critical time and charge density for spontaneous passivating of Fe -40%Cr- Ru alloys depended on the concentration of ruthenium in the alloy and the acid in which the corrosion takes place [1987Hig]. Tomashov [1986Tom] found that the general and pitting corrosion resistance were higher in the alloys containing ruthenium than in the alloys containing palladium. These observations were attributed to several factors [1991Pot]:

a) Ruthenium reduces the overvoltage of cathodic hydrogen generation more efficiently than palladium, thereby increasing the efficiency of the cathodic process.

b) Ruthenium, unlike palladium, reduces the rate of anodic dissolution by reducing the critical current density required for passivation especially in media containing chlorides. (Biefer [1970Bie] and Higginson [1987Hig] made this observation).

c) Ruthenium is susceptible to the adsorption of oxygen and the formation of oxides, and these affect the composition of the hydroxide and oxide layers formed on the surface of the steel which inhibits corrosion, while palladium remains as a separate metallic phase in the surface layer.

d) Although the passivating oxide layers on the steel contain ruthenium as well as chromium, the resistance of the steel to the activating effect of chloride ions increases, thus, Ru does not impair the resistance to pitting corrosion.

Higginson [1987Hig] found that Fe-40%Cr that had been alloyed with both 1.8% molybdenum and 0.1% ruthenium passivated far more quickly in sulphuric acid (0.5M) than the Fe-40%Cr-0.1%Ru alloy. According to Tomashov *et al.* [1980Tom2], the difference in passivation also occurred in solutions of dilute hydrochloric acid (1-3wt%), although Higginson [1987Hig] showed that the addition of 0.1 wt% Ru to an Fe-40%Cr-1.8%Mo steel did not spontaneously passivate in a solution of 0.5M hydrochloric acid. The discrepancies between the results of Tomashov *et al.* [1980Tom2] and Higginson [1987Hig] can be attributed to differing conditions, the environment or slight changes in concentrations of the acid, in their respective investigations [1991Pot]. Higginson [1987Hig] also found that the addition of 0.1% nickel to an Fe-40%Cr-0.1%Ru alloy increased the time needed for the occurrence of the spontaneous passivation in 0.5M sulphuric acid. He concluded that the inhibition of the anodic dissolution reaction in sulphuric acid was much greater for the alloy containing both nickel and ruthenium, even for only 0.1%Ru. The alloying of Fe-40%Cr -0.1%Ru with 1% Ni also caused spontaneous passivation to occur approximately seven times faster than for the Fe-40%Cr – 0.1%Ru alloy. Thus, while an addition of 1% nickel to Fe-40%Cr -0.1%Ru was advantageous and lowered the passivation time in hydrochloric acid, the same did not apply when the sulphuric acid was used, since the passivation time increased.

The effects of alloying additions on the polarization characteristics of Fe-Cr stainless steel in sulphuric acid are summarised in Figure 2.8 [1970Bie]. Ruthenium, Pd and Pt shift the corrosion potential to more noble values, and Mo, Ru, Pt and Re decrease the critical current density.

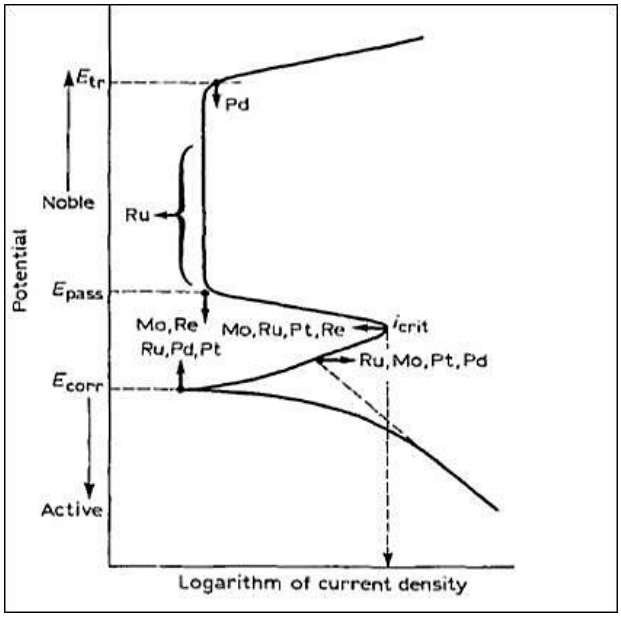

Figure 2.8. Summary of the effects of alloying additions on the polarization characteristics of Fe-Cr stainless steel in sulphuric acid [1970Bie].

Potgieter [1991Pot] concluded that cathodic alloying additives (e.g. PGMs) greatly increased the corrosion resistance of chromium in non-oxidizing acid environments, and the passivation of cathodically modified chromium in non-oxidizing acid environments. The process of active dissolution and passivation of cathodically-modified chromium can be satisfactorily interpreted from a comparison of the different electrochemical processes. The PGMs block the active sites in the crystal lattice of chromium, thereby preventing corrosion. A layer of the PGM atoms and trapped hydrogen in the pores between the cathodic component particles partly screen the surface of the alloy, also causing a decrease in the active anodic surface and in corrosion. It was also discovered that for all cathodically-modified alloys of titanium, stainless steel and chromium, there is an enrichment of the PGMs on the surface of the alloy during the corrosion process, which was explained by diffusion [1977Str].

The effect of ruthenium addition on microstructural modification and the formation of a second phase was shown by Olubambi *et al.* [2008Olu]. Figure 2.9 reveals that the microstructure of steel varied significantly and the grain sizes were refined as the amount of ruthenium increased. At 0.05% Ru addition, there were fine homogeneous equiaxed ferrite grains with dark particles (second phase) within the ferrite grains. The proportion of the second phase increased as the ruthenium content increased. This phase was shown by van der Lingen and Sanderbergh [2001Van] to possess better cathodic modification properties than pure ruthenium, and so act as enhanced cathodic active sites during exposure to corrosive environments.

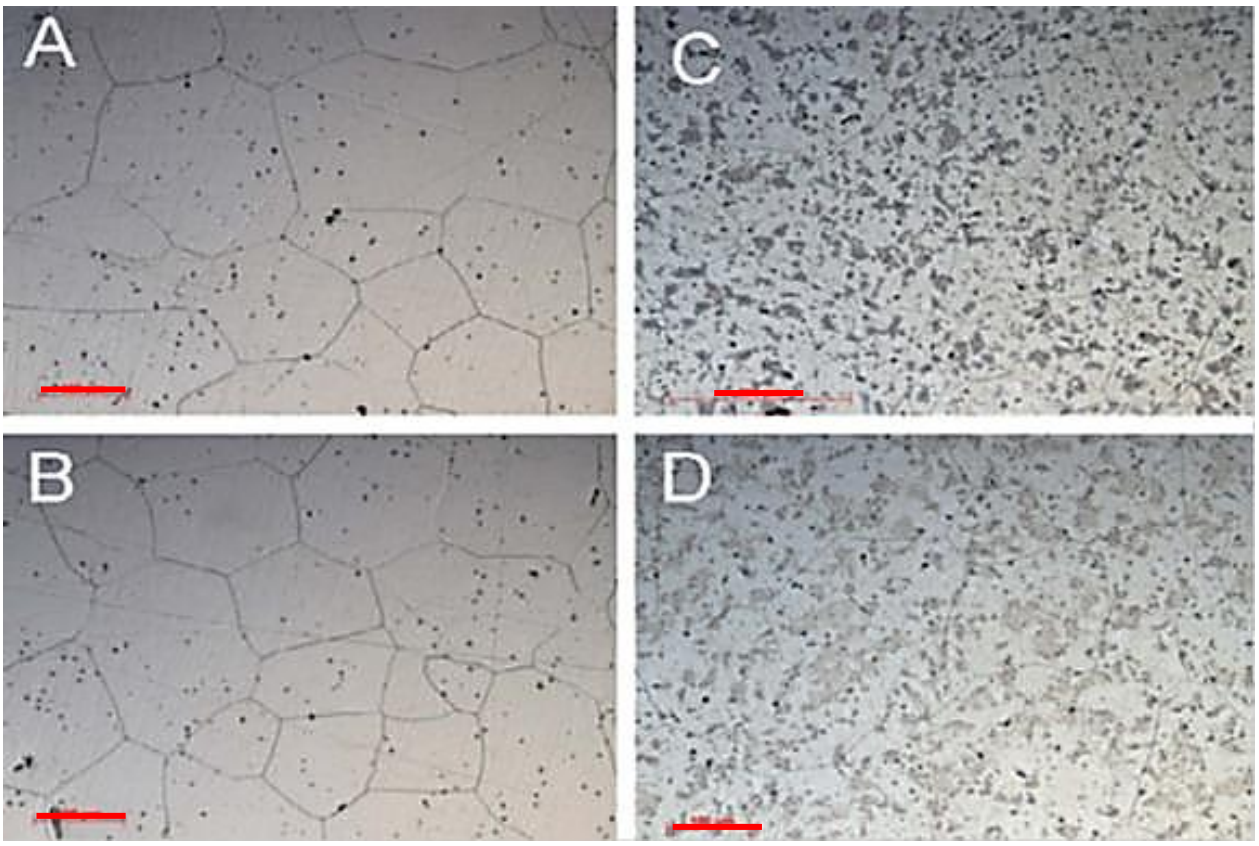

Figure 2.9. Optical micrographs of Fe-29Cr-2Ni-4Mo super-ferritic stainless steel alloys showing the influence of ruthenium on the microstructure: (A and B) 0.05% Ru and (C and D) 0.2%Ru [2008Olu]. Micron markers represent 100µm.

Figure 2.10 [2008Olu] shows the influence of temperature on the polarization behaviour of an Fe-29Cr-2Ni-4Mo super-ferritic stainless steel containing 0.2% Ru. As temperature increased, the corrosion current densities and corrosion rates increased. There was a major effect of temperature on the critical current density and active-passive transition, especially in

hydrochloric acid (Figure 2.11 [2008Olu]). The polarization curves in Figures 2.10 and 2.11 showed that an increasing temperature caused an increase in critical current density, which was more pronounced in hydrochloric acid solution. The active-passive transition widened as the temperature increased. Increased ruthenium contents were observed to be a major factor in improving the corrosion resistance of the alloys, due to the cathodic modification effects. Olubambi *et al.* [2008Olu] stated that ruthenium additions were more effective in sulphuric acid than in hydrochloric acid.

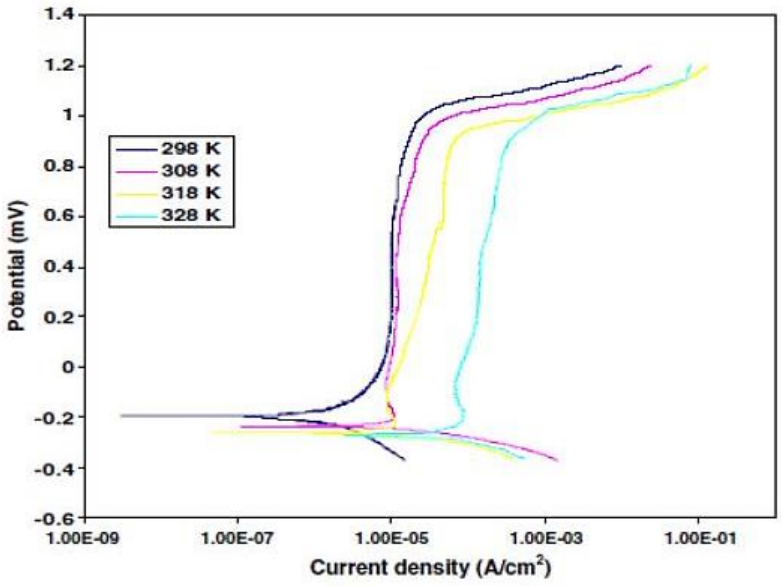

Figure 2.10. Influence of temperature on the corrosion behaviour of Fe-29Cr-2Ni-4Mo alloyed with 0.2% Ru in 1M sulphuric acid [2008Olu].

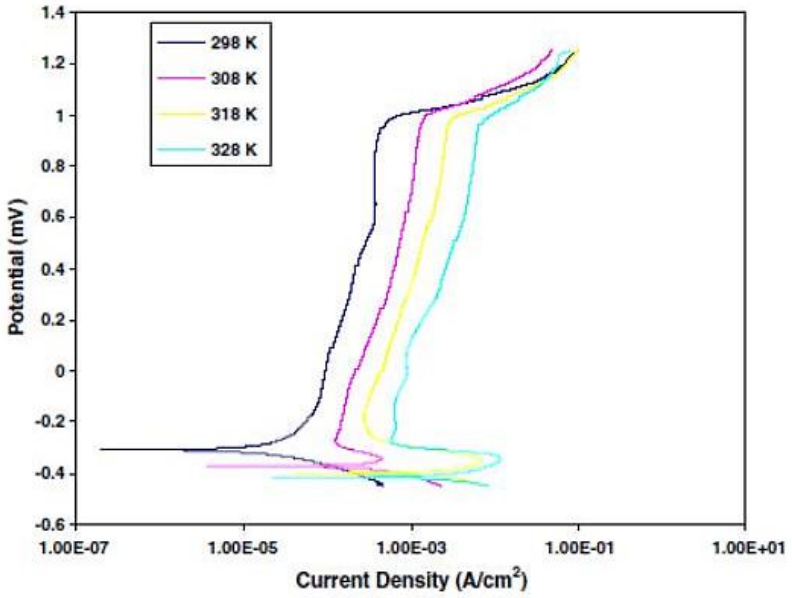

Figure 2.11. Influence of temperature on the corrosion behaviour of Fe-29Cr-2Ni-4Mo alloyed with 0.2% Ru in 1M hydrochloric acid [2008Olu].

2.2.2 Cathodic modification of duplex stainless steel

Investigations have been carried out on the cathodic modification of duplex stainless steel. Tomashov *et al.* [1977Tom] produced some duplex stainless steels that consisted of 18-25 wt% Cr, 7-l1 wt% Mn, 0 wt% Ni, ~2 wt% Mo, and nearly 1 wt% N, with varying ferrite proportions of 36 to 50%. These steels were additionally alloyed with 0.1-0.5 wt% Pd. Corrosion tests were conducted in solutions of 20-50% sulphuric acid at temperatures between 20°C and 100°C. It was reported that all the duplex alloys containing palladium initially corroded intensively after immersion and activation, before they became self-passivated. The time required for self-passivation decreased with an increase in both the palladium content of the steel and an increase in temperature, but increased with an increase in the concentration of acid (20 - 40% sulphuric acid). However, in a solution of 20% sulphuric acid at 100°C, only the steels containing 0.4 and 0.5 wt% palladium self-passivated. This investigation also showed that duplex stainless steels containing palladium had a greater corrosion resistance in 2 to 3% hydrochloric acid at 20°C to 50°C than did similar cathodically modified austenitic stainless steels with palladium.

Potgieter and Brookes [1995Pot] studied the effect of minor additions of Ru on the passivation of duplex stainless-steels in 40% H_2SO_4 and discovered that the presence of Ru inhibited the anodic dissolution behaviour when active corrosion took place. Significant improvements were achieved in the corrosion resistance of the alloys in H_2SO_4 solutions with ruthenium additions of up to 0.3 wt%. It was observed that the addition of ruthenium not only increased the efficiency of hydrogen evolution, and thereby changed the cathodic reaction kinetics, but it also inhibited anodic dissolution of the alloys by decreasing the critical and passive current densities. All three duplex alloys in the study: 29%Cr-14%Ni-3%Mo-0%Ru, 29%Cr-14%Ni-3%Mo-0.06%Ru and 29%Cr-14%Ni exhibited non-Tafel behaviour under severe conditions of active dissolution. Tafel type behaviour is a linear relationship of current and voltage under activation cotrol. Increasing ruthenium content always moved E_{corr} toward more noble values, regardless of whether spontaneous passivation or active dissolution occurred. The slight lowering of the hydrogen overpotential in the spontaneous passive state indicated an increased efficiency of hydrogen evolution, and a consequent shift in E_{corr} toward more noble values. Therefore, the cathodic modification effect contributed to the increased corrosion resistance of the alloys containing ruthenium [1995Pot]. In the case of the 29%-Cr duplex alloy series, lowering of the hydrogen overpotential and the cathodic modification phenomenon seemed much more marked and effective than in the case of the 22%-Cr duplex alloy series.

Myburg *et al.* [1998Myb] studied the surface composition of Ru-containing duplex stainless steel (DSS) after passivation in non-oxidizing media. From Auger electron spectroscopy (AES), chromium concentrations were slightly higher (about 3 wt% Cr) in the passive layers of both materials, compared to their bulk concentrations. Conversely, the Ni concentrations were reduced to less than half their bulk concentrations at the outer surfaces of the passive layers, with an increasing concentration gradient towards the bulk of the material. Enrichment of Mo at the outer surface of the passive layer was only observed in the case of the DSS-Ru samples which were passivated in HCl. The X-ray photoelectron spectroscopy (XPS) results indicated that the passive layer on the DSS-Ru samples contained more Cr_2O_3 and Fe^{2+} than $Cr(OH)_3$ and Fe^{3+}, compared to the DSS samples without Ru. These observations correlate the fact that Ru and Ni acted as blocking agents, which decreased the dissolution rates of Cr and Fe, and therefore increased the probability to form a stable passive layer.

Sherif *et al.* [2009She1] investigated the effects of minor additions of ruthenium (0.14%, 0.22%, and 0.28 wt%) on the passivation of duplex stainless-steel (Fe–22%Cr–9%Ni–3%Mo). The corrosion media was 2M HCl. Open-circuit potential (OCP) measurements showed an increased shift in the corrosion potential to more positive values with increasing Ru content. There was an agreement between the electron impedance spectroscopy (EIS) and polarization data. The increased addition of Ru is a powerful driving force to decrease the pitting and anodic dissolutions of DSS through increasing surface and polarization resistances, interface impedance, and maximum phase angle, which is the maximum angle between the vector and the x-axis. Weight-loss data confirmed that the presence of Ru greatly reduced the weight-loss and corrosion rate, while increasing the passivation efficiency of the alloy. This effect increased with increasing Ru contents and with decreased immersion times. The results from the combined measurements agreed well with one another and proved that the presence of Ru greatly enhanced the corrosion resistance of the DSS alloys against both general and pitting corrosion in the 2 M HCl solution.

Sherif *et al.* [2009She2] also investigated the effect of ruthenium additions on 2205 duplex stainless steel in 3.5% NaCl. Figure 2.12 [2009She2] shows that for curve 1, the chloride solution increased the potential to more negative values in the first few minutes, which may be due to the dissolution of the oxide films formed on the DSS alloy in air. Addition of 0.14 wt% Ru increased the potential to a positive direction; this effect decreased with increasing time with small fluctuations appearing on the curve, showing that 0.14 additions increased the general and pitting corrosion resistance of 2205. The presence of 0.22 and 0.28 wt% Ru shifted the OCP to more positive values, as shown in curves 3 and 4 with continued positive shifts with increasing time to be ≥400 and 500 mV more positive than the OCP obtained for the alloy in absence of ruthenium.

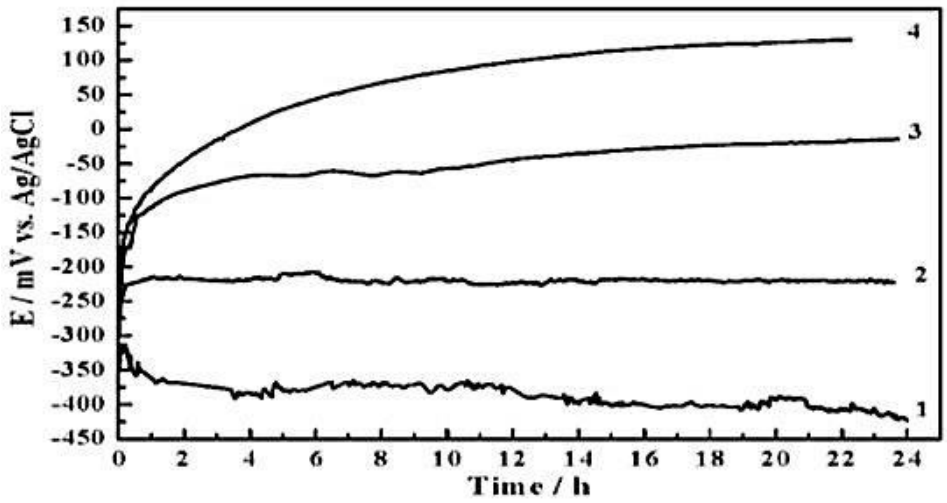

Figure 2.12. Variations of the open-circuit potential with time for the 2205 duplex stainless steel containing: (1) 0, (2) 0.14, (3) 0.22, and (4) 0.28wt% Ru in 3.5% NaCl solution [2009She2].

Increased ruthenium content showed a significant decrease in the cathodic, corrosion (i_{corr}), anodic and passivation currents (i_{pass}), as well as shifting both the corrosion and pitting potentials to more positive values [2009She2]. The area of the hysteresis loop of the polarisation decreased with increased ruthenium contents. This caused increased surface resistance to general and pitting corrosion (Figure 2.13 [2009She2]).

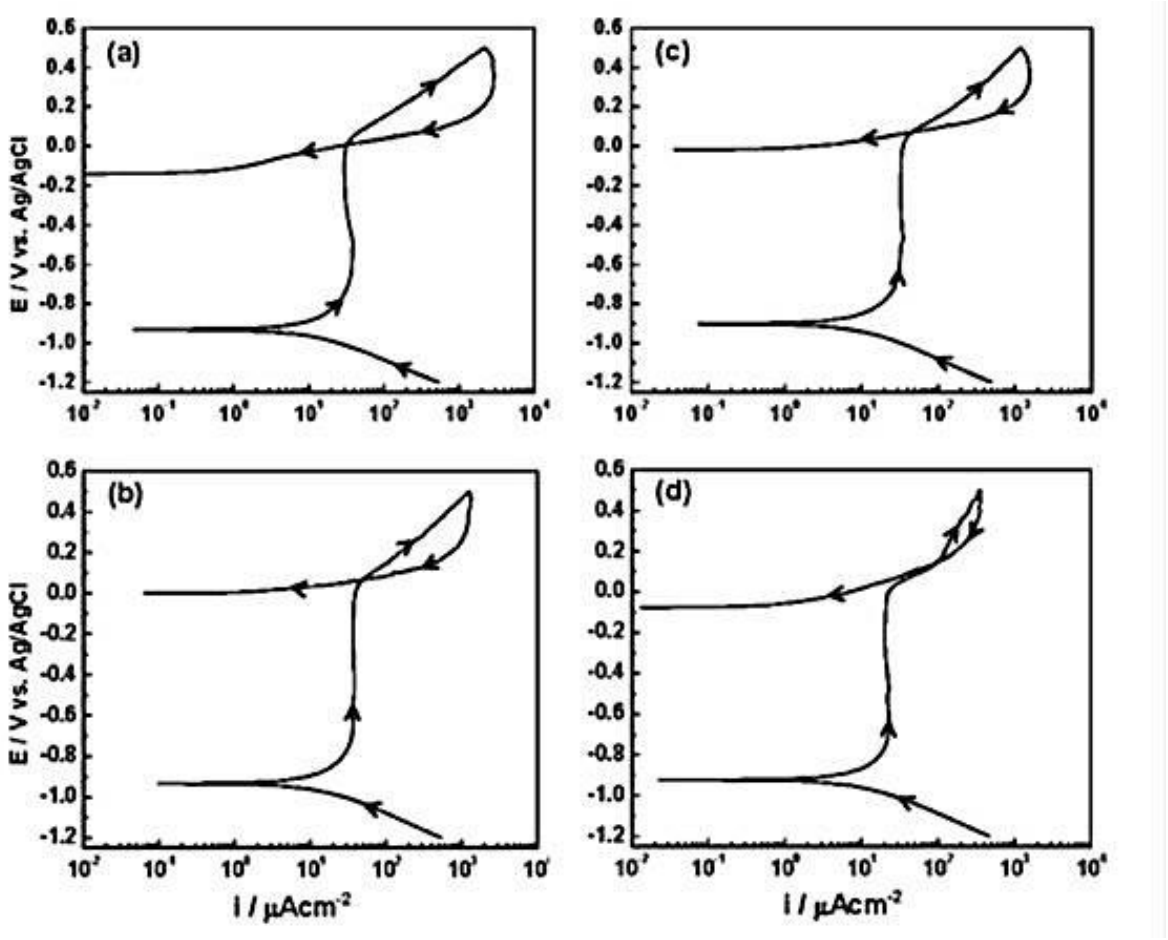

Figure 2.13. Potentiodynamic cyclic polarization curves for 2205 duplex stainless steel containing: (a) 0 wt% Ru, (b) 0.14 wt% Ru, (c) 0.22 wt% Ru, and (d) 0.28 wt% Ru in 3.5% NaCl solution; the measurements were recorded from the first moment of immersion [2009She2].

The influence of ruthenium additions after a long-term immersion period of 24 hours is shown in Figure 2.14 [2009She2]. Increasing the immersion time of DSS alloy without Ru in 3.5% NaCl solutions decreased the cathodic, i_{corr}, anodic and i_{pass} currents and also shifted i_{corr} and E_{pit} to more positive values. The decrease in the cathodic, i_{corr}, anodic and i_{pass} currents with increasing Ru content and further with immersion time are mainly due to the passivation of the DSS by Ru. The positive shift in the E_{corr} is apparently due to increasing the effectiveness of cathodic processes, which in turn decreases the rate of anodic reactions [1990Pot, 1995Bar].

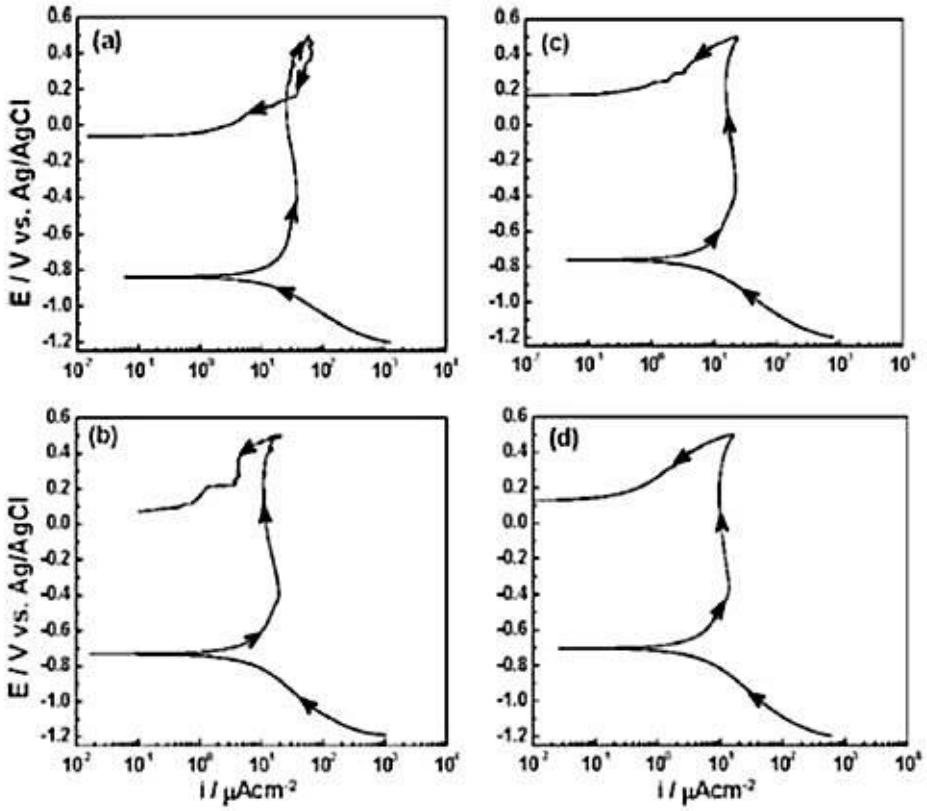

Figure 2.14. Potentiodynamic cyclic polarization curves for the 2205 duplex stainless steel containing: (a) 0 wt% Ru, (b) 0.14 wt% Ru, (c) 0.22 wt% Ru, and (d) 0.28 wt% Ru in 3.5% NaCl solution; the measurements were recorded after 24 h of immersion of the alloys in test solution [2009She2].

The potentiostatic current time measurements are shown in Figure 2.15 [2009She2]. In Figure 2.15a, curve 1 shows some current fluctuations with increasing time. The presence of 0.14 wt% Ru lowered the absolute current, but did not completely prevent the pitting attack. For alloys containing 0.22 and 0.28 wt% Ru, the current recorded was very low for both at first immersion and after 24 hours. This indicated the passivity of those two alloys against pitting corrosion.

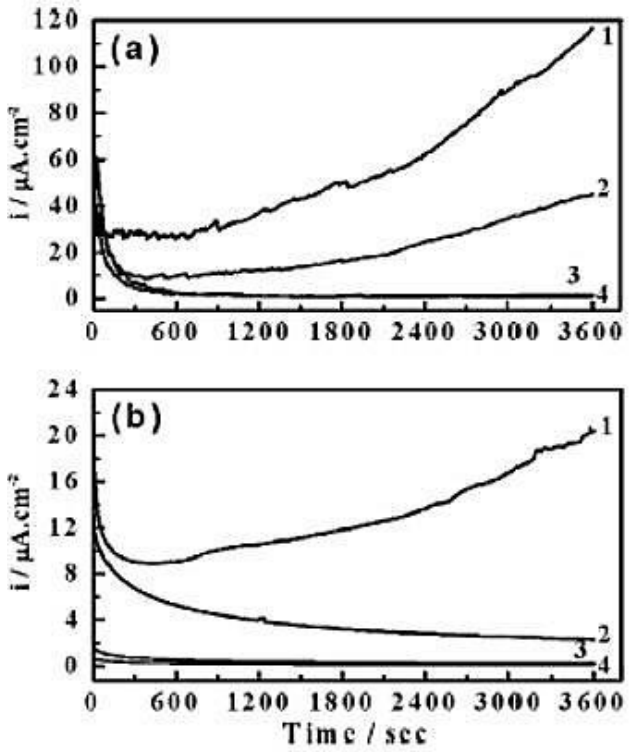

Figure 2.15. Potentiostatic current time measurements for 2205 duplex stainless steel in 3.5% NaCl solution at 100 mV after different immersion times: (a) 0 h, and (b) 24 h, containing: (1) 0 wt% Ru, (2) 0.14 wt% Ru, (3) 0.22 wt% Ru, and (4) 0.28 wt% Ru [2009She2].

The influence of 1 wt% palladium and ruthenium additions on intergranular stress corrosion craking (IGSCC) of 304 stainless steel were studied in simulated pressurised water reactor environments by Govender *et al.* [2012Gov]. The optical micrographs of 304, 304-Ru and 304-Pd after exposure to tetrathionate and stress corrosion cracking are shown in Figure 2.16 [2012Gov]. Figure 2.15a shows a smooth tensile specimen subjected to constant load testing in O_2 water (25°C, 2ppm O_2 and 244 MPa) with no IGSCC. Figure 2.16b shows 304 SS immersed in 0.1M $K_2S_4O_6$ for 2h with about 15–30 mm intergranular corrosion on surface of gauge length. Figure 2.16c shows 304 SS precracked in 0.1M $K_2S_4O_6$ for 2 h and subjected constant load testing in O_2 water (25°C, 2 ppm O_2, 168 h and 244 MPa) exhibiting IGSCC to depths of ~120 mm. Lastly, Figure 2.16d–f 304 SS, Pd-304 and Ru-304 respectively 'precracked' in 0.1M $K_2S_4O_6$ for 2h and subjected constant load testing in H_2 water (360°C, 30 $cc.kg^{-1}$ H_2, 500 h) with depth of ~100 μm, 300 μm and no IGSCC respectively [2012Gov]. The 304 stainless steel and palladium modified stainless steel showed secondary intergranular corrosion cracking (Figure

2.16c-e). There was no intergranular cracking observed in 304-Ru (Figure 2.16f). TEM analysis revealed enrichment of ruthenium and molybdenum within the oxide of the surface layers. Energy fitered TEM showed that cracks in hydrogenated water displayed dual layer oxides of chromium-rich oxide and an outer iron-rich oxide.

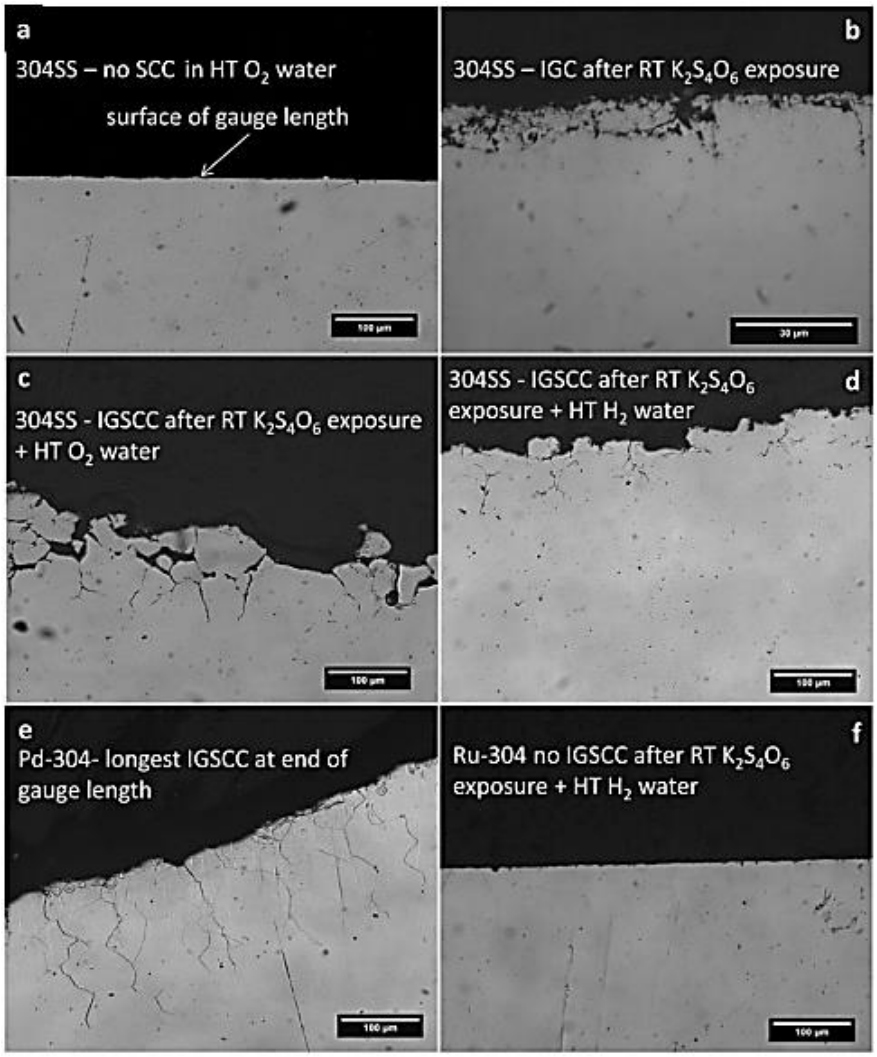

Figure 2.16. Optical micrographs of: (a) 304 SS (smooth tensile specimen), (b) 304 SS immersed in 0.1M $K_2S_4O_6$ for 2 h, (c) 304 SS precracked in 0.1M $K_2S_4O_6$ for 2 h and subjected constant load testing in O_2 water, (d) 304 SS, (e) Pd-304, and (f) Ru-304 'precracked' in 0.1M $K_2S_4O_6$ for 2 h, and subjected constant load testing in H_2 water [2012Gov].

2.3 Heat treatment of duplex stainless steels

Heat treatment is a solid state process consisting of heating materials to a specific predetermined temperature and holding them at the temperature for a set time, before finally cooling from this temperature. Heat treatments can also be complex, with different stages and temperatures. Heat treatment of steel is undertaken to give improvements in mechanical properties such as ductility, relieve internal stresses, refine grain size, and increase hardness or tensile strength, allowing changes in chemical composition of metal surfaces and in the bulk (if sufficient time is allowed). Properties such as hardness, strength, ductility, and toughness are dependent on the microstructure present in steel [1978Pic, 1984 Boy, 2008Can].

The size and distribution of the ferrite and austenite phases is dependent on both the thermo-mechanical cycles and heat treatment. This is important in developing the mechanical and physical properties of duplex stainless steels, specifically the higher tensile and yield strength when compared to austenitic or ferritic stainless steel [1978Sol, 1979Suu, 2009Row]. Thermo-mechanical treatment is where plastic deformation results in the production of crystal defects. This affects the phase transformation in metals and alloys by providing nucleation sites and aiding the diffusion process [1978Pic, 1988Raj].

Tavares *et al.* [2000Tav] observed that in the solution treated condition, the UNS S31803 (2205) duplex stainless steel had excellent corrosion resistance and mechanical properties. Intermetallic phases can form in duplex stainless steel during exposure in the temperature range of approximately 320°C to 955°C. The presence of these intermetallic phases is detrimental to toughness and corrosion resistance. The correct heat treatment and rapid cooling can eliminate these phases [1982Her, 1988Raj, 2006AST].

Fargas *et al.* [2009Far] studied the effect of annealing temperature on the mechanical properties, formability and corrosion resistance of hot rolled duplex stainless steel (2205). They evaluated the consequences of changing the annealing temperature from 1050°C, which is the industrial production of rolled duplex stainless steel (2205, EN 14462), to lower values in the range 975-850°C. They observed that annealing at around 875°C promoted the formation of the sigma phase. At annealing temperatures of 925°C and 975°C, the amount of sigma phase precipitated

was low, and in the form of isolated particles. Therefore, tensile properties and corrosion resistance were only slightly affected.

Lai *et al.* [1995Lai] studied the effect of solution treatment on ferrite morphology and subsequent ageing behaviour of 24.8 wt% Cr and 8 wt% Ni duplex stainless steel. They concluded that within the solution treatment range of 1050-1250°C, the austenite to ferrite ($\gamma \rightarrow \alpha$) transformation occurred and the solution treatment temperature affected the amount and morphology of the ferrite phase within the austenite matrix. When the temperature of the solution treatment increased, there were larger ferrite grains, which tended to be equiaxed. Within the ferrite, the chromium content decreased and the nickel content increased with increasing solution treatment time.

Jackson [1997Jac] investigated the kinetics of sigma formation and dissolution in duplex stainless steel. She showed that solution annealing had a retardation effect on the kinetics of intermetallic precipitation and revealed that detrimental intermetallic phase precipitation during cooling from annealing at 1050°C could be avoided by using cooling rates above 7°C/min. There was a fine dispersion of precipitates for ageing temperatures between 700°C and 800°C in the ferrite, and the precipitates along ferrite-austenite interfaces were suspected to be carbides. The amount of ferrite decreased with increasing intermetallic phases, due to the ferrite transforming into secondary austenite which is formed inadvertently at low temperature after the duplex structure has been established.

Duplex stainless steels cannot be hardened by heat treatment. The higher the annealing temperatures, the higher the ferrite content [1994Fro, 2009Zha1]. Formation of intermetallic phases, such as sigma, can occur in the temperature range 593-954°C. There is reformation of ferrite at 343-524°C (also responsible for 474°C embrittlement). The 2101 duplex stainless steel is solution annealed at 1020-1080°C, and rapid cooling is recommended after annealing [URLOut]. Figure 2.17(a) shows the schematic phase transformation diagram of the duplex stainless steel. The steel is melted to above 1400°C (I), and later cooled to 1080°C (II), the phases present were austenite and ferrite (γ and α). At 1080°C, it was held for about 120 minutes (III), before rapid cooling by water quenching (IV). Austenite and ferrite phases were present. The TTT (Time Temperature Transition) curves showing the narrow

temperature range at which stress relieving can be performed for some duplex stainless steel grades are shown in Figure 2.17(b)

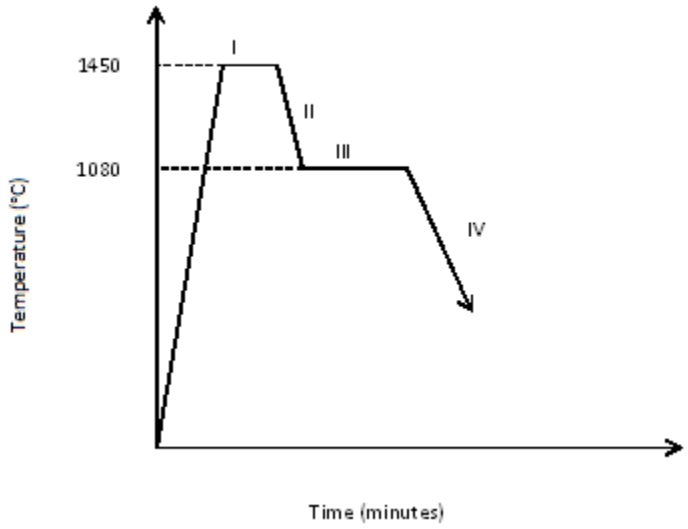

Figure 2.17 (a). Schematic phase transformation diagram of duplex stainless steel.

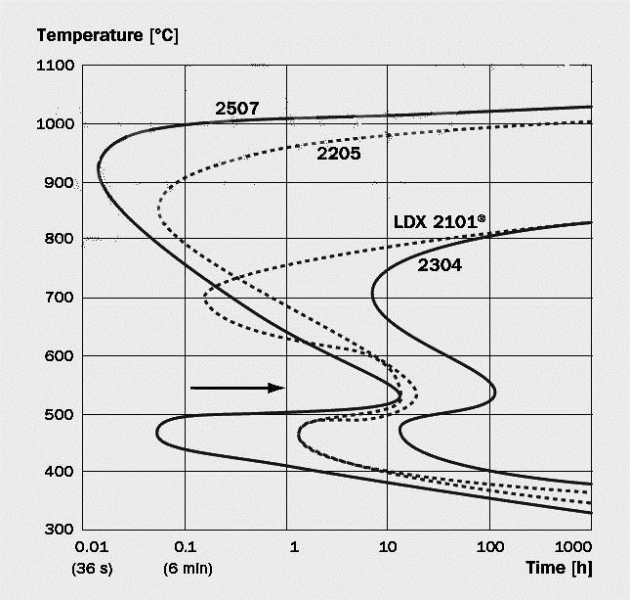

Figure 2.17 (b). TTT (Time Temperature Transition) curves showing the narrow temperature range in which it is possible to carry out stress relieving of duplex stainless steel grades [URLOut2].

2.4 Thermo–Calc

Thermo-Calc is a flexible software package developed in 1981, based on the Gibbs energy, for performing various kinds of thermodynamic and phase diagram calculations [1985Sun, 1986Sun]. It has been specifically developed for fields such as metallurgy, material science, alloy development, chemistry, geochemistry, semiconductors, energy conversation and power production. It also aids understanding of the factors that affect material behaviour and it helps in reducing costs by quickly identifying control parameters or alloy compositions. This software can calculate phase diagram sections and phase proportion diagrams with up to five independent variables in complex multicomponent and heterogeneous systems. It handles difficult problems involving the relations of many elements and phases and is particularly intended for systems and phases that show highly non-ideal behaviour.

TCFE3 is a recently-developed database for Thermo-Calc which includes sigma phase parameters. Thermo-Calc software with TCFE3 was used by Tavares *et al.* [2009Tav] in studying the microstructure changes and corrosion resistance of AISI 310S exposed to 600-800ºC. It was used for estimating the amount of sigma phase and $Cr_{23}C_6$ in equilibrium in a wide range of temperatures. Figure 2.18 [2009Tav] shows the weight fractions of austenite (γ), sigma (σ), liquid (L) and chromium carbide ($Cr_{23}C_6$) phases as function of temperature calculated by Thermo–Calc. This was then compared to experimental data. In equilibrium conditions, the amount of sigma phase decreased from 600°C to 800°C. However, as the $\gamma \rightarrow \sigma$ reaction is diffusion controlled, the experimental observations show the inverse trend, the increase in temperature enhanced the σ precipitation for ageing times up to 210 h.

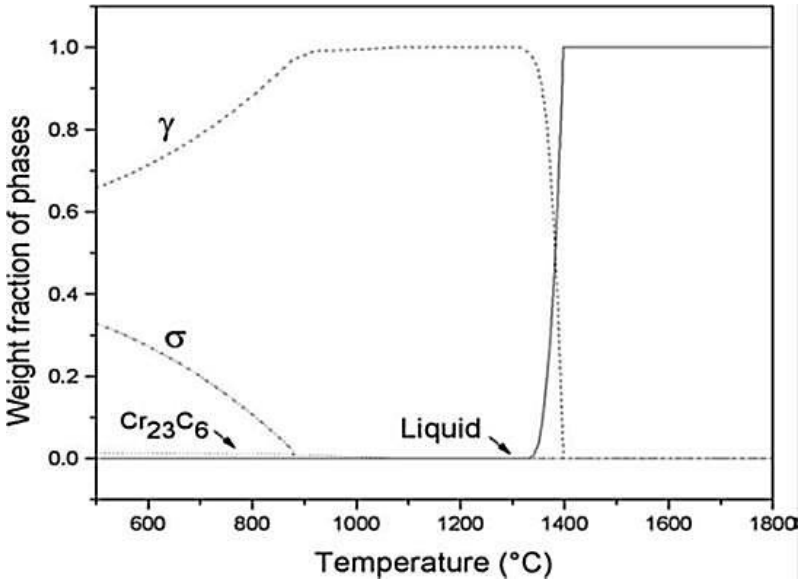

Figure 2.18. Phase proportion diagram showing equilibrium values of γ, σ and M23C6, for AISI 310S obtained with Thermo-Calc [2009Tav].

2.5 Corrosion of duplex stainless steels

The corrosion performance of stainless steel is affected by its design, fabrication, surface conditioning and maintenance. The corrosion resistance of stainless steel is always considered before selecting it for any application in a given environment. Corrosion failures in stainless steel can often be prevented by suitable changes in design or process parameters, and by the use of proper techniques or treatment. Inappropriate heat treatments can produce deleterious changes in the microstructure of stainless steels, thus reducing the corrosion resistance [1965Bak]. Precipitation of various intermetallic phases including carbides is deleterious to corrosion resistance, often as a result of chromium depletion along the grain boundaries [2005Gru].

Knowledge of the individual phases of duplex stainless steel is useful in understanding and assessing the corrosion mechanisms, mechanical properties and electrochemical behaviour [2006Vig]. For example, the pitting corrosion resistance of duplex stainless steel depends on the phases and microstructure, such as the ferrite-austenite proportion. Ferrite is the less pitting resistant phase of the duplex stainless steels [2008Zha]. The pitting corrosion resistance of super-duplex stainless is influenced by the annealing temperature [1982Her, 1996Gar]. The sigma phase may be harmful to the corrosion performance, by removing chromium and molybdenum

from the austenitic matrix. The modification of microstructures and phases within duplex stainless steels will therefore be an effective approach in improving their overall corrosion resistance and mechanical properties that are required in service. These modifications can be enhanced by the addition of suitable alloying elements.

Chloride solutions are the most widespread environments responsible for localized corrosion of duplex stainless steels. The aggressiveness of the environment increases with chloride content, redox potential, activity and temperature. Duplex stainless steel has good high temperature oxidation resistance, although it suffers from embrittlement if held for even short times at temperatures above 300ºC [1981Ber]. Thus, they are also limited for low temperature use because of ductile – brittle transformation.

Predictions on the corrosion behaviour of stainless steel can be made from anodic polarization curves [1991Fou]. The appearance of two active peaks in the polarisation diagrams has been used as an indication that selective attack will occur in duplex stainless steel [1987Sym, 1991Fou]. There are three patterns that could be observed in the corrosion patterns of duplex stainless steel according to Fourier [1991Fou]. The first pattern (A) shows that there is dissolution of both austenite and ferrite, and this yields a single active peak. The second pattern (B) shows that by increasing temperature, the cathodic current density becomes so high that at more active potentials the anodic current due to ferrite dissolution is masked and appears only as an anomaly in the cathodic branch of the curve. The third pattern (C) shows that higher corrosivity increases the critical anodic current density for ferrite dissolution to such an extent that a net anodic current is measured at these active potentials; this gives rise to two active peaks.

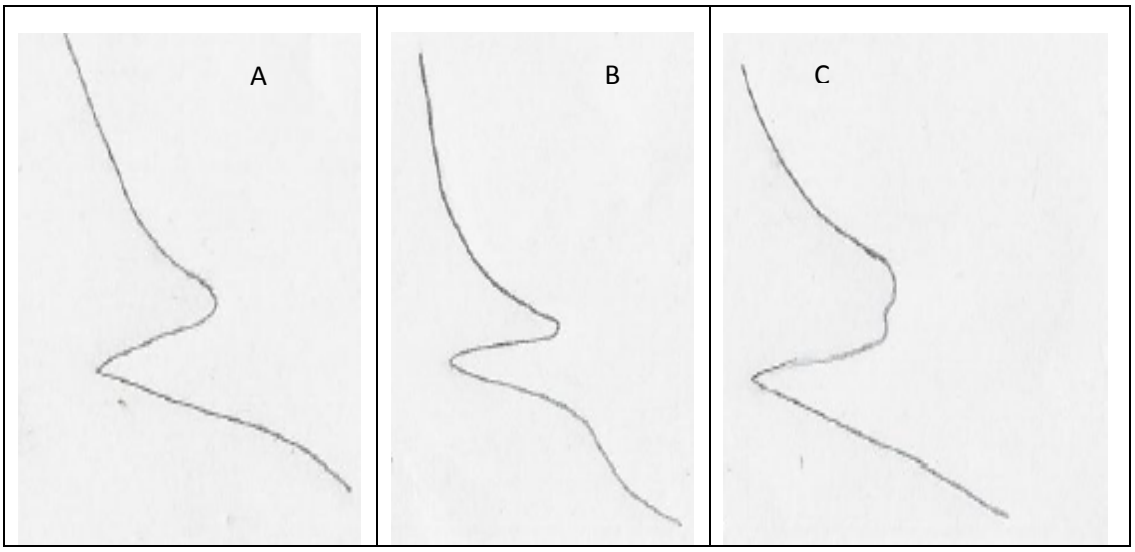

Figure 2.19. Schematic representation for duplex stainless steels of the three characteristic polarization plots obtained in H_2SO_4/NaCl mixtures [1991Fou].

2.5.1 Electrochemical methods

Mixed potential theory is the basis for electrochemical corrosion processes. It separates the oxidation and reduction reactions of corrosion and postulates that the total rates of all the oxidation reactions equals the total rates of all the reduction reactions on a corroding surface. Mixed potential theory proposes that all the electrons generated by the anodic reactions are consumed by corresponding reduction reactions.

When a metal is immersed in an acidic solution at equilibrium [1979Sed, 2009Mil], the rate of metal dissolution is equal to the rate of the cathodic reaction and the potential associated with the equilibrium condition is called the corrosion potential, E_{corr}.

Corrosion rates are determined by applying a current to produce a polarization curve. The variation of potential as a function of current enables the study of the effect of concentration and activation processes. Polarisation measurements can be used to determine the rate of the reactions involved in the corrosion process, which is the corrosion rate. The corrosion rate can be measured by extrapolation and linear polarisation. The corrosion current density (i_{corr}) cannot be measured directly, and is obtained by extrapolating the linear portion of measured potential-

current density curves. The more negative the standard electrode potential, the greater the tendency to form metal ions and hence to corrode.

Linear polarisation is based on the theoretical and practical demonstration that at potentials very close to E_{corr} ±10mV, the slope of the potential /applied current curve is approximately linear.

I_{corr} is related to the inverse of the slope $\frac{dE}{dl}$ by the equation derived by Stern and Geary [1957Ste]:

$$I_{corr} = \frac{I_{appi}}{2.3dE} \cdot \frac{\beta_c \beta_a}{\beta_c + \beta_a}$$

or

$$I_{corr} = \frac{1}{2.3R} \cdot \frac{\beta_c \beta_a}{\beta_c + \beta_a}$$

where β_c = Tafel constant for cathodic region

β_a =Tafel constant for anodic region

R = Polarisation resistance.

The linear polarisation method has many advantages in calculating instantaneous corrosion rates for many metals in various conditions. It can also be used to calculate inhibitors, protective coatings and change of corrosion rates with time [2008Rev]. An application of the linear polarisation technique is a non-destructive method of measuring the corrosion rates. The main advantage of the technique over periodic weight loss measurements is the possibility of continuously monitoring instantaneous corrosion rates of metal exposed to corrosive environments.

2.5.2 Corrosion as an electrochemical process

Corrosion can be defined as the deterioration of metals or materials by chemical or electrochemical methods [1945Eva]. The corrosion processes are most often electrochemical processes [1971Uhl]. A typical corrosion cell requires four elements: an anode, a cathode, an electrolyte and an electrical connection between the anode and cathode, which both have their own reactions.

The electrode at which chemical reductions occurs is called the cathode. Reduction involves a gain in electrons.

$2H^+ + 2e^- \longrightarrow H_2$ (acidic environments)

$O_2 + 4H^+ + 4e^- \longrightarrow 2H_2O$ (acidic environments)

$O_2 + 2H_2O + 4e^- \longrightarrow 4OH$ (neutral or alkaline environments)

and the area of corroding metal where there is reduction of hydrogen ions and oxygen is a cathode.

Examples of cathodic reactions include:

$M^{3+} + e^- \longrightarrow M^{2+}$

$M^{2+} + e^- \longrightarrow M^+$

$M^+ + e^- \longrightarrow M$

where M is metal.

The electrode in which chemical oxidation occurs is called the anode, and examples include:

$Zn \longrightarrow Zn^{2+} + 2e^-$

$Fe^{2+} \longrightarrow Fe^{3+} + e^-$.

The process of oxidation involves a loss of electrons by the reacting species, and the area of corroding metal where metal dissolution occurs is an anode.

The four main types of cells that take part in corrosion reactions are: dissimilar electrodes, concentration cells, differential temperature cells and differential aeration cells.

2.5.3 Electrochemical mechanism of corrosion

Corrosion occurs in a given environment because of the thermodynamic instability of a metal with respect to the oxidized form of the metal. There is an electron transfer between the metal and an electron acceptor in the solution because the reaction occurs at a metal/solution interface.

Anodic and cathodic areas are initiated [1963Shr]. In electrochemical mechanisms, the rate of a corrosion reaction can be interpreted in terms of transport of electrons from the corroding metals and molecules, and ions through the solutions and the electrode kinetics of the half reactions occurring [1963Shr]. Electrode kinetics is the study of the rates of the two half reactions at the interface between an electrode and a liquid.

The rate determining factors are [1963Shr]:

1. *Transportation* – transport of electrons to the cathode and of oxidised form of the metal away from the anode by diffusion, migration, convection and agitation.

2. *Activation energy* – if the activation energy or anodic process controls the rate, the process is said to be under activation control (Tafel parameters).

3. *Resistance overpotential* – if the resistance to passage of charge in the bulk solution or at the metal/solution interface is rate determining, the process is said to be resistance controlled.

2.5.4 Polarization diagram of corroding metal

Polarisation diagrams are graphs of potential with the log of current or log current density. In setting up an experiment to obtain polarisation diagrams, the working electrode, the reference electrode, and the inert counter electrode are required. Polarisation may be carried out either in potential steps which is potentiostatically, or continuously which is potentiodymically.

Figure 2.20 shows a hypothetical polarization diagram for a passivable system with active, passive and transpassive regions [1979Sed]. The corrosion parameters, corrosion potential (E_{corr}), critical current density (i_{crit}), passive current density (i_{pp}) are shown.

Oxidation of metal is the dissolution of metal: $M \rightarrow M^{2+} + 2e^-$

Reduction reactions are of the type: $R^{n+} + ne^- \rightarrow R$

In an aerated neutral or basic aqueous solution, the reduction reaction could be:

$O_2 + 2H_20 + 4e^- \rightarrow 4OH^-$,

whereas in a de-aerated acidic solution, the reduction reaction could be:

$2H^+ + 2e^- \rightarrow H_2$.

The chemical equivalents of a metal going into solution at the anodic sites are equal to the chemical equivalents of reduction products produced at cathodic sites.

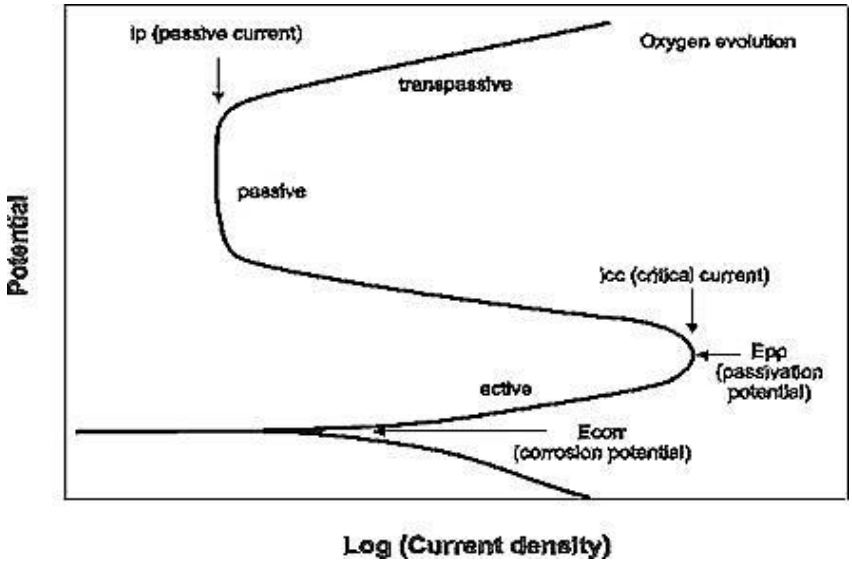

Figure 2.20. Hypothetical polarization diagram for a passivable system with active, passive and transpassive regions [1979Sed].

A metal is said to be passive if it substantially resists corrosion in a given environment resulting from marked anodic polarization. It could also be said to be passive if it substantially resists corrosion in a given environment, despite a marked thermodynamic tendency to react [1971Uhl]. Metals such as chromium are naturally passive when exposed to the atmosphere, and the passive property of chromium is conferred on stainless steel. Stainless steels exhibit very low corrosion rates when conditions are favourable for maintaining passivity [1975Eva]. When passivity is destroyed under conditions that do not permit the restoration of the protective oxide layer, the corrosion is more like a carbon or low alloy steel [1945Eva]. The presence of oxygen is vital to the corrosion resistance of a stainless steel to retain the oxide layer. The corrosion resistance is at the maximum when the steel is exposed and the surface is maintained free of deposits by a flowing bulk environment [1971Uhl].

Corrosion behaviour of duplex stainless steels in organic acid aqueous solutions was reported to be strongly dependent on the acid content and nature, temperature and contaminant type [2008Inv]. In aqueous solutions of acetic acid, 2205 and 2507 duplex stainless steels did not undergo corrosion in a wide range of acid concentrations and temperatures [2008Inv]. In 40% formic acid, 2507 was not subject to severe corrosion. The presence of sulphuric acid or sulphites decreased the duplex stainless steels corrosion performance in aqueous solutions of acetic acids and formic acids. It was observed that water and oxygen helped to maintain the protective oxide layer on duplex stainless ateels. There was a pronounced preferential dissolution of the austenitic phase with increasing solution aggressiveness [2008lnv].

Alloying is used for improving corrosion resistance; the alloying element may reduce i_{crit} or i_{pas} (Figure 2.8). As the corrosion potential is made more positive in the active region than the open circuit potential, the current density for metal dissolution increases, until it reaches the primary passivation potential E_{pp} and critical current density i_{crit}, where the current density decreases to a lower level (Figure 2.4). The decrease in current density is due to formation of protective oxide layer [1967Tom, 1970Bie, 1975Eva].

Passivity is a state of the metal in which the rate of anodic dissolution or corrosion in a given environment is much less than the rate at a less noble potential, or at a lower driving force for the corrosion reaction [1965Wag, 1978Sat]. Passivity also results from a noble metal added in small amounts to an active metal or alloy, which decreases the anodic current density to the critical value for passivity.

Wolff *et al.* [1998Wol] showed that the addition of Ru to Fe-40Cr lowered the corrosion current density, and gave a slight lowering of the passive current density. Cathodic Tafel slopes were lowered by the Ru addition, which can be explained in terms of improved hydrogen-evolution efficiency which resulted in a decrease of the hydrogen overpotential.

Myburg *et al.* [1998Myb] worked on the surface composition of Ru-containing duplex stainless steel after passivation in non-oxidizing media. The compositions of the passive films formed on the duplex stainless steels which passivated spontaneously were studied by Auger electron spectroscopy (AES) and X-ray photoelectron spectroscopy (XPS) in 0.1M HCl and 1M H_2SO_4. They observed that chromium concentration in the passive layer of the duplex stainless steel with

Ru was slightly higher compared to the case of no Ru. The XPS studies showed that Cr_2O_3 and Fe_3O_4 were present in higher concentrations in the Ru containing samples than in the normal duplex stainless steel without Ru.

Zhang *et al.* [2008Zha] studied the mechanical corrosion properties of 2101 duplex stainless steel and 304 austenitic stainless steel. Themo-Calc was used to calculate the volume fraction of the duplex stainless steel. They discovered that the volume fraction of austenite was higher than that determined by quantitative metallography, implying the samples were not at equilibrium, the samples were annealed at 1020°C and 1080°C for 30 minutes and water quenched. They found that the duplex stainless steel had higher yield strength and better ductility than 304 austenitic stainless steel at room temperature. The pitting resisistance was better than 304 austenitic stainless steel. Zhang *et al.* [2009Zha2] stated increasing annealing temperatures shifted the corrosion potential and the pitting potential to more negative values thereby decreasing the pitting resistance.

2.5.5 Comparison of the effect of ruthenium to chromium and stainless steels

The effect of ruthenium additions to chromium and different stainless steels is shown in Table 2.4, where the corrosion current density and corrosion rates were the comparison parameters. The alloys compared are chromium, ferritic and duplex stainless steels, there were limited data for the corrosion rates or corrosion current densities of austenitic stainless steels.

The addition of 1wt% Ru to 304 stainless steels improved the stress corrosion cracking susceptibility in high temperature water-containing residual oxygen. The yield strength of 304-1wt% Ru was higher than 304 stainless steels [2012Gov].

The corrosion resistance of welds in type 304 stainless steels made with nickel-copper-ruthenium consumables was higher in consumables containing ruthenium [2010Lia]. The corrosion measurements of the weld surface showed that the corrosion potential shifted to more positive values where Ni-10Cu-1Ru and Ni-10Cu-0.5Ru consumables were used, than for Ni-10Cu.

The addition of ruthenium greatly increased corrosion resistance of high chromium duplex stainless steel [1995Pot], The higher content of chromium in the ferrite promotes the formation

of passive layer in the duplex stainless steel [1990Pot], and although Ni is also beneficial to corrosion resistance, it does not aid in formation of passive layer, depending on the corrosive medium. Addition of ruthenium to ferritic stainless steels is more beneficial than to duplex stainless steel because the i_{corr} of ferrite is more affected by the additions than austenite. The improved behaviour of 304 austenitic stainless steel by the additions of ruthenium was attributed to synergestic effect between Ru and Mo [2012Sce]. Addition of Ru shifted the corrosion potential to more noble values. Potgieter [1996Pot] showed that corrosion rates of the ferritic and duplex alloys were of the same order of magnitude, with the DSS being lower. He stated that addition of 0.3wt% Ru was more effective in corrosion resistance in 1M H_2SO_4.

Table 2.4. Comparison of the effect of ruthenium to chromium and stainless steels.

Metal or steel	Ru (wt%)	i_{corr} (A/cm^2)	Corrosion rate (mm/y)	Comment	Comparison	Reference
Chromium	0.5	-	2	Boiling 10% sulphuric acid	Corrosion rate increased with increased temperature	[1961Gre]
	0.5	-	11	Boiling 20% sulphuric acid		
	0.5	-	17	Boiling 30% sulphuric acid		
	0.5	-	83	Boiling 40% sulphuric acid		
	0.5	-	7100	Boiling 50% sulphuric acid		
Fe-40Cr	0.22	7.4E-8	-	10% H_2SO_4 Ruthenium addition improved corrosion resistance	Addition of ruthenium improved corrosion resistance	[1998Wol]
Fe-35Cr-5Al	0.19	4.0E-8	-			
Fe-40Cr	0	7.7E-3	-	10% H_2SO_4 Optimum value = 0.16 wt% Ru	Corrosion rate and corrosion current reduced with increased ruthenium contents	[1995Pot]
	0.06	4.7E-7	-			
	0.11	5.0E-7	-			
	0.16	6.5E-7	-			
	0.22	1.1E-6				

Table 2.4. Comparison of the effect of ruthenium to chromium and stainless steels (continued).

Metal or steel	Ru (wt%)	i_{corr} (A/cm^2)	Corrosion rate (mm/y)	Comment	Comparison	Reference
Fe-30Cr	0	1.5E-3	-	10% H_2SO_4		
	0.06	2.3E-7	-			
	0.11	4.1E-7	-			
	0.16	7.9E-7	-			
	0.22	1.0E-7	-			
Fe-28.5Cr-Mo	0.015	-	62200	Active state boiling 10% H_2SO_4	Corrosion rate and corrosion current reduced with increased ruthenium contents	[1977Str]
	0.017	-	-	Active state		
	0.02	-	60	Passive		
	0.20	-	9	Passive		
	0.30	-	2	Passive		
	0.5	-	3	Self-repassivating		
Fe-28Cr-4M0	0	-	1.325	10% H_2SO_4 at 103°C Corrosion reduced with increased ruthenium addition	Ruthenium addition improved the corrosion rate	[1995Pot]
	0.20	-	0.23			
	0.30	-	0.05			
Fe-28Cr-14Ni-3Mo	0	-	0	10% H_2SO_4 at 90°C Ni improved the corrosion resistance		
	0.17	-	0			
	0.28	-	0			
Fe-22Cr-9Ni	0	-	4.00E-06	10% sulphuric acid at 25°C 0.28 wt% Ru = optimum value		[1996Pot]
	0.14	-	4.00 E-06			
	0.22	-	5.20 E-06			
	0.28	-	0.00			

Table 2.4. Comparison of the effect of ruthenium to chromium and stainless steels (continued).

Metal or steel	Ru (wt%)	i_{corr} (A/cm^2)	Corrosion rate (mm/y)	Comment	Comparison	Reference
Fe-29Cr-2Ni-4Mo	0.2	2.2E-5	-	2M HCl Corrosion current was low	Ruthenium addition improved the corrosion rate	[2009Olu]
Fe-22Cr-9Ni	0	-	4.01	2M HCl Corrosion rates decreased with increased ruthenium contents	Ruthenium addition improved the corrosion rate	[2009She]
	0.14	-	1.49			
	0.22	-	0.73			
	0.28	-	0.50			
	0	-	0.66	2M HCl at 25°C		[2012She]
	0.3	1.2E-4	0.33			
Fe-22Cr-9Ni	0	-	1.70E-06	0.5M HCl at 25°C	Corrosion rate and corrosion current reduced with increased ruthenium contents	[1996Pot]
	0.14	-	1.70 E-06			
	0.22	-	0.00			
	0.28	-	0.00			
	0	-	5.60 E-06	1M H_2SO_4 at 55°C Corrosion almost non-existent at 0.28 wt%		[1996Pot]
	0.14	-	6.80 E-06			
	0.22	-	4.30 E-06			
	0.28	-	0.00 E-06			
	0	-	4.09E-05	2M H_2SO_4 at 55°C Optimum value = 0.28 wt% Ru		[1996Pot]
	0.14	-	1.44E-05			
	0.22	-	1.25E-05			
	0.28	-	0.00			
Fe-22Cr-9Ni-3Mo	0	25.8E-2	-	1M H_2SO_4 at 25°C Lowest corrosion rate was found at 0.28 wt%Ru		[1996Pot]
	0.14	2.9E-2	-			
	0.22	1.8E-2	-			
	0.28	0.7E-3	-			

Table 2.4. Comparison of the effect of ruthenium to chromium and stainless steels (continued).

Metal or steel	Ru (wt%)	i_{corr} (A/cm^2)	Corrosion rate (mm/y)	Comment	Comparison	Reference
Fe-22Cr-9Ni-3Mo	0	5.6E-6	0.056	3.5% NaCl Corrosion rate high, and decreased with increased ruthenium contents	Ruthenium addition improved the corrosion rate	[2009She2]
	0.14	4.9E-6	0.049			
	0.22	4.4E-6	0.044			
	0.28	3.5E-6	0.036			
Fe-29Cr-14Ni-3Mo DSS	0	0	-	10% H_2SO_4 acid at room temperature Corrosion was almost non-existent		[1995Pot]
	0.06	0	-			
	0.17	0	-			
	0.28	0	-			
Fe-Cr-Ni-Mo	0	-	0.010	1M H_2SO_4 at 25°C		[1996Pot]
	0.1	-	0.009			
	0.2	-	0.008			
	0.3	-	0.009			
	0	-	0.5	1M H_2SO_4 at 95°C Higher ruthenium concentration had best corrosion resistance		
	0.1	-	1.995			
	0.2	-	1.305			
	0.3	-	0.848			
Fe-22Cr-5Ni	0	-	0.004	1M H_2SO_4 at 25°C Optimum value = 0.3 wt% Ru	Corrosion rate and corrosion current reduced with increased ruthenium contents	
	0.1	-	0.004			
	0.2	-	0.005			
	0.3	-	0.000			
	0	-	3.155	1M H_2SO_4 at 95°C Optimum value = 0.3 wt% Ru		
	0.1	-	0.572			
	0.2	-	0.409			
	0.3	-	0.000			

Table 2.4. Comparison of the effect of ruthenium to chromium and stainless steels (continued).

Metal or steel	Ru (wt%)	i_{corr} (A/cm^2)	Corrosion rate (mm/y)	Comment	Comparison	Reference
Fe-24Cr	Ru-Ti	~10E-6	-	Ru-Ti and Ru implanted on the surface, i_{corr} reduced with ruthenium addition, improved corrosion rate	Ruthenium addition improved the corrosion rate	[1990Tjo]
	Ru	2.0E-6	-			
	0.4		3.12E-02			
	0.6		2.69E-02			
	0.8		2.19E-02			
	1.0		1.12E-02			

CHAPTER 3

EXPERIMENTAL PROCEDURE

3.1 Introduction

This study builds on alloy development and corrosion studies at the University of the Witwatersrand. It focused on the heat treatment and corrosion behaviour of 2101 LDX cathodically modified with various percentages of ruthenium. The microstructures were studied to ascertain the effect of ruthenium, and hardness tests were done to ensure that there was no deleterious effect by Ru on the mechanical properties. Additionally, two other duplex stainless steel grades (2205 and 2507) and an austenite grade (316) were studied, to compare them with the 2101 without ruthenium additions. Understanding of the corrosion properties was achieved through the examination of the morphologies of the surfaces and observation of the electrochemical behaviour of the alloys in acidic and acidic chloride solutions. This could aid in future commercialization of the alloy with Ru additions.

3.1.1 Production of alloys

Samples of 316 austenitic stainless steel, and 2101, 2205 and 2507 duplex stainless steels were obtained from the Southern Africa Stainless Steel Development Association (SASSDA), in the as-rolled condition.

The 2101 duplex stainless steel was cut into small chips, sizes of 0.47mm x 0.015mm x 0.05mm (length x breadth x thickness) with the aid of a Struers Secotom-10 cutting machine. Ruthenium powder was added to the chips, which were later compacted. The compacted samples were melted in the button-arc furnace at Mintek under an argon atmosphere using titanium as an oxygen-getter, and were cooled in the furnace, on a water-cooled copper hearth. The alloys were designed to have the compositions shown in Table 4.2.

3.1.2 Phase proportion–temperature diagrams

Phase proportion-temperature diagrams of 2101 duplex stainless steel were calculated using Thermo-Calc with the TCEFS and SSOL4 databases. The austenite (fcc), ferrite (bcc), hexagonal (hcp), sigma and liquid phases were considered in the calculations. For the 2101 duplex stainless steel containing Ru, the SSOL4 database was used for the calculations, since this database contained Ru and the TCFES database did not. The composition variations of ferrite, austenite and hcp structures were also determined using Thermo–Calc.

3.1.3 Heat treatment of samples

Annealing was done in a tube furnace in air, followed by rapid cooling in water. The as-cast samples were annealed at temperatures of 1080°C for 10, 30, 90 and 120 minutes and 1100°C for 120 minutes, followed by quenching in water. This treatment was necessary to obtain the austenite in a ferrite matrix.

3.1.4 Metallographic investigation of samples

In order to understand the corrosion behaviour, the microstructure had to be known. It was also necessary to verify the proportions of the austenite:ferrite phases in the alloys with ruthenium additions, to ensure that the heat treatment had been effective to give a near 50:50 proportion. As-received samples of 2101 duplex stainless steel and 316 austenitic stainless steel were used in the experiments. (LDX 2101 is a trade name for EN14162 registered to Outokumpu Steel Limited.)

Specimens for microstructural and morphological examinations were cut into square samples measuring $1cm^3$ then hot mounted in bakelite. The samples were ground with 320, 600, 800 and 1000 grit silicon carbide papers , and polished using 3μm and 1 μm diamond pastes to obtain a mirror-like surface. The samples were rinsed in distilled water and degreased with acetone. The 316 austenitic steel samples were electro-etched with 10g oxalic acid in 100ml of distilled water to reveal the details of their microstructures, while the duplex stainless steels were electro-etched using 40g sodium hydroxide in 100ml of distilled water.

The alloys of 2101 with ruthenium were polished with diamond polish from 3μm down to 1μm, followed by an oxide polishing (OPS) (1μm) to obtain a mirror-like surface, after which they were washed with distilled water and ethanol. The surfaces were immersed in 40% NaOH without allowing the surface to dry, and were electrochemically etched at a potential of 3V for 8–10 seconds using a platinum electrode, according to the ASTM standard [2006AST]. After etching, each sample was examined using an optical microscope.

The proportion of each phase was determined. The volume fractions of the austenite phase were measured by quantitative metallography, using a grid [1968Rhi]. Five different micrographs were used for each sample. The mean was calculated, divided by the number of points in the grid, and multiplied by one hundred, to give the results in terms of the volume percent of phase.

3.1.5 Sample characterization

Microstructural observations of the samples were performed using an Axiotech microscope with an AxioCam MRc digital camera. The microstructure of the samples before exposure to the corrosive environment was observed using a JEOL 840 Scanning Electron Microscope (SEM) with a backscattered electron detector and a secondary electron detector, with accelerating voltage of 20 kV. Both of these modes were used to study the specimens. Quantitative analysis was carried out using Energy dispersive X-ray (EDX) Analysis. The phases were confirmed using X-ray diffractometry (XRD) with Philips X-pert Highscore software.

3.1.6 Corrosion measurements

3.1.6.1 The electrochemical cell

The electrochemical cell consisted of a 500ml Pyrex glass conical flask suitable for a conventional three-electrode system: comprising the sample, a silver/silver chloride 3M KCl solution reference electrode and a graphite counter electrode. The cover of the cell had five holes for the reference electrode, working electrode, counter electrode, thermometer and aeration/de-aeration.

The heat treated samples were cold-mounted in epoxy resin after an electrical connection was provided by attaching a conductive wire to the rear using aluminium conducting tape. The samples were wet ground on 320, 600, 800 and 1000 grit SiC grinding papers on a automated wheel, degreased with ethanol, and washed with distilled water. The areas exposed to the corrosive solution were traced onto tracing paper, which was then measured to obtain the surface area.

The test corrosion solutions (0.5M H_2S0_4, 0.5M HCl, 1M H_2S0_4, 1M H_2S0_4+1% NaCl and 3.5 M NaCl) were prepared using chemicals of analytical grade and distilled water. All electrochemical measurements were made at different temperatures (±1°C) in the range of 25-80°C. The temperature was maintained in a water-bath and measured with a thermometer.

3.1.6.2 Electrochemical measurements

Electrochemical measurements were carried out using an Auto Lab Potentiostat (PGSTAT20 computer controlled) using the General Purpose Electrochemical Software (GPES) Version 4.9 and NOVA Version 1.7. All tests were carried out in triplicate and recorded; the tests with good reproducibility were used.

3.1.6.3 Open-circuit potential measurement

Open-circuit potential measurements (OCP) were used to determine the reactivity of the alloys (tendency of the alloys to corrode) in different media with time. The variations in the OCP values of the alloys at zero applied current immediately after the immersion of the alloys in different media up until about eight hours were measured. The open circuit potential was measured by maintaining a constant current. Potential-time graphs were obtained.

3.1.6.4 Potentiodynamic polarisation

The potentiodynamic polarisation responses of the alloys were investigated in naturally aerated and de-aerated solutions at different temperatures. Polarisation curves were obtained at a scan rate of 1mV/s, starting from -500mV to 1500mV with respect to the open circuit potential (OCP). Samples were polished, and rinsed with ethanol to remove the products that might have

formed on the surface before undertaking further measurements. These products were too small to collect for subsequent analysis.

3.1.6.5 Cyclic potentiodynamic polarisation measurement

Cyclic polarisation measurements were carried out to determine the corrosion rates, evaluate the passivity behaviour, and determine the pitting and repassivation behaviour of the alloys. This is a non-destructive test. Before potentiodynamic polarisation, the alloys were immersed in the electrolytes for sufficient time to stabilise at the OCP. Cyclic polarisation curves were measured at a scan rate of 1mV/s, starting from -200 mV (with respect to the OCP) to about 1200 mV, before reversing. Calibration was done with respect to 2101 steel samples used.

3.1.6.6 Chronoamperometry technique

Chronoamperometric tests were carried out to further assess the pitting corrosion behaviour of the alloys and to determine stability of the passive films formed by the alloys in the different media. The chronoamperometry behaviour was studied for about eight to twelve hours in different media, within the passivity regions obtained from the cyclic potentiodynamic polarisation measurements. After each scan, the electrolyte was replaced with fresh electrolyte, and the samples were freshly polished, rinsed in water and washed with acetone to remove the products that might have formed on the surface that could affect the following measurements. These products were too small to collect for further analysis.

3.1.6.7 Post corrosion measurement characterization

Types and morphologies of identified pits on the surfaces of the corroded samples after potentiodynamic and chronoamperometry studies were examined using a JEOL SEM.

3.1.7 Chemical composition

The chemical compositions of as-received samples were determined using a Bruker Q8 Magellan spark optical emission spectrometer, after grinding the samples to ensure that they were flat and

clean to avoid rough, uneven burning. They were clamped and sparked. The emitted radiation was split using a prism to produce a spectrum. The emitted spectra were seen as different colours, depending on the wavelength. The intensity of an emission line (colour) is proportional to the concentration of each element present. The spark was repeated thrice and the average results were reported.

CHAPTER 4

RESULTS

4.1 Overview

The chemical compositions analyses were carried out to ascertain and quantify the elements that were present in the alloys under study. Thermo-Calc was used to determine the best heat treatment temperature and also to deduce the phases present in the 2101 alloys with ruthenium additions. The temperature to obtain the 50:50 duplex phase was calculated by Thermo-Calc and a temperature 20°C higher than this calculated temperature was also used for comparism, to see if a higher temperature would affect the microstructure. Optical microscopy was done to assess the microstructure and understand the phases present and to ensure that ruthenium had no negative effect on the phases present or the ferrite:austenite ratio. It was also used to check whether the samples produced were homogeneous, and done on all the samples heat treated at 1080°C for different holding times. The best microstructures were those of the samples annealed for 120 minutes because they had more austenite (and so more representative of the equilibrium condition), and these were used for further studies. Three etchants were tried to obtain the best contrast for the microstructures. The scanning electron microscope with EDX analysis were also used to obtain detailed microstructures and the composition of phases in the alloys. The volume fractions were calculated to show the percentage of the phases in the alloys and to ascertain that near 50:50 duplex microstructures were obtained. The identification of the phases was done with X-ray diffractometry to ensure that the major phases were austenite and ferrite. Hardness tests were done to verify that the additions of ruthenium did not affect the mechanical properties of the 2101 alloy, and were chosen because they were easier and cheaper than other mechanical tests, especially on small samples. The electrochemical tests were done to compare the corrosion behaviour of 2101 with 316, 2205 and 2507 stainless steels. The corrosion behaviour of the manufactured 2101 alloy with ruthenium were also studied and compared to the other alloys.

4.2 Chemical composition

Table 4.1 shows the chemical composition of 2101, 2001, 2205 and 2507 duplex stainless steels which were analysed by a Bruker Q8 Magellan spark emission spectrometer.

Table 4.1. Chemical composition (wt%) of as-received samples of 2101, 2001, 2205, 2507 duplex stainless steels.

Alloy	**Element (wt%)**					
	Cr	**Ni**	**Mn**	**N**	**Mo**	**Fe**
2101	21.5±0.7	1.5±0.3	4.8±0.0	0.2±0.0	0.5±0.5	Balance
2001	20.5±1.4	2.0±1.4	5.0±1.4	0.1±0.1	0.6±0.0	
2205	22.5±0.7	5.5±1.4	2.0±0.0	0.2±0.0	3.3±0.4	
2507	25.0±1.4	7.0±1.4	1.2±0.0	0.3±0.1	4.0±1.4	

Table 4.2 shows the compositions and weight of the targetted alloys, with the different weight percentages of ruthenium added to 2101 duplex stainless steel. The first batch of alloys to be produced were Alloys 1-6. The highest ruthenium content was 0.2 wt% Ru. The weights before melting were 5g, while the weights after were not determined.

The second batch of samples were Alloys 7-12, and had an initial weight of 6g. The weight after melting indicated metal loss during melting, so it was assumed that there was also weight loss in the first batch. The lowest ruthenium content was 0.05wt% Ru, while the highest was 10wt% Ru for this batch.

The last batches were Alloys 13-23. The decrease in the weight after melting shows that metal loss also occurred during melting (Table 4.2). The lowest ruthenium content added for this batch was 0.05 wt% Ru, while the highest was 2.50 wt% Ru.

Table 4.2. Ruthenium compositions and weight of designed Fe-21Cr-01Ni (wt%) (2101) DSS alloys.

Alloy	2101-Ru (wt%)	Weight before melting (g)	Weight after melting (g)
1	0.00	5.0000	Not measured
2	0.05	5.0000	Not measured
3	0.10	5.0000	Not measured
4	0.15	5.0000	Not measured
5	0.20	5.0000	Not measured
6	0.20	5.0000	Not measured
7	0.05	6.0000	5.9432
8	0.10	6.0000	5.8802
9	0.15	6.0000	5.9224
10	0.20	6.0000	5.9294
11	2.50	6.0000	5.8975
12	10.00	6.0000	5.7854
13	0.05	44.5554	44.3429
14	0.10	45.7057	45.5182
15	0.15	40.8992	40.7235
16	0.20	41.2819	40.3043
17	0.40	38.4207	38.2409
18	0.60	45.3259	45.1027
19	0.80	42.2580	41.9972
20	1.00	32.4500	32.2020
21	1.50	34.3191	34.2216
23	2.50	38.2243	37.7704

4.3 Thermo-Calc results

The calculated diagrams using Thermo-Calc with SSOL4 and TFECS5 databases are presented in Figures 4.1-4.20. They cover a temperature range from above melting to 600°C which is considered the lowest temperature at which the calculations were accurate, as expected, due to kinetic restraints (primarily diffusion) on the thermodynamic equilibrium as the temperature is lowered, because of the slowing down of diffusion at low temperatures. The calculations helped to define the temperature of heat treatment. The Thermo-Calc calculations were done for 2101 lean duplex stainless steels containing compositions of 0, 0.05, 0.1, 0.15, 0.2, 5 and 10 wt% Ru

and were to help in predicting the microstructures. Sigma phases were also calculated for 0 wt%, 2.5 wt%, 5 wt% and 10wt% Ru to show the effect of ruthenium on sigma formation in 2101 lean duplex stainless steel. Although SSOL4 is not a specialised ferrous database, TCFE5 database is a ferrous database. The latter does not contain ruthenium, hence the more general SSOL4 database had to be used. There was no significant difference between the diagrams calculated by TCFE5 and SSOL4 (Figures 4.1 and 4.2), which indicated that it was acceptable to use the SSOL4 data base for the calculations. Phase proportion-temperature or ‘‘Property diagrams’’ were drawn for all the alloys, which show the proportion of the phases with different temperatures. The elemental compositions of the phases were calculated, together with the temperature ranges for the phases. It was observed that the temperature at which ferrite has the highest composition, is where austenite will have the lowest composition, which is expected.

4.3.1 Alloy designation 2101 DSS

The phase proportion diagram of 2101 lean duplex stainless steel obtained with the TCFES database above 600°C is shown in Figure 4.1. The ferrite started to solidify at 1480°C and solidification was complete at ~1400°C. The maximum ferrite was between ~1407°C and~1380°C, and dropped to the minimum of 22% at ~873°C. The austenite phase, designated FCC_A1#1 in Thermo-Calc, started to form at ~1380°C. The HCP phase started to precipitate at 873°C with maximum proportion ~2%. The 50:50 austenite: ferrite ratio was achieved at ~1120°C and ~700°C. The duplex structure was observed at various ratios between 1380°C to about 880°C. The austenite phase precipitated at 1380^{o}C and it reached the maximum at 873°C. It has the same proportion with ferrite at ~700°C and ~1120°C. Table 4.3 shows the phase information: average composition, range of stability and maximum proportion.

Table 4.3. Phase information for 2101 using TCFES.

Phase	Average Composition (wt%)	Minimum stability temperature (°C)	Maximum stability temperature (°C)	Maximum proportion (%)
Liquid		1407	>1480	100
BCC_A2	$Fe_{0.70}Cr_{0.22}Mn_{0.04}$	<600	1480	100
FCC_A1	$Fe_{0.72}Cr_{0.18}Mn_{0.05}$	<600	1380	79
HCP		<600	873	~2

4.3.2 Alloy designation 2101 SSOL4

Figure 4.2 shows multi-component diagrams calculated with the SSOL4 database. The main component on solidification was ferrite. The ferrite started to exist at ~1480°C and austenite started to precipitate at ~1380°C, and the HCP phase started forming at 870°C. The liquid phase existed until 1407°C, when solidification was complete. Figure 4.2 shows that the sample can be heat treated between 1000°C and 1200°C to obtain a duplex structure. The extracted data are given in Table 4.4. There was no difference between the calculated results using SSOL4 and TCFE5 databases, which was good, because it meant that the databases were giving the same answers. This meant that the SSOL4 database (which had ruthenium) could be used instead of TCFE5 (which did not have ruthenium).

Table 4.4. Phase information for 2101 using SSOL4.

Phase	Average composition (wt%)	Minimum stability temperature (°C)	Maximum stability temperature (°C)	Maximum proportion (%)
Liquid	-	~1407	>1480	100
BCC_A2	$Fe_{.70}Cr_{.22}Mn_{0.04}$	<600	1480	100
FCC_A1	$Fe_{.72}Cr_{.18}Mn_{0.05}$	<600	1380	79
HCP		<600	873	~2

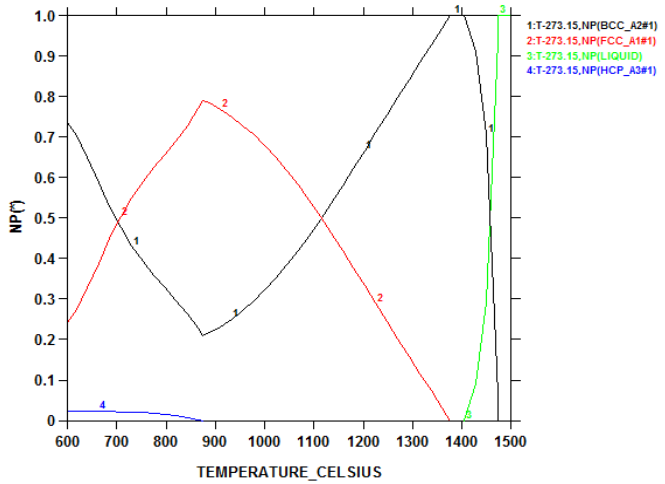

a) Phase-proportion-temperature diagram of 2101.

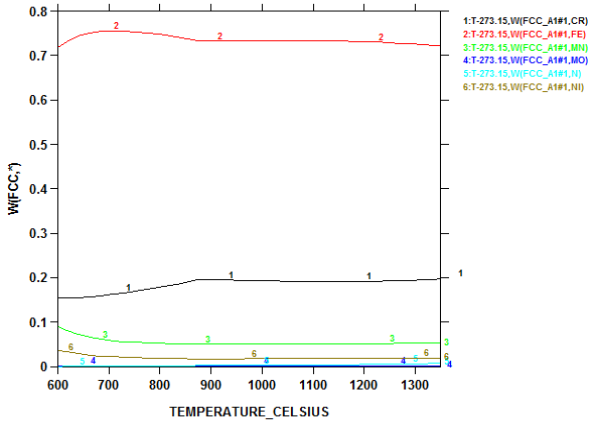

b) Composition diagram of austenite

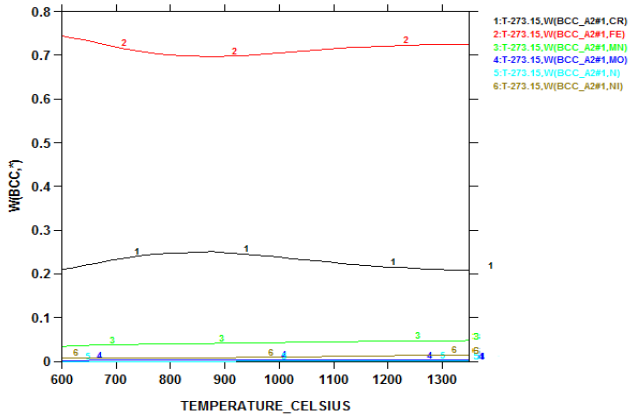

c) Composition diagram of ferrite

Figure 4.1. Multi-component and compositional plots for Alloy 2101 with TCFE5: (a) Phase proportion-temperature diagram, (b) Composition diagram of austenite, and (c) composition diagram of ferrite.

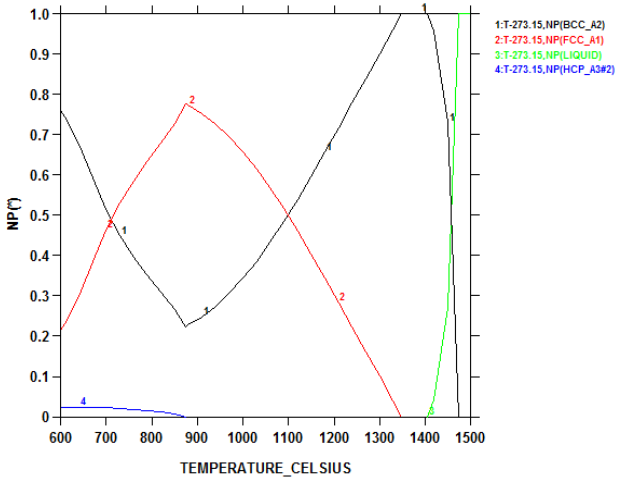

a) Phase proportion-temperature diagram.

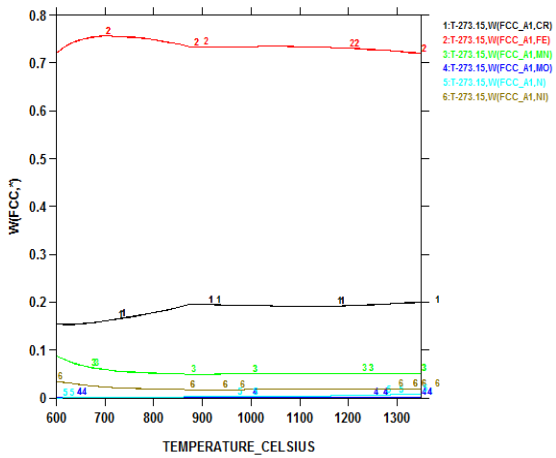

b) Composition of austenite.

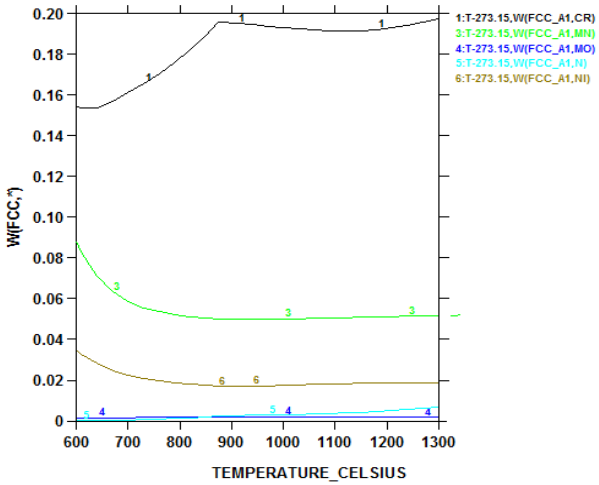

c) wt% of the minor components of austenite.

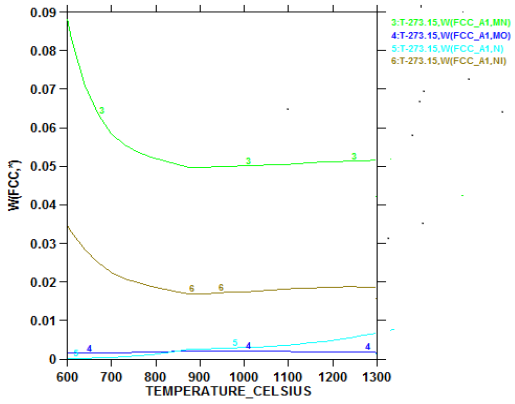

d) wt% of the very minor components of austenite.

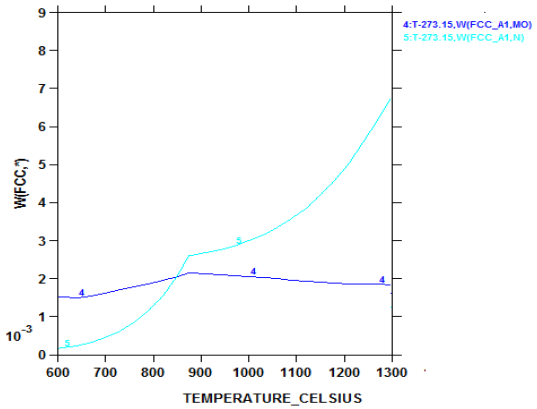

e) wt% of the very minor components of austenite.

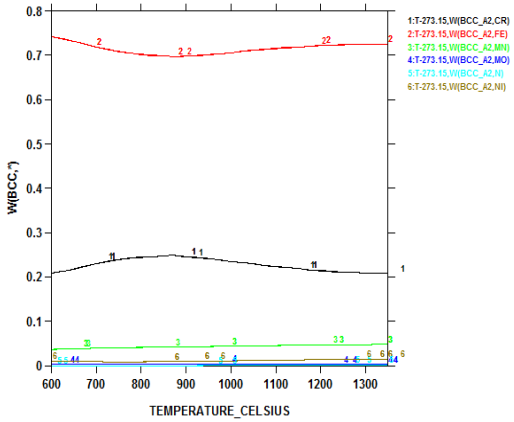

f) Composition of ferrite.

Figure 4.2. Multi-component and compositional plots for Alloy 2101 with SSOL4.

4.3.3 Alloy designation 2101-0.05wt% Ru DSS

With 0.05wt% Ru, the liquid phase was present above 1500°C to about 1400°C, and there was solidification to ferrite between 1480°C and 1400°C. The ferrite proportion was maximum between 1345°C and 1407°C; it reached the minimum at about 880°C. It had an equal proportion with austenite at 1080°C and at around 700°C. The duplex structure (austenite and ferrite) was calculated with 50:50 austenite:ferrite ratio at 1080°C, so heat treatment would yield 50:50 austenite:ferrite ratio, providing the time would be sufficient for diffusion to occur.The hcp precipitated out at 875°C. The composition variation of austenite (Figure 4.3) shows the iron content was between 74% at 1300°C, and around 72% at 600°C; chromium varied between 18% to 15% from 1300°C to 600°C. Manganese increased slightly with decreased temperature from about 5% at 1300°C to about 9% at 600°C. Ruthenium was very close to 0, due to the minor ruthenium amount, and the ruthenium partitioned fairly equally between austenite and ferrite. This would be advantageous for corrosion resistance, because then Ru would benefit both phases. The plots are given in Figure 4.3 and the data obtained from them are shown in Table 4.5.

Table 4.5. Phase information for 2101-0.05wt% Ru using SSOL4.

Phase	**Average composition (wt%)**	**Minimum stability temperature (°C)**	**Maximum stability temperature (°C)**	**Maximum proportion (%)**
Liquid	-	1400	>1500	100
BCC_A2	$Fe_{0.72}Cr_{0.21}Mn_{0.032}$	<600	1345	100
FCC_A1	$Fe_{0.75}Cr_{0.18}Mn_{0.05}Ni_{0.025}$	<600	1350	72.7
HCP		<600	875	2

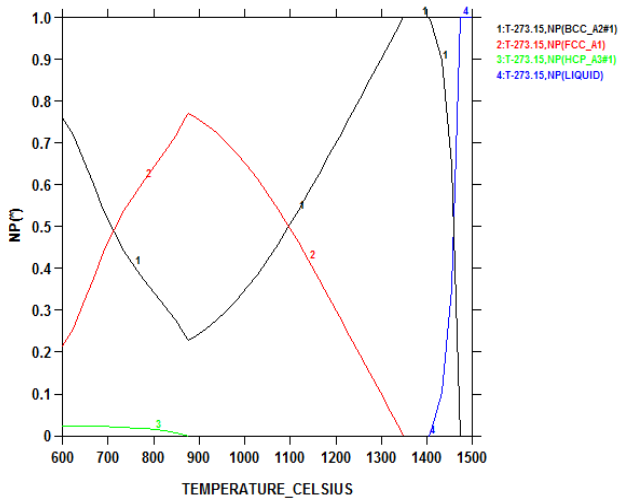

a) Phase proportion-temperature diagram.

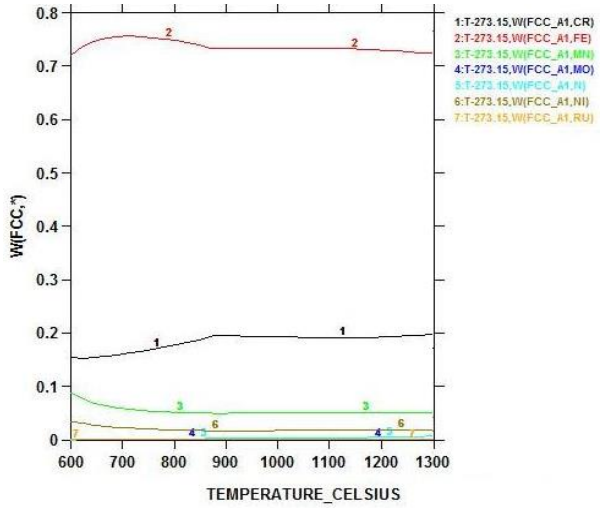

b) Composition of austenite.

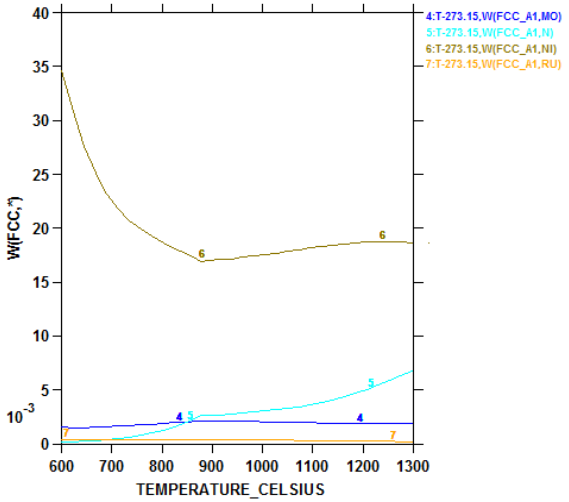

c) Minor amounts of elements in austenite.

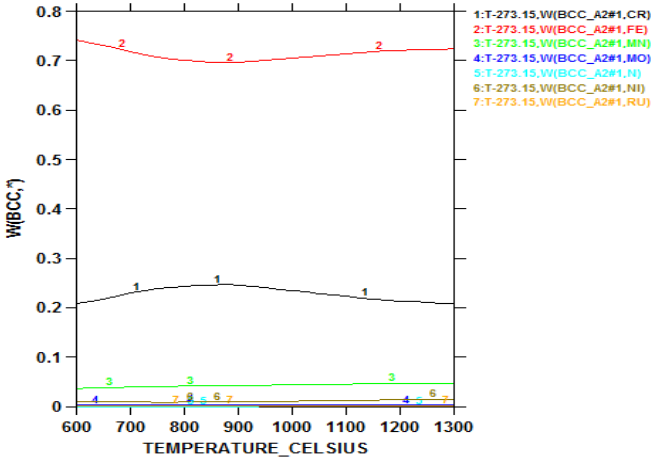

d) Composition of ferrite.

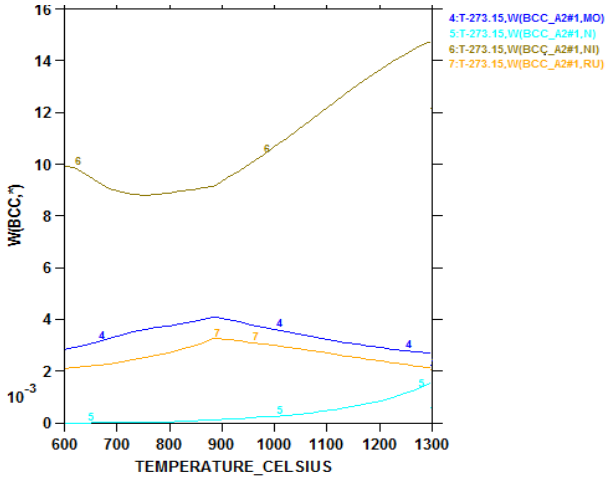

e) Minor amounts of elements in ferrite.

Figure 4.3. Multi-component and compositional plots for Alloy 2101 with 0.05wt% Ru calculated using SSOL4.

4.3.4 Alloy designation 2101-0.1wt% Ru DSS

Figure 4.4 presents the phase proportions and composition variation of phases for 2101-0.1wt% Ru duplex stainless steel. Liquid existed above 1500°C, and liquid and ferrite were seen from 1480°C to 1350°C, during solidification. Austenite and ferrite phases were obtained between ~1350°C to ~600°C. Ferrite had the maximum proportion between 1400°C and 1350°C. The minimum ferrite proportion was at about ~875°C. Ferrite had an equal ratio with austenite at ~1080°C and ~720°C. The HCP structure precipitated at around 880°C, the maximum proportion was ~2%.

The composition variation of ferrite in 2101-0.1wt% Ru is shown in Figure 4.4. Iron had the maximum composition, of course, followed by chromium and manganese. The ferrite had the highest ruthenium composition at around 880°C, and the ruthenium content reduced as the HCP started to precipitate at 875°C. Molybdenum had the highest peak at about 875°C. The composition of elements in austenite in descending order was: Fe, Cr, Mn (Figure 4.4). Ruthenium increased with a decrease in temperature from about 0.07 % at 1300°C to about 0.09% at 600°C in ferrite phase (Figure 4.4e). The data obtained from the plots are shown in Table 4.6.

Table 4.6. Phase information for 2101-0.1wt% Ru using SSOL4.

Phase	**Average composition (wt%)**	**Minimum stability temperature (°C)**	**Maximum stability temperature (°C)**	**Maximum proportion (%)**
Liquid	-	1400	>1600	100
BCC_A2	$Fe_{0.72}Cr_{0.21}Mn_{0.032}$	<600	1467	100
FCC_A1	$Fe_{0.75}Cr_{0.18}Mn_{0.05}Ni_{0.025}$	<600	1350	78
HCP		<600	875	2

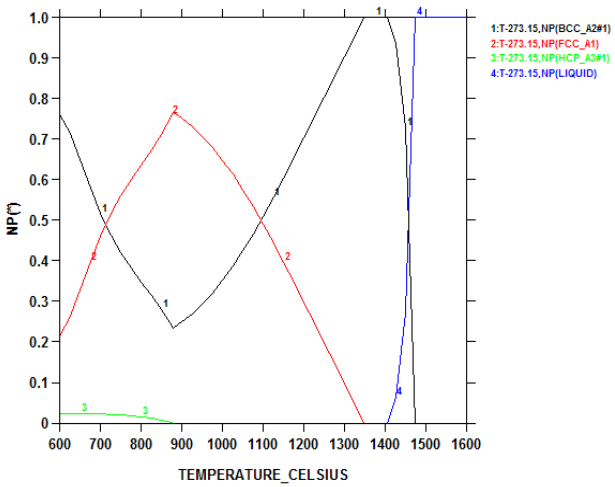

a) Phase proportion-temperature diagram.

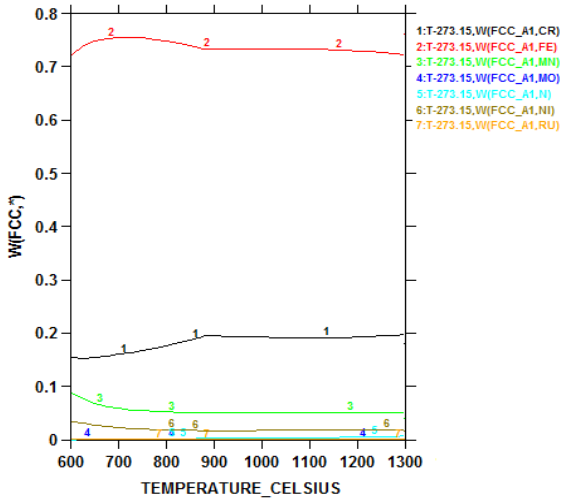

b) Composition of austenite.

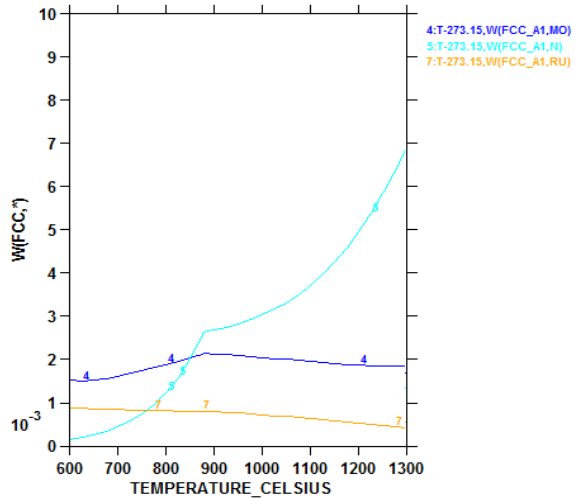

c) Minor components of austenite.

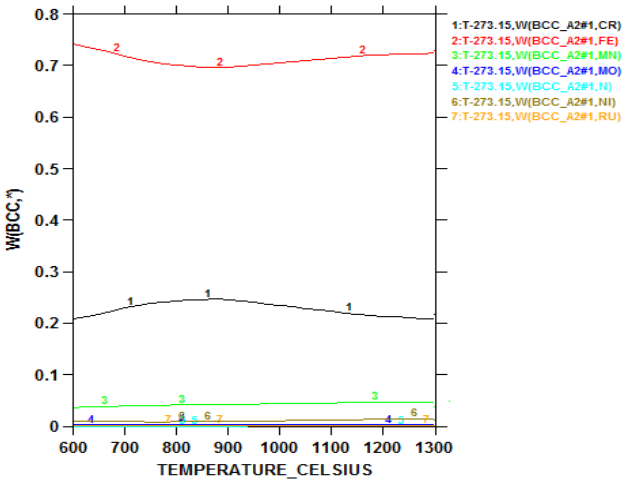

d) Composition of ferrite.

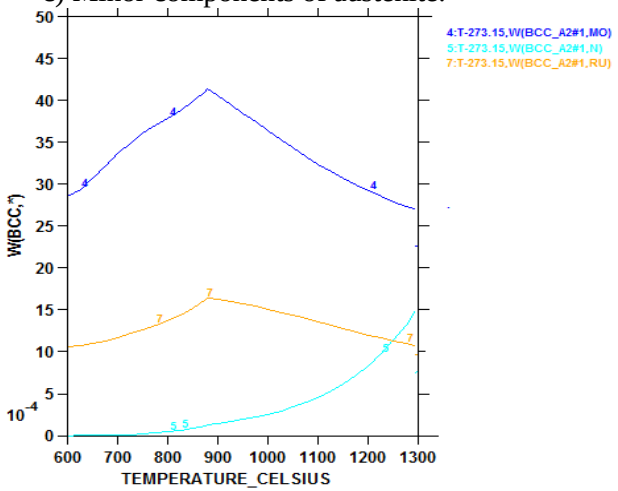

e) Minor components of ferrite.

Figure 4.4. Multi-component and compositional plots for duplex stainless steel Alloy 2101 with 0.1wt% Ru, using the SSOL4 database.

4.3.5 Alloy designation 2101-0.15wt% Ru DSS

The multi-component diagram of 2101-0.15 wt% Ru duplex stainless steel drawn with the SSOL4 database is presented in Figure 4.5. The liquid phase was calculated above 1400°C. Ferrite solidified between 1480°C and 1400°C. The highest proportion of ferrite (100%) was observed at around 1400°C to 1380°C, while the lowest proportion was at 880°C. The austenite and ferrite had equal ratios at 1080°C and 740°C. The composition variation of austenite was calculated for the temperature range of 1300°C to 600°C (Figure 4.5b). The Fe content was greater than 72%, chromium was lower than 20% and there was an increase in ruthenium as the temperature decreased. In Figure 4.5e, the iron content in ferrite varied with temperature, and the minimum percentage was less than 70%; the chromium content was less than 20%. Table 4.7 shows the minimum and maximum stability temperatures and the maximum proportion of the phases in 2101-0.15wt% Ru DSS. The hcp phase started to precipitate at 883°C.

Table 4.7. Phase information for 2101-0.15wt% Ru using SSOL4.

Phase	**Average composition (wt%)**	**Minimum stability temperature (°C)**	**Maximum stability temperature (°C)**	**Maximum proportion (%)**
Liquid	-	1400	>1500	100
BCC_A2	$Fe_{0.72}Cr_{0.22}Mn_{0.04}$	<600	1471	100
FCC_A1	$Fe_{0.75}Cr_{0.18}Mn_{0.06}$	<600	1342	76
HCP		<600	883	2

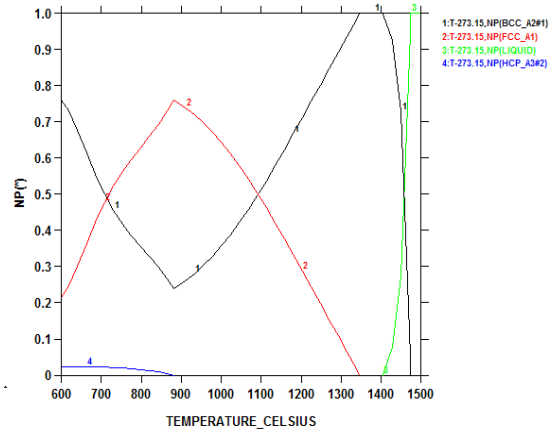

a) Phase proportion-temperature diagram.

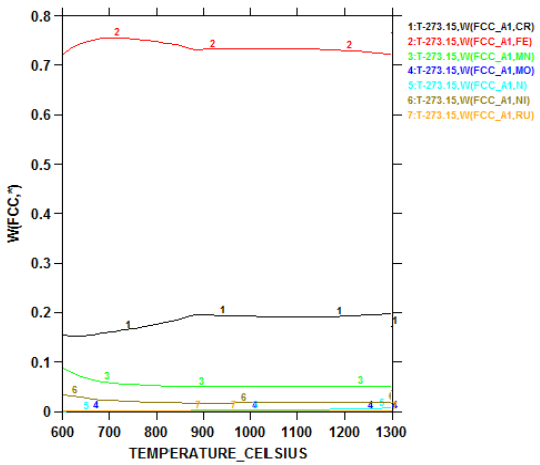

b) Composition of austenite.

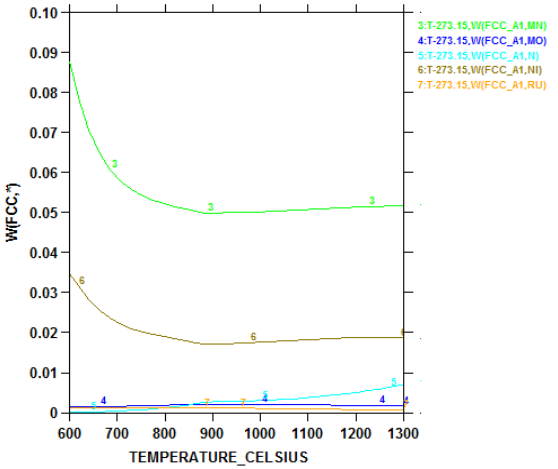

c) Minor components of austenite.

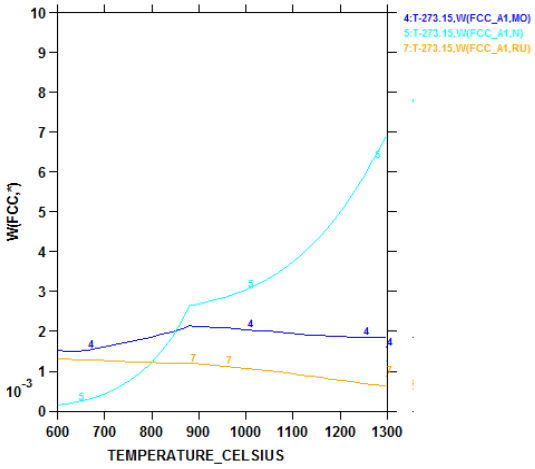

d) Minor components of austenite.

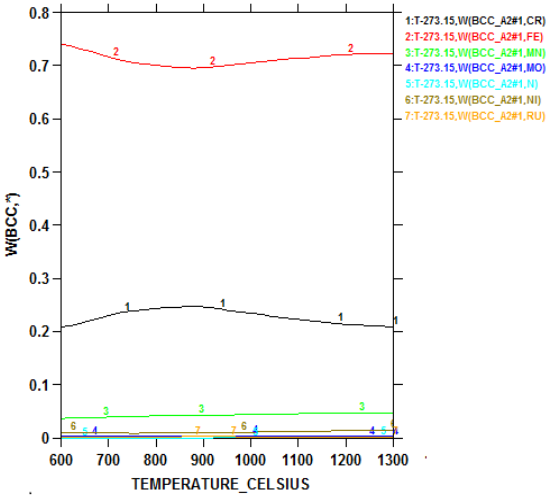

e) Composition of ferrite.

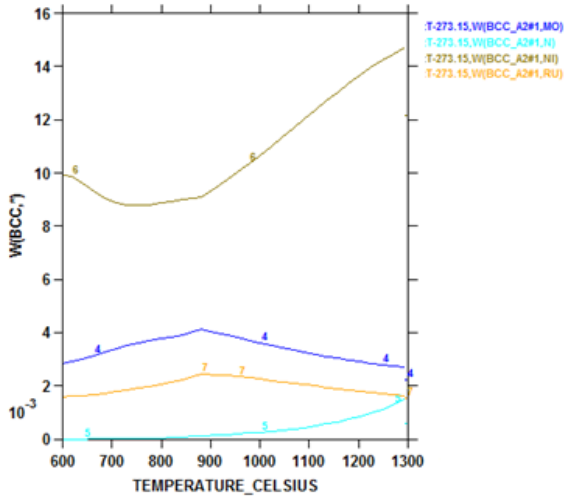

f) Minor components of ferrite.

Figure 4.5. Multi-component and compositional plots for duplex stainless steel Alloy 2101 with 0.15wt% Ru using the SSOL4 database.

4.3.6 Alloy designation 2101-0.2wt% Ru DSS

The phase proportion diagram of 2101-0.2 wt% Ru gave two phases: austenite and ferrite in the temperature range of 1350°C to ~900°C (Figure 4.6). Liquid began to solidify at about 1480°C to form ferrite. The austenite phase started to form at 1350°C; it had the highest proportion at 880°C with about 78%.

Figure 4.6b presents the composition variation of austenite in 2101-0.2 wt% Ru duplex stainless steel. The chromium was less than 20%. The ruthenium content in austenite was between 0.14% and 0.11% between 1300°C and 600°C.

The composition variation of ferrite is shown in Figure 4.6e. The iron proportion throughout the calculated temperature range was less than or equal to 72%, while the chromium content was greater than 20%, which was expected. The ruthenium content was less than 0.3% and greater than 0.2%. The ruthenium composition was higher between 900 and 600°C. This was the temperature range where there was an HCP structure in Figure 4.6a. The data are presented in Table 4.8.

Comparing Figures 4.6b and 4.6e, it can be seen that the elements that aid the formation of each phase are higher in content; e.g. chromium partitioned more to ferrite than to austenite. This agrees with chromium being a ferrite former. Ruthenium partitioned slightly more to ferrite than to austenite, although the difference was very minimal.

Table 4.8. Phase information for 2101-0.2wt% Ru using SSOL4.

Phase	**Average composition (wt%)**	**Minimum stability temperature (°C)**	**Maximum stability temperature (°C)**	**Maximum proportion (%)**
Liquid		1400	>1500	100
BCC_A2	$Fe_{0.70}Cr_{0.22}Mn_{0.04}$	<600	1475	100
FCC_A1	$Fe_{0.72}Cr_{0.18}Mn_{0.06}$	<600	1341	75
HCP		<600	883	2

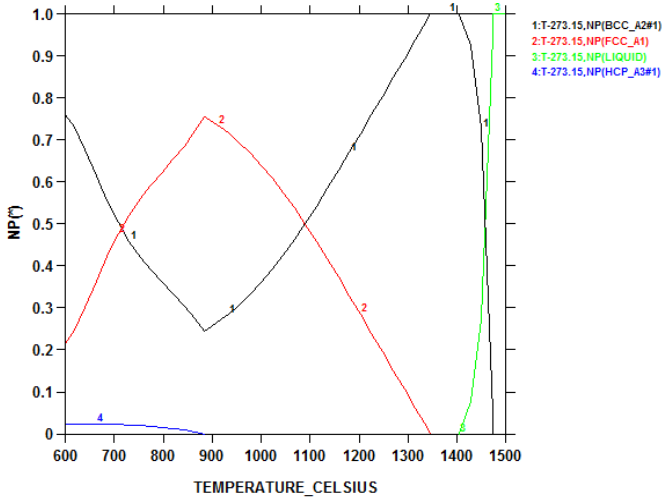

a) Phase proportion-temperature diagram.

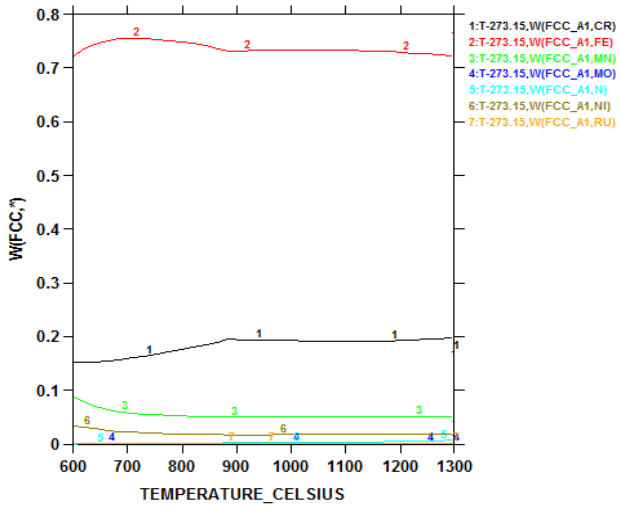

b) Composition of austenite.

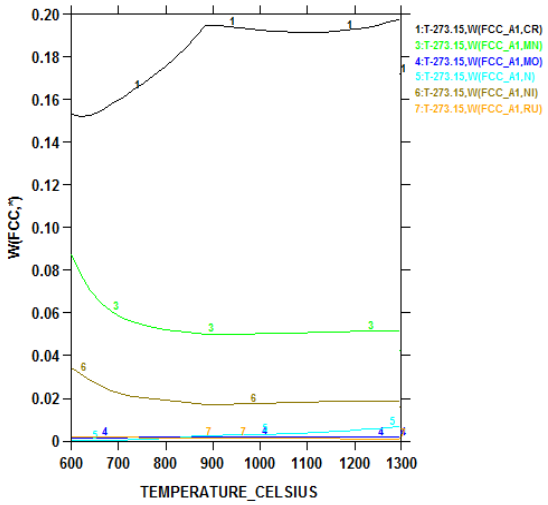

c) Minor components in austenite.

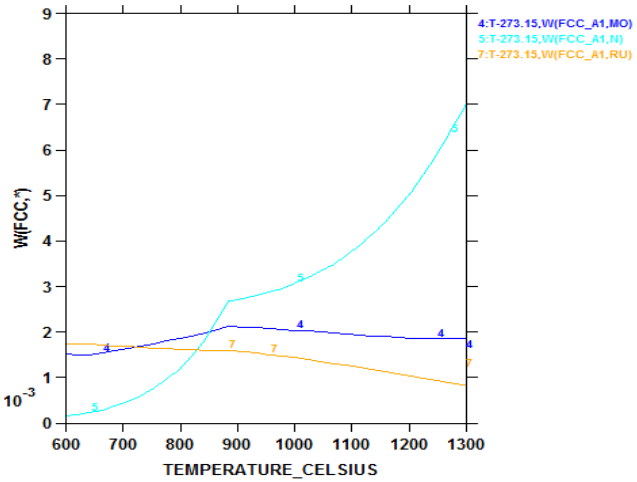

d) Minor components in austenite.

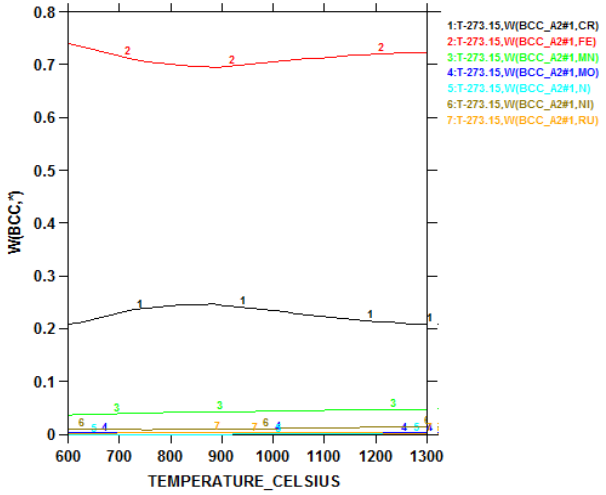

e) Composition of ferrite.

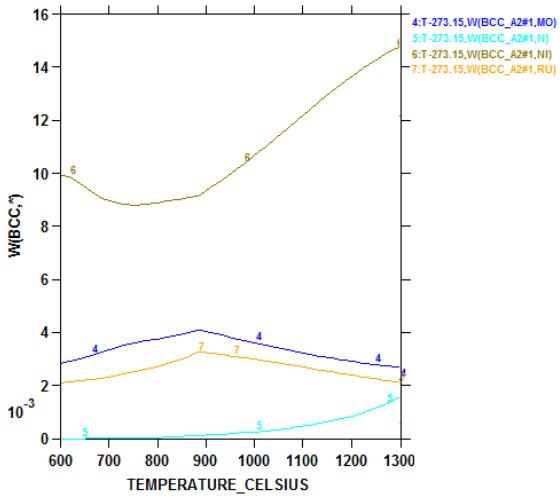

f) Minor components in ferrite.

Figure 4.6. Multi-component and compositional plots for Alloy 2101 with 0.2wt% Ru.

4.3.7 Alloy designation 2101-2.5wt% Ru DSS

The phase proportion diagram of 2101-2.5wt% is shown in Figure 4.7. Ferrite started to solidify above 1350°C. The ferrite was above 85% in the temperature ranges of 1300°C to 700°C. The austenite phase was observed at about 1280°C down to 600°C (the limit of calculations), but the maximum proportion was lower than 15%, and the phase proportion was reduced to almost 0% at 1050°C. Thus, 2.5wt% Ru did not give a duplex stainless steel. The HCP phase started to precipitate at about 1150°C, which is much higher at lower ruthenium contents.. Sigma phase precipitated out at about 640°C, with 13% at 600°C.

Figure 4.7e shows the composition variation of sigma in 2101-2.5 wt% Ru duplex stainless steel calculated between the temperature range of 600°C to 635°C. Table 4.9 shows that Fe, Cr and Mn were the prominent elements, with compositions less than 5%, 45% and 15% respectively.

Table 4.9. Phase information for 2101-2.5wt% Ru using SSOL4.

Phase	**Average composition (wt%)**	**Minimum stability temperature (°C)**	**Maximum stability temperature (°C)**	**Maximum proportion (%)**
Liquid		1330	>1440	100
BCC_A2	$Fe_{0.71}Cr_{0.2}Mn_{0.02}Ni_{0.04}$	1330	1440	100
FCC_A1	$Fe_{0.74}Cr_{0.17}Mn_{0.072}Ni_{0.036}$	760	1273	12
HCP	$Fe_{0.50}Ru_{0.24}Mn_{0.04}$	<600	1160	3
Sigma	$Fe_{0.48}\ Cr_{0.41}Mn_{0.12}$	<600	640	13

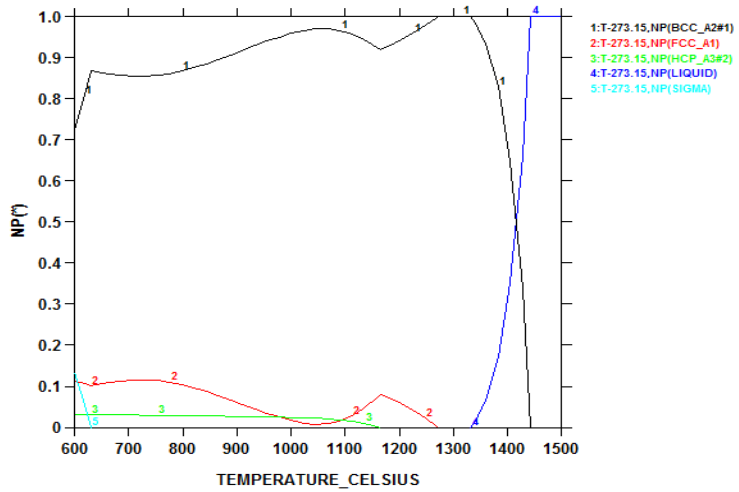

a) Phase proportion-temperature diagram.

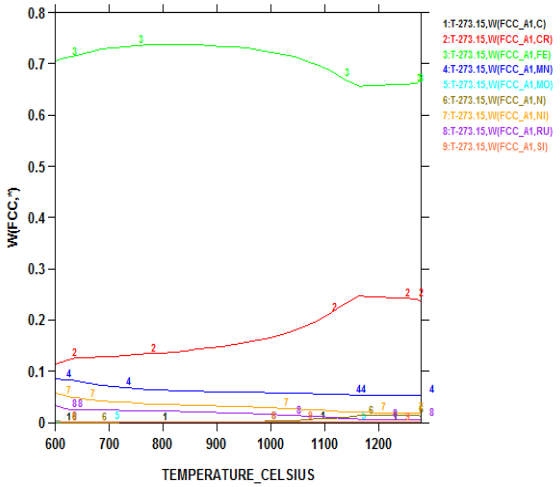

b) Composition of austenite.

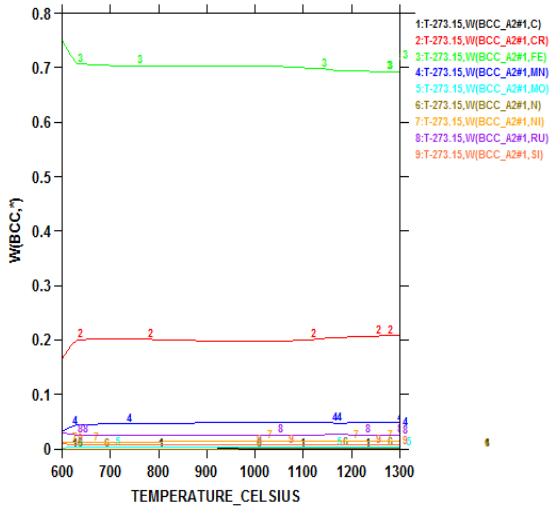

c) Composition of ferrite.

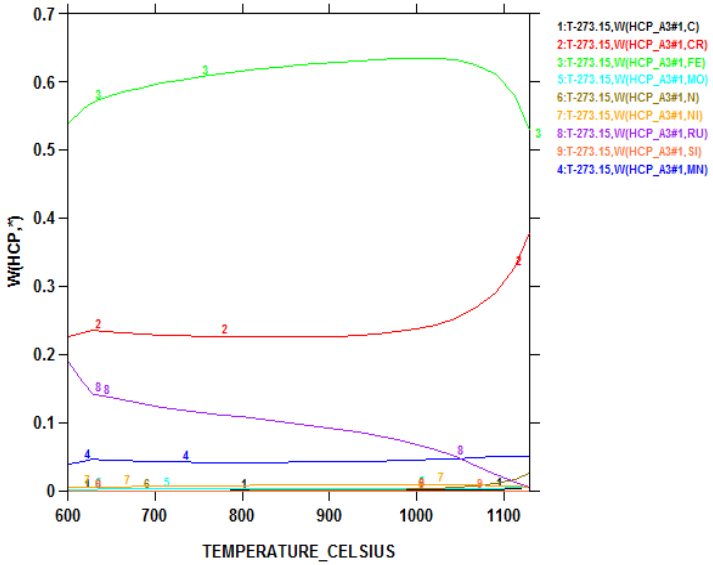

d) Composition of HCP.

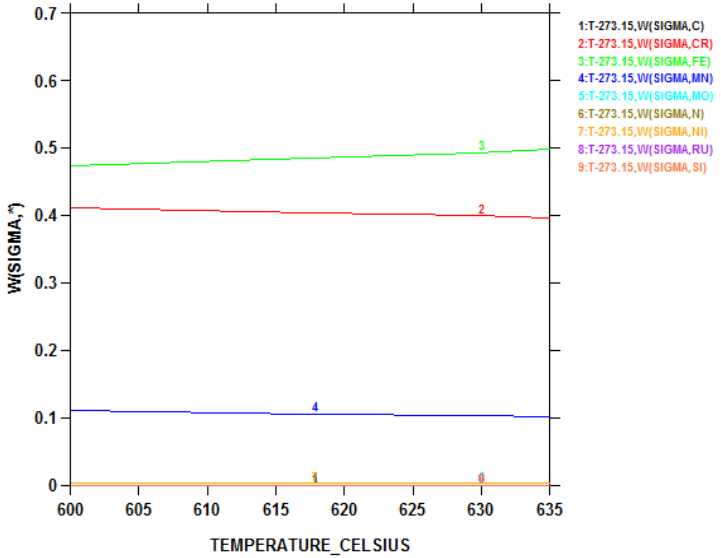

e) Composition of sigma

Figure 4.7. Multi-component and compositional plots for Alloy 2101 with 2.5wt% Ru.

4.3.8 Alloy designation 2101-5wt% Ru

The major phase was the ferrite phase (BCC-A2). The minor phases comprised less than 15%. At 1260°C, the HCP_A3#1 phase started to form, and FCC started to form at 900°C. The sigma phase started to precipitate at 630°C. The plots are given in Figure 4.8, and the data obtained from these are provided in Table 4.10.

Figure 4.8f presents the composition variation of sigma in 2101-5wt% Ru, was calculated at the temperature range of 600-620°C. Ruthenium, Fe, Cr and Mn were present. Chromium was greater than or equal to 4% and iron was less than 5%.

Table 4.10. Phase information for 2101-5 wt% Ru using SSOL4.

Phase	**Average composition (wt%)**	**Minimum stability temperature (°C)**	**Maximum stability temperature (°C)**	**Maximum proportion (%)**
Liquid		1310	>1440	100
BCC_A2	$Fe_{0.69}Cr_{0.20}Mn_{0.05}Ru_{0.05}$	1310	1440	100
FCC_A1	$Fe_{0.71}Cr_{0.12}Mn_{0.08}Ru_{0.05}$	<700	890	12
HCP_A3#2	$Fe_{0.51}Cr_{0.23}Ru_{0.24}Mn_{0.04}$	<600	1260	4.5
Sigma	$Fe_{0.48}\ Cr_{0.41}Mn_{0.12}$	<600	630	2

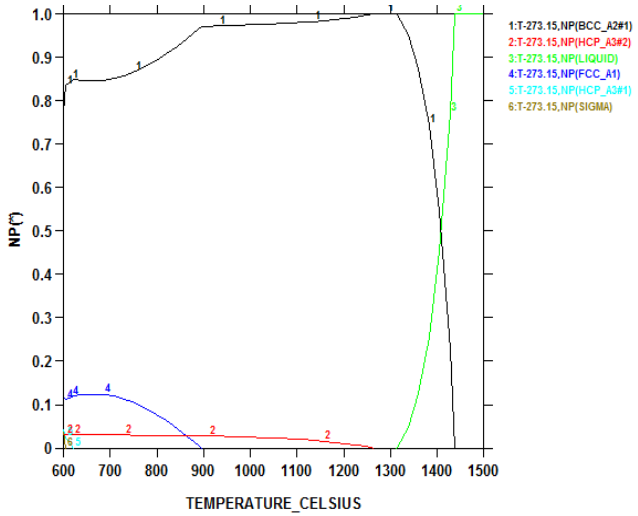

a) Phase proportion-temperature diagram.

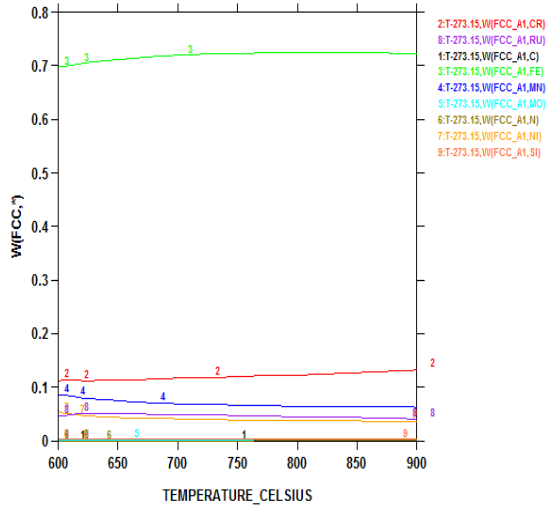

b) Composition of austenite

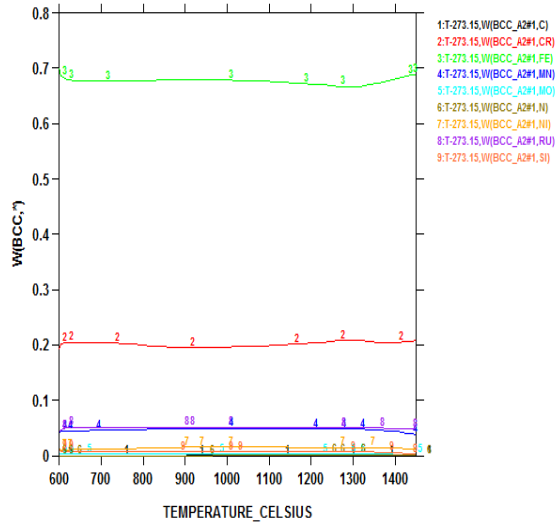

c) Composition of ferrite.

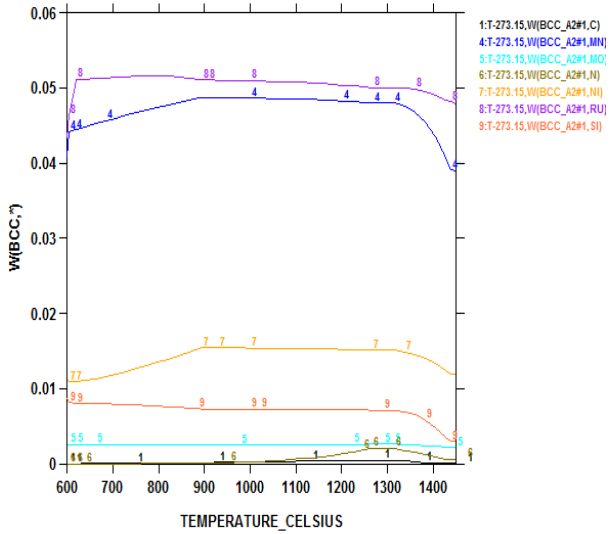

d) Minor components of ferrite.

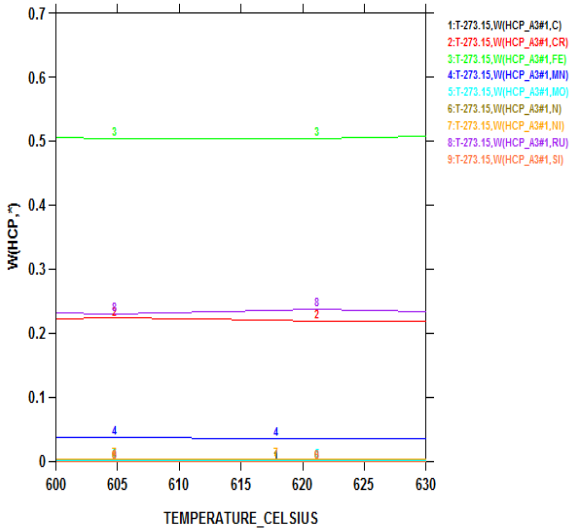

e) Composition of HCP.

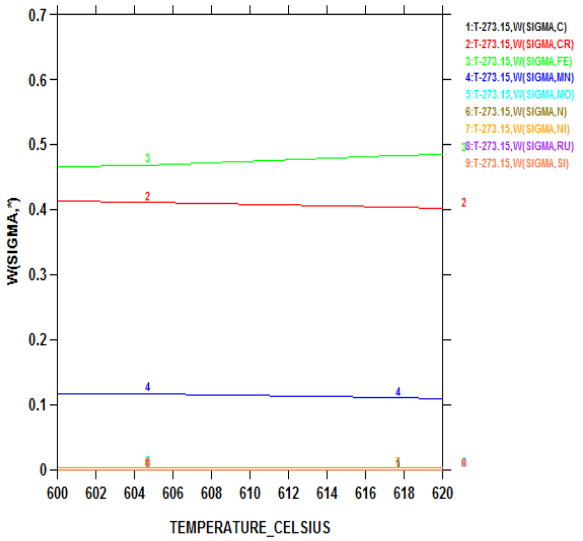

f) Composition of sigma.

Figure 4.8. Multi-component and compositional plots for Alloy 2101 with 5wt% Ru.

4.3.9 Alloy designation 2101-10wt% Ru

The phase proportion diagram of 2101duplex stainless steel containing 10 wt% Ru is shown in Figure 4.9. Five different phases were observed. The liquid phase was observed from above 1500°C to 1280°C. Ferrite started to solidify at around 1450°C; its maximum proportion was at about 1290°C. The proportion of ferrite between 1330°C to 900°C was above 90%, and decreased to less than 60% at 600°C. The HCP_A3#2 phase, which formed in the solid state, precipitated at about 1280°C; it was less than 5% proportion for the whole temperature range where it appeared. Another HCP phase (HCP_A3#1) phase was calculated in the temperature range of 800 to 600°C; it was ~28% at 600°C. The maximum proportions of the phases are presented in Table 4.11.

Table 4.11. Phase information for 2101-10wt% Ru using SSOL4.

Phase	**Average composition (wt%)**	**Minimum stability temperature (°C)**	**Maximum stability temperature (°C)**	**Maximum proportion (%)**
Liquid		1275	>1430	100.0
BCC_A2#1	Mainly Fe	1276	1430	99.0
FCC_A1	$Fe_{0.69}Cr_{0.10}Mn_{0.05}Ru_{0.06}Ni_{0.04}$	<600	850	12.0
HCP_A3#1	$Fe_{0.48}Ru_{0.25}Cr_{0.20}Mn_{0.04}$	<600	804	27.6
HCP_A3#2	$Cr_{0.80}$ $N_{0.08}$	<600	1275	3.8

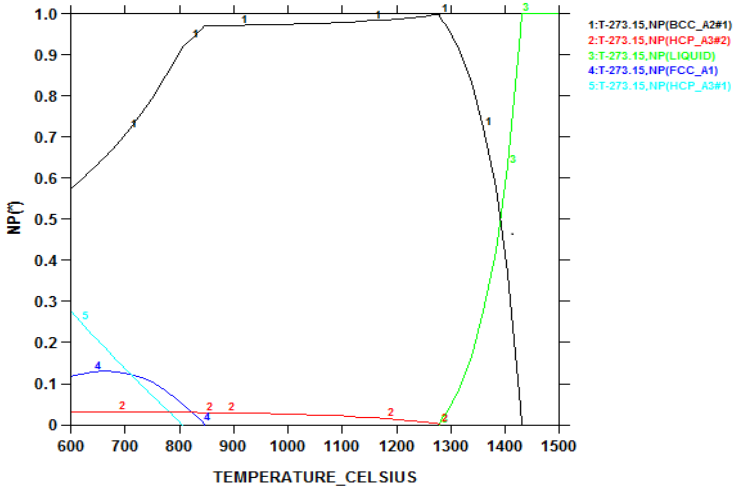

a) Phase proportion-temperature diagram.

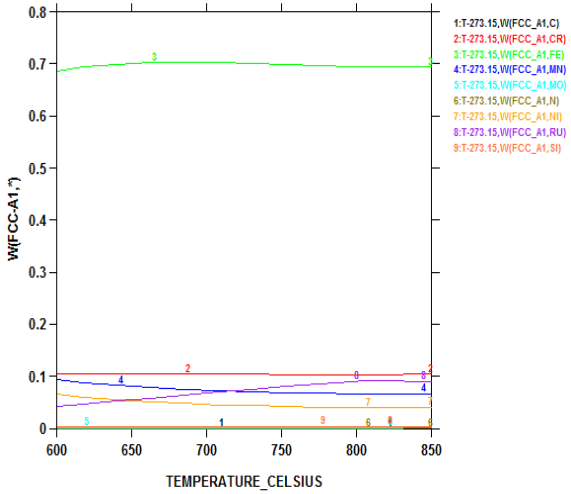

b) Composition of austenite.

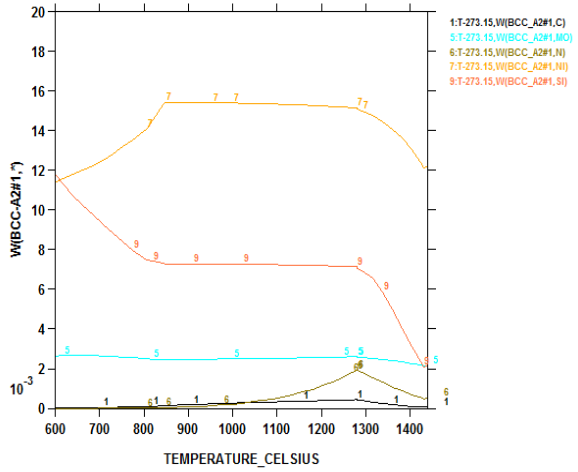

c) Composition of ferrite.

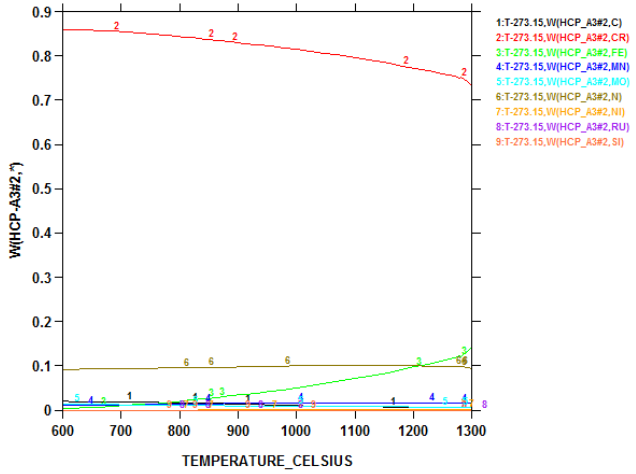

d) Composition of HCP_A3#2.

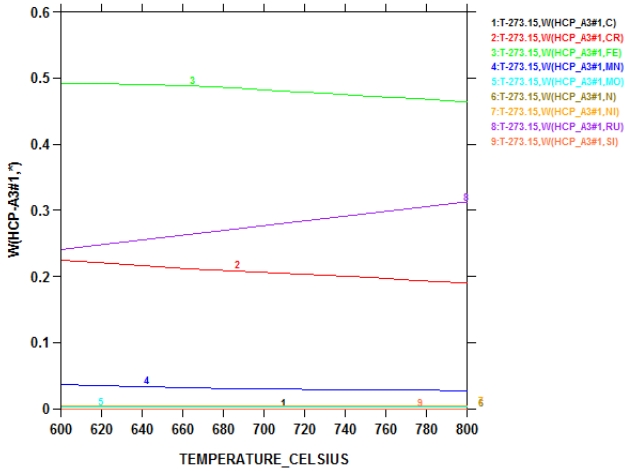

e) Composition of HCP_A3#1.

Figure 4.9. Multi-component and compositional plots for Alloy 2101 with 10 wt% Ru.

4.3.10 Summary of Thermo-Calc analysis

- Thermo-Calc indicated the phases to expect at each temperature, but it did not reveal the duration for the heat treatment, since the calculations are for equilibrium conditions. The heat treatment time was later determined by experiment.

- The 2101 duplex stainless steel with ruthenium up to 0.2 wt% had equal amounts of ferrite and austenite at 1080°C and 880°C.

- The temperature at which the liquid disappeared in 2101-10 wt% Ru was at 1280°C, which was lower than the other 2101 compositions with lower percentages of ruthenium.

- Ruthenium additions up to 0.2 wt% did not give a significant change to the phase proportion diagram, retaining the duplex structure.

- For higher percentage of ruthenium (2.5, 5 and 10 wt% Ru), there were changes in the phases of the duplex stainless steel, reducing the proportions of austenite, to less than a duplex structure. Thus, these compositions would not be suitable for a duplex stainless steel.

- The ruthenium was found to be in both ferrite and austenite phases, with little difference between them. This would be advantageous for corrosion resistance, because the Ru would benefit both phases.

- As the ruthenium content increased, the HCP_A3#2 phases precipitated out at higher temperatures.

- The higher temperature 50:50 range is at 1080°C for the duplex structure. This is preferred for heat treatment because the diffusion would be higher at 1080°C than at 700°C. Also, another phase, hcp, was calculated to be present at 700°C and this would be undesirable.

4.4 Material characterization

4.4.1 Optical microscopy

Metallographic examination of all the alloys showed the phases that were present in the etched samples. The etchant with the best contrast for the duplex stainless steels was 40g sodium hydroxide in 100ml distilled water; The etched duplex stainless steel showed ferrite being dark and the lighter phase as austenite. No intermetallic phase was observed in these samples. Figure 4.10 shows the optical micrograph of 316 austenitic stainless steel electrochemically etched with 10g oxalic acid in 100ml distilled water, revealing the austenite grains.

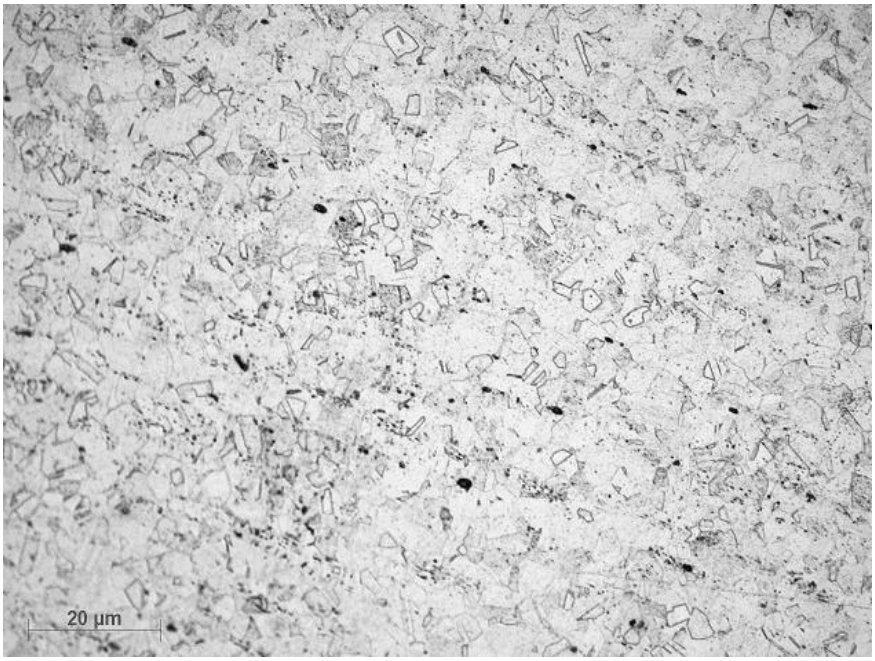

Figure 4.10. Optical micrograph of 316 austenitic stainless steel, showing austenite grains, electrochemically etched with10g oxalic acid in distilled water.

Figure 4.11 shows the optical micrograph of as-received 2101 lean duplex stainless steel. The ferrite was coloured dark by the 40g NaOH in 100ml distilled water, while the austenite phase was not coloured. The austenite and ferrite showed alternating bands, in the direction of rolling.

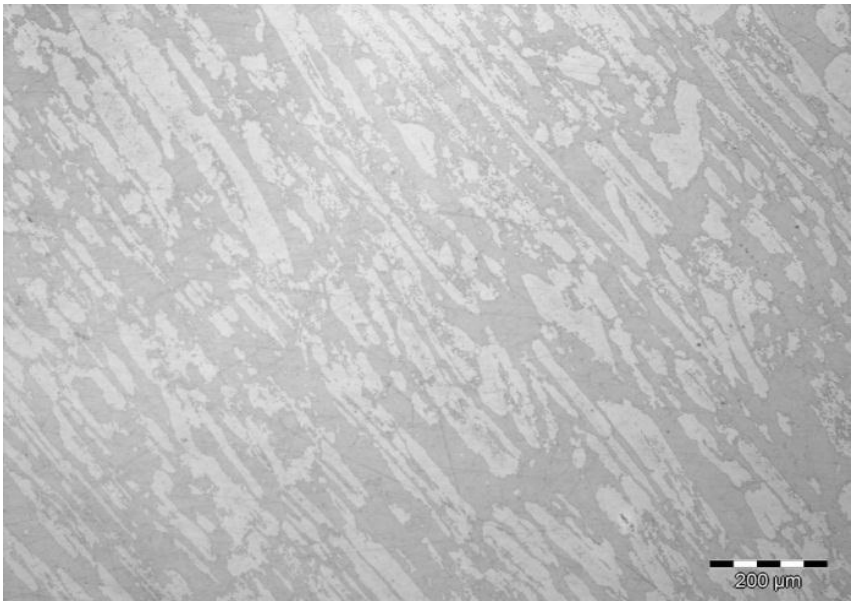

Figure 4.11. Optical micrograph of as-received 2101 DSS showing ferrite (dark) and austenite (light), electrochemically etched with 40g NaOH in 100ml distilled water.

The microstructure revealed in the optical micrograph of 2001 duplex stainless steel by 40g sodium hydroxide in 100ml distilled water is presented in Figure 4.12. The etch coloured ferrite dark and austenite white; these two phases were the only phases observed. The very dark spots were porosity.

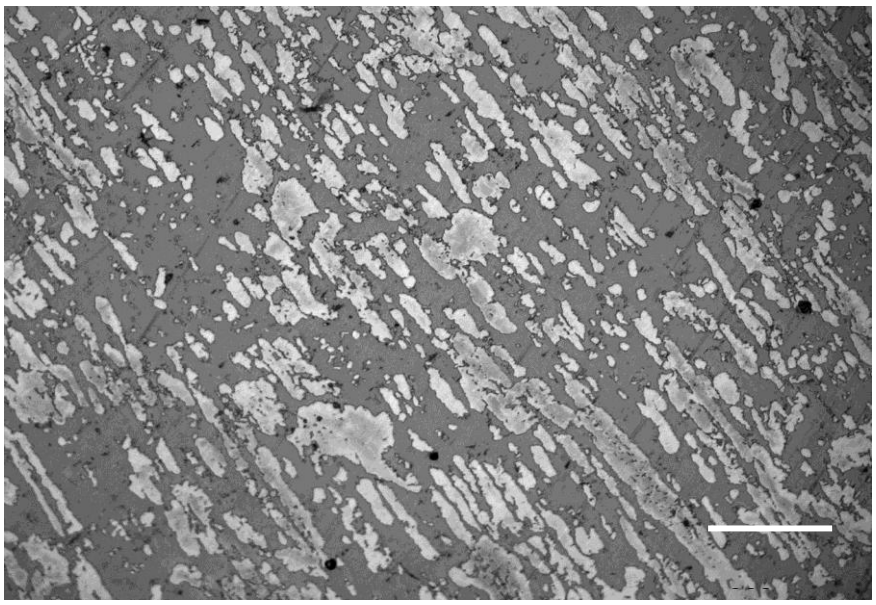

Figure 4.12. Optical micrograph of as-received 2001 DSS showing ferrite (dark) and austenite (light), electrochemically etched with 40g sodium hydroxide in 100ml water. Micron marker represents 200µm.

The optical micrograph of the as-received 2205 duplex stainless steel is presented in Figure 4.13, showing alternating bands of austenite and ferrite. The phases were elongated along the rolling direction.

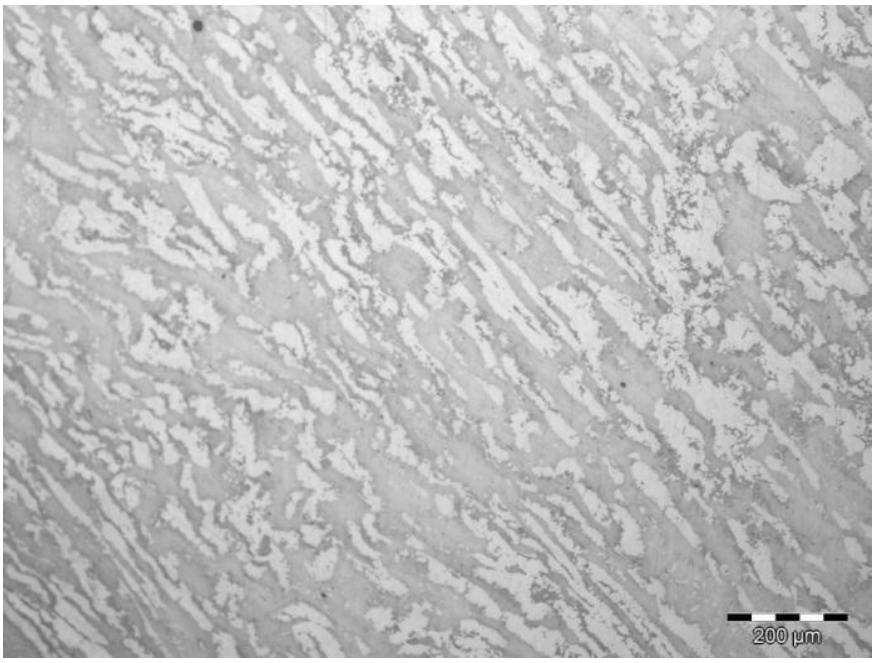

Figure 4.13. Optical micrograph of as-received SAF 2205 DSS showing ferrite (dark) and austenite (light), etched electrochemically with 40g NaOH in 100ml distilled water .

An optical micrograh of 2507 duplex stainless steel is shown in Figure 4.14. Two distinct phases were revealed: austenite and ferrite. They were in alternating bands.

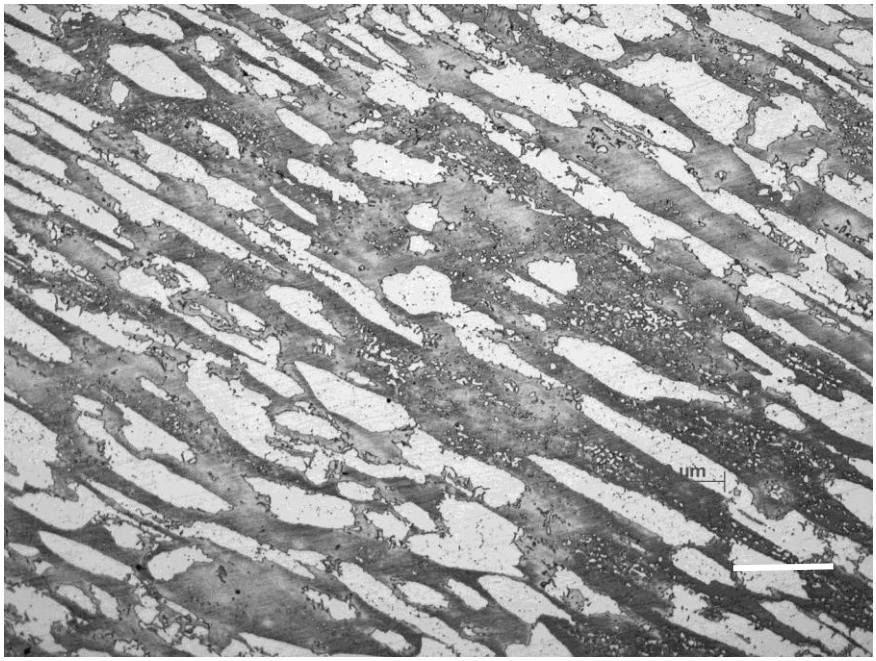

Figure 4.14. Optical micrograph of 2507 DSS showing ferrite (dark) and austenite (light), etched with 40g NaOH in100ml distilled water. Micron marker represents 100µm.

Figure 4.15 shows the optical micrograph of the heat treated 2101 ruthenium-free sample, showing the grain boundaries with the austenite deposited along them. The dark round particles were austenite dispersed in a matrix of ferrite. The austenite and ferrite ratio was 16.0±8.0:84.0±8.0.

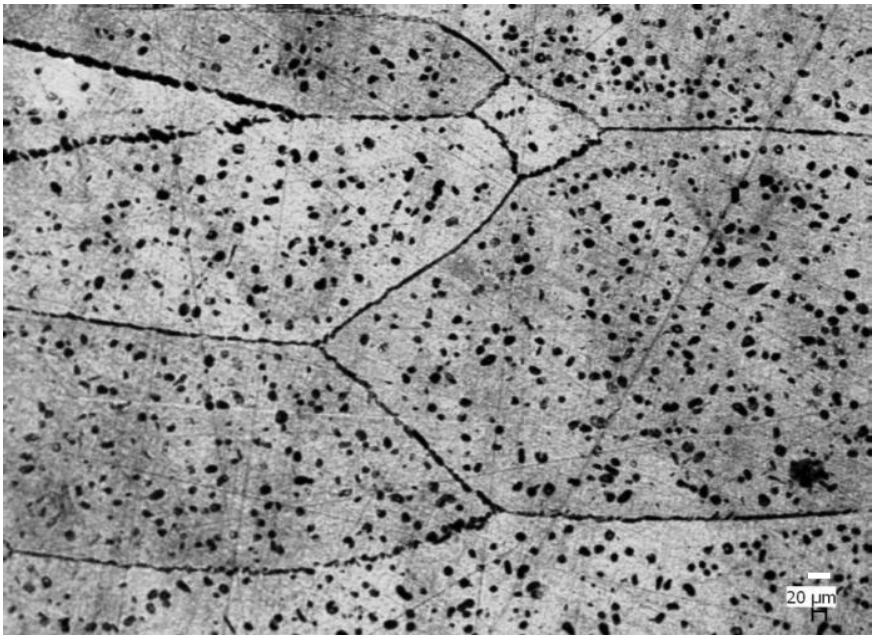

Figure 4.15. Optical micrograph of the 2101 Ru-free sample annealed for 10 minutes at 1080°C and rapidly cooled to room temperature, electrochemically etched with 40g NaOH in 100ml water, showing austenite in ferrite matrix. Micron marker represents 20µm.

Figure 4.16 shows an optical micrograph of the 2101 sample without ruthenium, consisted of randomly dispersed austenite particles in a matrix of ferrite, and some precipitates were formed along the grain boundaries. The volume fraction was 72:28 ferrite:austenite.

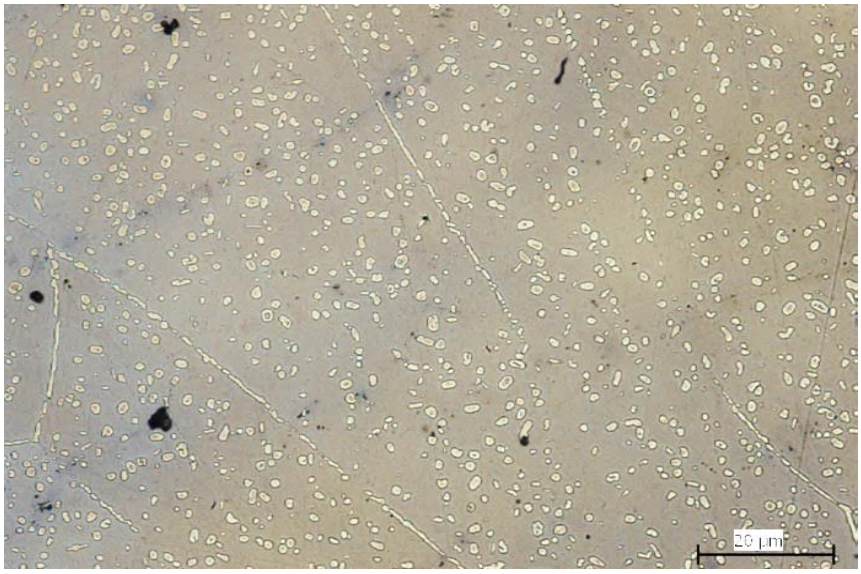

Figure 4.16. Optical micrograph of 2101 sample without ruthenium, annealed at 1080°C for 120 minutes and rapidly cooled to room temperature, etched with 40g NaOH in 100ml distilled water. The lighter particles are austenite dispersed in a matrix of ferrite.

Figure 4.17 shows an optical micrograph of 2101-0.1wt% Ru. The austenite phase was dispersed in the matrix of ferrite; the austenite particles were small, and they were randomly dispersed within grains, and along some of the grain boundaries. The austenite was finer along the grain boundaries and formed fairly continuous precipitates there. No intermetallic phase was observed. The volume fraction of austenite was 21.3±4.1.

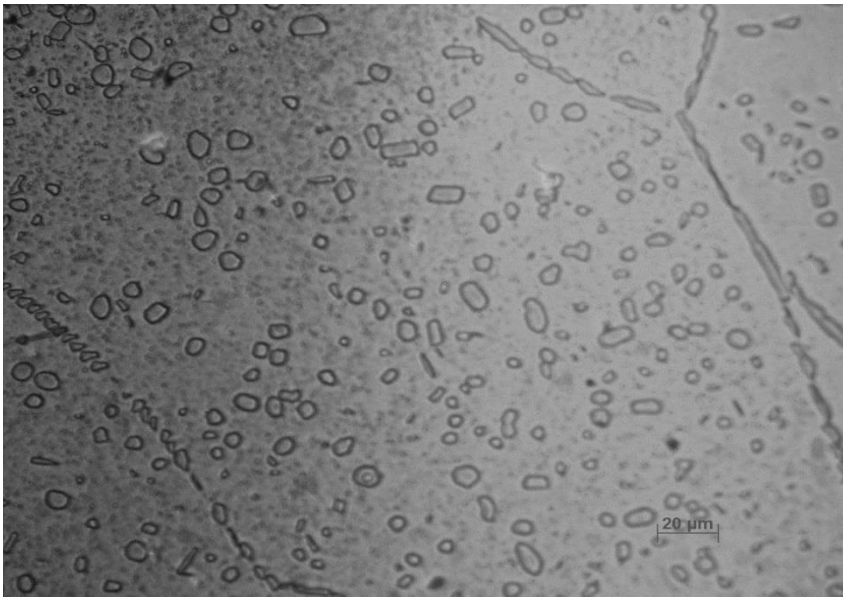

Figure 4.17. Optical micrograph of the 2101 sample with 0.1 wt% Ru annealed for 90 minutes at 1080°C and cooled rapidly in water, showing austenite particles in a ferrite matrix.

Figure 4.18, the optical micrograph of the 2101 sample with 0.15wt% Ru, shows the microstructure had austenite particles growing at the grain boundaries and some were dispersed in the ferrite grains. Inside the ferrite grains, the austenite was fairly round, but they were joined together on some of the grain boundaries, forming ‘decorated grain boundaries’. There were also light particles with irregular interfaces, which were not identified. The volume fraction was 34.9:66.1 austenite:ferrite.

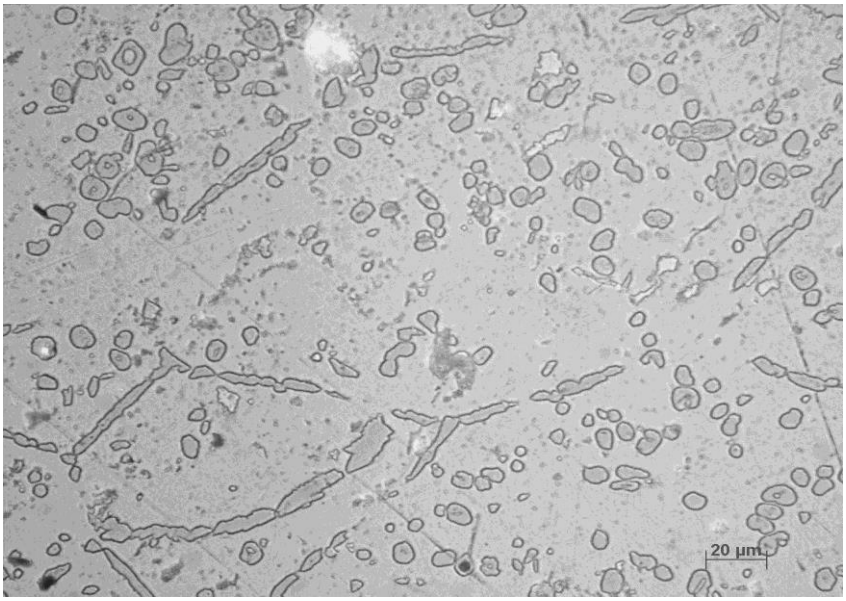

Figure 4.18. Optical micrograph of the 2101 sample with 0.15 wt% Ru annealed for 90 minutes at 1080°C and rapidly cooled, showing austenite (dark) and ferrite (light).

The microstructure of nominal composition of 0.2 wt% Ru in 2101 sample (Figure 4.19) shows the austenite phase as discrete particles, randomly dispersed in the ferrite matrix. The austenite was smaller along the grain boundaries and were joined together to form near continuous precipitation. The volume fraction of austenite was 22.4±6.0.

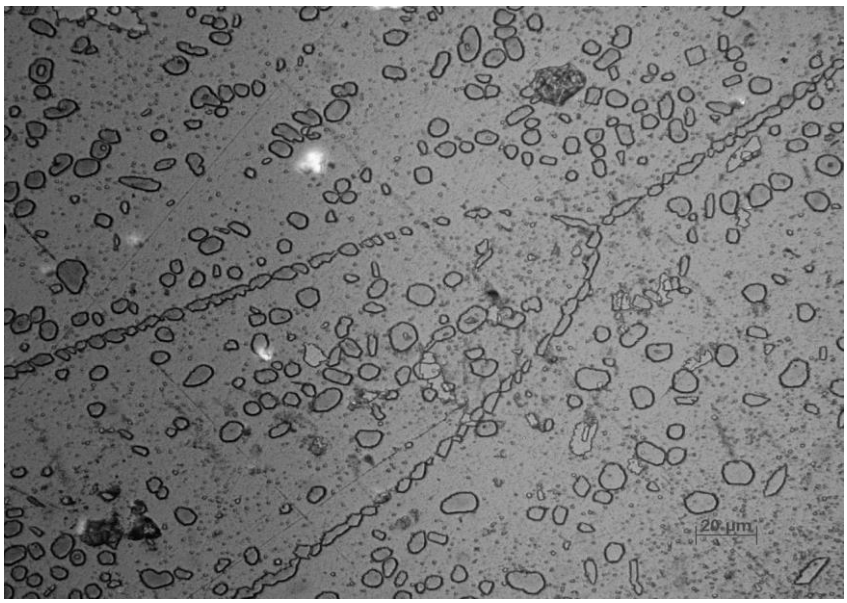

Figure 4.19. Optical micrograph of the 2101 sample with 0.2 wt% Ru (a) annealed for 90 minutes at 1080°C and rapidly cooled, etched with 40g NaOH in 100ml distilled water, showing austenite (light), ferrite (dark). Micron marker represents 20µm.

The microstructure of the 2101 sample with 0.2 wt% Ru (Figure 4.20) shows the austenite particles as fairly round, dispersed in ferrite matrix. The grain boundaries were all decorated with austenite. The austenite proportion had increased with increasing soaking time. The volume fraction of austenite was 30.7±2.3.

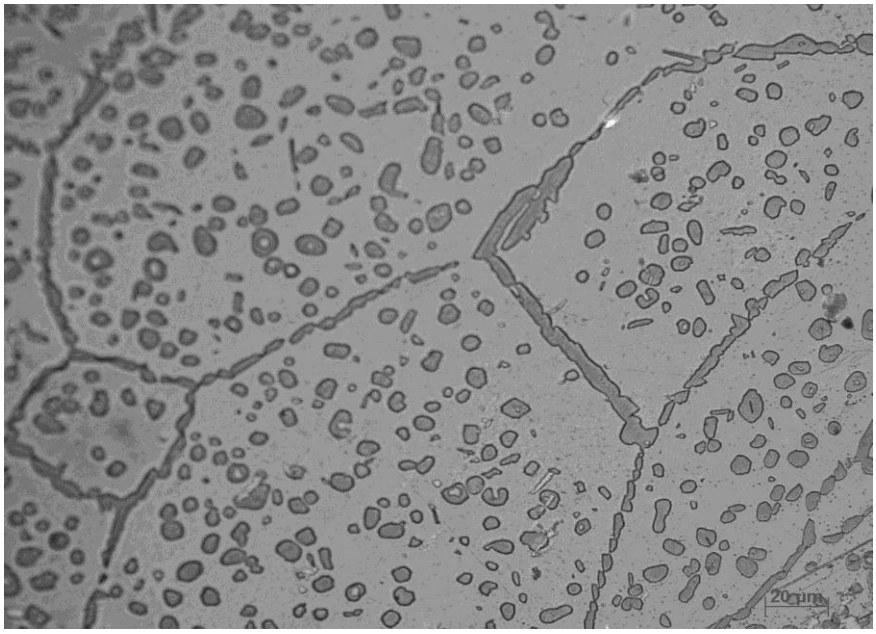

Figure 4.20. Optical micrograph of the 2101 sample with 0.2wt% Ru (b) annealed at 1080°C for 90 minutes and rapidly cooled, etched with 40g NaOH showing ferrite (light) and austenite (dark).

Figure 4.21 shows the microstructure of the 2101 sample with 0.2wt% Ru annealed at 1100°C for 120 minutes, which was very different from the previous micrographs. There was a higher amount of austenite, and while the ferrite grains were less coarse, the austenite was more coarse and fewer than in the sample annealed at 1080°C (Figure 4.20). The volume fraction of austenite was 30.7±9.2.

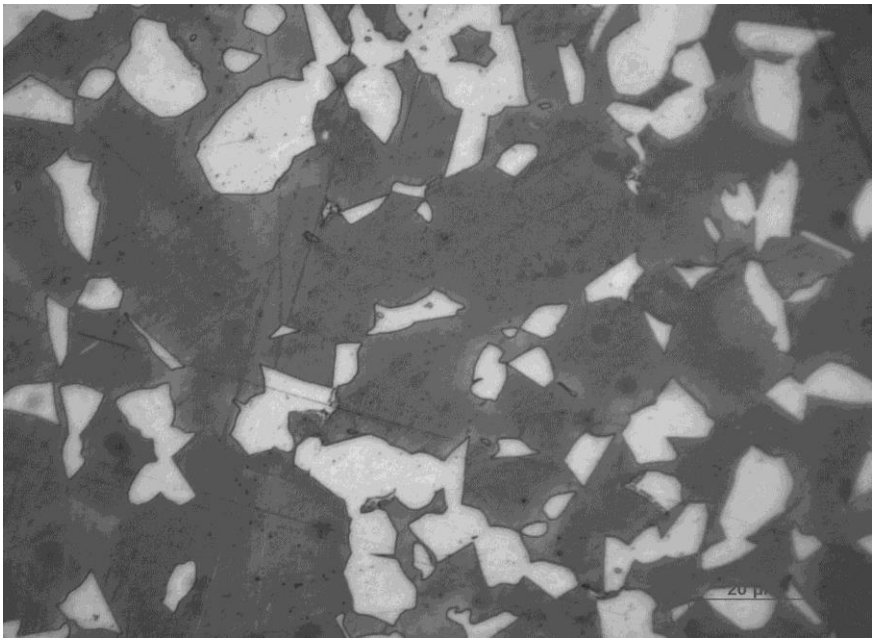

Figure 4.21. Optical micrograph of 2101-0.2 wt% Ru annealed at 1100°C for 120 minutes, electrochemically etched in 40g NaOH in 100ml water, revealing austenite (light) and ferrite (dark).

The 2101 sample with 0.2 wt% Ru was heat treated at 1080°C (Figure 4.22) because Thermo-Calc showed that this was the highest temperature at which the 50:50, austenite:ferrite phase could be obtained. At higher temperature there is more diffusion, and there is much more chance for the desired microstructure to be obtained. The temperature 1100°C was chosen because the duplex structure is expected at these temperature and the diffusion would be quicker, although it might not give 50:50 ratio, while 1080°C is expected to give exactly 50:50 austenite to ferrite ratio.

The optical micrograph of 2101-0.2wt% Ru in Figure 4.22 revealed two phases, austenite and ferrite. The austenite particles were homogenously distributed in the ferrite matrix. The 10g oxalic acid was used to reveal the phases, but the sodium hydroxide produced the best result. The volueme fraction of austenite was 51.0±2.0.

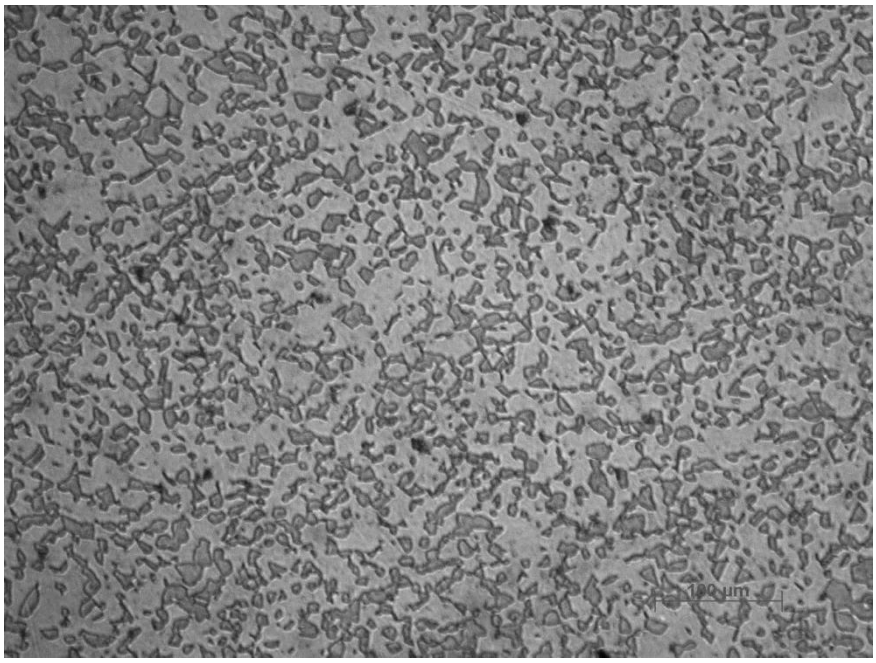

Figure 4.22. Optical micrograph of 2101-0.2 wt% Ru annealed at 1080°C for 120 minutes, electrochemically etched with 10g oxalic acid in 100ml distilled water, showing austenite (dark) and ferrite (light). Micron marker represents 100µm.

Figure 4.23 shows a dark phase in a matrix of the light phase: austenite in ferrite matrix. The austenite had very rounded interfaces. The phase proportion of austenite and ferrite were amost equal, and this was different from the previous microstructure at that temperature. However, the distribution of the phases was not homogeneous.

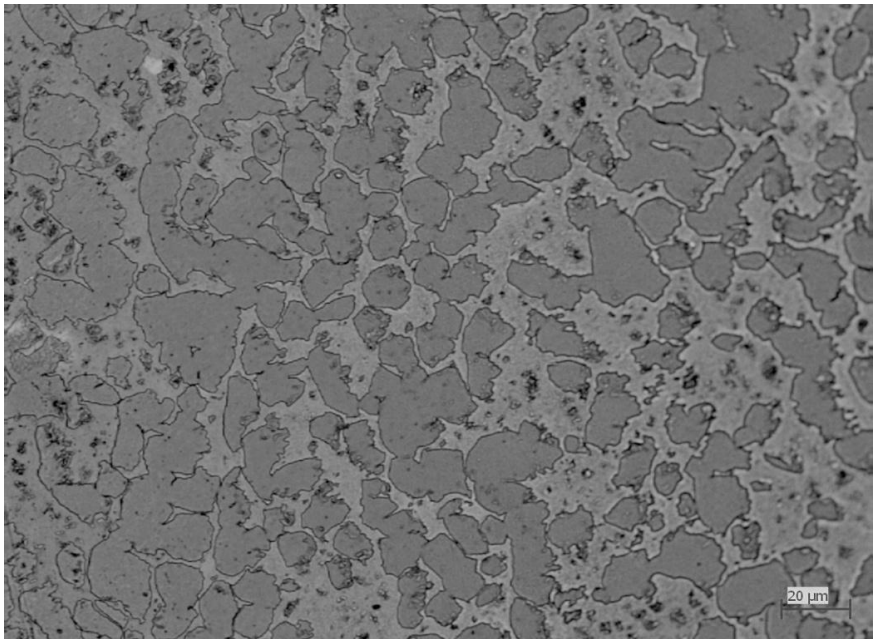

Figure 4.23. Optical micrograph of 2101-0.2 wt% Ru annealed at 1080°C for 90 minutes, etched electrochemically by 40g NaOH in 100ml distilled water, showing austenite (dark) and ferrite (light). The volume fraction was 59:41 austenite:ferrite.

Optical micrographs showing of 2101-2.5 wt% Ru are shown in Figure 4.24. The austenite particles were roundish, with some facetted interfaces, and dispersed throughout the microstructure. The ferrite structure was revealed in the micrograph, with coarse austenite on the ferrite boundaries (Figure 4.24(a)). Murakami's etch was used to reveal the ferrite, but the sodium hydroxide etch produced the best results.

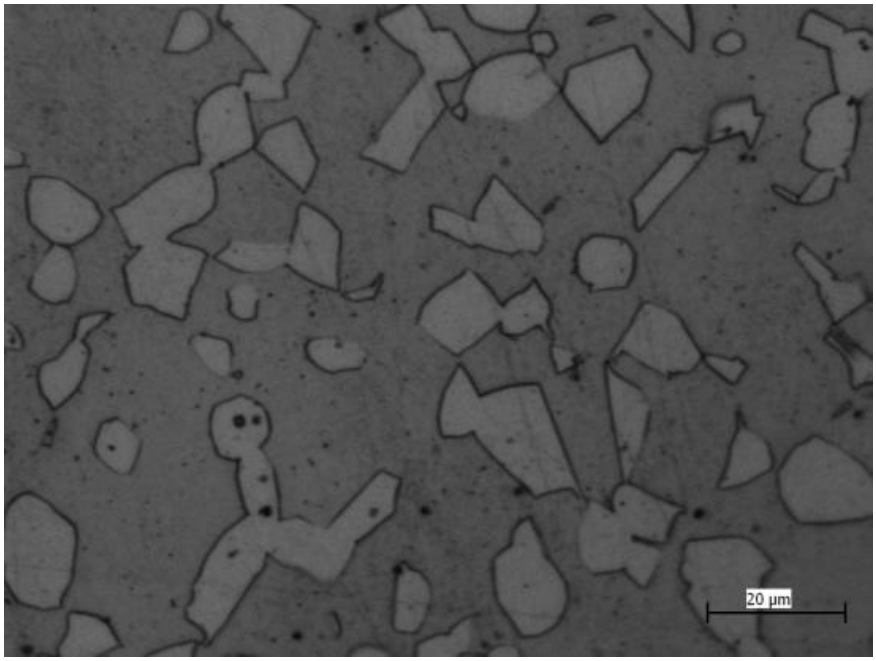

Figure 4.24(a). Optical micrograph of 2101-2.5wt% Ru heat treated at 1080°C for 120 minutes, showing austenite (light) in ferrite (dark), etched with 40g NaOH in 100ml distilled water.

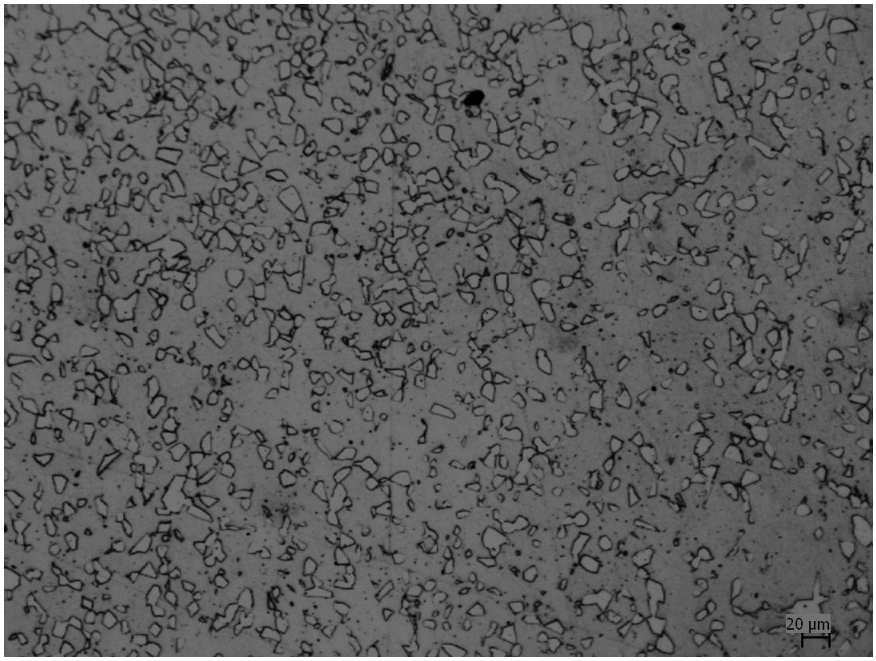

Figure 4.24(b). Optical micrograph of 2101-2.5wt% Ru heat treated at 1080°C for 120 minutes, austenite (light) dispersed in ferrite (dark), etched with Murakami's reagent.

Figure 4.25 shows the microstructure of nominal 2101-10wt% Ru annealed at 1080°C for 120 minutes and rapidly cooled to room temperature. There were apparently four different contrasts observed with optical microscopy, but with scanning electron microscopy (Figure 4.42), only two contrasts were observed. These were ferrite (darker) and hcp (lighter), where the matrix was ferrite.

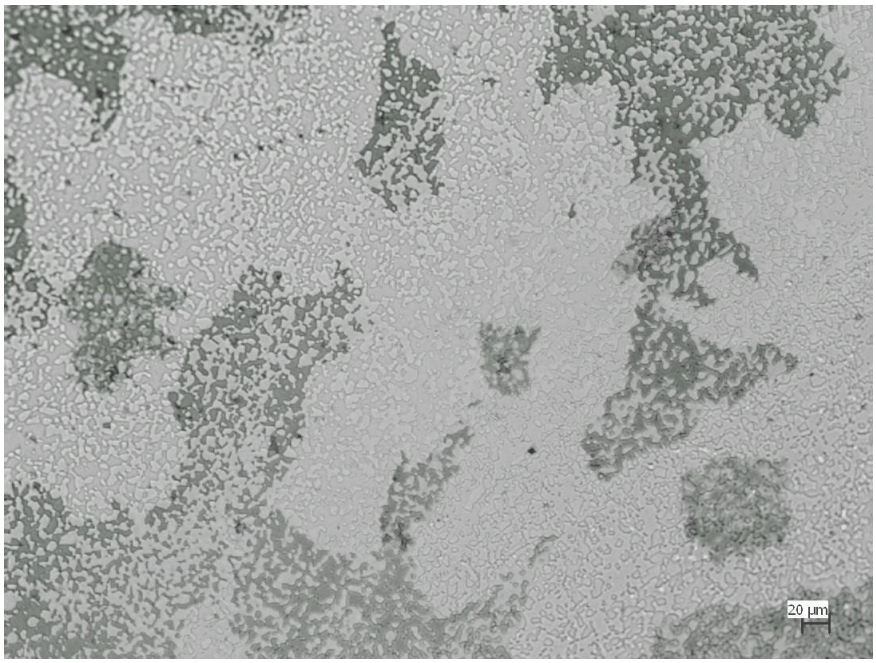

Figure 4.25. Optical micrograph of 2101-10wt% Ru annealed at 1080°C for 120 minutes, etched electrochemically by 40g NaOH in 100ml distilled water, and showing four apparent contrasts, showing hcp in a ferrite matrix.

4.5 SEM and EDX results

4.5.1 SEM images of as-received samples

SEM analysis was done using a high resolution scanning electron microscope (HR-SEM), mainly in back-scattered electron mode. The SEM micrographs obtained in BSE for 2101, 2001, 2205 and 2507 are shown in Figures 4.26 - 4.30.

Figure 4.26 shows 316 stainless steel, the microstructure was austenite. Some porosity was observed.

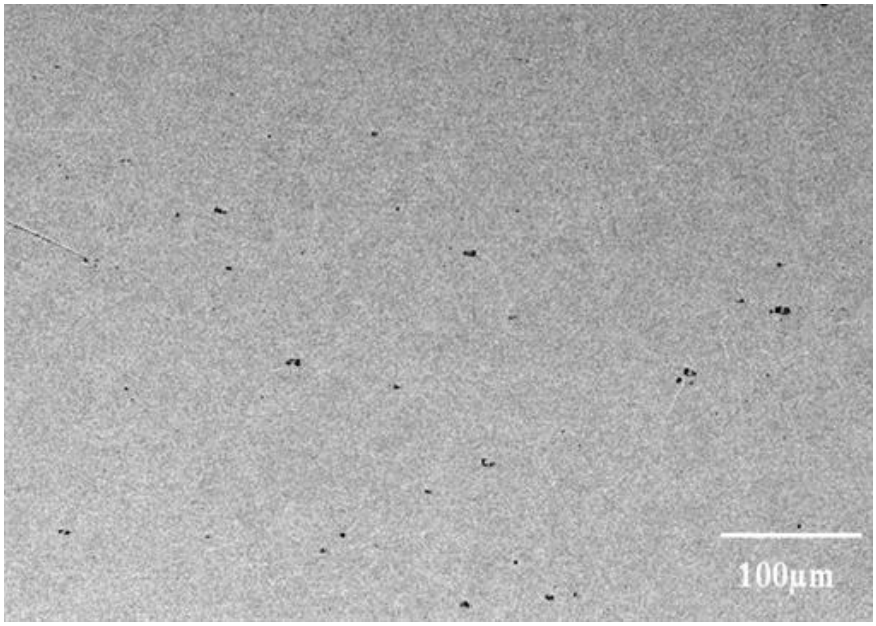

Figure 4.26. Type 316 stainless steel showing austenite grains, and porosity etched with 10g oxalic acid in 100ml distilled water.

The SEM micrograph of as-received 2101 is presented in Figure 4.27 showing austenite in a ferritic matrix. The austenite particles showed irregular interfaces.

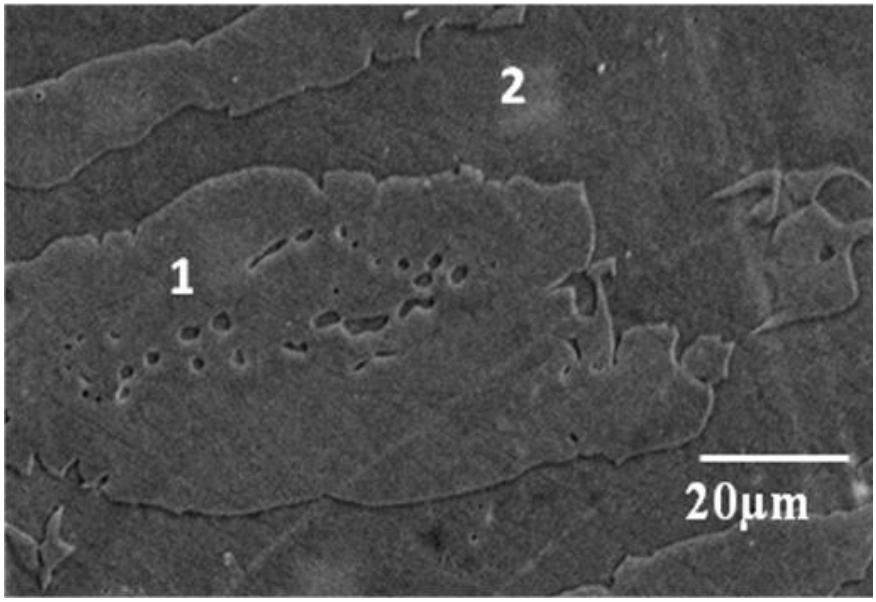

Figure 4.27. BSE- SEM micrograph of as-received 2101 DSS showing ferrite (dark, 2), austenite (light, 1), etched with 40g NaOH in 100ml distilled water.

Figure 4.28 shows the backscattered electron SEM image of 2001 DSS showing coarse austenite in a matrix of ferrite. The interfaces of the austenite were irregular.

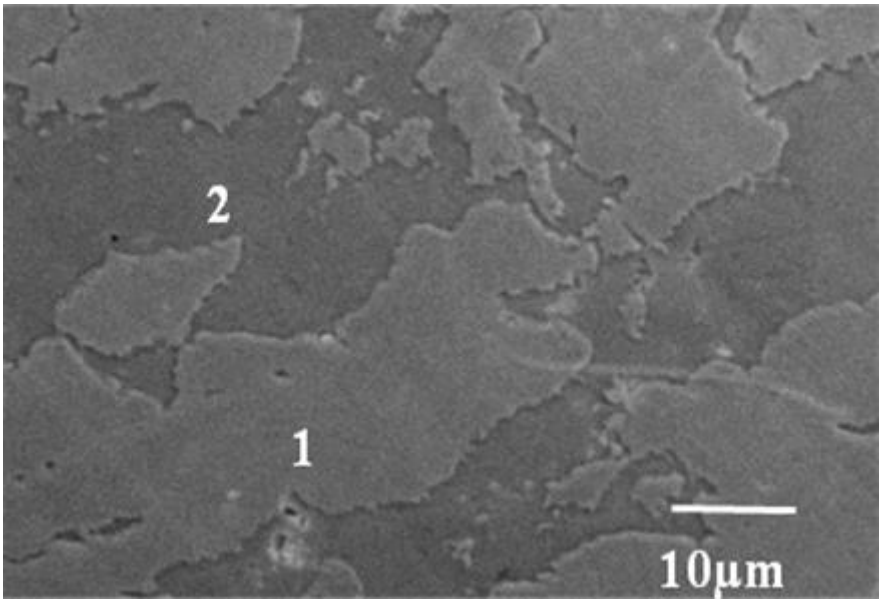

Figure 4.28. SEM- BSE micrograph of as-received 2001 DSS showing austenite (1) and ferrite (2) etched with 40g sodium hydroxide in 100ml distilled water.

The SEM image of 2205 duplex stainless steel is presented in Figure 4.29, showing austenite particles randomly dispersed in a matrix of ferrite. Porosity was also observed in the micrograph and the interfaces were irregular.

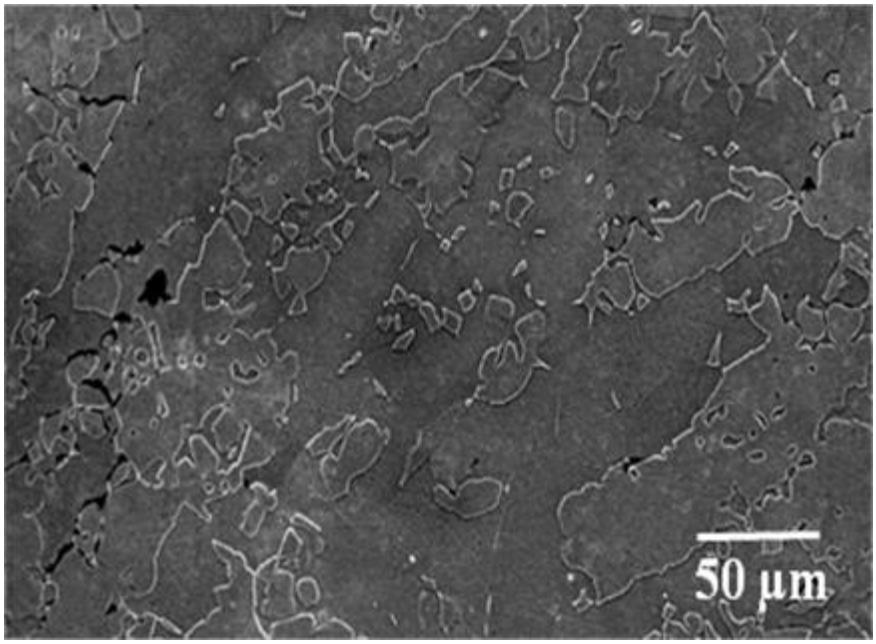

Figure 4.29. SEM-BSE micrograph of as-received 2205 DSS showing ferrite (dark), and austenite (light), etched with 40g NaOH in 100ml distilled water.

Figure 4.30 presents the SEM micrograph of 2507 duplex stainless steel in which alternate bands of austenite and ferrite were observed. Annealing twins in the austenites were also seen and the ferrite grains were usually larger. The phases were difficult to differentiate in the microstructure, although the banding was clearly seen.

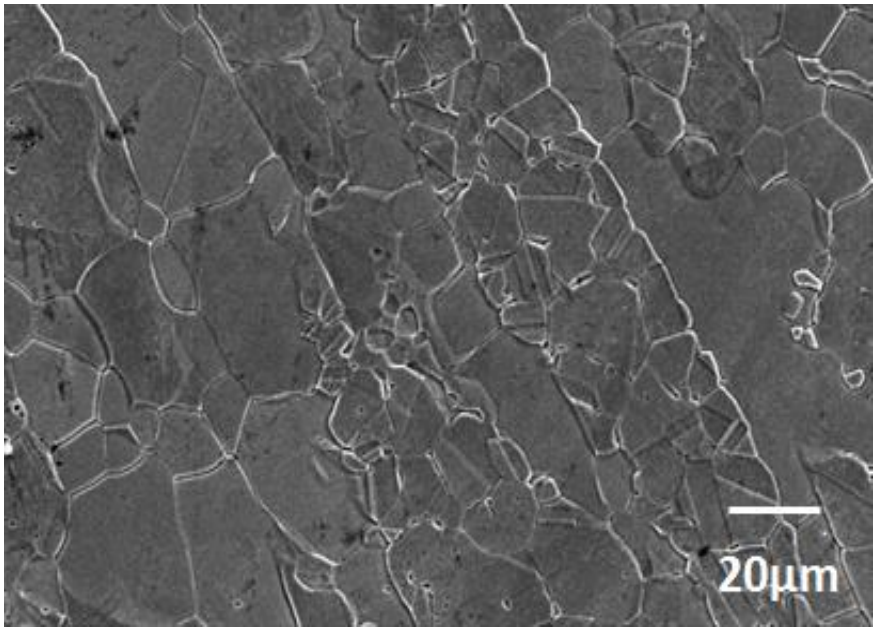

Figure 4.30. BSE-SEM micrograph of as-received 2507 DSS showing ferrite (dark) and austenite (light), etched with 40g NaOH in 100ml distilled water.

4.4.1 SEM images of 2101 with ruthenium samples heat treated at 1080°C

Figure 4.31 shows the austenite phase dispersed in the ferrite matrix. Small precipitates of austenite were also on the grain boundary. The area analyses of the dark and medium regions were similar, which showed they are the same phase. The difference in contrast could be due to sample preparation [2012Van]. The austenite within the grains often had ferrite cores. The interfaces were smoother after annealing. The austenite proportion was 16.0±8.0.

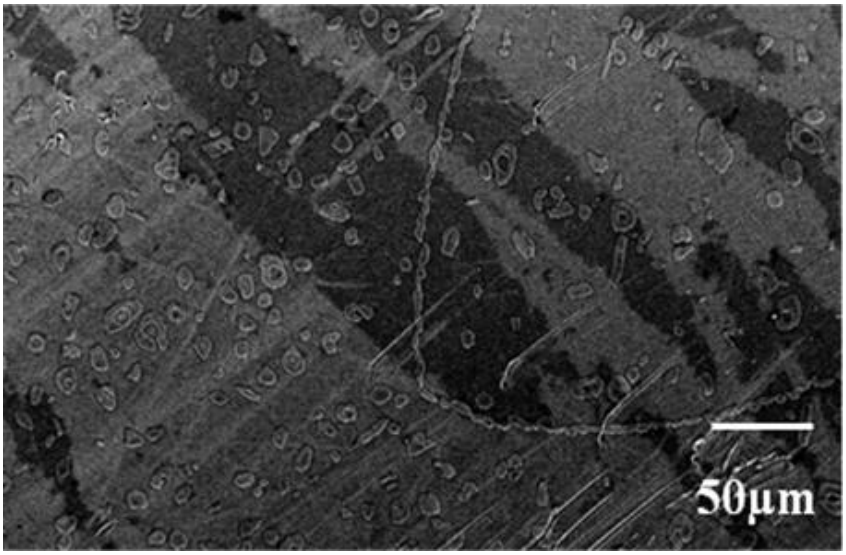

Figure 4.31. SEM-BSE micrograph of heat treated Ru-free 2101 sample annealed for 10 minutes at 1080°C, showing austenite (light) and ferrite (dark), etched with 40g NaOH in 100ml distilled water.

Figure 4.32 shows the SEM–BSE image of a (badly polished) 2101 Ru-free sample soaked for 30 minutes. The austenite phase was randomly dispersed in a matrix of ferrite, and formed at the grain boundaries. The austenite proportion was 18.0±2.3%.

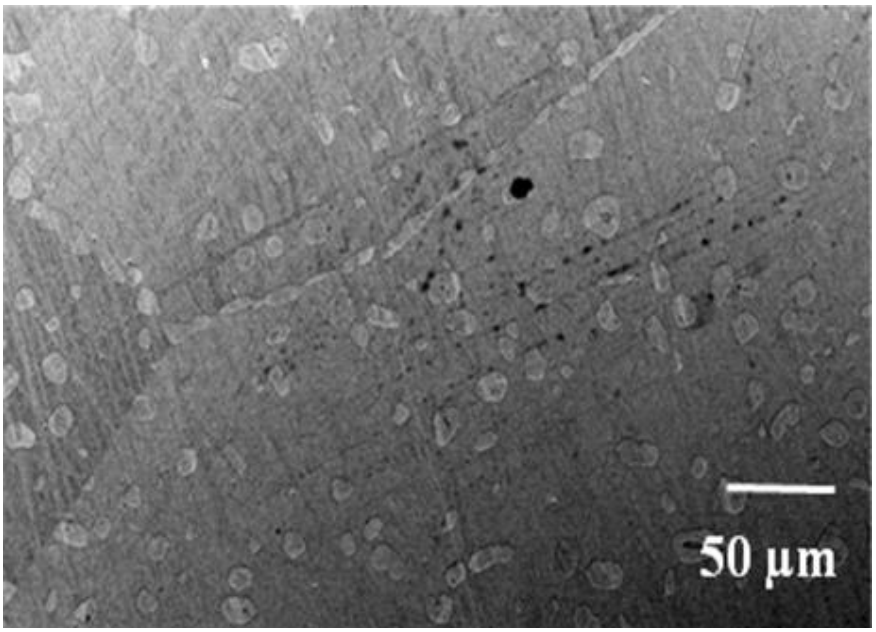

Figure 4.32. SEM-BSE image of Ru-free 2101 heat treated sample annealed for 30 minutes at 1080°C, showing austenite (light) and ferrite (dark) etched with 40g NaOH in 100ml distilled water.

Figure 4.33 shows the SEM–BSE image of the 0.15wt% Ru alloy annealed for 30 minutes. The austenite was randomly dispersed in a matrix of ferrite, as well as forming at the grain boundaries. The austenite within the grains also had a ferrite core. The austenite proportion was 18.7±6.3. The interfaces were smooth.

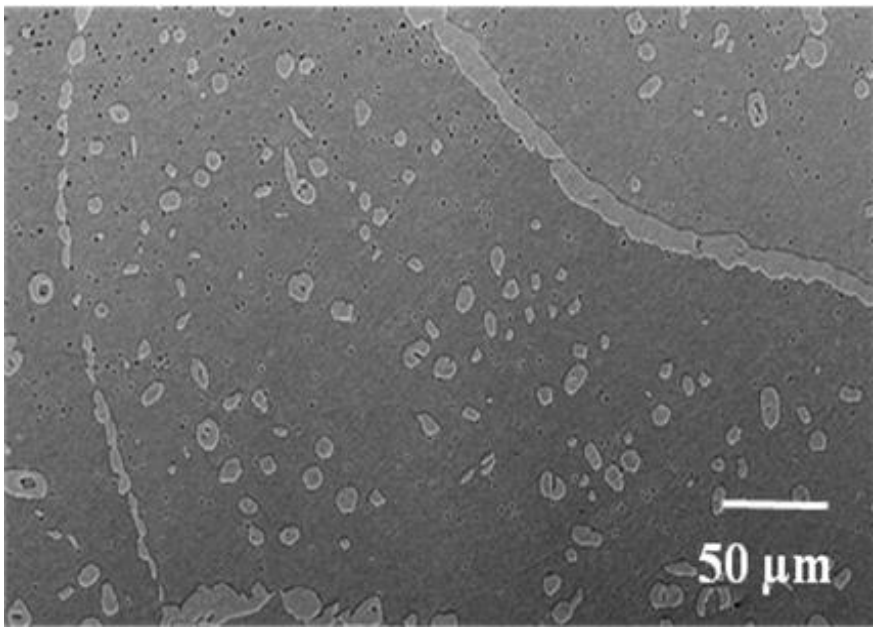

Figure 4.33. SEM-BSE image of heat treated 2101 sample with 0.15 wt % Ru annealed for 30 minutes at 1080°C, showing austenite (light) and ferrite (dark), etched with 40g NaOH in 100ml distilled water.

Figure 4.34 shows the SEM–BSE image of the 2101 with 0.2 wt% Ru sample annealed for 30 minutes. The austenite grew in a matrix of ferrite, and could also be seen growing into the grains from the grain boundaries. The austenite to ferrite ratio was 17:83. The austenite within the ferrite grains had a more complex form, with some enclosed ferrite. The interfaces were smooth.

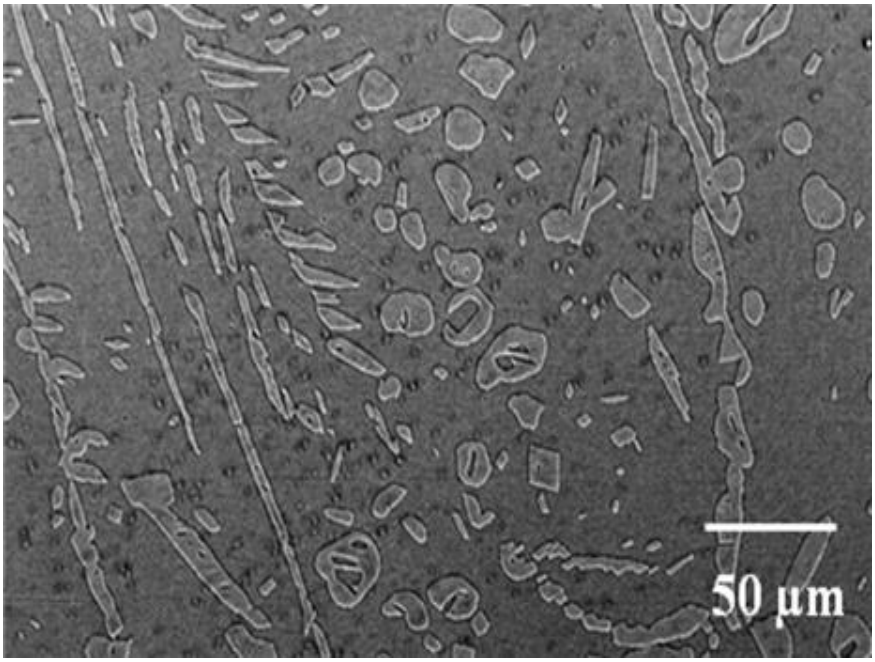

Figure 4.34. SEM-BSE images of heat treated 2101 with 0.2 wt% Ru annealed for 30 minutes at 1080°C: austenite (light), ferrite (dark), etched with 40g NaOH in 100ml distilled water.

For the 2101 Ru-free samples, more austenite was observed for 30 minutes annealing time than for 10 minutes, which shows that as the soaking time increased the volume fraction of austenite increased. Thus, 10 minutes was too short to attain the microstructures required, hence equilibrium was not reached. Therefore, it would have been helpful to investigate the effect of soaking time on the microstructure at 120 minutes, but because of limited samples available this was not done.

Figures 4.35-4.42 present SEM-BSE images of the 2101duplex stainless steel alloyed with various percentages of ruthenium between nominal 0.15 and 10 wt%. The images revealed austenite and ferrite, or ferrite and hcp. The austenite particles were randomly dispersed in the ferrite matrix, and no intermetallic phases were observed. In Figures 4.36 and 4.38, some of the ferrite was enclosed in the austenite grains. The austenite also formed along some of the grain boundaries for some samples. In Figures 4.37, 4.39 - 4.42, the addition of ruthenium did not change the phases formed for up to nominal 2.5 wt%, but at 10 wt% Ru the microstructure contain ferrite and hcp phases, with no austenite, and a ferrite percentage of 49.0±7.5 and hcp 51.0±7.5.

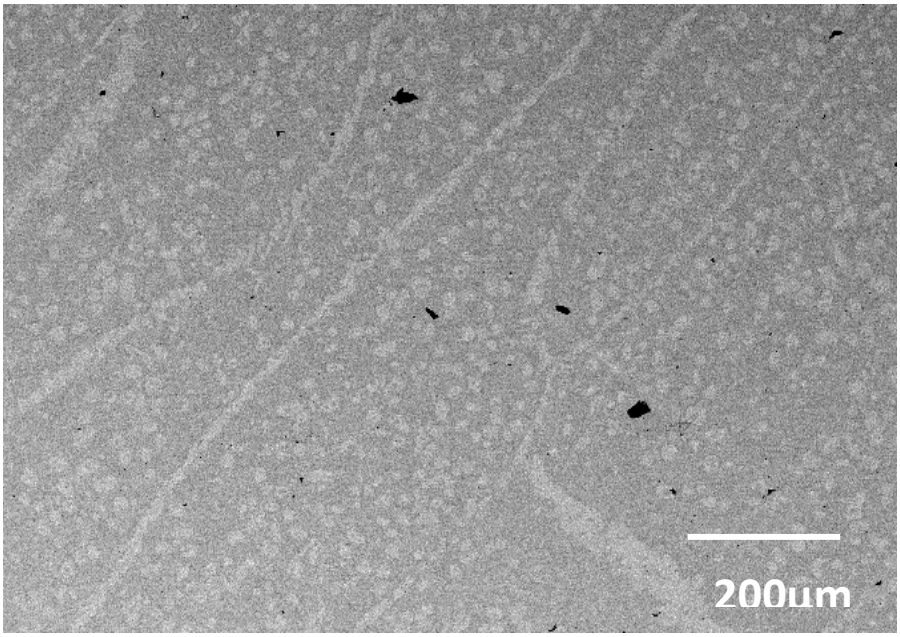

Figure 4.35. SEM–BSE image of 2101 duplex stainless steel containing nominal 0.15 wt% ruthenium, annealed at 1080°C for 120 minutes: austenite (light), ferrite (dark), etched with 40g NaOH in 100ml distilled water.

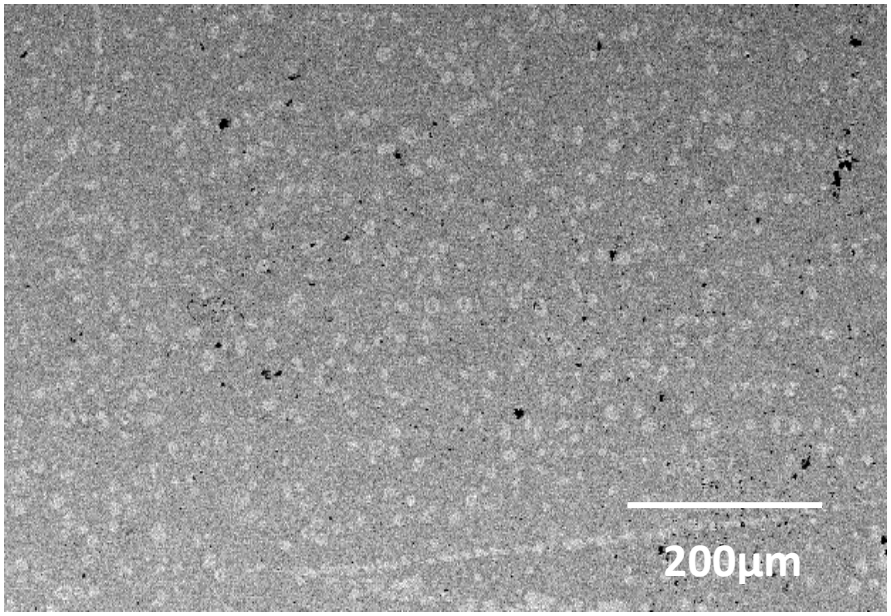

Figure 4.36. SEM–BSE image of 2101 duplex stainless steel containing nominal 0.2 wt% ruthenium, annealed at 1080°C for 120 minutes, showing austenite (light) and ferrite (dark), etched with 40g NaOH in 100ml distilled water.

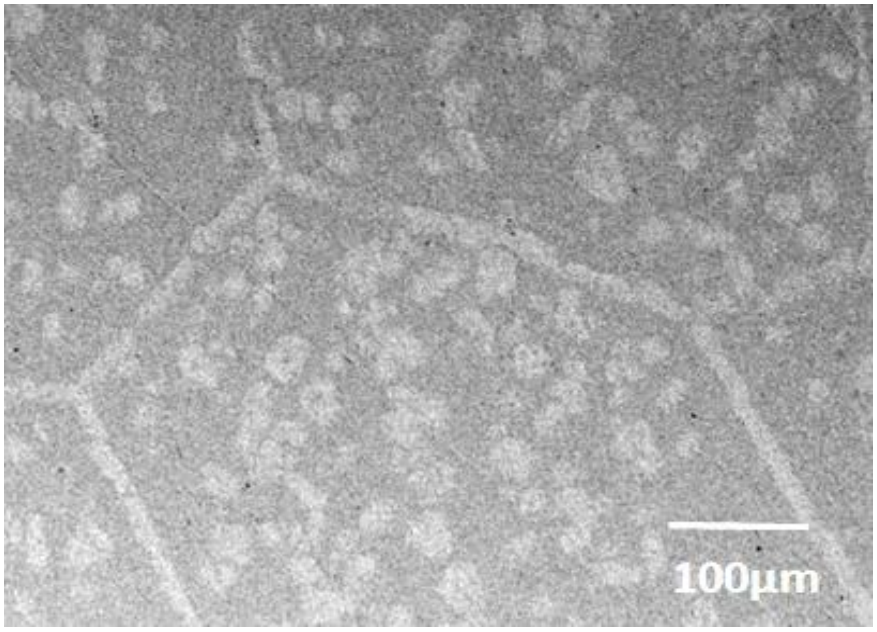

Figure 4.37. SEM–BSE image of 2101 duplex stainless steel containing nominal 0.4 wt% ruthenium, annealed at 1080°C for 120 minutes 40g NaOH in 100ml distilled water, showing ferrite (dark) and austenite (light).

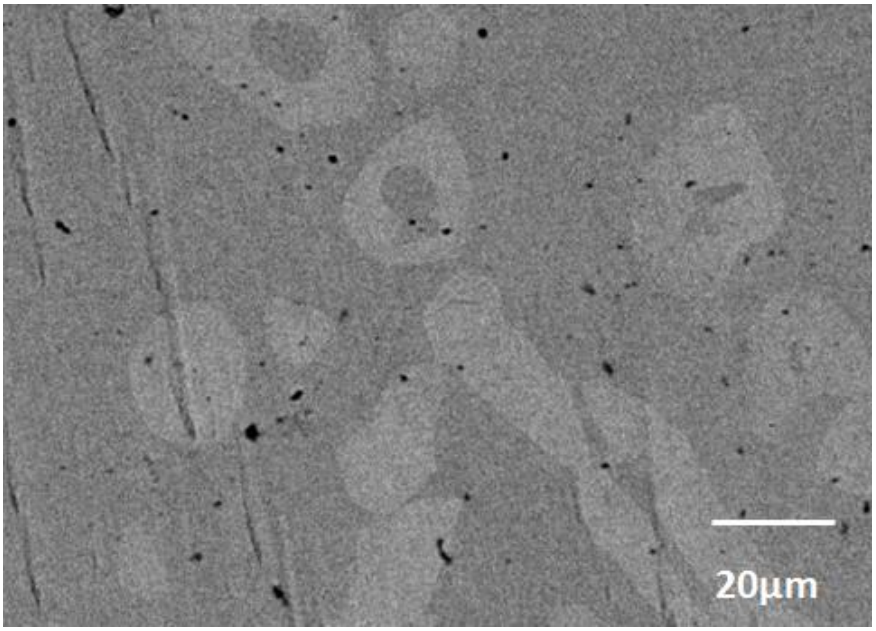

Figure 4.38. SEM–BSE image of 2101 duplex stainless steel containing nominal 0.6 wt% ruthenium, annealed at 1080^{o}C for 120 minutes 40g NaOH in 100ml distilled water, showing austenite (light) and ferrite (dark).

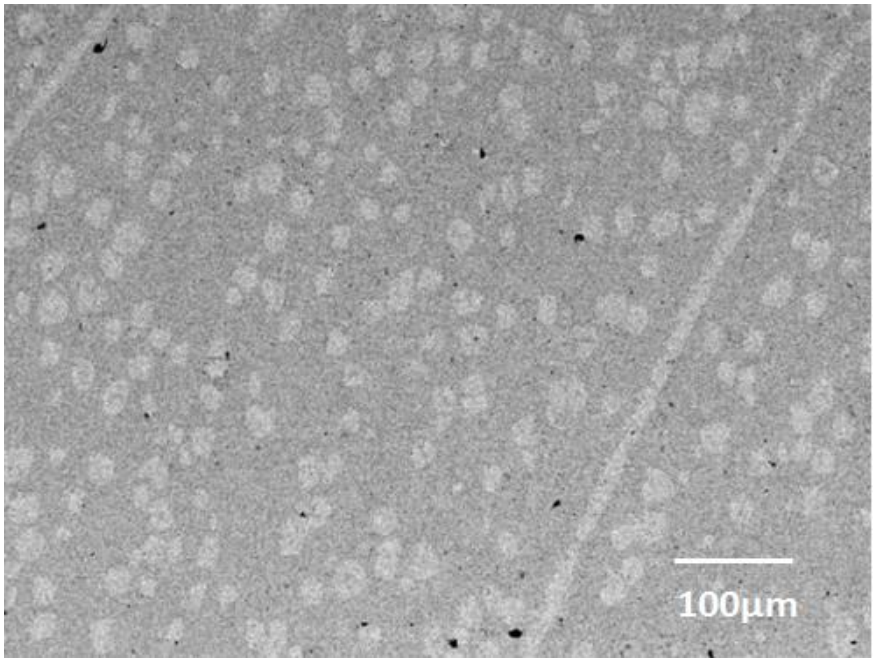

Figure 4.39. SEM–BSE image of 2101 duplex stainless steel containing nominal 0.8 wt% Ru, annealed at 1080°C for 120 minutes, showing austenite (light) and ferrite (dark), etched with 40g NaOH in 100ml distilled water.

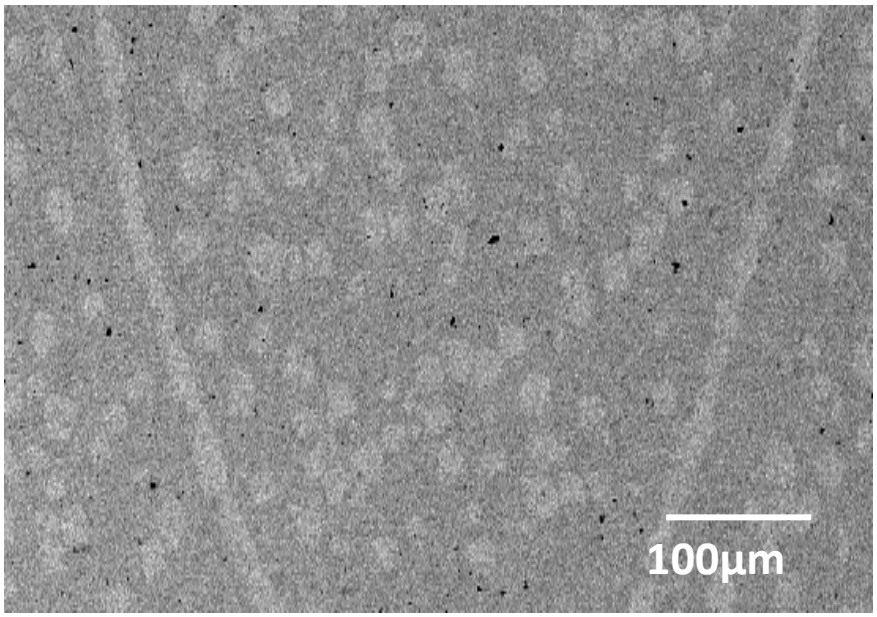

Figure 4.40. SEM–BSE image of 2101 duplex stainless steel containing nominal 1 wt% Ru, annealed at 1080°C for 120 minutes, showing austenite (light) and ferrite (dark), etched with 40g NaOH in 100ml distilled water.

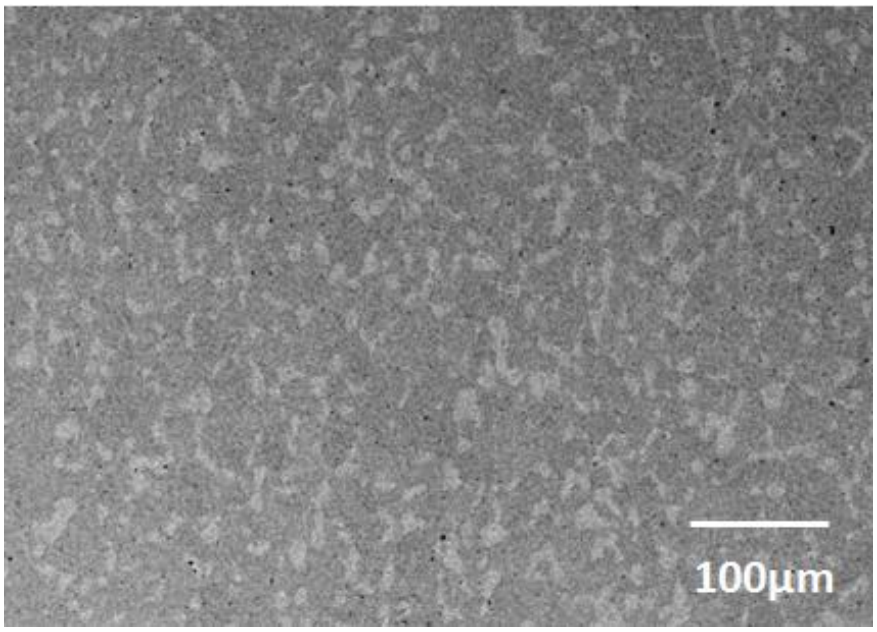

Figure 4.41. SEM–BSE image of 2101 duplex stainless steel containing nominal 2.5 wt% Ru, annealed at 1080°C for 120 minutes, etched with 40g sodium hydroxide in 100ml distilled water, showing austenite (light) and ferrite (dark).

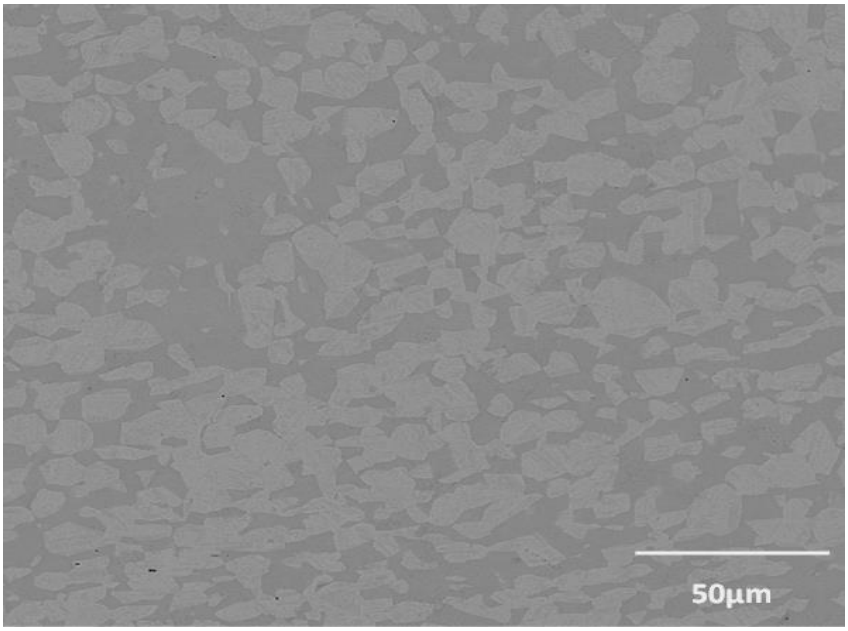

Figure 4.42. SEM–BSE image of 2101 duplex stainless steel containing nominal 10 wt% Ru, annealed at 1080°C for 120 minutes, showing ferrite (dark) and hcp (light), etched with 40g NaOH in 100ml distilled water.

4.5.3 SEM images of samples heat treated at 1100°C

The SEM images of samples heat treated at 1100°C for 120 minutes are presented in Figures 4.43- 4.52. Phases of austenite and ferrites were observed in all the micrographs. The austenite particles were well dispersed in the ferrite matrix and some were formed at the grain boundaries. Porosity was observed in some micrographs and was generally round. The addition of ruthenium did not reveal any significant change in the microstuctures.

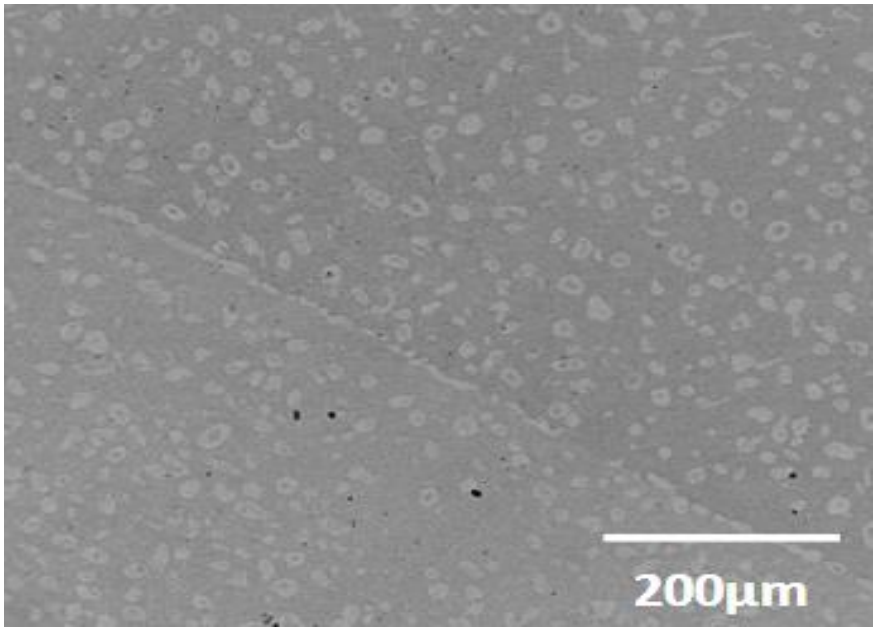

Figure 4.43. SEM–BSE image of 2101 duplex stainless steel containing nominal 0.05 wt% Ru, annealed at 1100°C for 120 minutes, etched with 40g sodium hydroxide in 100ml distilled water revealing austenite (light) and ferrite (medium) phases.

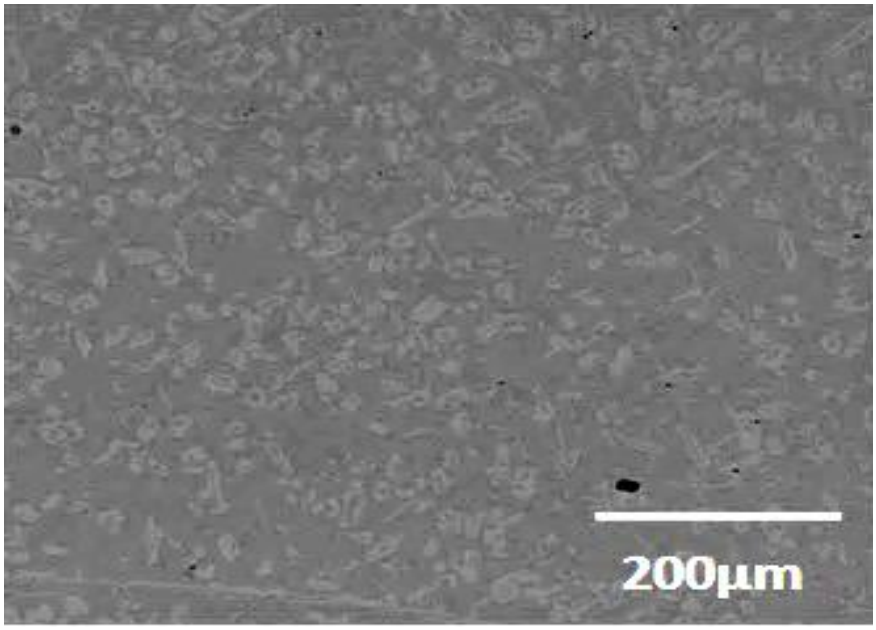

Figure 4.44. SEM–BSE image of 2101 duplex stainless steel containing nominal 0.1 wt% Ru, annealed at 1100°C for 120 minutes, showing austenite (light) and ferrite (dark), etched with 40g NaOH in 100ml distilled water.

Figures 4.35 and 4.45 are the SEM-BSE images of the 2101-0.15 wt% Ru duplex stainless steels annealed at 1080°C and 1100°C for 120 minutes respectively. The austenite was randomly dispersed in the ferrite matrix and some ferrite was enclosed in austenite grains. More austenite was seen at the grain boundaries in the sample annealed at 1080°C than in the sample annealed at 1100°C. The ferrite was coarser at 1100°C than at 1080°C. The volume fraction of austenite on 1080°C was 58.0±8.6, while for 1100°C was 40.0±4.4.

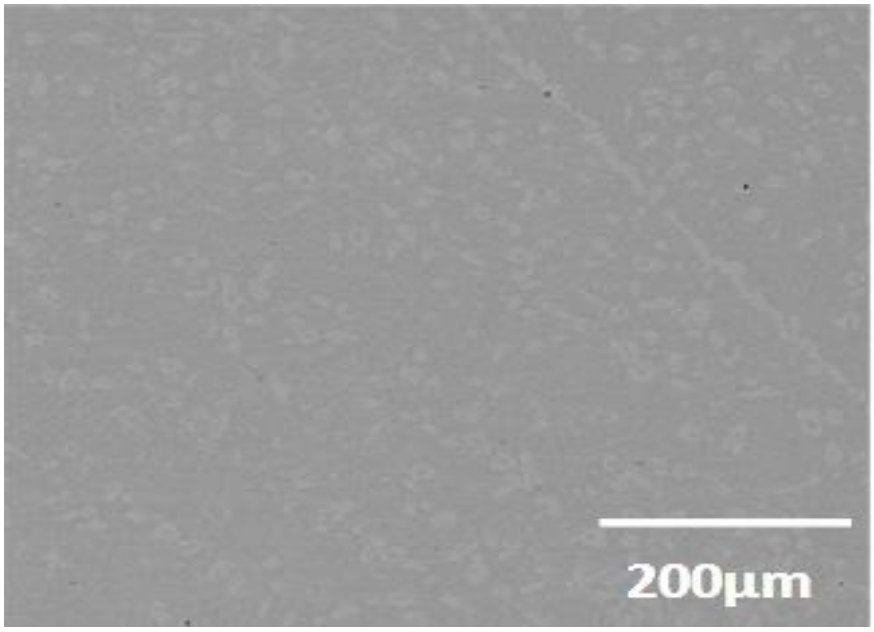

Figure 4.45. SEM–BSE image of 2101 duplex stainless steel containing nominal 0.15 wt% Ru, annealed at 1100°C for 120 minutes, showing austenite (light) and ferrite (dark), etched with 40g NaOH in 100ml distilled water.

The SEM micrograph of 2101-0.2wt% Ru samples annealed at 1080°C and 1100°C for 120 minutes are shown in Figures 4.36 and 4.46 respectively. Austenite was dispersed randomly in the ferrite matrix, and some of the ferrite was enclosed in austenite grains for both temperatures. At 1100°C, the ferrite grain boundaries were continuously decorated with austenite. The volume fraction of austenite at 1080°C was 51.0±2.0, and for 1100°C was 40.7±4.7.

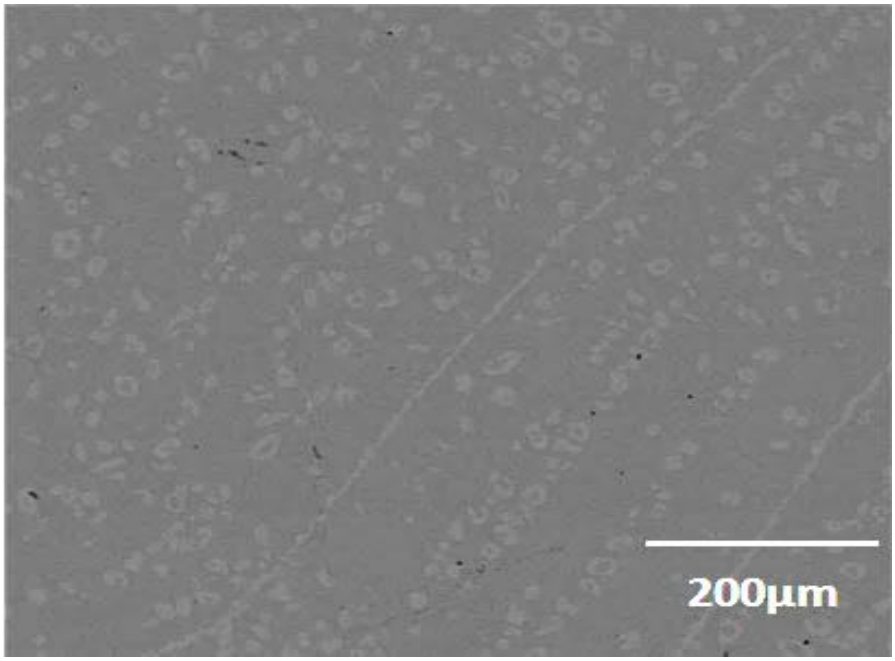

Figure 4.46. SEM–BSE image of 2101 duplex stainless steel containing nominal 0.2 wt% Ru, annealed at 1100°C for 120 minutes, showing austenite (light) and ferrite (dark), etched with 40g NaOH in 100ml distilled water.

The SEM micrographs of 2101-0.4 wt% Ru samples annealed at 1080°C and 1100°C are shown in Figures 4.37 and 4.47. Austenite was randomly dispersed in ferrite matrix, with some austenite formed at the grain boundaries at both temperatures. Ferrite grains were coarser at 1100°C than at 1080°C. The percentage of austenite at 1080°C was 61.0±7.6, which was higher than 40.0±4.2 at 1100°C.

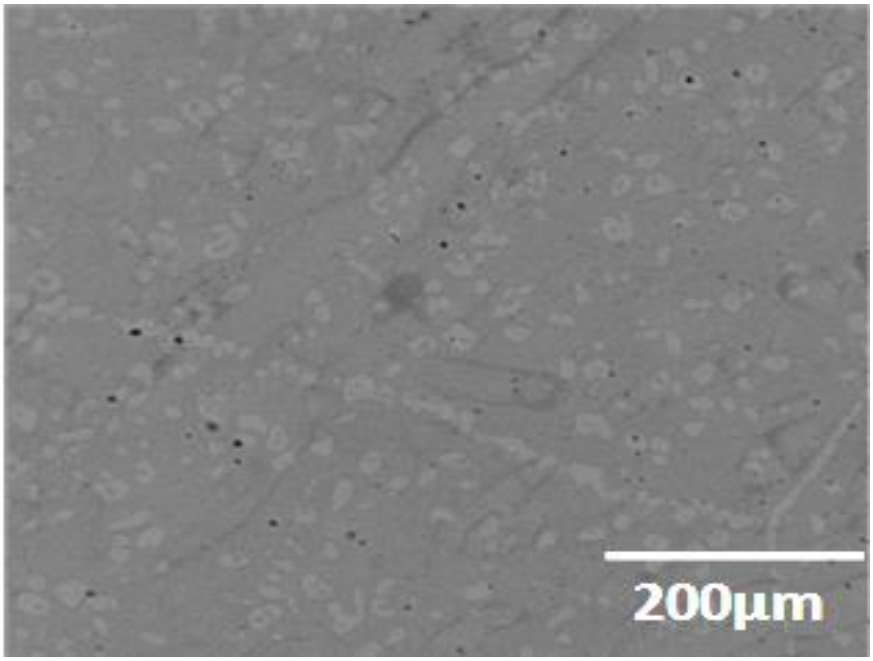

Figure 4.47. SEM–BSE image of 2101 duplex stainless steel containing nominal 0.4 wt% Ru, annealed at 1100°C for 120 minutes, showing austenite (light) and ferrite (dark), etched with 40g NaOH in 100ml distilled water.

Figures 4.38 and 4.48 present the SEM micrographs of 2101-0.6wt% Ru samples annealed at 1080°C and 1100°C for 120 minutes respectively. Ferrite was occasionally enclosed in austenite grains in the ferrite matrix. Austenite grains were dispersed randomly in the ferrite, and some austenite also formed on the grain boundaries. The volume fraction of austenite at 1080°C was 51.0 ±6.0while at 1100°C it was 37.0±8.8.

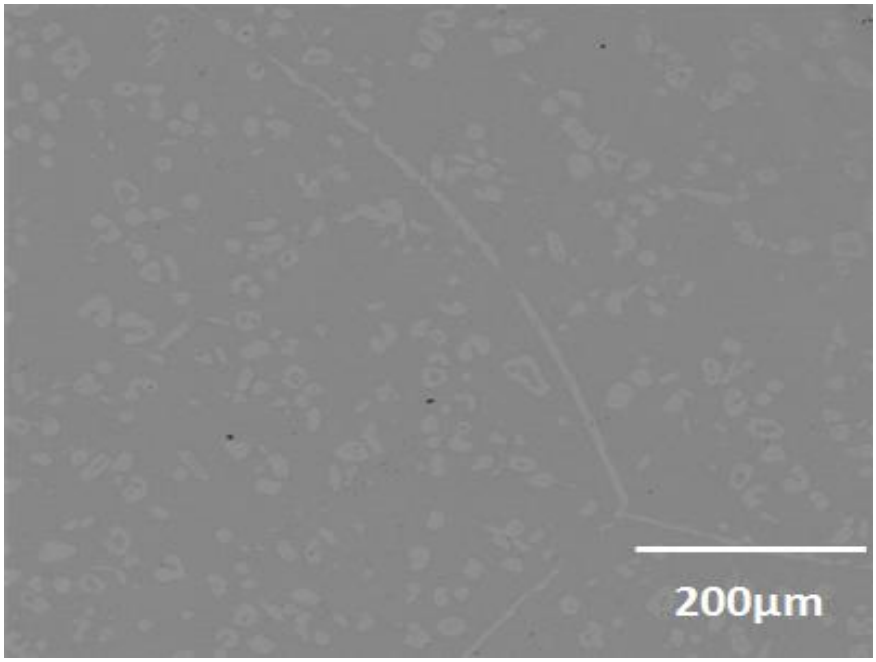

Figure 4.48. SEM–BSE image of 2101 duplex stainless steel containing nominal 0.6 wt% Ru, annealed at 1100°C for 120 minutes, showing austenite (light) and ferrite (dark), etched with 40g NaOH in 100ml distilled water.

For the 2101-0.8 wt% Ru samples in Figures 4.39 and 4.49, annealed at 1080°C and 1100°C respectively, austenite was randomly dispersed in ferrite, and some also formed at the grain boundaries. Austenite was coarser at 1080°C than at 1100°C. The percentages of austenite present at 1080°C and 1100°C were 69.0±5.0 and 38.0±8.3 respectively.

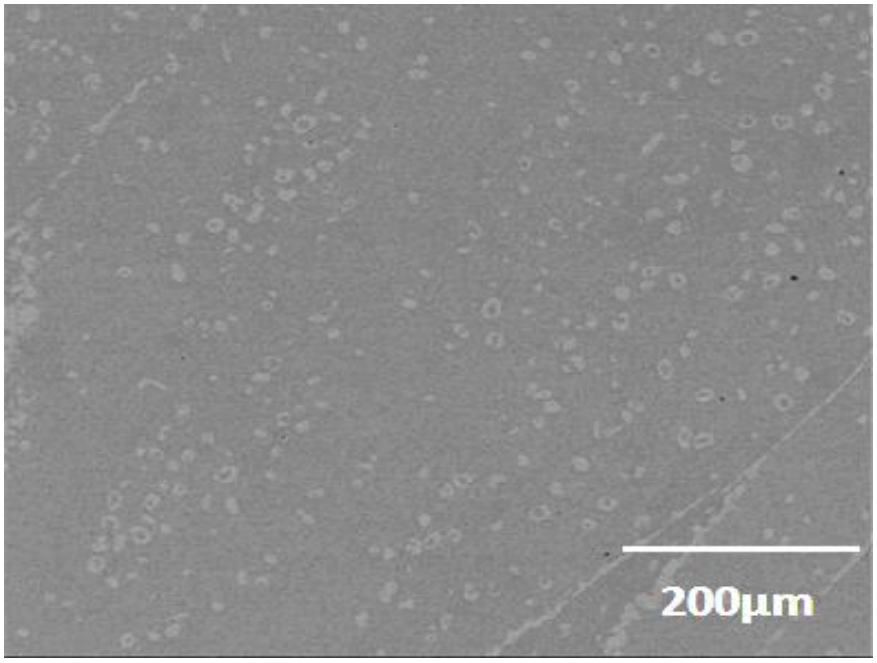

Figure 4.49. SEM–BSE image of 2101 duplex stainless steel containing nominal 0.8 wt% Ru, annealed at 1100°C for 120 minutes, showing austenite (light) and ferrite (dark), etched with 40g NaOH in 100ml distilled water.

Similar to the other samples, the austenite was randomly dispersed in the ferrite matrix, and also on the grain boundaries in the 2101-1wt% Ru samples annealed at 1080°C and 1100°C for 120 minutes (Figures 4.40 and 4.50 respectively). The austenite grains were coarser at 1080°C. The austenite volume fraction at 1080°C was 53.0±5.0 and 38.0±8.3 at 1100°C.

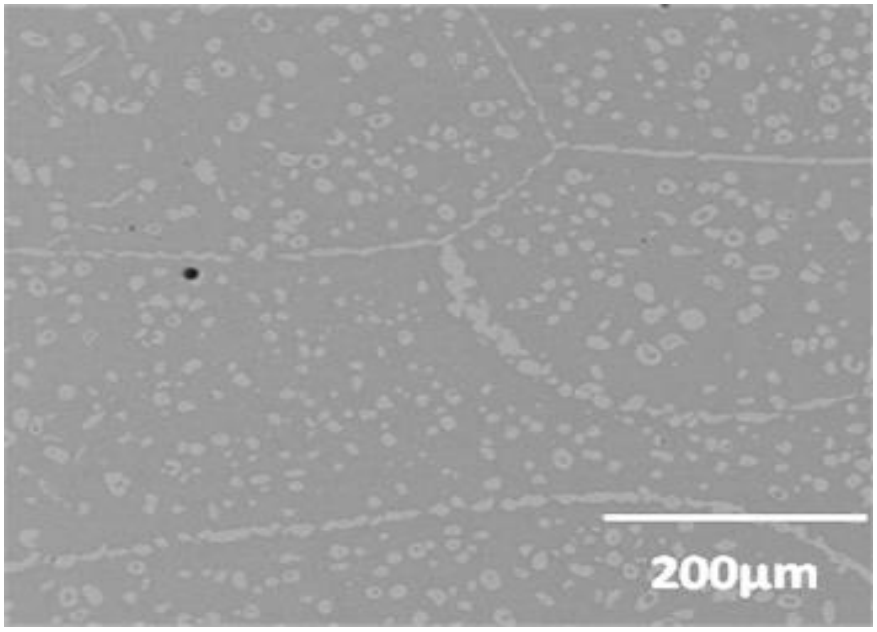

Figure 4.50. SEM–BSE image of 2101 duplex stainless steel containing nominal 1 wt% Ru, annealed at 1100°C for 120 minutes, showing austenite (light) and ferrite (dark), etched with 40g NaOH in 100ml distilled water.

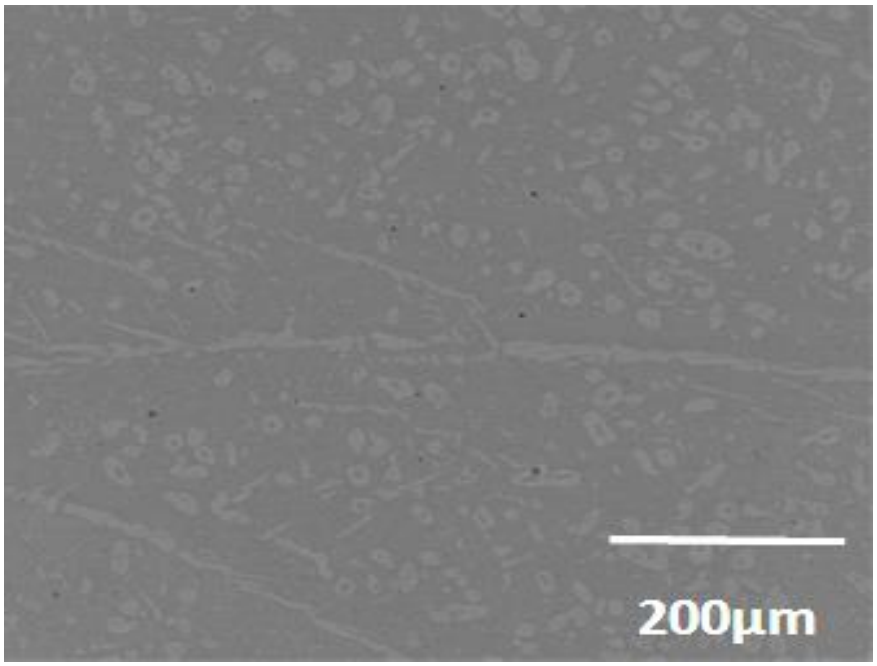

Figure 4.51. SEM–BSE image of 2101 duplex stainless steel containing nominal 1.5 wt% Ru, annealed at 1100°C for 120 minutes, showing austenite (light) and ferrite (dark), etched with 40g NaOH in 100ml distilled water.

The SEM micrographs of 2101-2.5wt% Ru samples annealed at 1080°C and 1100°C are shown in Figures 4.41 and 4.52. The austenite particles were randomly dispersed in the ferrite, and were coarser at 1080°C. They were more rounded in 1100°C, while at 1080°C they were more angular. Some austenite particles were formed on the grain boundaries at both temperatures. The percentages of austenite in 1080°C and 1100°C were 40.0±7.3 and 45.5±6.0 respectively.

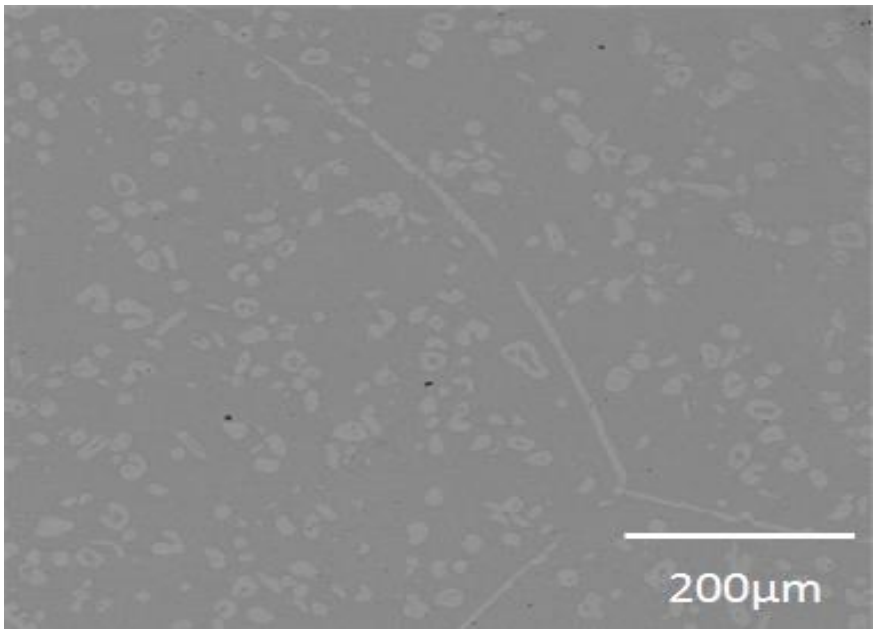

Figure 4.52. SEM–BSE image of 2101 duplex stainless steel containing nominal 2.5 wt% Ru, annealed at 1100°C for 120 minutes, showing austenite (light) and ferrite (dark), etched with 40g NaOH in 100ml distilled water.

The sample containing 1.5wt% Ru was not annealed at both temperatures, because of a lack of material, and so could not be compared at the different temperatures.

Overall, the volume fractions showed that, for most samples, the 50:50 austenite:ferrite ratios were better achieved at 1080°C than at 1100°C. This agrees with the Thermo-Calc calculations, which showed that 1080°C was the temperature where the 50:50 proportion was expected. The Thermo-Calc calculation predicted a higher proportion of ferrite than austenite at 1100°C, and this agreed with the volume fractions calculated.

4.5.4 EDX analyses of samples

Table 4.12 shows the EDX analyses of the two phases, austenite and ferrite, in as-received 2101, 2001, 2205 and 2507 duplex stainless steels. The EDX analyses of 2101 gave the following elements: Cr, Ni, Mo, Mg, Al, Si, S, Ca, Mn, Fe. The ferrite phase had a higher proportion of Mg, Si, Ca, Cr and Mo, while austenite had a higher proportion of Al, S, Mn, Fe and Ni. (The overall analyses were done by spark emission spectroscopy (Table 4.1)).

The 2001 DSS had two phases, the compositions were analysed by EDX and the following elements: Cr, Ni, Mo, Mg, Al, Si, S, Ca, Mn, Fe, Ti, Ca were found in both phases. The ferrite content contained the higher Si, V, Cr and Mo contents, while the austenite contained the higher Al, S, Mn, Fe, Ni contents.

The EDX analysis of the phases of 2507 (Table 4.12) gave the following elements: Mg, Al, Si ,Ca, Ti, V, Cr, Mn, Fe, Ni, Cu and Mo in the phases. Ferrite had a higher proportion of Mo, Be, Si and Cr, while austenite contained higher Cu, Mg, Al, Mn, Fe and Ni contents.

EDX analysis of 2205 duplex stainless steel confirmed the two phases of austenite and ferrite. The phases comprised Mg, V, Co, Fe, Si, Mn, Cr, Ni and S. Ferrite had a higher proportion of Mg, Co, Cr and S, while the austenite was richer in V, Mn, Fe and Ni.

Table 4.13 shows the analyses of the as-cast samples of 2101 containing different percentages of ruthenium ranging from 0 wt% Ru to 0.2 wt% Ru. The elements that were predominant were iron, chromium, manganese and nickel, as expected. The ruthenium content was not accurate, because it was lower than 1 wt%, which is beyond the capability of EDX. There were large variations in the carbon contents, but the error values were also large.

Table 4.14 presents the analyses of the different phases in 2101 heat treated samples containing different percentages of ruthenium. Chromium partitioned more to the ferrite, while nickel was more in the austenite phase, for all the alloys up to 2.5 wt% ruthenium. Ruthenium partitioned more to the hcp phase in 10 wt% Ru, which is expected, since ruthenium is hexagonal.

Overall compositions of the heat treated samples with ruthenium additions analysed by EDX are presented in Table 4.15. The predominant elements were iron, chromium, manganese and molybdenum as expected. The chromium contents in the as-cast samples in Table 4.12 were slightly higher than the heat treated samples in Table 4.14. This was unexpected, since

chromium diffusion rates are slow, since chromium is a large atom (compared to carbon and nitrogen).

The ruthenium analyses were not as expected, probably because the ruthenium was not homogeneously distributed in the samples. Also, EDX is not really the appropriate technique for analysing small amounts of ruthenium (less than 1wt%), and WDS would have been better.

Table 4.12. Overall composition (wt%) of as-cast 2101 with ruthenium additions analysed by EDX.

Ru addition (wt%)	Fe	Ni	Cr	Mn	Mo	Mg	Si	S	Cl	C	O	Ru
0	68.0±0.4	1.8±0.1	21.3±0.1	4.5±0.3	0.2±0.0	-	0.8±0.1	-	-	1.6±0.4	2.0±0.3	-
0.05	66.7±1.9	1.8±0.2	20.6±0.9	4.3±0.3	0.2±0.2	-	0.8±0.2	-	-	1.7±1.5	4.7±0.9	0.1±0.1
0.10	66.9±1.2	1.6±0.2	20.5±0.3	4.6±0.6	0.2±0.2	-	0.9±0.2	0.3±0.0	0.1±0.0	2.0±1.2	4.1±0.2	0.0±0.1
0.15	69.6±1.2	1.6±0.2	21.2±0.6	5.5±0.3	0.2±0.3	-	0.9±0.2	-	0.1±0.0	0.6±0.8	4.0±0.0	0.1±0.1
0.20	68.1±0.5	1.6±0.2	20.9±0.4	4.4±0.5	0.2±0.2	0.3±0.0	0.9±0.1	-	-	0.3±0.9	3.9±0.3	0.1±0.2

Table 4.13. Compositions (wt%) of heat treated 2101 duplex stainless steel samples with ruthenium additions analysed by EDX.

Ru addition (wt%)	Phase	Fe	Ni	Cr	Mn	Mo	Si	Ru	C	O
0.05	**Ferrite**	63.5±0.1	1.5±0.1	20.4±0.2	4.6±0.2	0.7±0.2	1.2±0.1	0.6±0.1	4.6±0.8	3.0±0.2
	Austenite	66.0±1.0	2.0±0.2	18.2±0.6	5.0±0.5	0.5±0.2	1.0±0.2	0.6±0.2	4.5±0.5	2.3±0.1
0.1	**Ferrite**	64.6±0.4	1.4±0.2	20.7±0.3	4.7±0.2	-	0.9±0.1	0.5±0.1	3.9±0.4	3.3±0.2
	Austenite	66.6±0.5	1.4±0.2	20.7±0.3	4.7±0.2	-	0.9±0.2	0.5±0.1	2.3±0.2	3.7±0.4
0.15	**Ferrite**	63.5±0.8	1.6±0.2	20.1±0.3	4.6±0.3	0.7±0.3	1.0±0.1	0.8±0.2	4.5±0.7	3.1±0.1
	Austenite	66.6±0.4	2.4±0.1	17.7±0.4	5.4±0.1	0.5±0.1	0.8±0.1	0.6±0.1	4.0±0.7	2.0±0.1
0.2	**Ferrite**	62.3±0.6	1.4±0.2	19.8±0.4	4.5±0.2	0.7±0.1	1.0±0.1	0.6±0.3	6.0±0.7	3.7±0.1
	Austenite	65.9±0.2	2.3±0.3	17.3±0.3	5.2±0.2	0.8±0.1	1.0±0.1	0.7±0.2	4.4±0.3	2.5±0.1
0.4	**Ferrite**	58.5±0.9	1.4±0.2	18.7±0.5	4.2±0.3	0.7±0.2	1.0±0.1	0.8±0.3	11.2±1.1	3.6±0.2
	Austenite	62.5±0.9	2.0±0.1	16.5±0.3	5.1±0.2	0.6±0.2	1.0±0.1	0.9±0.2	8.9±1.7	2.6±0.3
0.6	**Ferrite**	64.6±0.8	1.5±0.2	20.5±0.4	4.9±0.2	0.5±0.2	1.0±0.2	0.9±0.1	3.2±1.4	2.9±0.3
	Austenite	66.4±0.5	2.3±0.2	17.5±0.3	5.4±0.2	0.4±0.1	0.9±0.1	1.0±0.1	3.8±0.4	2.2±0.1
0.8	**Ferrite**	63.0±0.5	1.6±0.3	19.8±0.2	4.3±0.3	0.5±0.1	1.0±0.1	1.4±0.1	5.1±0.4	3.3±0.1
	Austenite	65.6±0.5	2.5±0.1	17.0±0.3	5.0±0.1	0.7±0.2	1.0±0.1	1.5±0.2	4.6±0.5	2.2±0.2
1	**Ferrite**	62.6±0.9	1.5±0.2	19.5±0.1	4.3±0.1	0.6±0.2	1.0±0.1	1.2±0.2	5.7±0.8	3.5±0.2
	Austenite	67.0±0.8	2.3±0.2	17.0±0.4	5.3±0.1	0.6±0.1	0.9±0.1	1.3±0.0	3.6±1.5	2.0±0.8
1.5	**Ferrite**	61.7±0.6	1.5±0.1	19.6±0.3	4.4±0.2	-	1.0±0.1	1.7±0.2	6.1±0.4	4.0±0.1
	Austenite	65.3±0.8	2.0±0.3	17.3±0.2	5.2±0.1	-	1.0±0.2	2.1±0.2	4.5±0.8	2.6±0.2
2.5	**Ferrite**	61.5±0.2	1.5±0.2	19.9±0.4	4.4±0.1	0.6±0.2	1.0±0.1	1.9±0.2	6.0±0.2	3.2±0.1
	Austenite	64.9±0.7	2.1±0.1	17.6±0.3	5.1±0.1	0.5±0.2	0.9±0.1	2.0±0.3	4.52±0.6	2.2±0.2
10	**Ferrite**	60.0±0.7	1.3±0.1	20.2±0.7	3.5±0.1	0.7±0.1	0.9±0.0	6.6±0.4	5.7±0.9	3.2±0.3
	HCP	61.6±0.6	1.6±1.1	16.6±1.1	4.1±0.3	0.6±0.1	0.8±0.0	7.9±0.4	4.6±0.8	2.0±0.1

Table 4.14. Overall composition (wt%) of heat treated 2101 with ruthenium additions analysed by EDX.

Ru addition (wt%)	Fe	Ni	Cr	Mn	Mo	Si	Ru	C	O
0.05	63.5±0.4	1.6±0.2	20.1±0.4	4.7±0.1	0.6±0.1	1.0±0.2	0.5±0.1	5.1±0.5	2.9±0.1
0.10	64.5±0.6	1.6±0.2	20.1±0.4	4.7±0.1	-	1.1±0.1	0.5±0.1	4.2±0.5	3.2±0.2
0.15	64.6±0.6	1.6±0.1	19.9±0.3	4.7±0.1	0.5±0.2	1.0±0.1	0.6±0.1	4.1±0.4	3.0±0.1
0.20	63.0±0.5	1.6±0.1	19.8±0.2	4.5±0.1	0.7±0.2	1.1±0.2	0.6±0.1	5.2±0.4	3.6±0.1
0.40	57.7±0.8	1.5±0.1	18.1±0.2	4.3±0.2	0.6±0.1	0.9±0.1	0.8±0.1	12.3±0.9	3.8±0.1
0.60	68.9±0.5	1.6±0.3	19.9±0.3	4.8±0.1	0.7±0.2	1.1±0.1	1.0±0.2	4.1±0.4	2.9±0.2
0.80	63.5±0.3	1.7±0.1	19.6±0.2	4.4±0.1	0.5±0.1	1.0±0.0	1.3±0.1	4.7±0.3	3.4±0.1
1.00	62.8±0.4	1.5±0.2	19.3±0.3	4.5±0.2	0.6±0.1	0.9±0.1	1.3±0.1	5.5±0.8	3.5±0.2
1.50	62.5±0.3	1.5±0.1	19.2±0.3	4.5±0.3	-	1.0±0.1	1.7±0.1	5.7±0.3	3.9±0.2
2.50	63.1±0.6	1.7±0.1	19.4±0.2	4.6±0.3	0.6±0.1	1.0±0.0	2.0±0.3	4.6±0.3	3.2±0.2
10.00	60.7±0.3	1.3±0.2	18.3±0.5	3.9±0.3	0.5±0.1	0.9±0.0	7.4±0.3	4.5±0.3	2.7±0.1

4.6 Volume fraction of phases

The volume fractions were calculated using quantitative metallography, using a grid, and the results of the as-received samples are given in Table 4.15. The errors were quite high and were probably due to the technique used, rather than inhomogeneity in the as-received samples.

Table 4.15. Volume fraction (%) ferrite and austenite in the as-received samples.

Alloys	**2101**	**2001**	**2507**	**2205**
Ferrite	51.2±5.9	41.8±4.4	49.3±4.6	31.2±5.2
Austenite	48.8±5.9	58.2±4.4	50.7±4.6	68.8±5.2

Table 4.16 shows the volume fractions of the phases in the 2101 samples as measured by quantitative metallography. An increase in soaking time at 1080^{o}C produced an increase in the proportion of the austenite phase. The duplex structures were better achieved and the amount of austenite increased with temperature, as shown in Table 4.16.

Table 4.16. Volume fractions of austenite and ferrite in samples of 2101-Ru heat treated at 1080°C.

Ru addition (wt%)	Soaking time (minutes)	Austenite (%)	Ferrite (%)
0	10	16.0±8.0	84.0±8.0
0	30	18.0±2.3	82.0±2.3
0	120	28.0±9.0	72.0±9.0
0.05	90	39.3±6.9	60.7±6.9
0.1	90	21.3±4.1	78.7±4.1
0.15	30	18.7±6.3	81.3±6.3
0.15	90	34.9±2.3	65.1±2.3
0.15	120	58.2±8.6	42.0±8.6
0.2	30	17.0±6.0	83.0±6.0
0.2	90	22.4±6.0	77.6±6.0
0.2	120	51.0±2.0	49.0±2.0
0.4	120	61.0±7.6	39.0±7.6
0.6	120	51.0±6.0	49.0±6.0
0.8	120	57.0±8.0	43.0±8.0
1	120	53.0±5.0	47.0±5.0
2.5	120	40.0±7.3	60.0±7.3

Table 4.17. Volume fractions of austenite and ferrite in samples of 2101-Ru heat treated at 1100°C for 120 minutes.

Ru addition (wt%)	Austenite (%)	Ferrite (%)
0.05	45.1±4.5	54.9±4.5
0.1	44.8±4.0	55.2±4.0
0.15	40.0±4.4	60.0±4.4
0.2	40.0±4.2	60.0±4.2
0.4	40.7±4.7	59.3±4.7
0.6	37.0±8.8	63.0±8.8
0.8	38.0±8.3	62.0±8.3
1	38.0±2.8	62.0±2.8
1.5	30.3±6.4	69.7±6.4
2.5	45.5±6.0	54.5±6.0

4.7 X-Ray diffractometry

4.7.1 XRD of as-received samples

Figures 4.53-4.55 show the X-ray diffraction patterns of the as-received samples. The peaks corresponding to austenite and ferrites were identified. The pattern from the as-received sample 2101 is shown in Figure 4.53. XRD showed that the 2101 DSS sample was composed of ferrite and austenite. The strongest X-ray peaks were those of ferrite. This is a good pattern with low background. Figure 4.54 presents the XRD pattern for 2205 duplex stainless steel, with austenite having the highest peak intensity. The highest peak for 2507 (Figure 4.56) was the ferrite peak. 2001 was not analysed further in the study because of the closeness of its chemical composition to 2101.

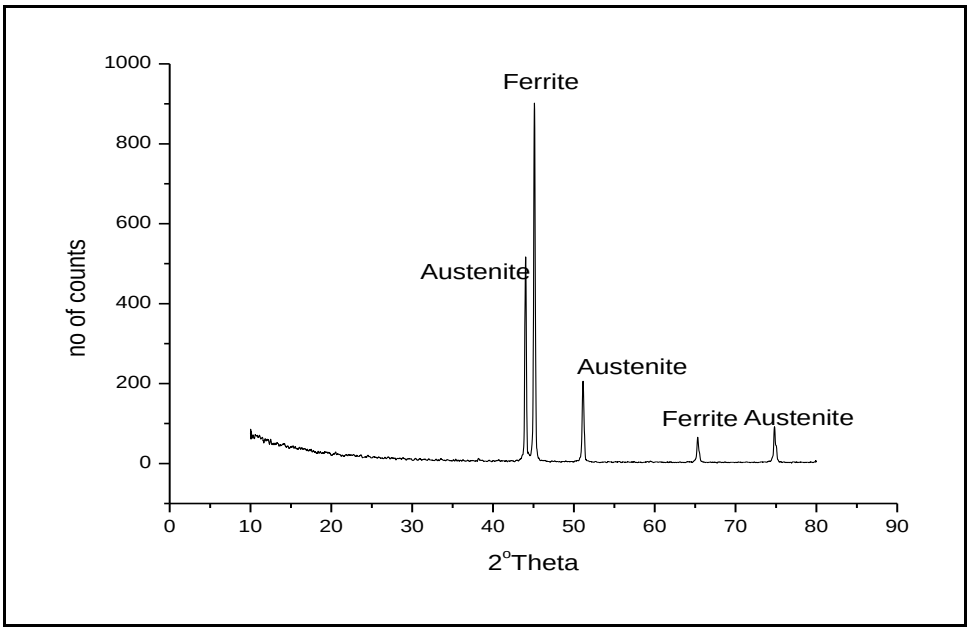

Figure 4.53. XRD pattern of as-received 2101 showing austenite and ferrite peaks.

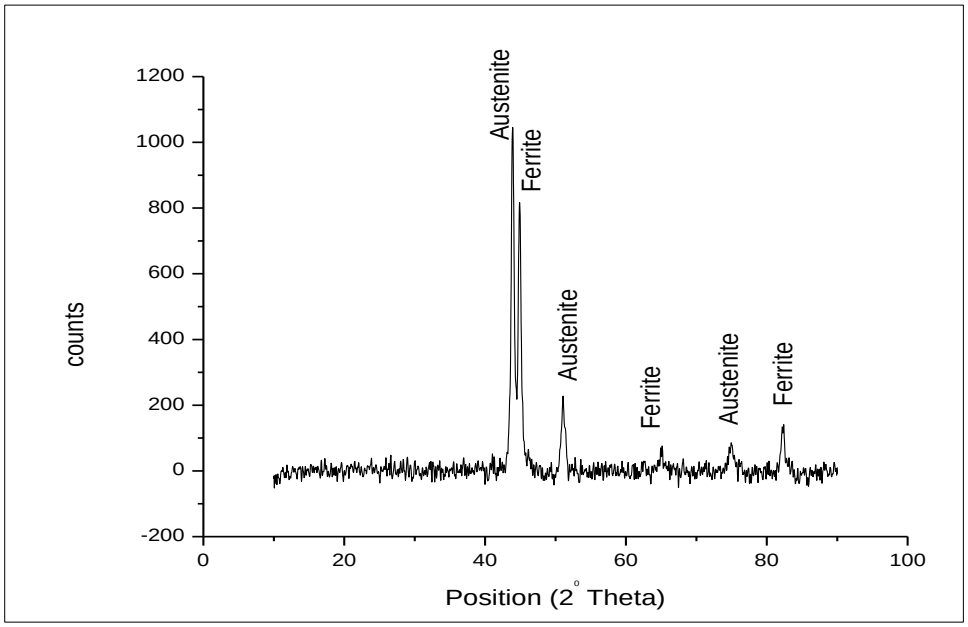

Figure 4.54. XRD pattern of as-received 2205 duplex stainless steel.

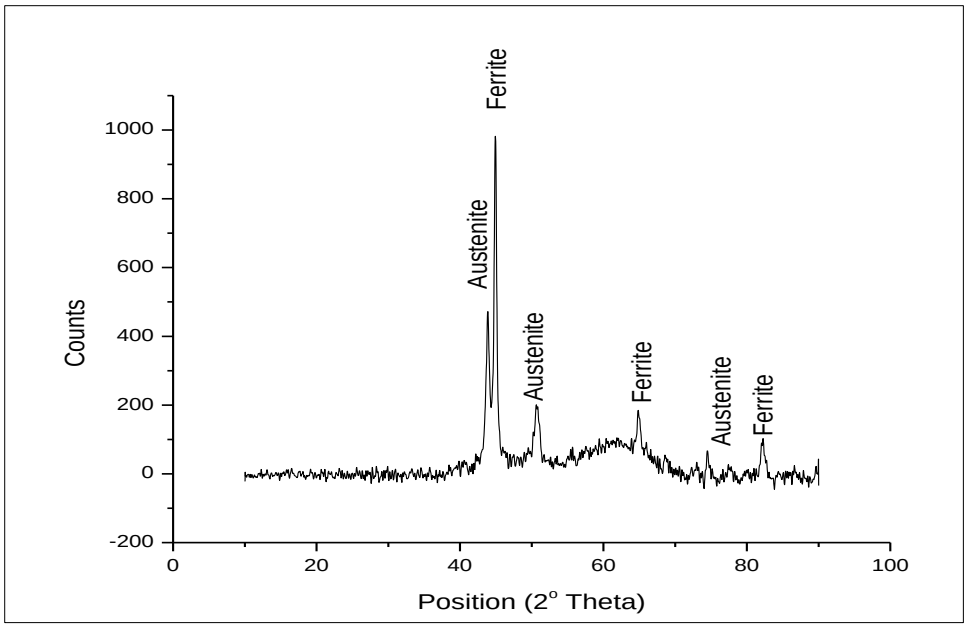

Figure 4.55. XRD pattern of as-received 2507 duplex stainless steel.

4.7.2 XRD of 2101 samples with ruthenium

The X-ray analyses of samples containing ruthenium are presented in Figures 4.56-4.61. The peaks of austenite and ferrite were identified. There were humps in the background of samples containing 0.05, 0.1, 0.15 and 0.2 wt% ruthenium (Figures 4.56, 4.58 and 4.59). Figure 4.56 shows the pattern of 2101 with 0.05 wt% Ru ruthenium heat treated at 1080°C for 120 minutes. Ferrite had the highest peaks in the samples containing 0.05, 0.1, 0.15 and 0.2 wt% Ru. The XRD pattern of the 2101-2.5 wt% Ru sample heat treated at 1080°C for 120 minutes is shown in Figure 4.60. The phases present in the specimen were austenite and ferrite, and the highest peak was for ferrite, although the austenite peaks were higher for all the other Ru-containing 2101 samples, except for that with 0.05wt% Ru. The 2101 had the highest austenite peaks. The 2101-2.5 wt% Ru peaks were similar to the peaks of 2101 without ruthenium. The intensity of the peaks was higher in 2101-2.5wt% Ru than in 2101 without ruthenium. The XRD analysis of sample containing 2101-10wt% Ru had identified peaks of ferrite and hcp, but the latter had shifted due to the Ru content. However, The 2101 samples with ruthenium annealed at 1100°C were not analysed.

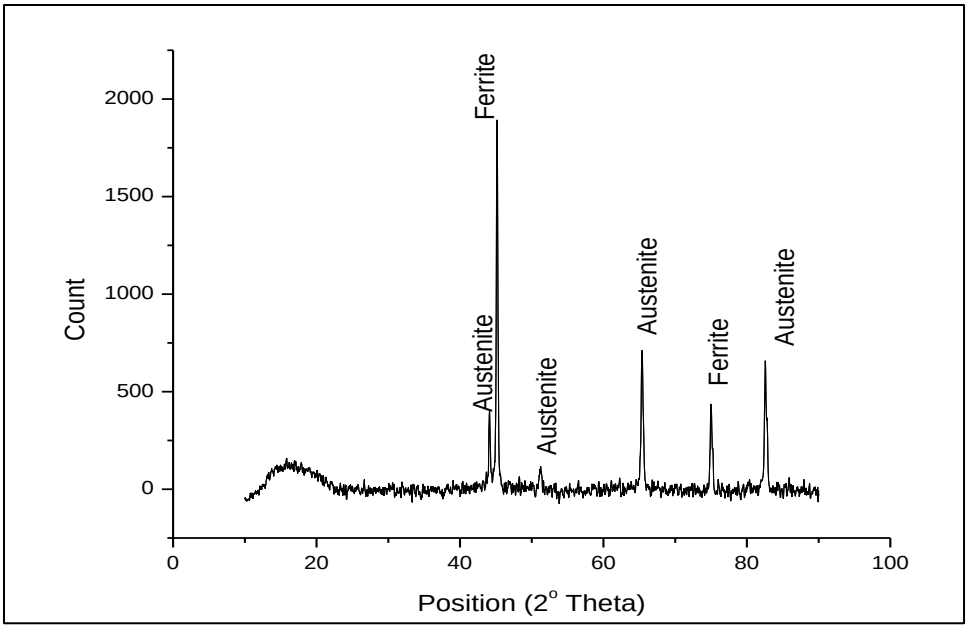

Figure 4.56. XRD pattern of 2101-0.05 wt% Ru heat treated at 1080°C for 120 minutes.

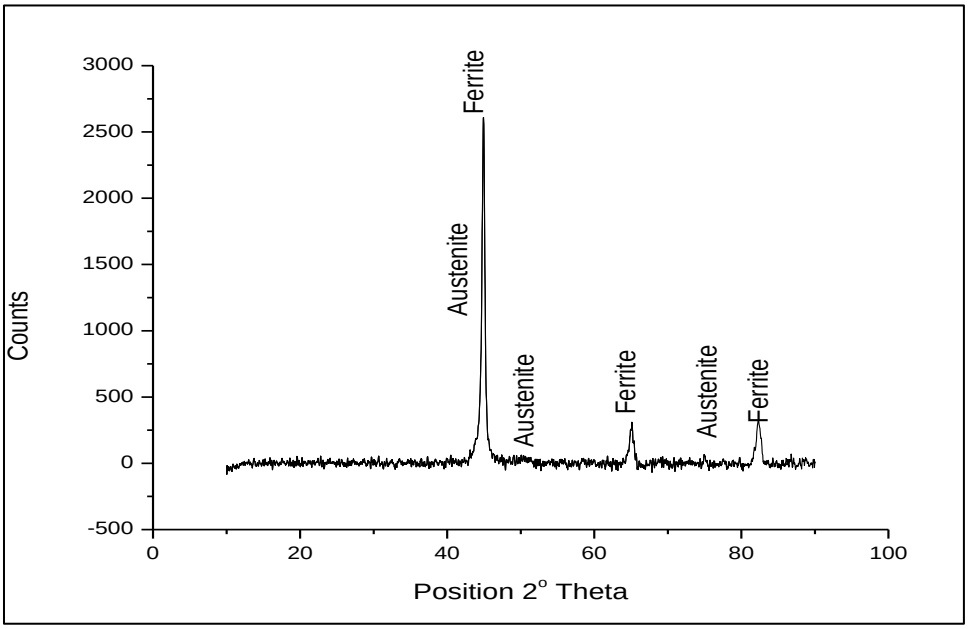

Figure 4.57. XRD pattern of 2101-0.1 wt% Ru heat treated at 1080°C for 120 minutes.

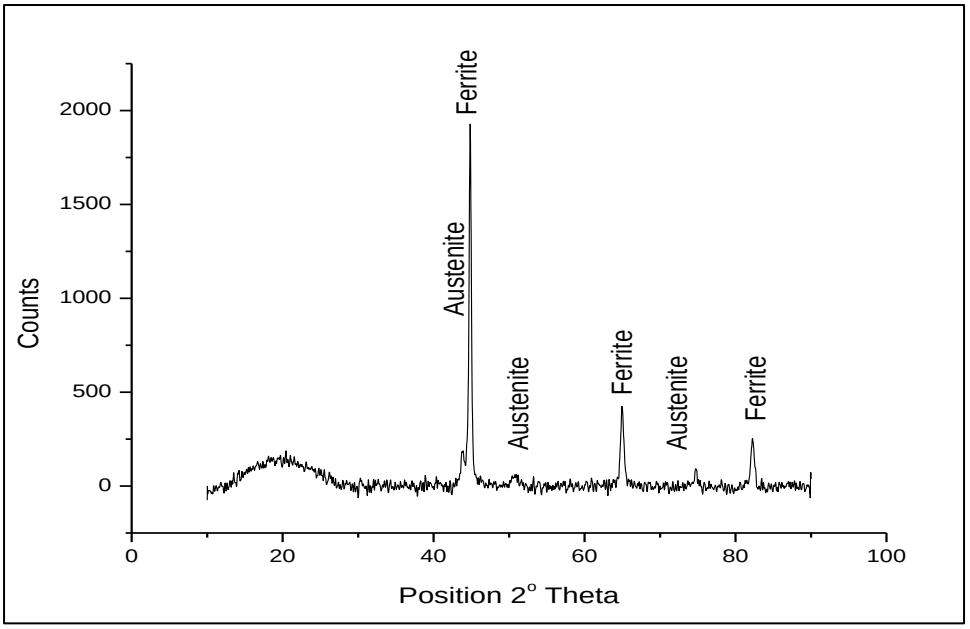

Figure 4.58. XRD pattern of 2101-0.15 wt% Ru heat treated at 1080°C for 120 minutes.

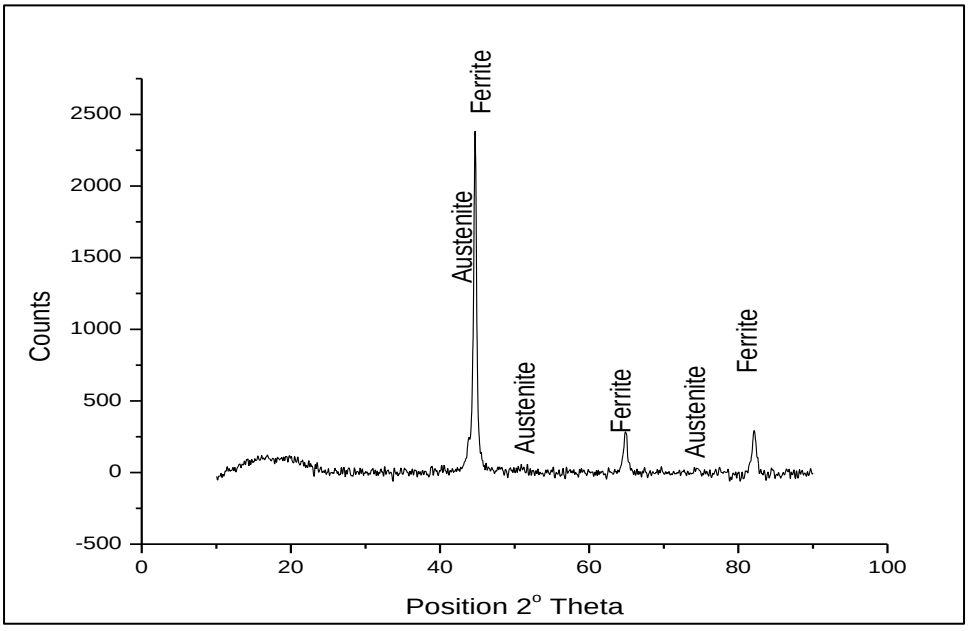

Figure 4.59. XRD pattern of 2101-0.2 wt% Ru heat treated at 1080°C for 120 minutes.

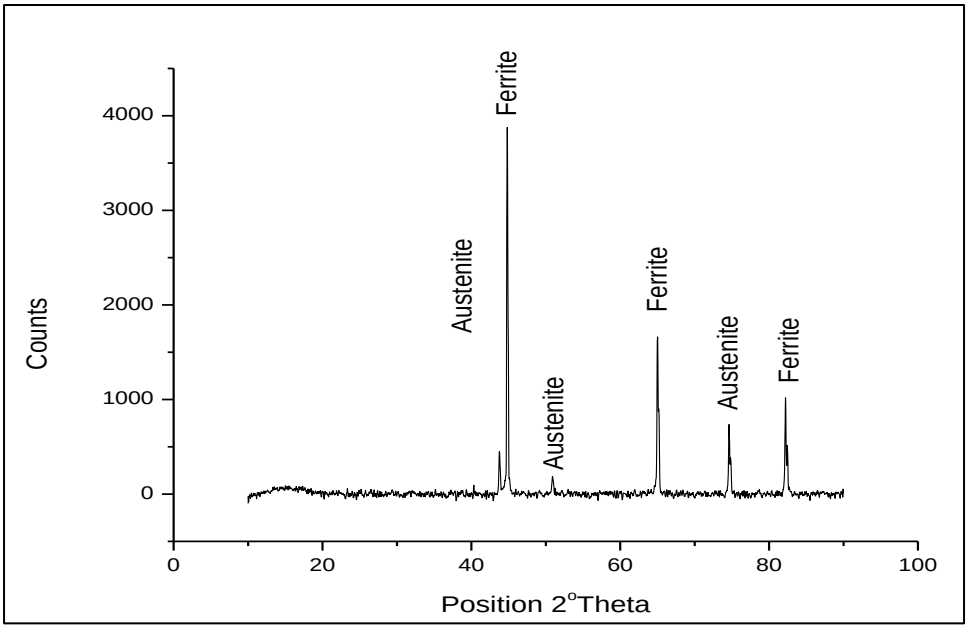

Figure 4.60. XRD pattern of 2101-2.5 wt% Ru heat treated at 1080°C for 120 minutes.

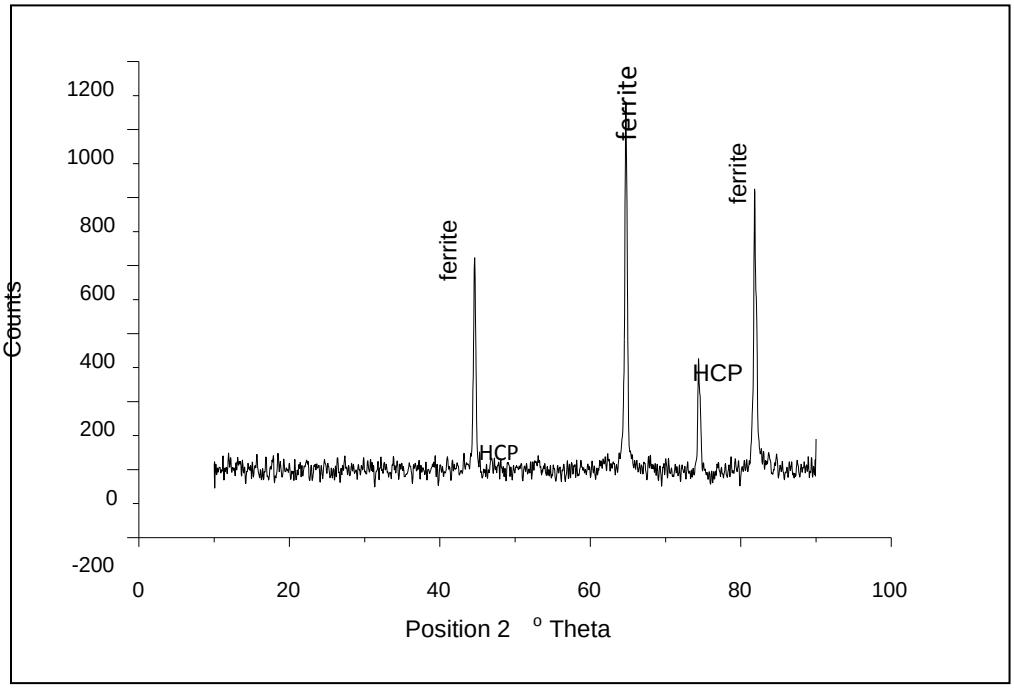

Figure 4.61. XRD pattern of 2101-10 wt% Ru heat treated at 1080°C for 120 minutes.

4.8 Hardness tests

Vickers hardness tests were conducted on the samples, and the results are presented in Table 4.18 and Figure 4.62. The results of the alloys varied from a minimum of 222±4 HV to 240±6 HV. The variation in hardness was relatively small with low errors. It was assumed that ruthenium was not homogeneously distributed, which gave these variations, and thus no direct conclusion could be drawn, except that after 1 wt% Ru thre was a slight increase in hardness.

Table 4.18. Effects of ruthenium content (wt%) on hardness of 2101 duplex stainless steels.

2101 –Ru (wt%)	Hardness (HV)
0	230±1
0.05	231±3
0.1	222±4
0.15	230±3
0.2	227±6
0.4	233±2
0.6	240±3
0.8	240±6
1.5	234±6
2.5	237±3

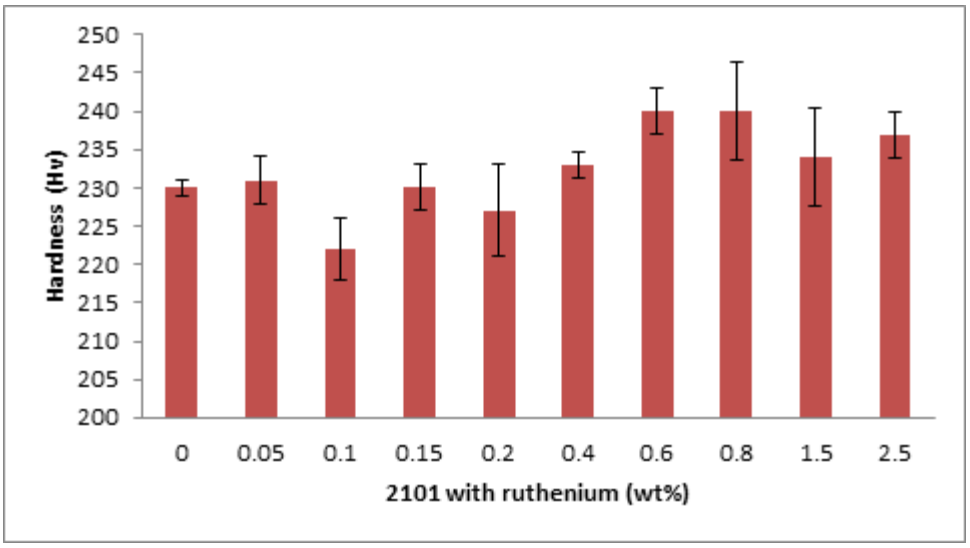

Figure 4.62. The effects of ruthenium content (wt%) on hardness of 2101 duplex stainless steels.

4.9 Corrosion results

4.9.1 Comparison of LDX2101 duplex stainless steels with 2205 and 2507 duplex stainless steels in acidic and acidic chloride environments

The electrochemical measurement results are hereby reported for 2101, 2205 and 2507 duplex stainless steels. A minimum of three tests were done for each sample, and the closest two were accepted. The repeatability curves are shown in Appendix 2.

The corrosion behaviour of these duplex stainless steels in sulphuric acid without chloride and sulphuric acid with chloride additions at 25°C, 40°C, 60°C and 80°C is shown in Figures 4.63 - 4.66. The chloride additions were made to ascertain the effect of chloride contaminants in sulphuric acid solution.

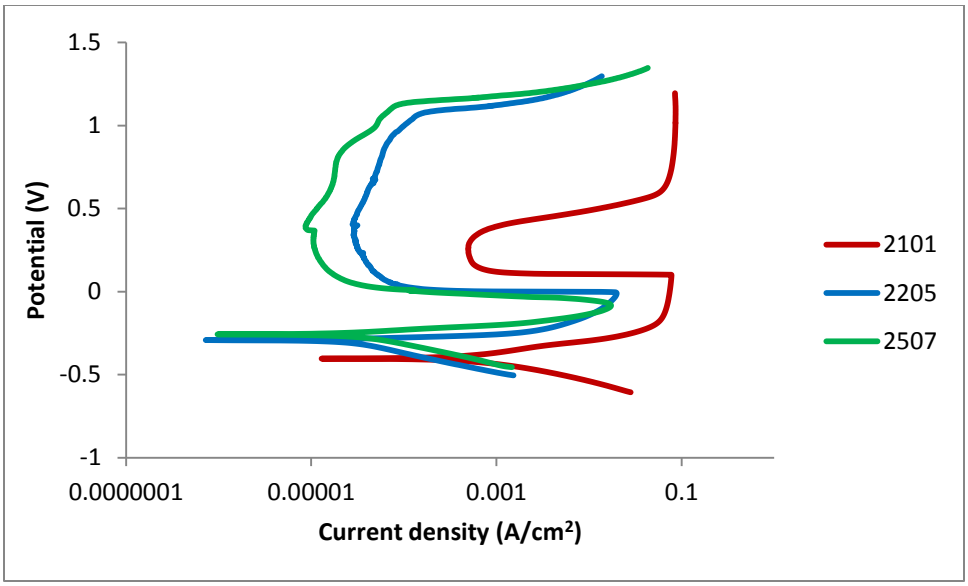

Figure 4.63. Potentiodynamic curves of 2101, 2205 and 2507 duplex stainless steels in 1M H_2SO_4 at 25°C.

At 25°C, the 2101 duplex stainless steel had lower corrosion resistance than 2205 and 2507 in 1M sulphuric acid (Figure 4.63). The i_{crit} was higher for 2101 than for 2507 and 2205. In sulphuric acid, there was an active-passive transition for only 2205 and 2507.

The results in 1M sulphuric acid solution containing 0.1% sodium chloride (Figure 4.64) showed similar potentiodynamic curves for 2101, 2205 and 2507 duplex stainless steels. There were no i_{crit} values for the samples, because pseudo-passivation occurred immediately.

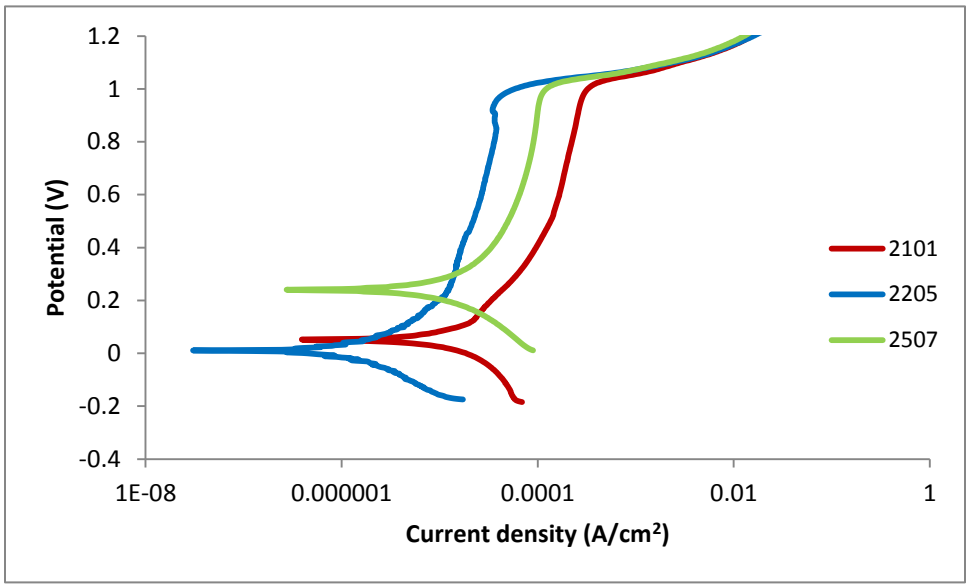

Figure 4.64. Potentiodynamic curves of 2101, 2205 and 2507 duplex stainless steels in 1M H_2SO_4 and 1% NaCl at 25°C.

At 40°C in 1M sulphuric acid (Figure 4.65), the 2101 duplex stainless steel had a more active corrosion potential than 2205 and 2507 duplex stainless steels. The passive range in 1M sulphuric acid was shorter in 2101 than for the other duplex stainless steels. The i_{crit} values for 2205 and 2507 were almost the same, and lower than 2101.

In the solution containing 1M sulphuric acid and 1% sodium chloride at 40°C (Figure 4.66), the 2205 sample had the lowest i_{pp} in 1M sulphuric acid at 40°C. The 2101 sample had the most positive corrosion potential and 2205 had the most negative corrosion potential, although all were fairly similar.

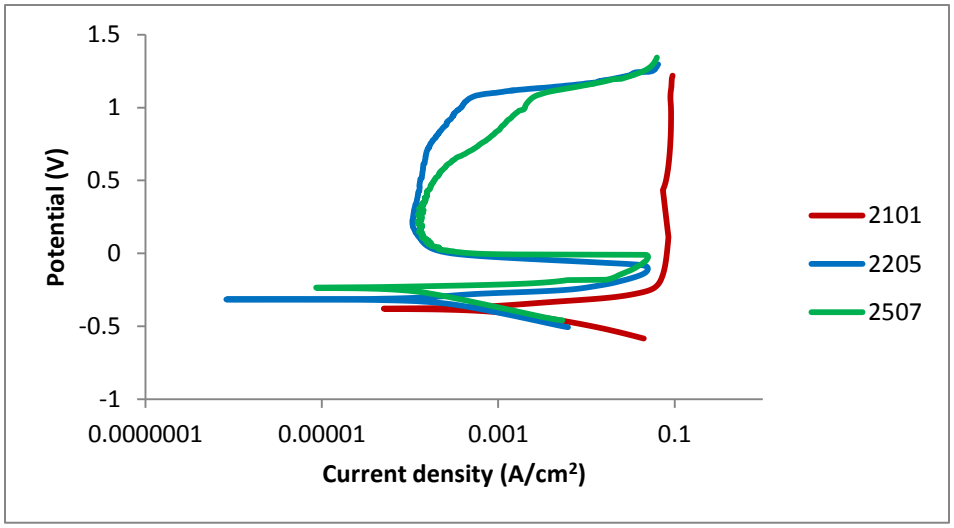

Figure 4.65. Potentiodynamic diagram of 2101, 2205 and 2507 duplex stainless steels in 1M H2SO4 at 40°C.

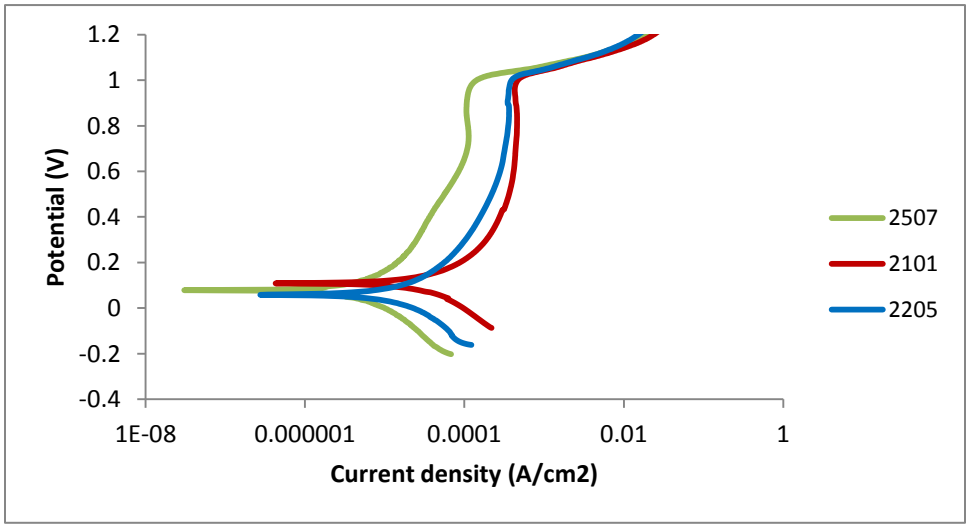

Figure 4.66. Potentiodynamic curves of 2101, 2205 and 2507 duplex stainless steels in 1M H_2SO_4 and 1% NaCl at 40°C.

The electrochemical responses of 2101, 2205 and 2507 in 1M sulphuric acid, and 1M sulphuric acid with sodium chloride at 60°C are presented in Figures 4.67 and 4.68 respectively. The ranking of the corrosion potentials were 2101 < 2205 < 2507 was the same in 1M sulphuric acid with or without the additions of Cl. As would be expected, the chloride addition to sulphuric acid resulted in a reduction in the passive range for all three steels.

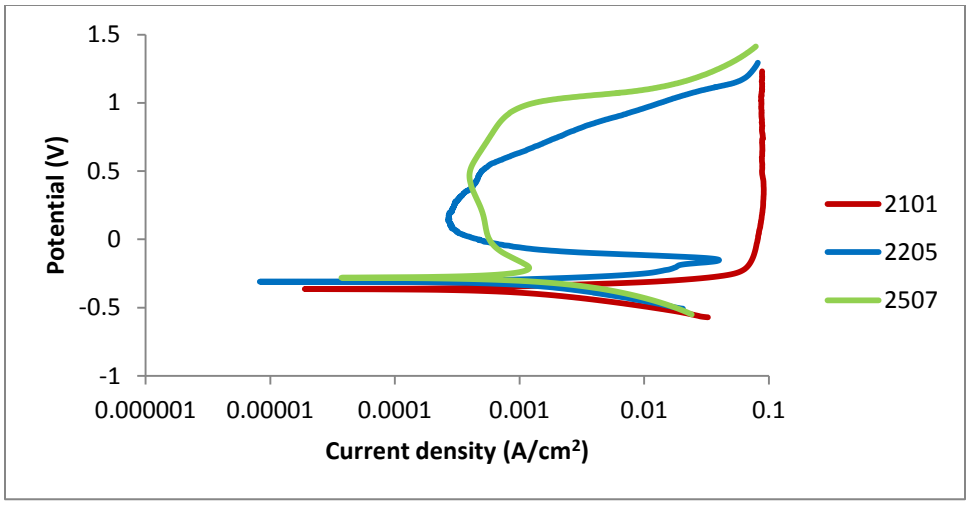

Figure 4.67. Potentiodynamic curves of 2101, 2205 and 2507 duplex stainless steels in 1M H_2SO_4 at 60°C.

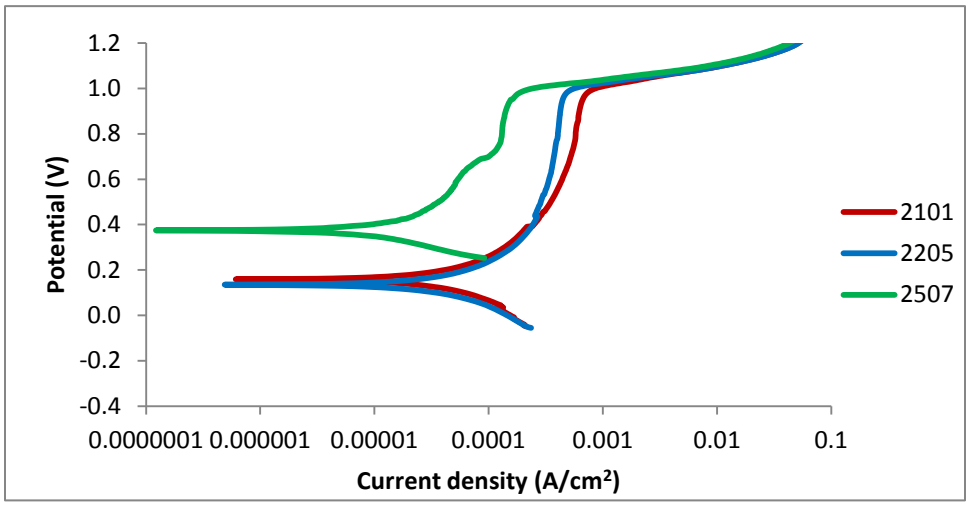

Figure 4.68. Potentiodynamic curves of 2101, 2205 and 2507 duplex stainless steels in 1M H_2SO_4 and 1% NaCl at 60°C.

Figures 4.69 and 4.70 present the potentiodynamic curves of 2101, 2205 and 2507 at 80°C in 1M sulphuric acid, and 1M sulphuric acid with 1% NaCl respectively. The 2507 duplex stainless steel had the highest corrosion potential of 445 mV in 1M sulphuric acid, and 124 mV in 1M sulphuric acid with 1% NaCl, followed by 2205 and 2101 in 1M sulphuric acid. The corrosion potential trends in 1M sulphuric acid with 1% sodium chloride were 2101 < 2205 < 2507. The 2205 alloy did not have i_{crit} values in Figure 4.70, because it exhibited pseudo-passivity. The

lowest passive current density for 1 M sulphuric acid and 1M sulphuric acid with 1% sodium chloride were observed for alloy 2507. These results are given in Table 4.19.

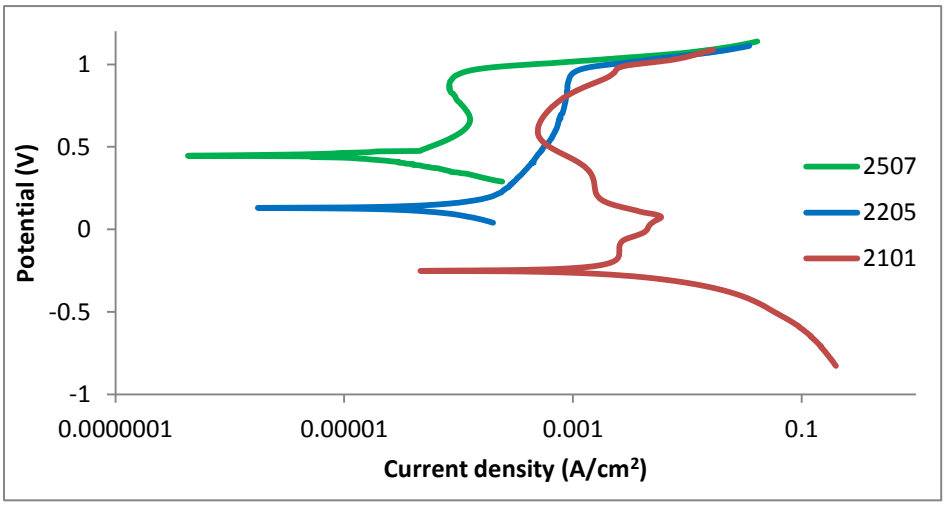

Figure 4.69. Potentiodynamic curves of 2101, 2205 and 2507 duplex stainless steels in 1M H_2SO_4 at 80°C.

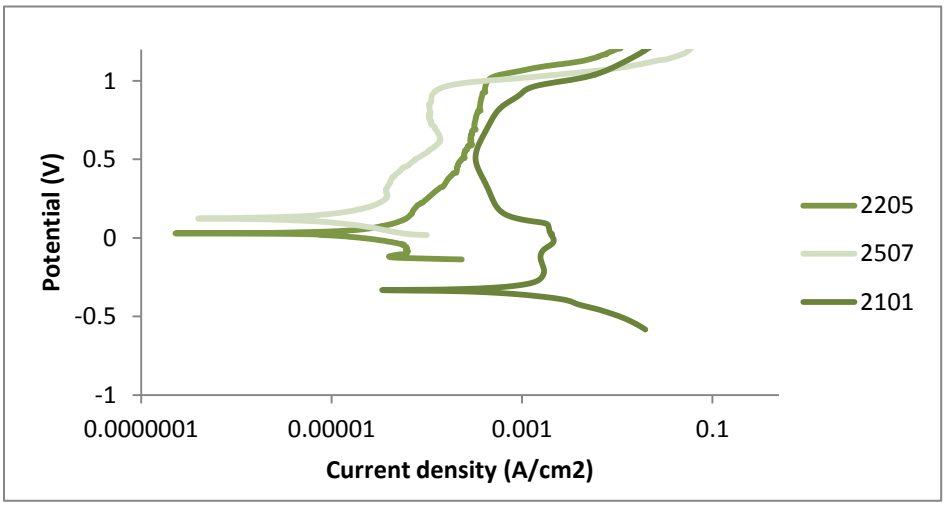

Figure 4.70. Potentiodynamic curves of 2101, 2205 and 2507 duplex stainless steels in 1M H_2SO_4 and 1% NaCl at 80°C.

Table 4.19. Potentiodynamic data for duplex stainless steel samples in H_2SO_4 with and without NaCl.

Corrosive medium	Concentration	Temperature (°C)	Alloy	E_{corr} (mV)	Corrosion rate (mm/y)	i_{pass} (A/cm^2)
H_2SO_4	1 M	25	2101	-403	5.68E+04	6.57E-04
			2205	-292	2.89E+03	2.89E-05
			2507	-257	1.66E+03	1.10E-05
H_2SO_4	1 M	40	2101	-380	9.07E+04	7.36E-02
			2205	-314	7.89E+03	1.28E-04
			2507	-236	6.24E+03	1.35E-04
H_2SO_4	1 M	60	2101	-363	9.63E+04	8.65E-02
			2205	-309	4.96E+04	2.79E-04
			2507	-281	2.49E+04	3.98E-04
H_2SO_4	1 M	80	2101	-251	1.41E+05	3.19E-04
			2205	130	4.34E+03	2.63E-04
			2507	445	9.86E+01	8.40E-05
H_2SO_4 NaCl	1 M 1%	25	2101	49	7.83E+02	7.10E-04
			2205	11	5.47E+02	2.12E-05
			2507	241	3.58E+02	3.91E-05
H_2SO_4 NaCl	1 M 1%	40	2101	109	1.48E+03	3.31E-04
			2205	58	6.68E+02	1.69E-04
			2507	78	2.66E+02	4.73E-05
H_2SO_4 NaCl	1 M 1%	60	2101	159	6.59E+02	3.30E-04
			2205	135	6.37E+02	2.82E-04
			2507	374	3.04E+02	5.18E-05
H_2SO_4 NaCl	1 M 1%	80	2101	-331	1.04E+06	3.53E-04
			2205	29	1.26E+03	2.12E-04
			2507	124	5.39E+02	1.00E-03

4.9.2 Comparison of 316 austenitic stainless steel with 2101 duplex stainless steel in different concentrations of sulphuric acid

The potentiodynamic tests were carried out for 2101 and 316 stainless steels in sulphuric acid with molarities of 2M and 3M at 25°C, and are presented in Figures 4.71 and 4.72. Table 4.20 shows the electrochemical data calculated with the GPES software. The corrosion resistance of 316 was superior to that of 2101 in 2M H_2SO_4, since Figure 4.71 shows that 2101 had a higher critical current density than 316, the corrosion potential was lower than 316, and the passive current density was lower in 2101 than in 316. The 316 stainless steel had a lower corrosion rate of 1.61E-01 mm/y compared to 5.72E+0 mm/y for 2101 (Table 4.20). Figure 4.72 shows that 2101 had the highest critical current density, lower corrosion potential in 3M sulphuric acid than 316. Thus, the corrosion rate of 2101 was higher than 316. Figure 4.73 shows that with increasing sulphuric acid molarity (from 1M to 3M), the corrosion potential of 316 increased slightly, and the corrosion current density increased from 1M to 2M.

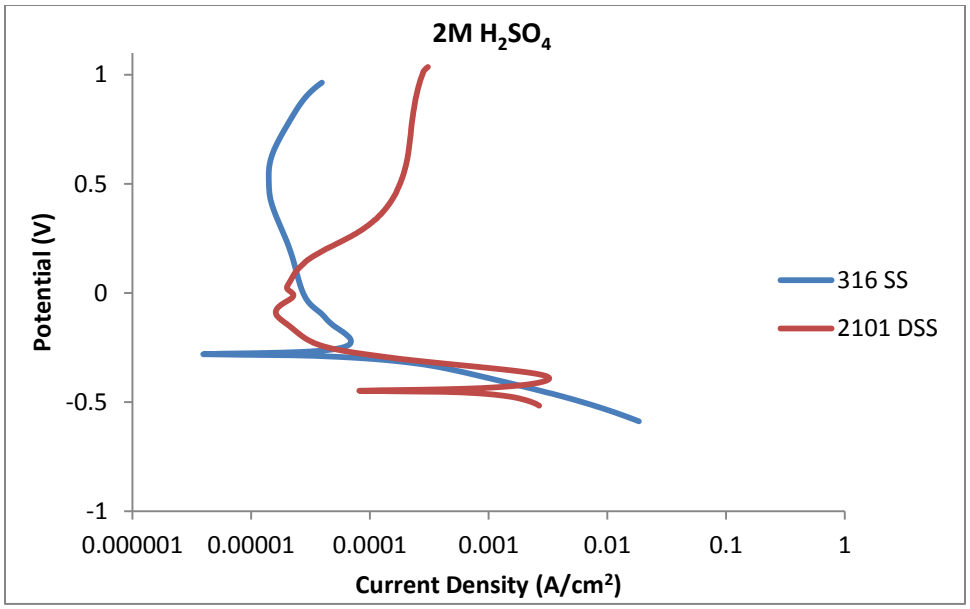

Figure 4.71. Potentiodynamic curves of 2101 duplex stainless steel and 316 austenitic stainless steel in 2M sulphuric acid at 25°C.

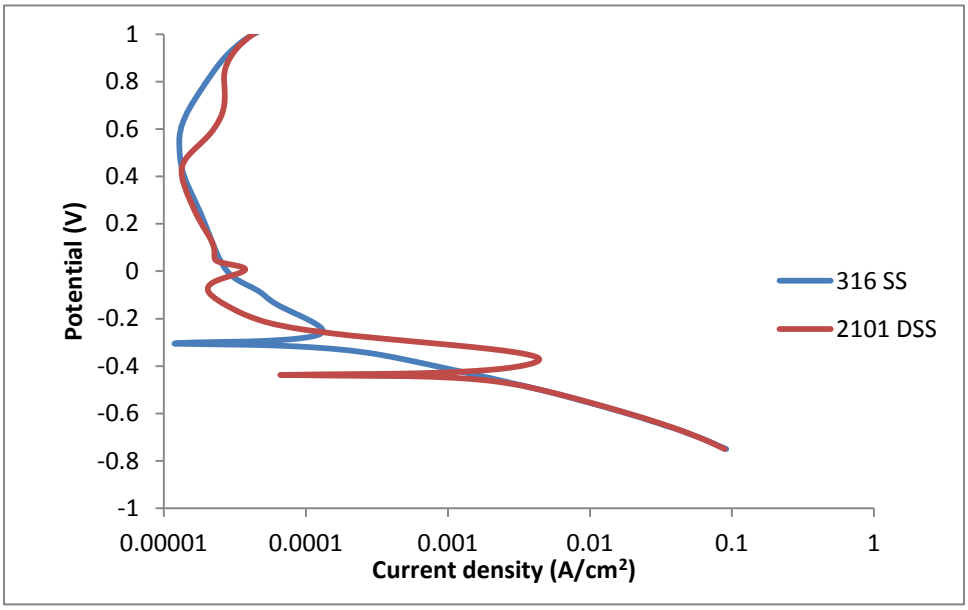

Figure 4.72. Potentiodynamic curves of 2101 duplex stainless steel and 316 austenitic stainless steel in 3M sulphuric acid at 25°C.

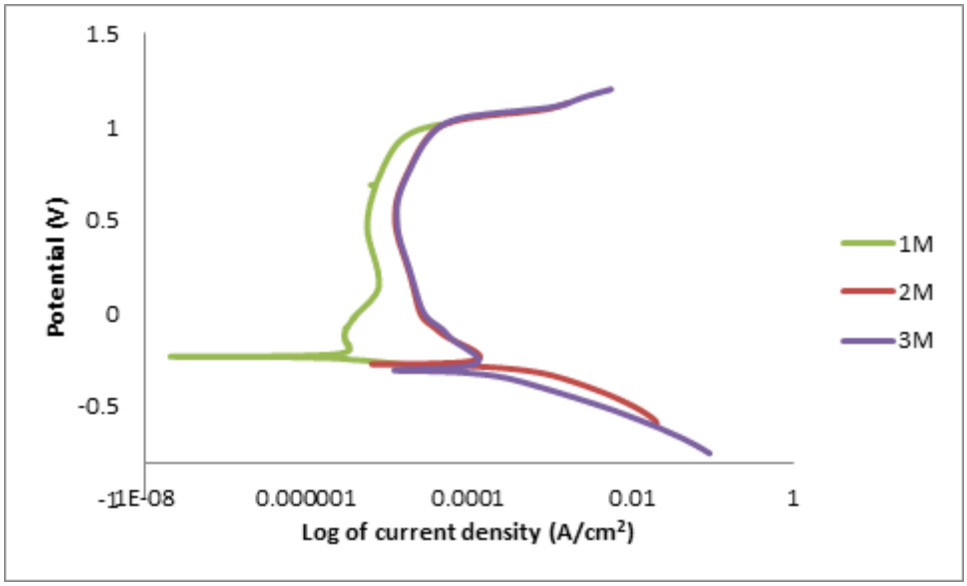

Figure 4.73. Potentiodynamic curves of 316 austenitic stainless steel in different molarities of sulphuric acid at 25°C.

Table 4.20. Potentiodynamic data for 2101 and 316 stainless steel samples in H_2SO_4 at different concentrations.

Steel	H_2SO_4 concn. (M)	E_{corr} (V)	i_{corr} (A/cm^2)	Corrosion rate (mm/y)
2101	2	-0.45	3.8E-4	4.41E+0
2101	3	-0.41	4.9E-4	5.72E+0
316	2	-0.28	1.0E-5	1.087E-1
316	3	-0.30	1.5E-5	1.612E-1

4.9.3 Potentiodynamic results of 2101 with ruthenium in 0.5M H_2SO_4

The results for electrochemical corrosion tests performed in 0.5M H_2SO_4 are presented in Figures 4.74 – 4.83 and are summarised in Table 4.21. From these figures, it can be seen that the critical current density, the passive current density and the corrosion rate decreased with increasing ruthenium content. The corrosion potential (E_{corr}) became more noble with the addition of ruthenium. The E_{corr} observed for 2101 without ruthenium was -325mV, while for 2101 with 1wt% Ru, the E_{corr} was 132mV (Table 4.21). The alloy containing 1 wt% Ru displayed pseudo-passivity. Instability was observed in the anodic curve of 2101 with no ruthenium (Figure 4.74).

Figure 4.74 shows the potentiodynamic curve of 2101 without ruthenium in 0.5M sulphuric acid. An active to passive transition was observed. The i_{crit} was at $1.10\times10^{-3}A/cm^2$ and i_{pass} was $2.5\times10^{-5}A/cm^2$. Anodic dissolution occurred in the anodic parts of the curve. Instability was observed in the curve.

The potentiodynamic curve for 2101 with 0.15wt% Ru in 0.5 M H_2SO_4 is shown in Figure 4.75. There was no i_{crit}; the curve went straight to passivation. The i_{pass} was at $5.70\times10^{-6}A/cm^2$ compared to $2.5\times10^{-5}A/cm^2$ for 2101 with no Ru, and one order of magnitude lower with 0.15wt% Ru.

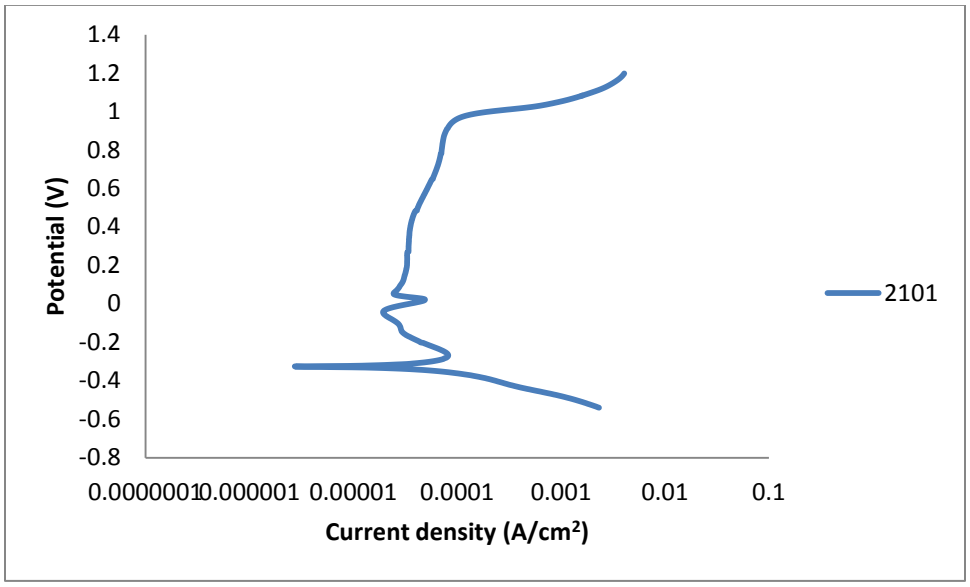

Figure 4.74. Potentiodynamic curve of 2101 duplex stainless steel in 0.5 M sulphuric acid at 25°C.

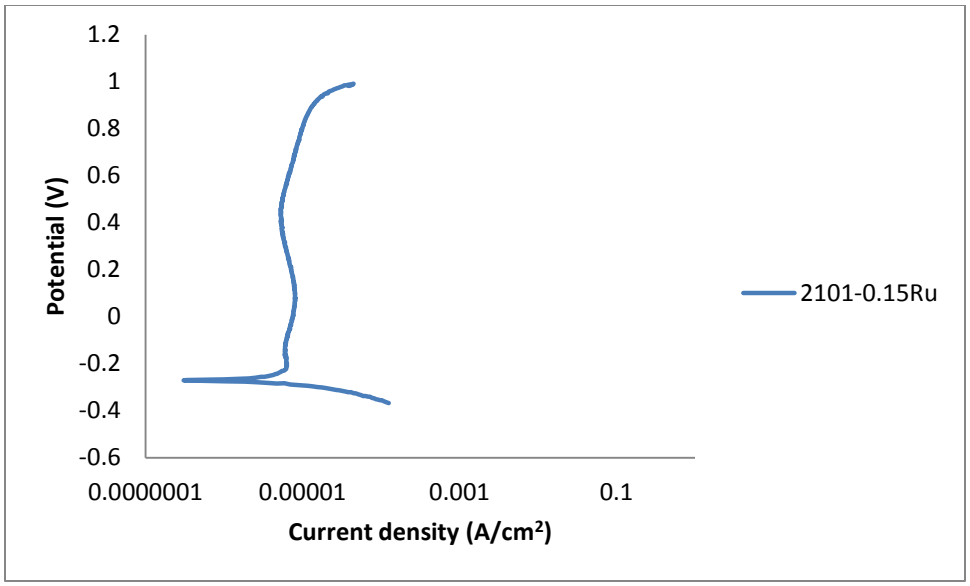

Figure 4.75. Potentiodynamic curve for 2101-0.15 wt% Ru in 0.5 M H_2SO_4 at 25°C.

Figure 4.76 shows the potentiodynamic curve for 2101-0.2 wt% Ru. There was no active nose and as the curve went straight to passivation, i_{crit} did not exist. E_{corr} was -264mV, while i_{pass} was 6.30×10^{-6}A/cm^2, almost the same value as at 0.15wt% Ru.

The potentiodynamic curve for 2101-0.4wt% Ru is shown in Figure 4.77. The i_{crit} was observed and measured to be 2.90×10^{-6}A/cm^2 and E_{corr} was -258mV.

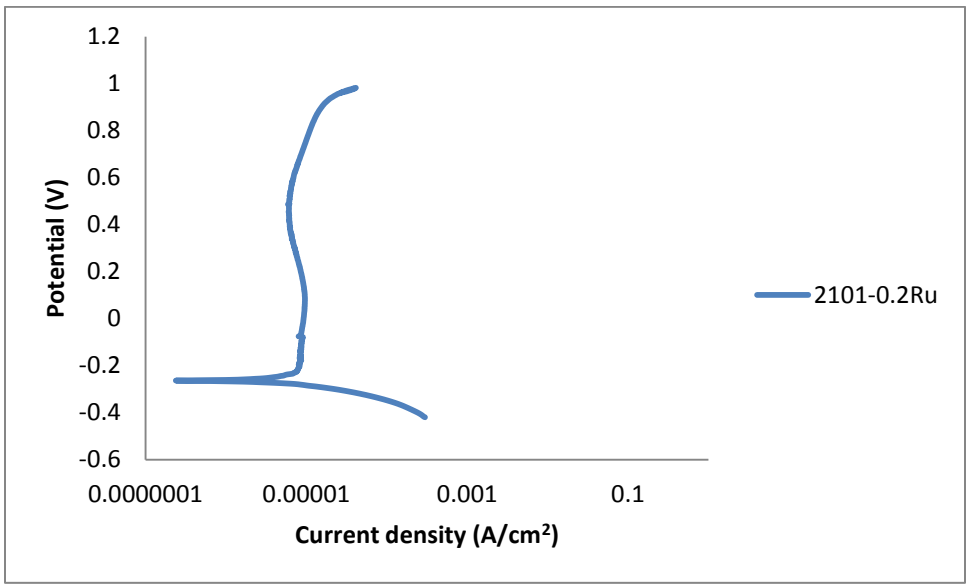

Figure 4.76. Potentiodynamic curve for 2101-0.2 wt% Ru in 0.5M H_2SO_4 at 25°C.

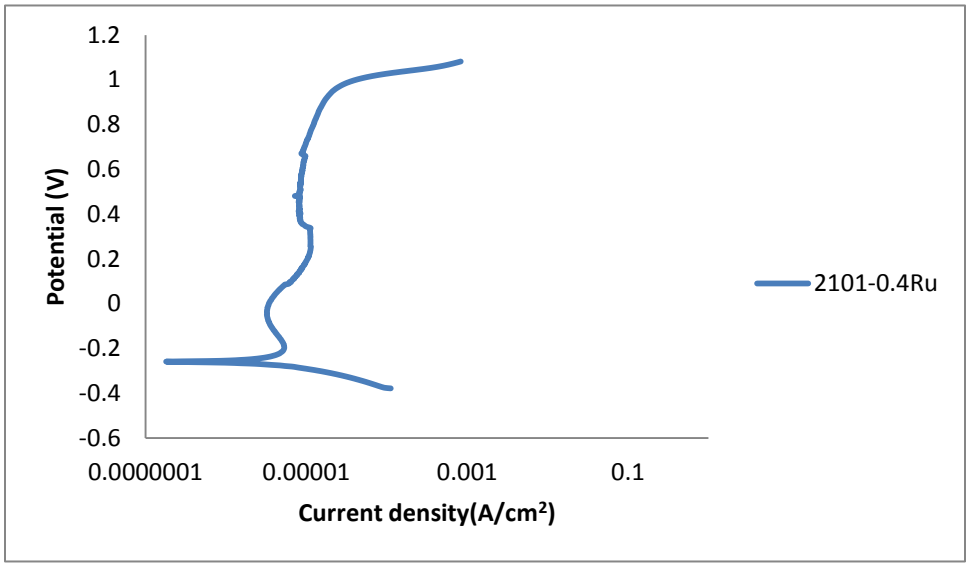

Figure 4.77. Potentiodynamic curve for 2101-0.4 wt% Ru in 0.5M H_2SO_4 at 25°C.

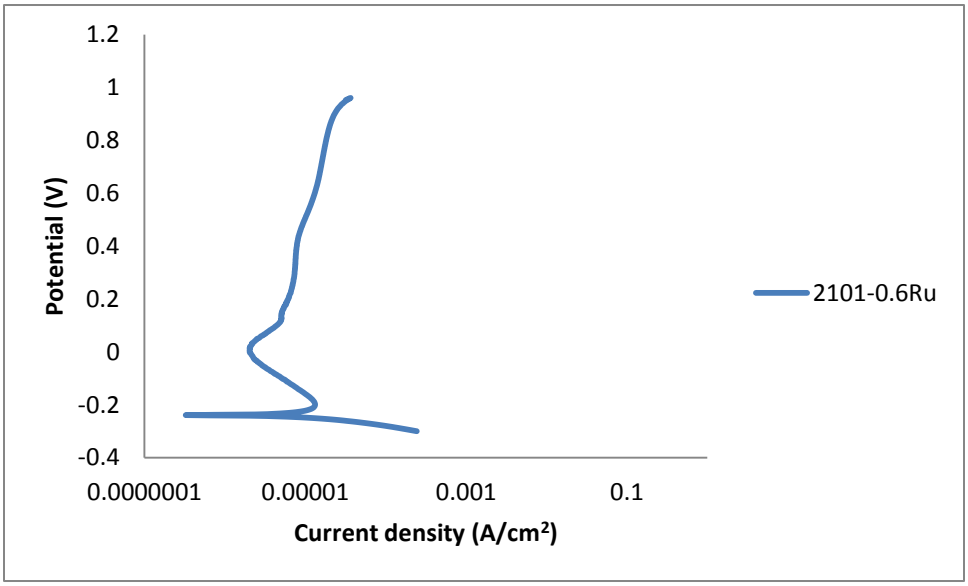

Figure 4.78. Potentiodynamic curve for 2101-0.6 wt% Ru in 0.5M H_2SO_4 at 25°C

Figure 4.78 shows the potentiodynamic curve 2101-0.6wt% Ru. The corrosion potential was at -239 mV.

The potentiodynamic curve for 2101-0.8 wt% Ru is presented in Figure 4.79. Anodic dissolution was observed. The i_{crit} value was 1.60×10^{-6}A/cm^2 and i_{pass} was 2.10×10^{-6}A/cm^2, similar to the other Ru contents.

Figure 4.80 shows the potentiodynamic curve for 2101-1 wt% Ru in 0.5M sulphuric acid. A marked drop in current densities was observed compared to Figures 4.78 and 4.79, which could be due to the improved resistance of the passive films formed, which could also be a barrier to diffusion. This effect was observed in the anodic part of the curve. The corrosion potential E_{corr} was 132 mV, which is the most noble of all the alloys in the 0.5 M sulphuric acid solution.

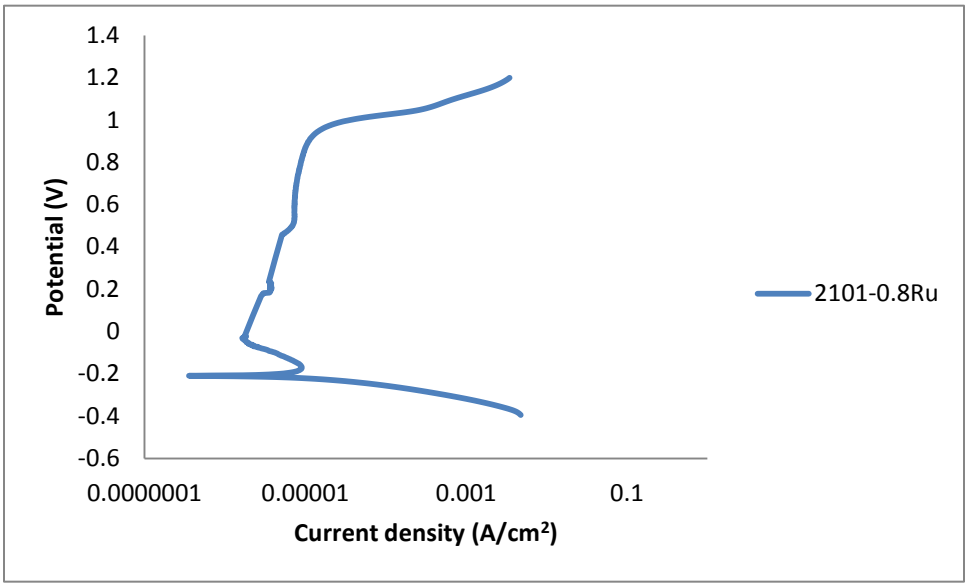

Figure 4.79. Potentiodynamic curve for 2101-0.8 wt% Ru in 0.5M H_2SO_4 at 25°C.

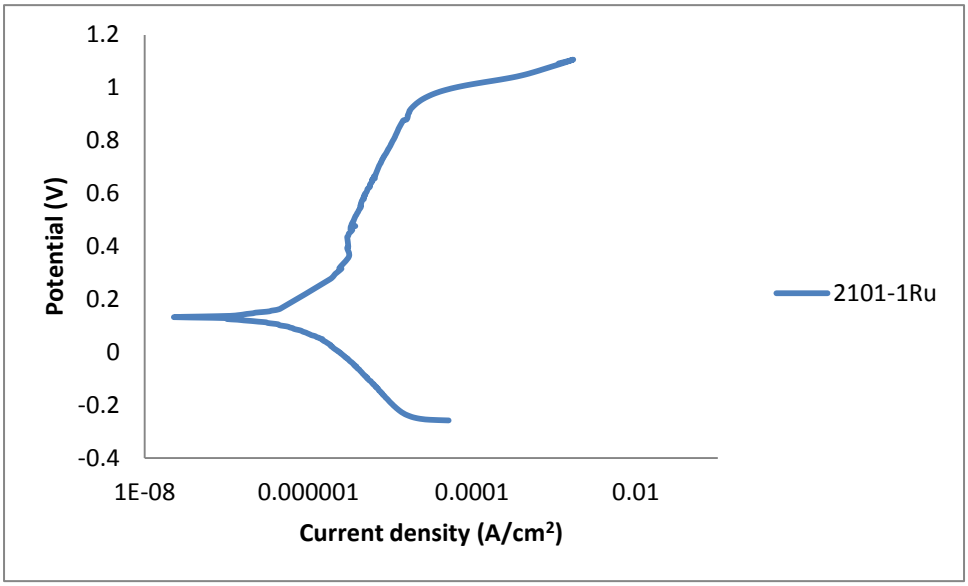

Figure 4. 80. Potentiodynamic curve for 2101-1 wt% Ru in 0.5M H_2SO_4 at 25°C.

Figures 4.81 – 4.83 present the potentiodynamic curves for 2101 with 0.1, 0.8 and 1.5 wt% Ru additions heat treated at 1100°C for 120 minutes. In Figure 4.81, i_{crit} was observed to be 1.24×10^{-6} A/cm^2 for 2101-0.1 wt% Ru, and anodic dissolution was observed. The i_{crit} value for 2101-0.8wt% Ru was 2.38 $\times10^{-5}$ A/cm^2, while for 1.5 wt% Ru addition it was 3.18 $\times10^{-5}$ A/cm^2 (Figures 4.81 and 4.82). The electrochemical results deduced from the curves are presented in Table 4.21.

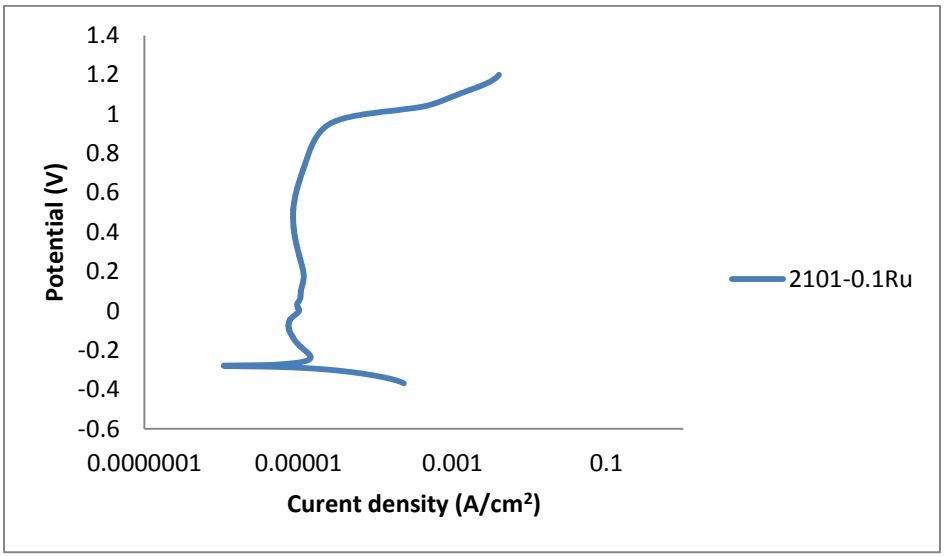

Figure 4.81. Potentiodynamic curve for 2101-0.1 wt% Ru heat treated at 1100°C in 0.5M H_2SO_4 at 25°C.

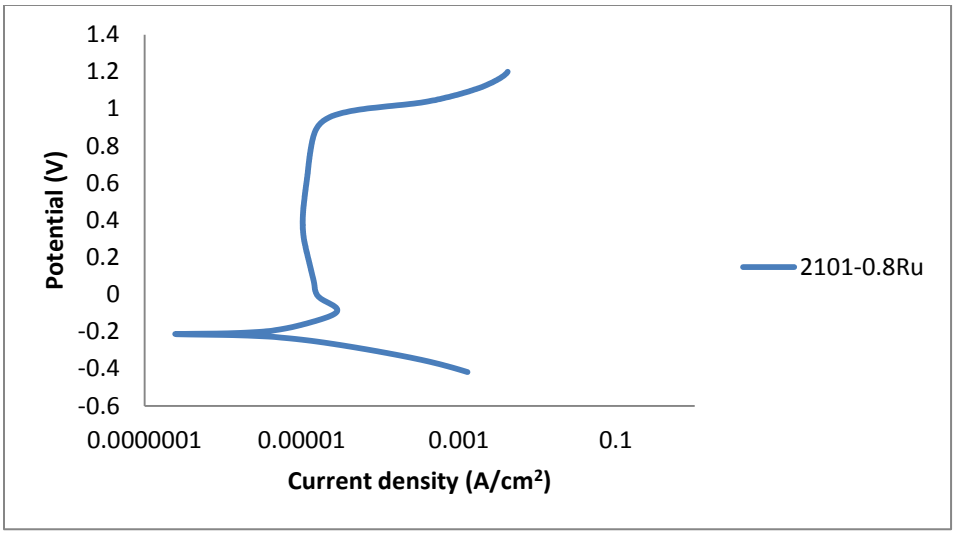

Figure 4.82. Potentiodynamic curve for 2101-0.8 wt% Ru heat treated at 1100°C in 0.5M H_2SO_4 at 25°C.

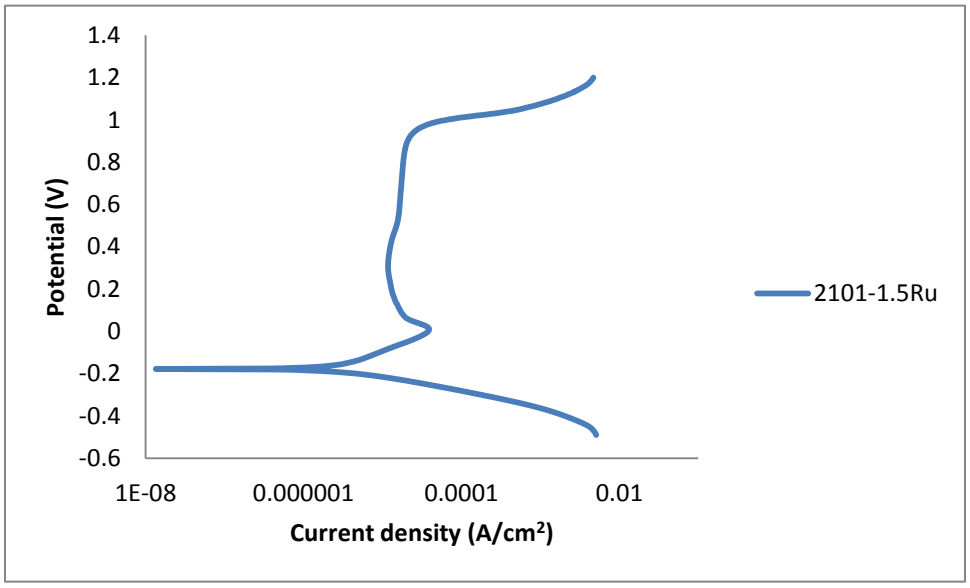

Figure 4.83. Potentiodynamic curve for 2101-1.5 wt% Ru heat treated at 1100°C in 0.5M H_2SO_4 at 25°C.

Table 4.21. Potentiodynamic data for 2101 steel samples with ruthenium in 0.5M H_2SO_4.

Heat treatment temp (°C)	Ru addition (wt%)	i_{crit} (A/cm^2)	E_{corr} (mV)	i_{corr} (A/cm^2)	Corrosion rate (mm/y)	i_{pass} (A/cm^2)
1080	0	1.10E-03	-325	4.93E-05	5.75E-01	2.5E-05
	0.15	-	-275	3.60E-06	4.20E-02	5.7E-06
	0.20	-	-264	3.43E-06	4.00E-02	6.3E-06
	0.40	2.90E-06	-258	9.70E-07	1.13E-02	3.1E-06
	0.60	1.80E-05	-239	2.03E-07	2.37E-03	2.3E-06
	0.80	1.60E-06	-200	1.27E-07	1.48E-03	2.1E-06
	1.00	-	132	1.18E-07	1.38E-03	8.9E-07
1100	0.10	1.24E-06	-281	3.40E-04	3.97E+00	8.6E-06
	0.80	2.38E-05	-212	8.95E-07	1.04E-02	1.0E-05
	1.50	3.18E-05	-179	2.27E-04	2.65E+00	1.2E-05

4.9.4 Electrochemical response of alloys in 1M sulphuric acid

The potentiodynamic response of 2101 stainless steel was investigated and the curves were reversed to evaluate the pitting potential of the alloys in 1M sulphuric acid at 25°C. The direction of the scans is shown by means of the red arrows on the graphs. Figure 4.84 shows the reversed scan for 2101 (with no Ru) exposed to 1M sulphuric acid at 25°C.

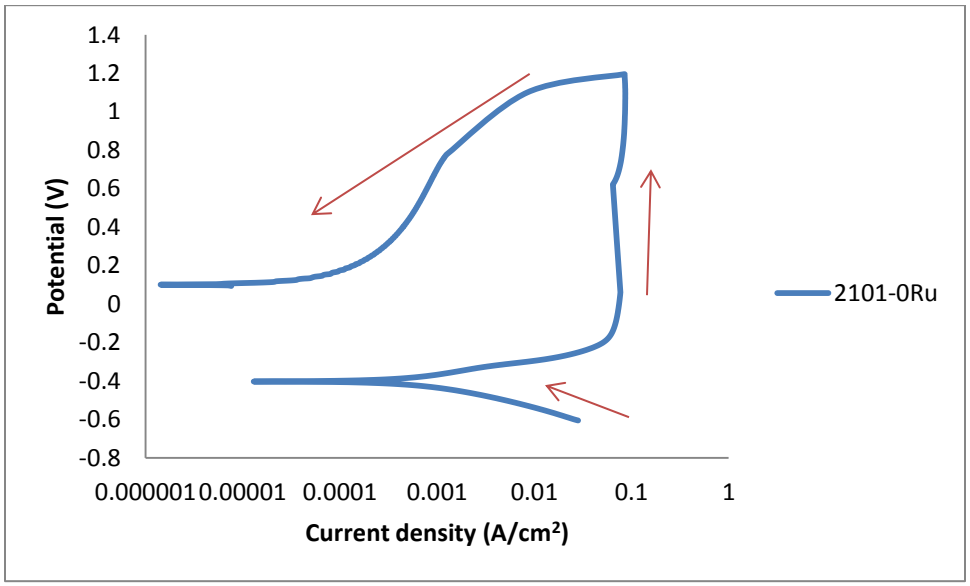

Figure 4.84. Potentiodynamic curve of 2101 duplex stainless steel in 1M H_2SO_4 at 25°C.

The effect of ruthenium addition to 2101 in 1M sulphuric acid at 25°C is shown in Figures 4.85 – 4.90. The corrosion potential increased with increasing ruthenium content, and the corrosion current and corrosion rate decreased with increases in ruthenium content. The electrochemical data are presented in Table 4.22.

Figure 4.85 shows the potentiodynamic curve of 2101-0.15 wt% Ru duplex stainless steel in 1M H_2SO_4 at 25°C. The curve has an active-passive transition, i_{crit} was observed at 2.26×10^{-5} A/cm^2, corrosion potential was at -231mV, and the passive current density was 1.1×10^{-5} A/cm^2.

The potentiodynamic curve of 2101-0.2 wt% Ru duplex stainless steel in 1M H_2SO_4 at 25°C is presented in Figure 4.86; the i_{crit} was seen at 6.61×10^{-6}A/cm^2, the corrosion potential was -208 mV, while the passive current was 9.75×10^{-6} A/cm^2. The corrosion potential of 2101-0.4 wt% Ru duplex stainless steel in 1M sulphuric acid solution at 25°C was -191 mV and the passive current density was 1.2×10^{-5} A/cm^2, the curve is presented in Figure 4.87. Figure 4.88 shows the potentiodynamic curve of 2101 duplex stainless steel with 0.6 wt% Ru in 1M H_2SO_4 at 25°C. The corrosion potential was -120 mV, the passive current density, i_{pass}, was 6.9×10^{-6} A/cm^2. The potentiodynamic curve of 2101-0.8 wt% Ru duplex stainless steel in 1M H_2SO_4 at 25°C is presented in Figure 4.89. It had a corrosion potential of -2 mV, and a passive current density of 7.1×10^{-6} A/cm^2. The effect of 1 wt% ruthenium addition to 2101 in 1M sulphuric acid at 25°C is shown in Figure 4.90. corrosion potential was 22 mV and the passive current density was 7.8×10^{-6} A/cm^2.

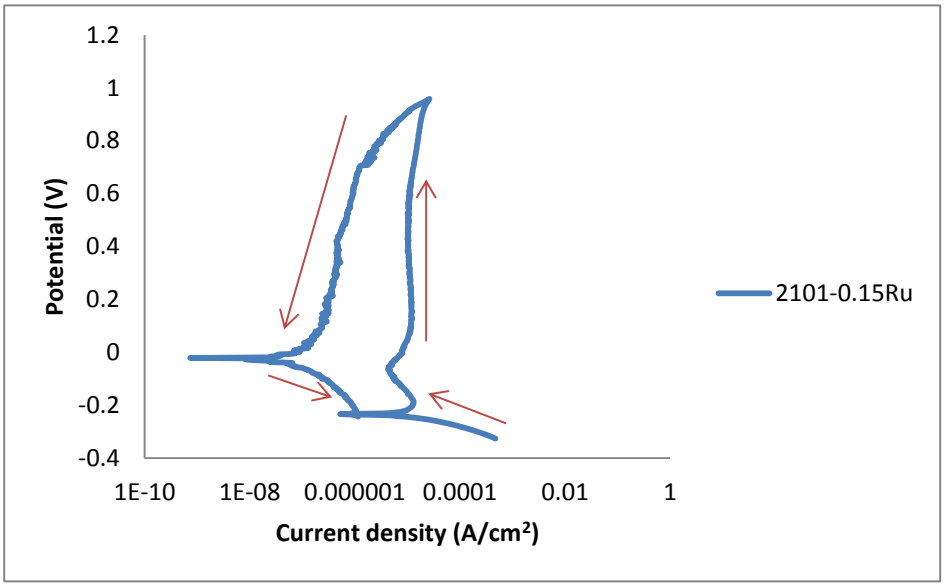

Figure 4.85. Potentiodynamic curve of 2101-0.15 wt% Ru duplex stainless steel in 1M H_2SO_4 at 25°C.

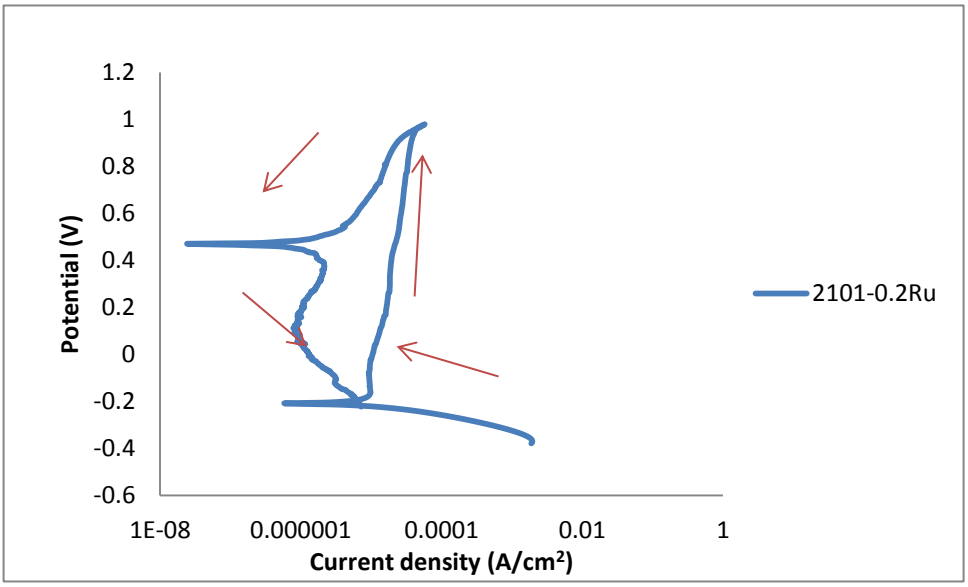

Figure 4.86. Potentiodynamic curve of 2101-0.2 wt% Ru duplex stainless steel in 1M H_2SO_4 at 25°C.

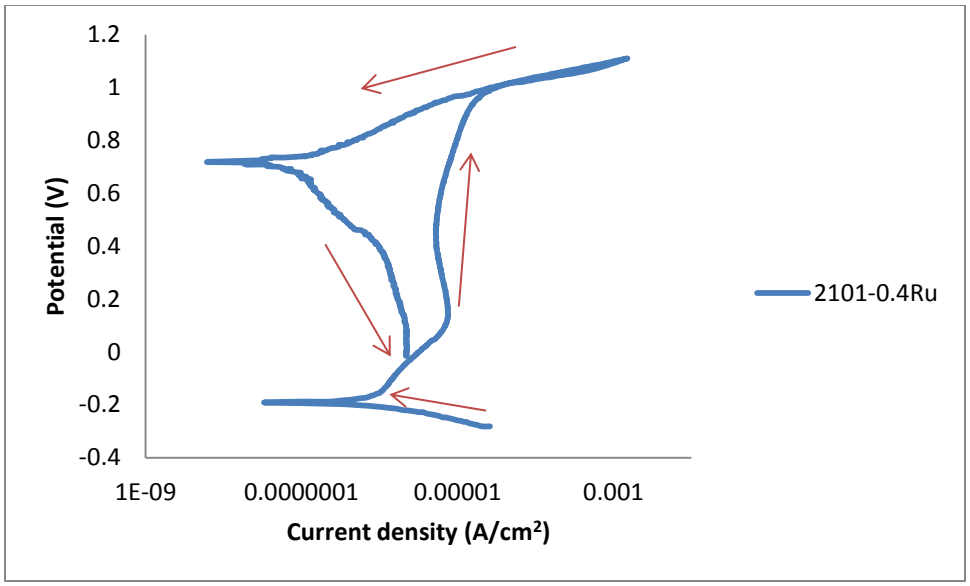

Figure 4.86. Potentiodynamic curve of 2101-0.4 wt% Ru duplex stainless steel in 1M H_2SO_4 at 25°C.

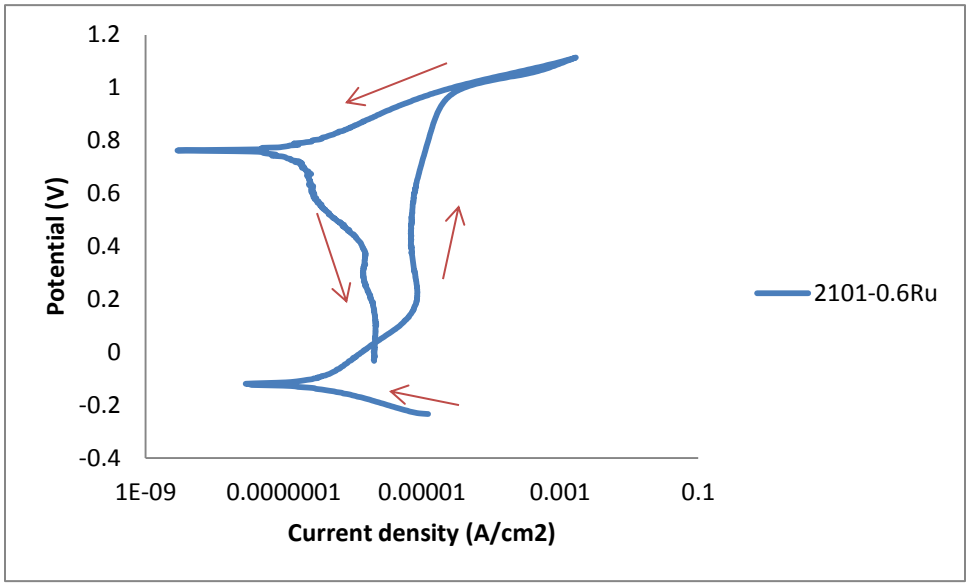

Figure 4.88. Potentiodynamic curve of 2101-0.6 wt% Ru duplex stainless steel in 1M H_2SO_4 at 25°C.

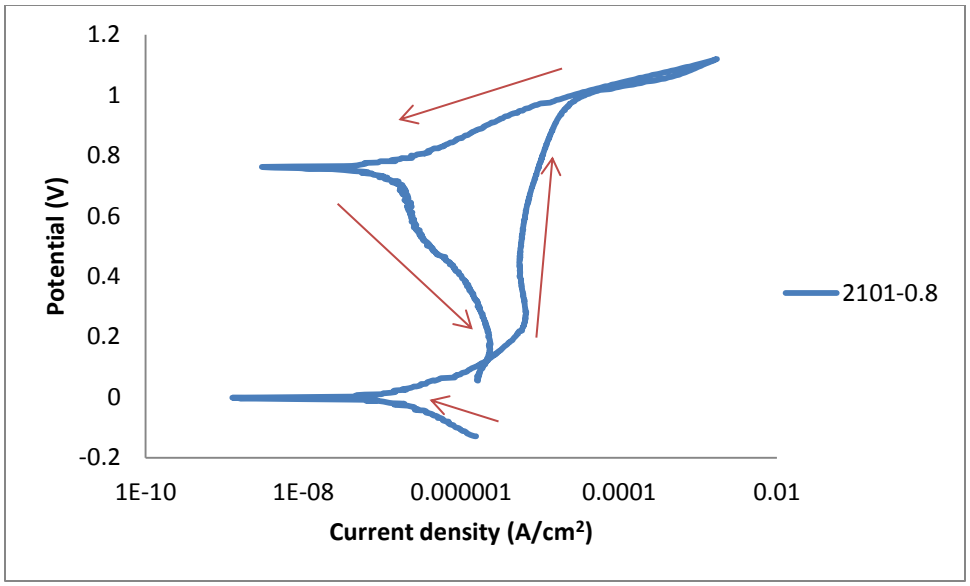

Figure 4.89. Potentiodynamic curve of 2101-0.8 wt% Ru duplex stainless steel in 1M H_2SO_4 at 25°C.

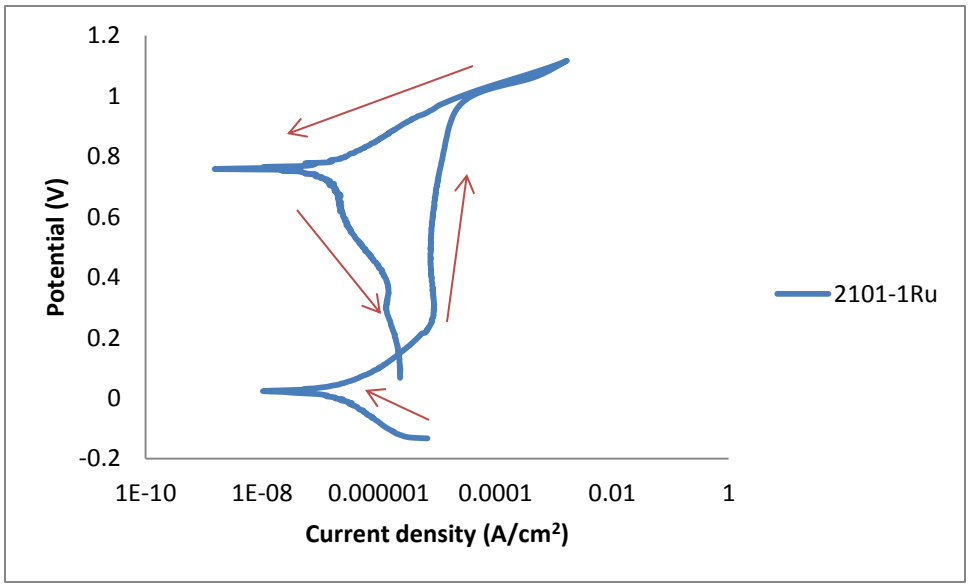

Figure 4.90. Potentiodynamic curve of 2101-1 wt% Ru duplex stainless steel in 1M H_2SO_4 at 25°C.

The responses of the 2101 alloy with 0.2, 0.4, 0.6, 0.8 and 1 wt% Ru in 1M sulphuric acid at 40°C are presented in Figures 4.91-4.95. The important electrochemical results are presented in

Table 4.22. Active to passive transitions were observed in the 2101 alloys containing 0.2, 0.4 and 0.6% wt% Ru, while the 2101 alloys containing 0.8 and 1wt% Ru (Figures 4.94 and 4.95) showed pseudo-passivity. The corrosion potential moved towards more noble values as the ruthenium content increased. The corrosion rate and the corrosion current decreased with increasing ruthenium contents in 2101 steel.

Figure 4.91 shows the potentiodynamic curve of 2101-0.2 wt% Ru duplex stainless steel in 1M sulphuric acid at 40°C. The corrosion potential was -408mV; it had a high critical current density of 1.97×10^{-3} A/cm^2, and passive current density of 1.2×10^{-4} A/cm^2.

The effect of 0.4 wt% ruthenium addition to 2101 duplex stainless steel in 1M sulphuric acid at 40°C is shown in Figure 4.92. The electrochemical parameters measured were i_{crit}, i_{pass}, and E_{corr}, and their values were 4.03×10^{-4} A/cm^2, 1.8×10^{-4} A/cm^2 and -198 mV, respectively.

The potentiodynamic curve of 2101-0.6 wt% Ru duplex stainless steel in 1M H_2SO_4 at 40°C is presented in Figure 4.93. It had a corrosion potential of -169mV, a passive current density of 2.4×10^{-4} A/cm^2, and a critical current density of 3.5×10^{-4} A/cm^2. The corrosion rate was 3.73mm/y

The corrosion potential of 2101-0.8 wt% Ru duplex stainless steel in 1M sulphuric acid solution at 40°C was -148 mV, passive current density was 2.4×10^{-4} A/cm^2 and the corrosion rate was 4.63×10^{-2} mm/y. The curve is presented in Figure 4.94.

The potentiodynamic curve of 2101-1wt% Ru duplex stainless steel in 1M H_2SO_4 at 40°C is presented in Figure 4.95. The corrosion potential was -59 mV.

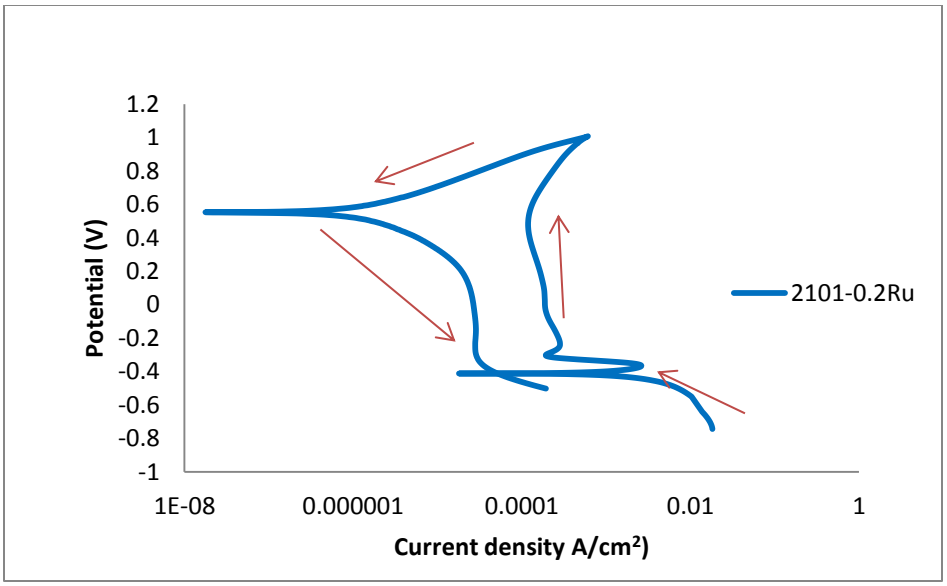

Figure 4.91. Potentiodynamic curve of 2101-0.2 wt% Ru duplex stainless steel in 1M H_2SO_4 at 40°C.

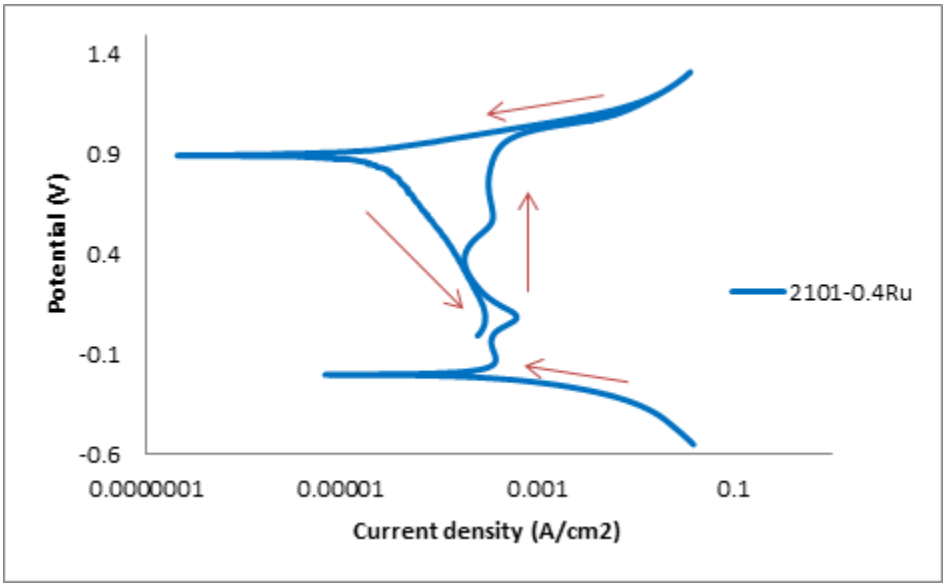

Figure 4.92. Potentiodynamic curve of 2101-0.4 wt% Ru duplex stainless steel in 1M H_2SO_4 at 40°C.

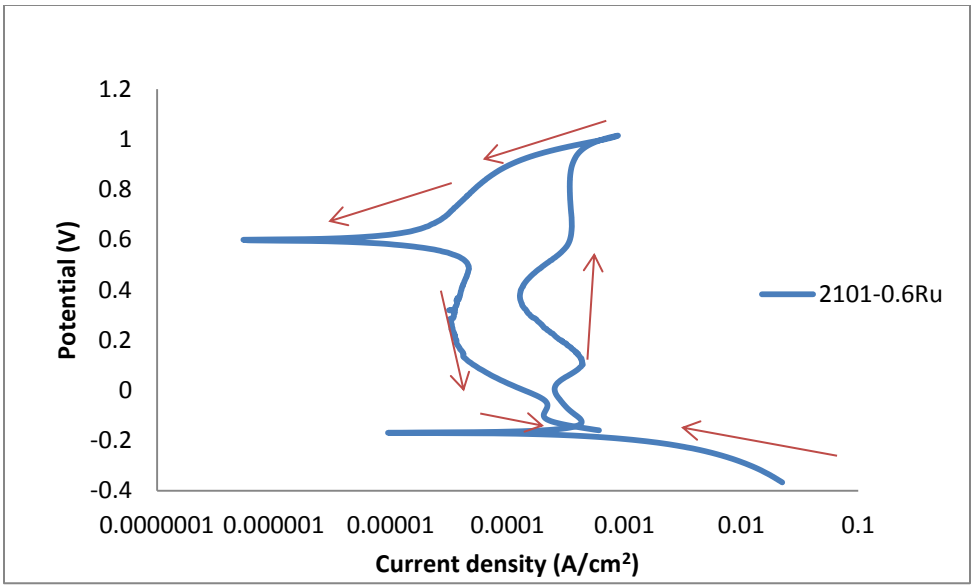

Figure 4.93. Potentiodynamic curve of 2101-0.6 wt% Ru duplex stainless steel in 1M H_2SO_4 at 40°C.

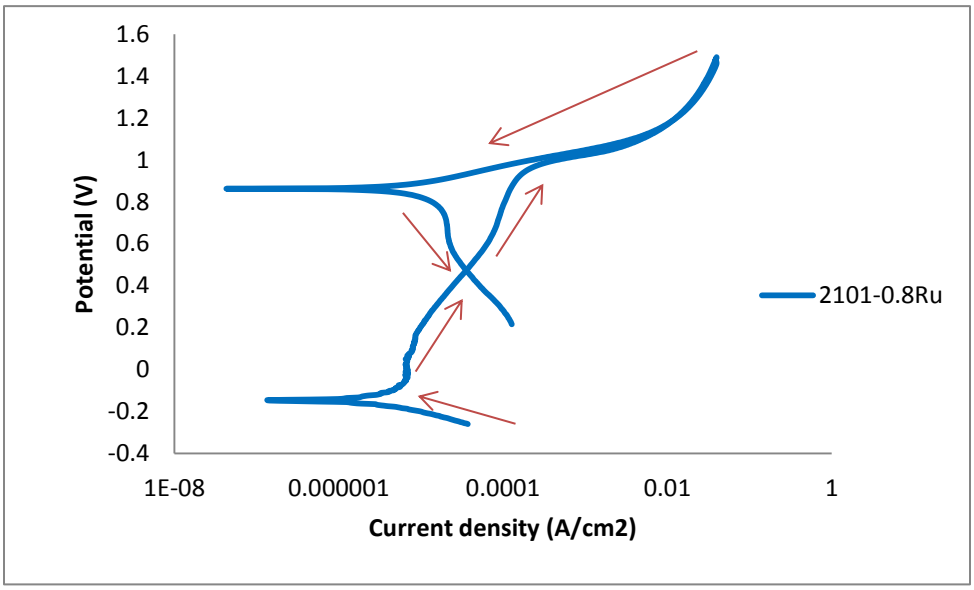

Figure 4.94. Potentiodynamic curve of 2101-0.8 wt% Ru duplex stainless steel in 1M H_2SO_4 at 40°C.

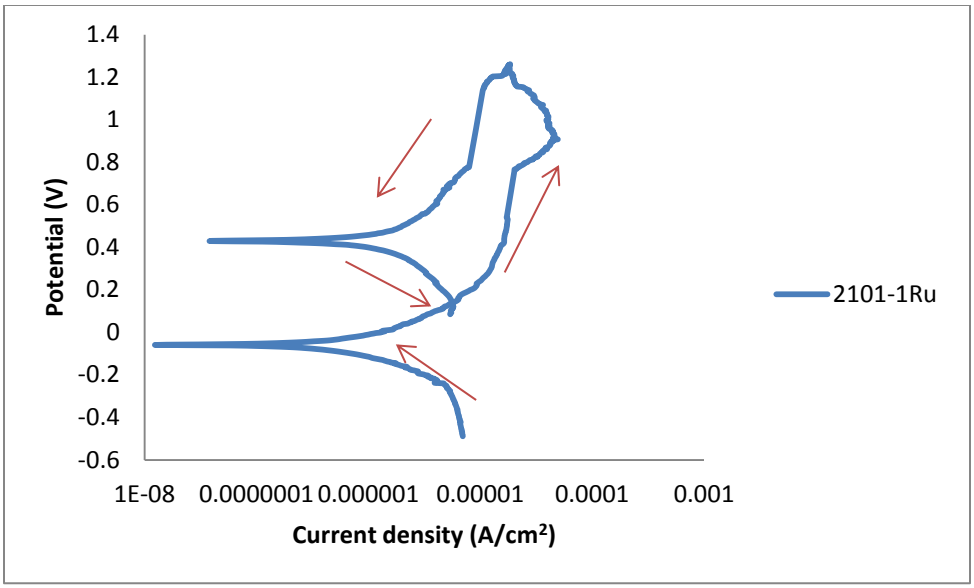

Figure 4.95. Potentiodynamic curve of 2101-1 wt% Ru duplex stainless steel in 1M H_2SO_4 at 40°C.

The potentiodynamic curves of 2101 with ruthenium in 1M H_2SO_4 at 60°C are shown in Figures 4.96-4.100. The corrosion potential increased with increasing ruthenium content, while the corrosion current and corrosion rate decreased. The electrochemical data are presented in Table 4.22. The shapes of the curves show active to passive transitions for the 2101 alloys containing 0.2 and 0.4 wt% Ru (Figures 4.96 and 4.97). Pseudo-passivity was observed for ruthenium additions of 0.6 - 1wt% Ru (Figures 4.98-4.100).

Figure 4.96 shows the potentiodynamic curve of 2101-0.2 wt% Ru duplex stainless steel in 1M H_2SO_4 at 60°C. The curve shows an active-passive transition, i_{crit} at 6.08×10^{-3} A/cm^2, E_{corr} was at -410 mV, and passive current density was 2.2×10^{-4} A/cm^2.

The potentiodynamic curve of 2101-0.4 wt% Ru duplex stainless steel in 1M H_2SO_4 at 60°C is presented in Figure 4.97. The i_{crit} was at 1.35^{-3}A/cm^2, the corrosion potential was -254 mV, while the passive current was 1.4×10^{-4} A/cm^2, slightly lower than the 0.2wt% Ru alloy.

The effect of 0.6 wt% ruthenium addition to 2101 in 1M sulphuric acid solution at 60°C is shown in Figure 4.98. E_{corr} was -244 mV and the passive current density was 6.6×10^{-4} A/cm^2.

The potentiodynamic curve of 2101-0.8 wt% Ru duplex stainless steel in 1M H_2SO_4 at 60°C is presented in Figure 4.99. It had a corrosion potential of -225 mV and the passive current density of 1.6×10^{-5} A/cm^2.

Figure 4.100 shows the. potentiodynamic curve of 2101-1 wt% Ru duplex stainless steel in 1M sulphuric acid at 60°C. It had a corrosion potential of -140mV.

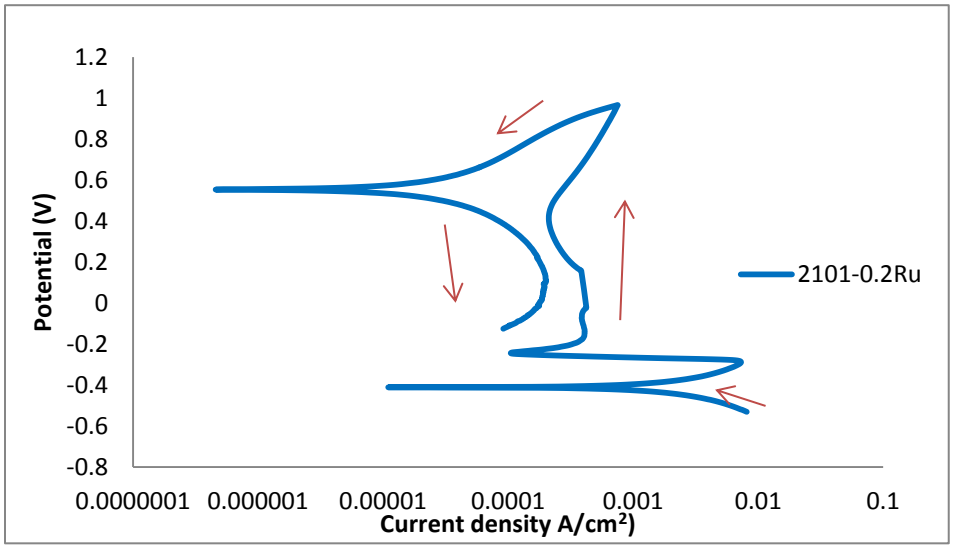

Figure 4.96. Potentiodynamic curve of 2101-0.2 wt% Ru duplex stainless steel in 1M H_2SO_4 at 60°C.

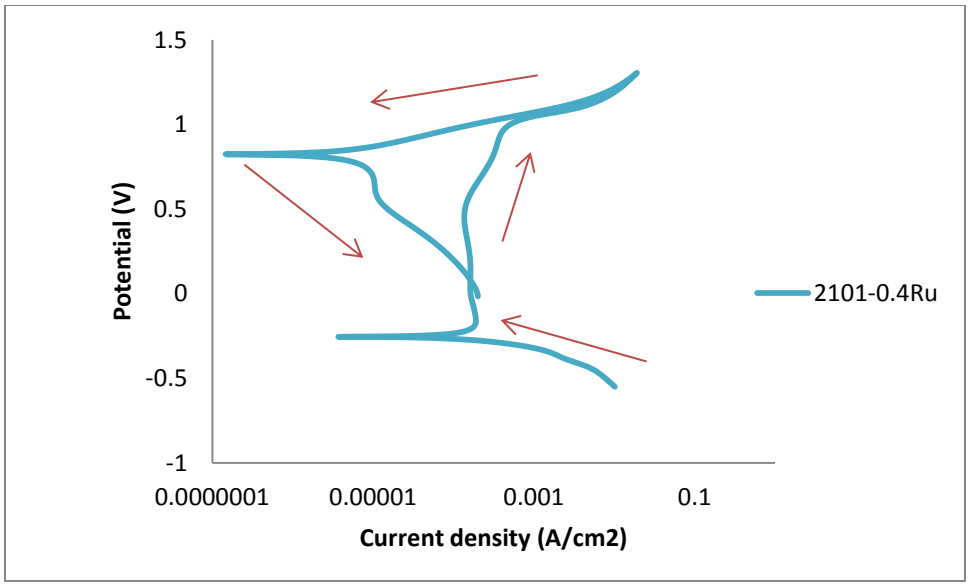

Figure 4.97. Potentiodynamic curve of 2101-0.4 wt% Ru duplex stainless steel in 1M H_2SO_4 at 60°C.

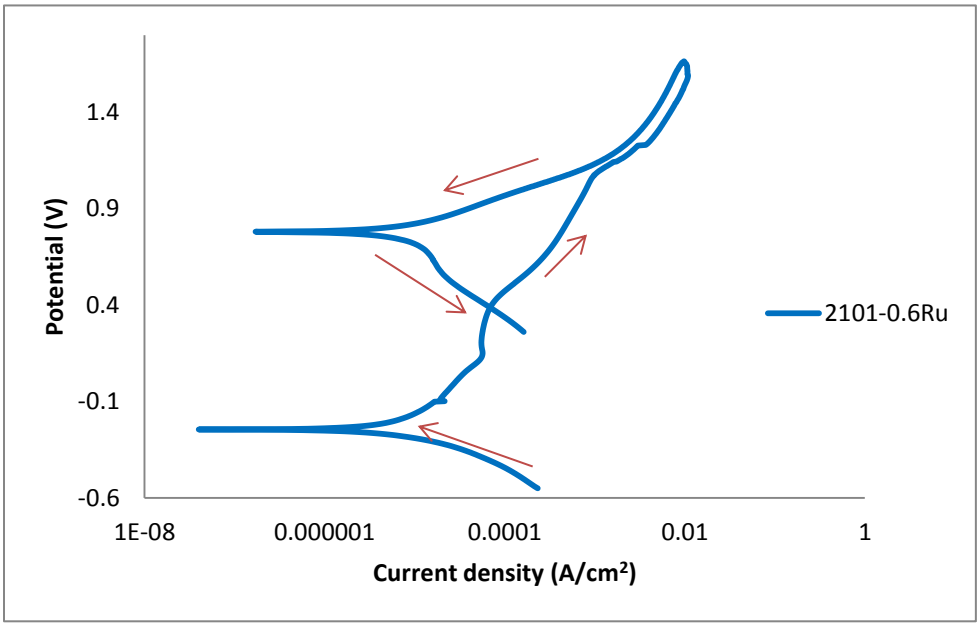

Figure 4.98. Potentiodynamic curve of 2101-0.6 wt% Ru duplex stainless steel in 1M H_2SO_4 at 60°C.

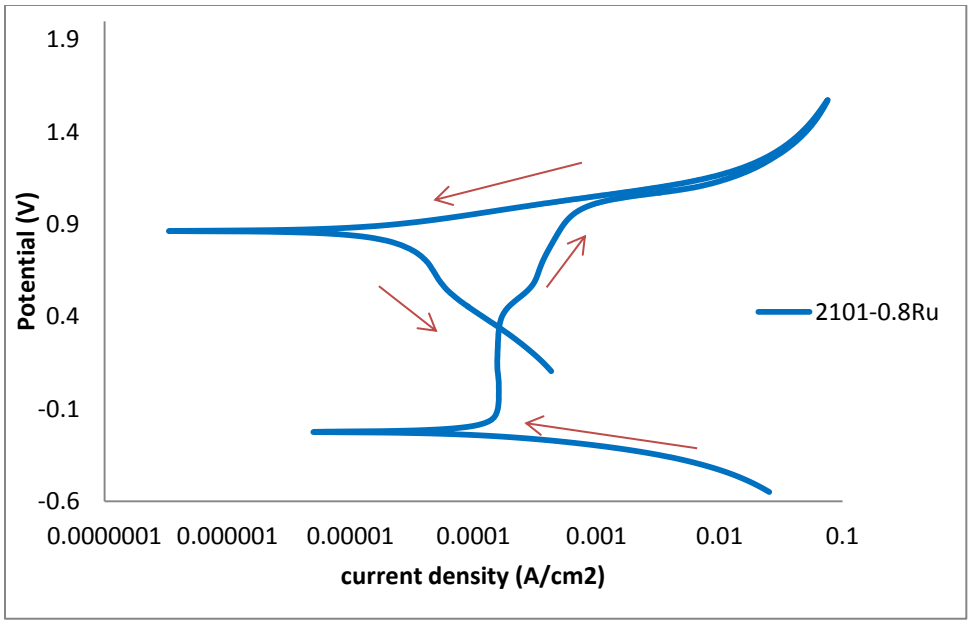

Figure 4.99. Potentiodynamic curve of 2101-0.8 wt% Ru duplex stainless steel in 1M H_2SO_4 at 60°C.

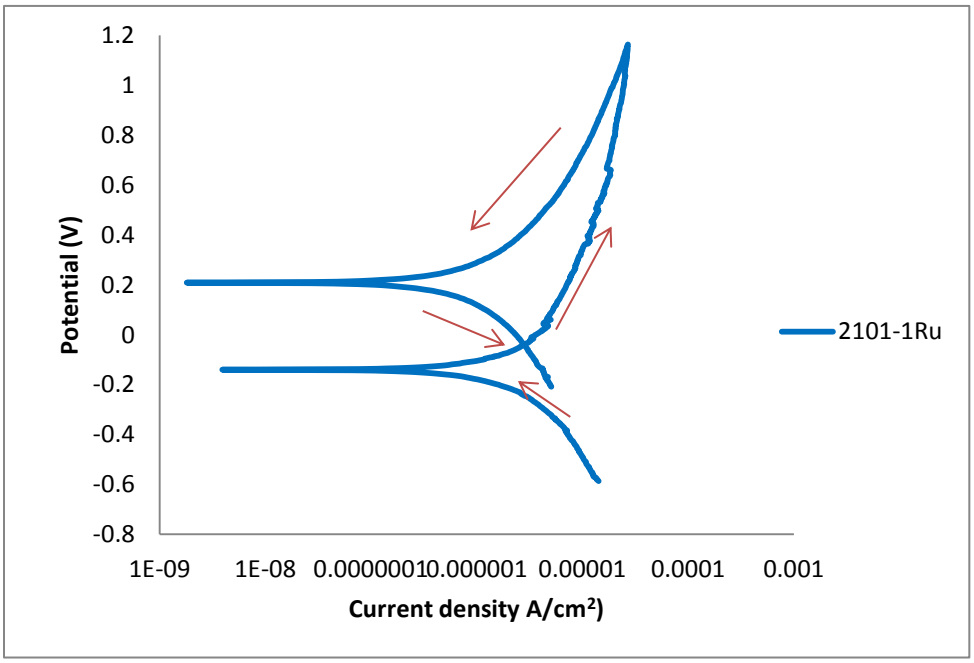

Figure 4.100. Potentiodynamic curve of 2101-1 wt% Ru duplex stainless steel in 1M H_2SO_4 at 60°C.

Table 4.22. Potentiodynamic data for 2101 steel samples with ruthenium in 1M H_2SO_4.

Temperature (°C)	Alloy type (wt% Ru)	E_{corr} (mV)	i_{corr} (A/cm^2)	Corrosion rate (mm/y)	i_{pass} (A/cm^2)
25	0	-403	1.42E-03	1.66E+01	6.57E-04
	0.15	-231	1.20E-05	1.40E-01	1.1 E-05
	0.20	-208	9.03E-06	1.06E-01	1.1 E-05
	0.40	-191	1.08E-06	1.26E-02	1.2 E-05
	0.60	-120	4.04E-07	4.72E-03	6.9E-06
	0.80	-002	2.16E-07	2.53E-03	7.1 E-06
	1.00	22	1.80E-07	2.10E-03	7.8 E-06
40	0.20	-408	1.90E-03	2.22E+01	1.2E-04
	0.40	-198	6.87E-04	8.03E+00	1.8E-04
	0.60	-169	3.19E-04	3.73E+00	2.4 E-04
	0.80	-148	3.96E-06	4.63E-02	2.7 E-05
	1.00	-59	4.66E-07	5.45E-03	4.4 E-05
60	0.20	-410	2.00E-03	2.34E+01	2.2 E-04
	0.40	-254	3.33E-04	3.89E+00	1.4E-04
	0.60	-244	3.18E-04	3.72E+00	6.6E-04
	0.80	-225	5.83E-05	6.82E-01	1.6E-05
	1.00	-140	8.22E-07	9.61E-03	1.0E-05

4.9.5 Electrochemical behaviour of 2101 duplex stainless steel in 0.5M HCl

The potentiodynamic tests were performed in triplicate in 0.5M HCl solution. These tests were only performed with a forward scan and not reversed, in order to only study passivation characteristics. The whole range of alloys showed active–passive transitions at 25°C (Figures 4.101-107) and i_{crit} values were observed for all the alloys at room temperature. The passive current densities were high, the passive ranges were short and anodic dissolution was observed.

Figure 4.101 shows the potentiodynamic curve of 2101-0 wt% Ru duplex stainless steel in 0.5M hydrochloric acid. The corrosion potential was -460mV, critical current density was 2.2×10^{-3} A/cm^2, and passive current density was 1.4×10^{-4} A/cm^2.

The potentiodynamic curve of 2101-0.05 wt% Ru duplex stainless steel is presented in Figure 4.102. It exhibited an active to passive transition, and had a critical current density of 4.88×10^{-3} A/cm^2 and a passive current density of 4.4×10^{-4} A/cm^2.

The effect of 0.15 wt% ruthenium addition on 2101 duplex stainless steel in 0.5M hydrochloric acid was shown in Figure 4.103. The electrochemical parameters measured were i_{crit}, i_{pass}, and E_{corr}, and their values were 1.6×10^{-3} A/cm^2, 4.8×10^{-6} A/cm^2 and -445 mV respectively.

The potentiodynamic curve of 2101-0.4 wt% Ru duplex stainless steel in 0.5M HCl is presented in Figure 4.104. It had a corrosion potential of -420mV, a passive current density of 6.1×10^{-4} A/cm^2, and a critical current density of 7.9×10^{-4} A/cm^2.

The potentiodynamic curve of 2101-0.6 wt% Ru duplex stainless steel in 0.5M HCl is presented in Figure 4.105. The corrosion potential was -417 mV, critical current density was. 4.3×10^{-4} A/cm^2 and the passive current density of 1.0×10^{-4} A/cm^2.

The corrosion potential of 2101-0.8 wt% Ru duplex stainless steel in 0.5M HCl acid solution was -405mV, passive current density was 1.0×10^{-4} A/cm^2 and the critical current density of 1.3×10^{-4} A/cm^2. The curve is presented in Figure 4.106, and showed an active to passive transition. The nose at the critical current density was pronunced.

Figure 4.107 shows the potentiodynamic curve of 2101-1 wt% Ru duplex stainless steel in 0.5M hydrochloric acid. The corrosion potential was 138mV; it had a passive current density of 9.7×10^{-6} A/cm^2.

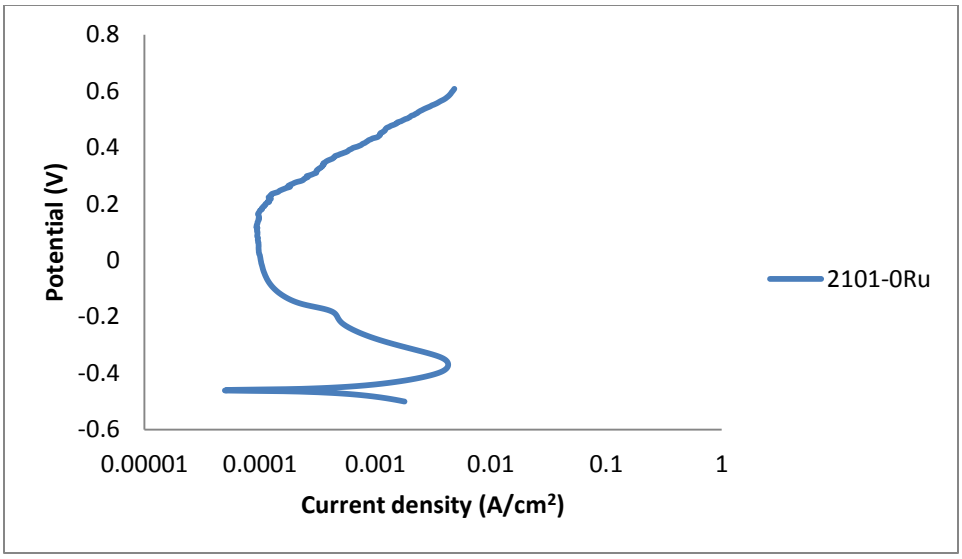

Figure 4.101. Potentiodynamic curve of 2101duplex stainless steel in 0.5M HCl.

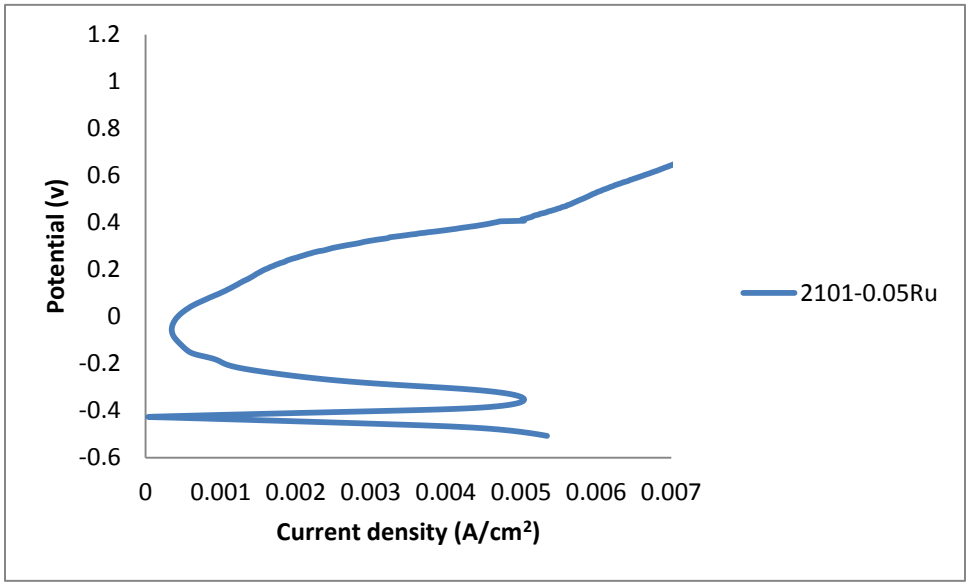

Figure 4.102. Potentiodynamic curve of 2101-0.05 wt% Ru duplex stainless steel in 0.5M HCl.

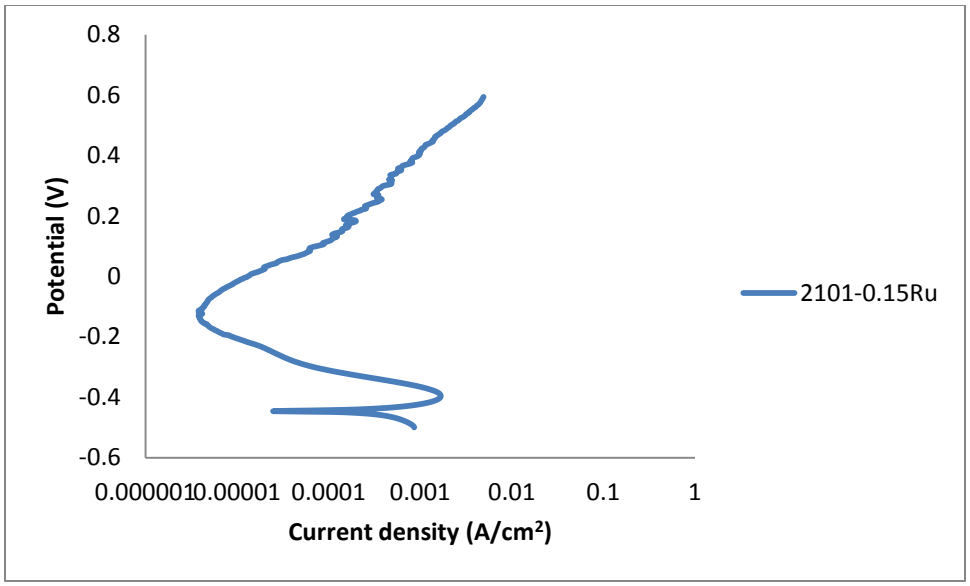

Figure 4.103. Potentiodynamic curve of 2101-0.15 wt% Ru duplex stainless steel in 0.5M HCl.

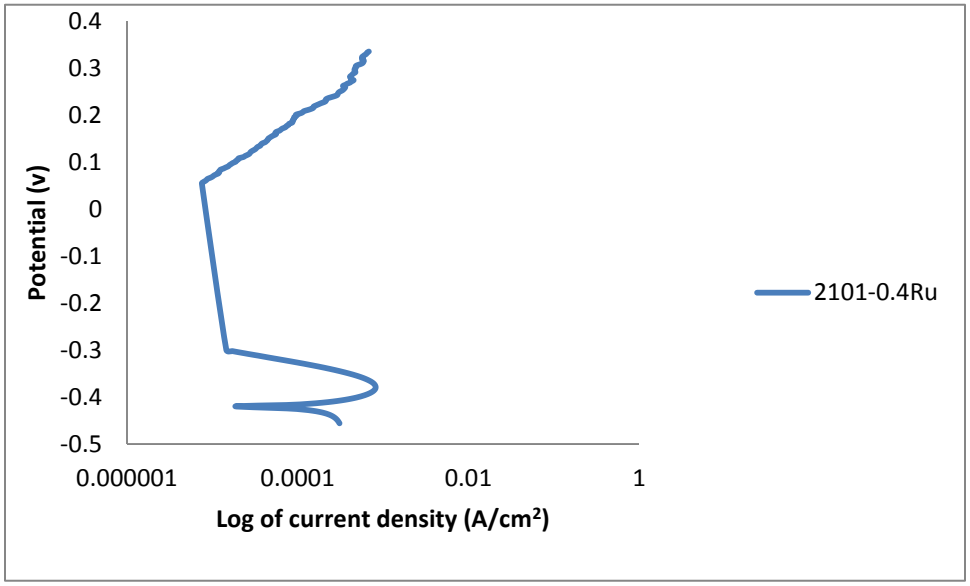

Figure 4.104. Potentiodynamic curve of 2101-0.4 wt% Ru duplex stainless steel in 0.5M HCl.

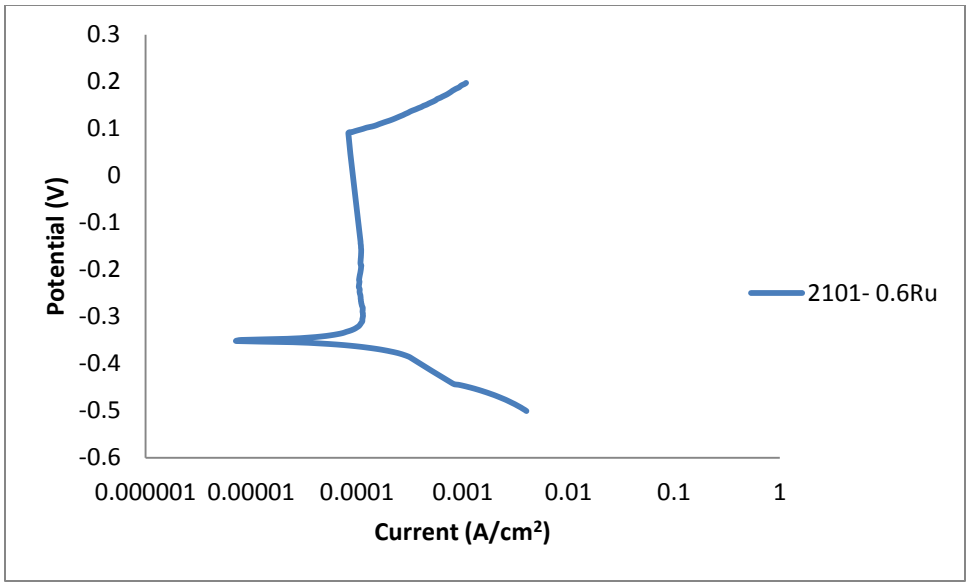

Figure 4.105. Potentiodynamic curve of 2101-0.6 wt% Ru duplex stainless steel in 0.5M HCl.

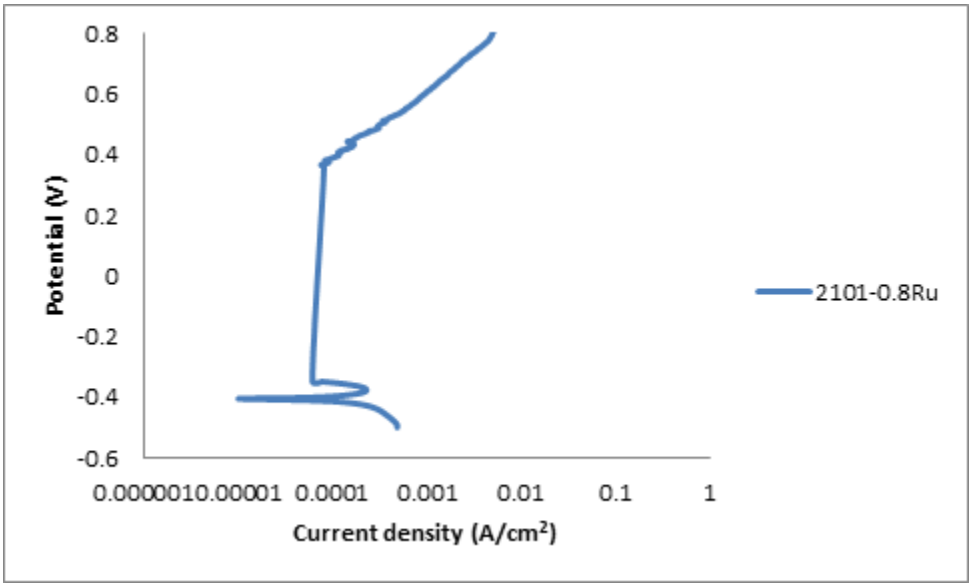

Figure 4.106. Potentiodynamic curve of 2101-0.8 wt% Ru duplex stainless steel in 0.5M HCl.

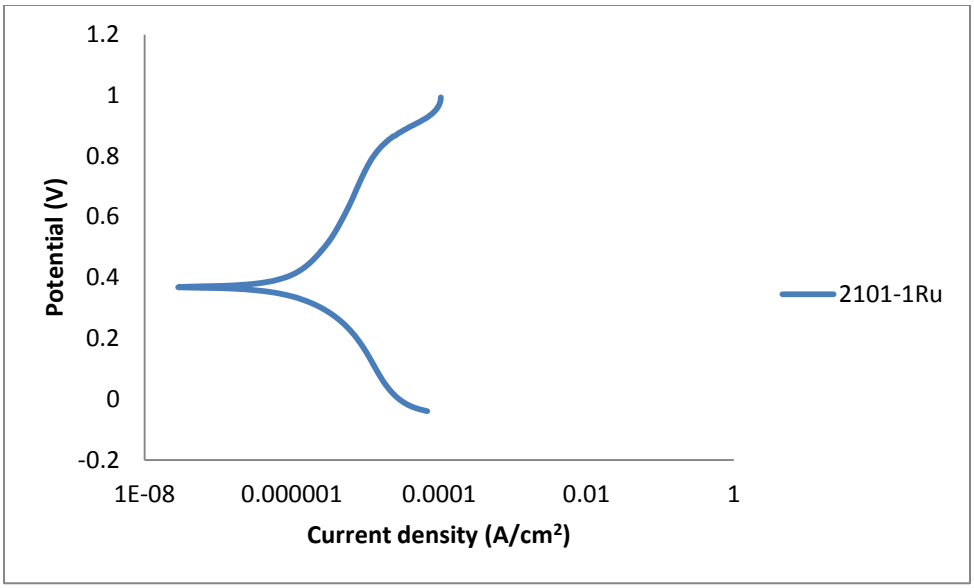

Figure 4.107. Potentiodynamic curve of 2101-1 wt% Ru duplex stainless steel in 0.5M HCl.

Table 4.23. Potentiodynamic data for 2101 steel samples with ruthenium in 0.5M HCl.

Ru addition (wt%)	i_{crit} (A/cm^2)	E_{corr} (mV)	i_{corr} (A/cm^2)	Corrosion rate (mm/y)	i_{pass} (A/cm^2)
0	2.2E-03	-460	7.6E-01	8.88E+03	1.4E-04
0.15	1.6E-03	-445	8.3E-02	9.70E+02	4.8E-06
0.40	7.9E-04	-420	4.6E-02	5.38E+02	6.1E-04
0.60	4.3E-04	-417	3.7E-02	4.33E+02	1.0E-04
0.80	1.3E-04	-405	2.8E-02	3.27E+02	1.0E-04
1.00	2.3E-06	138	1.4E-11	1.64E-07	9.7E-06

4.9.6 Cyclic potentiodynamic tests

Cyclic potentiodynamic polarization measurements were done to determine the corrosion rates, evaluate the passivity and repassivation behaviour of the alloys, and to assess the pitting of the alloys in 3.5M sodium chloride solution (Figures 4.108- 4.113). The electrochemical results from cyclic potentiodynamic tests in 3.5M sodium chloride at 25°C are presented in Table 4.24. The corrosion potential increased and the size of the hysteresis loop decreased with increasing

ruthenium content, hence showing resistance to pitting corrosion as the ruthenium content increased. The corrosion current and corrosion rate decreased with increasing ruthenium content. The cathodic slopes, β_c (the slope of the cathodic part of the curve), became more negative as the ruthenium contents increased, indicating a slight increase in corrosion resistance (Table 4.24).

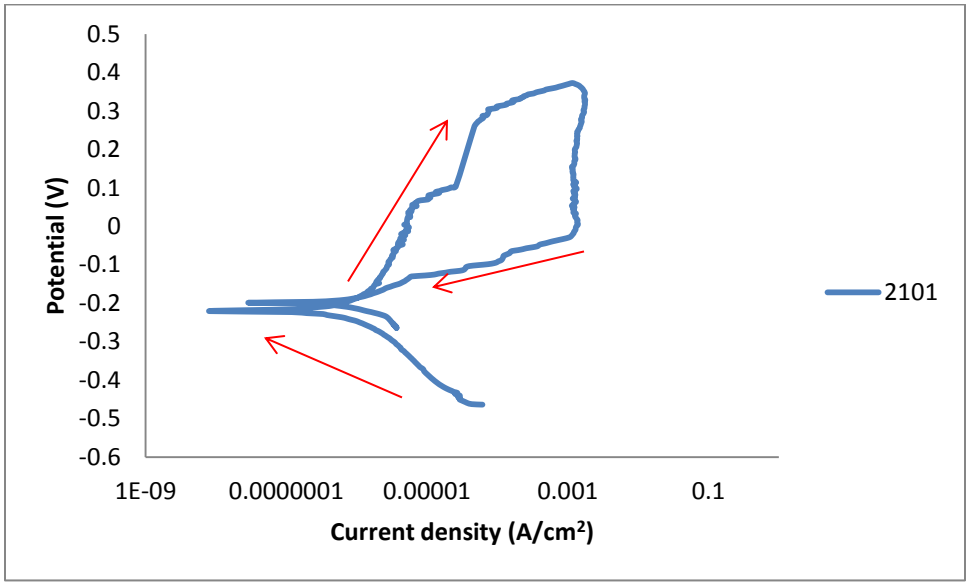

Figure 4.108. Cyclic polarization curve of 2101 in 3.5M NaCl.

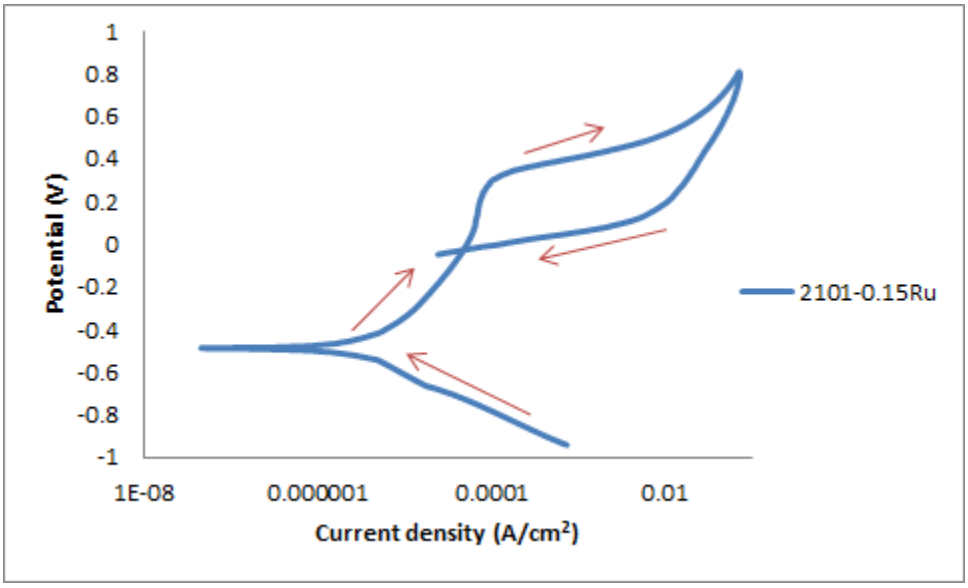

Figure 4.109. Cyclic polarization curve of 2101-0.15 wt% Ru in 3.5M NaCl.

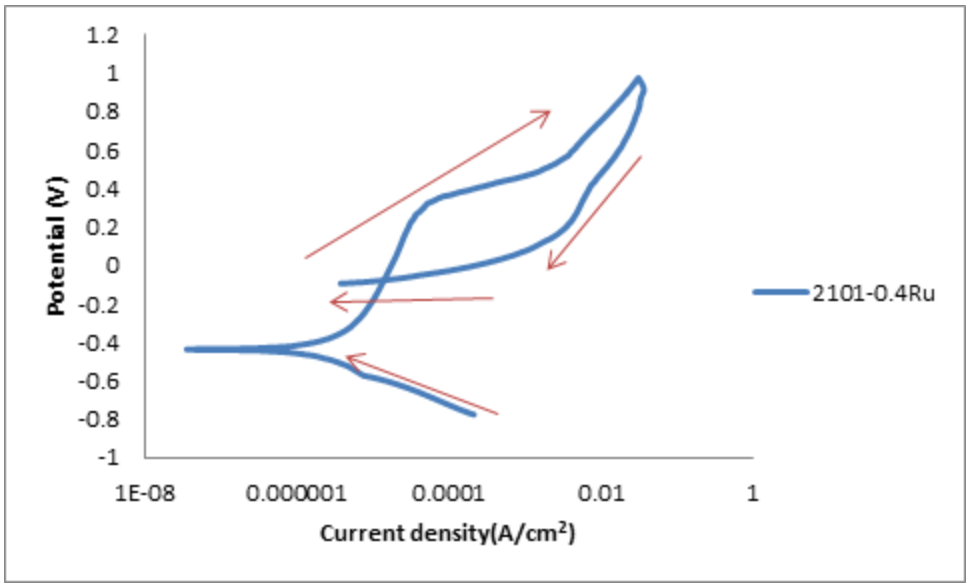

Figure 4.110. Cyclic polarization curve of 2101-0.4 wt% Ru in 3.5M NaCl.

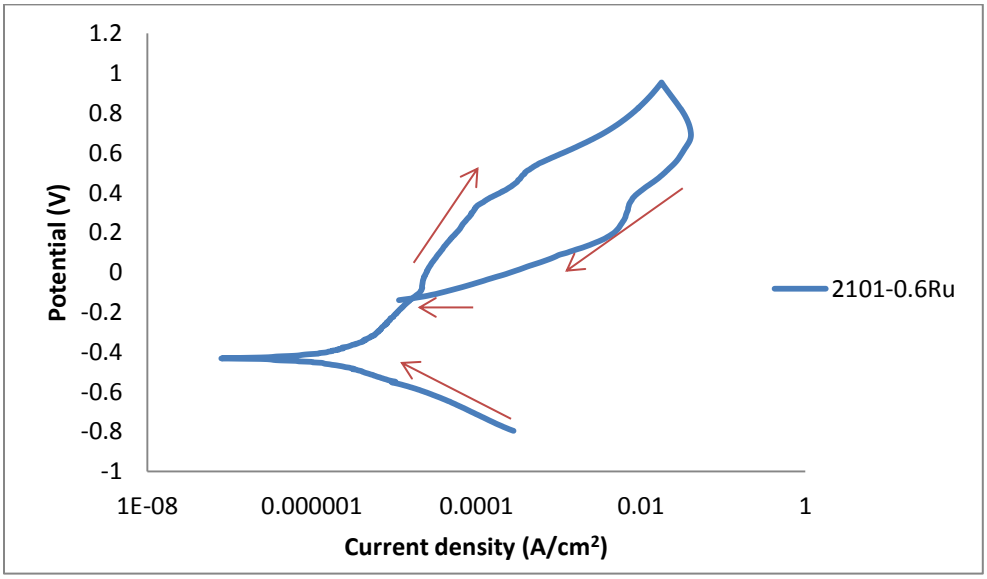

Figure 4.111. Cyclic polarization curve of 2101-0.6 wt% Ru in 3.5M NaCl.

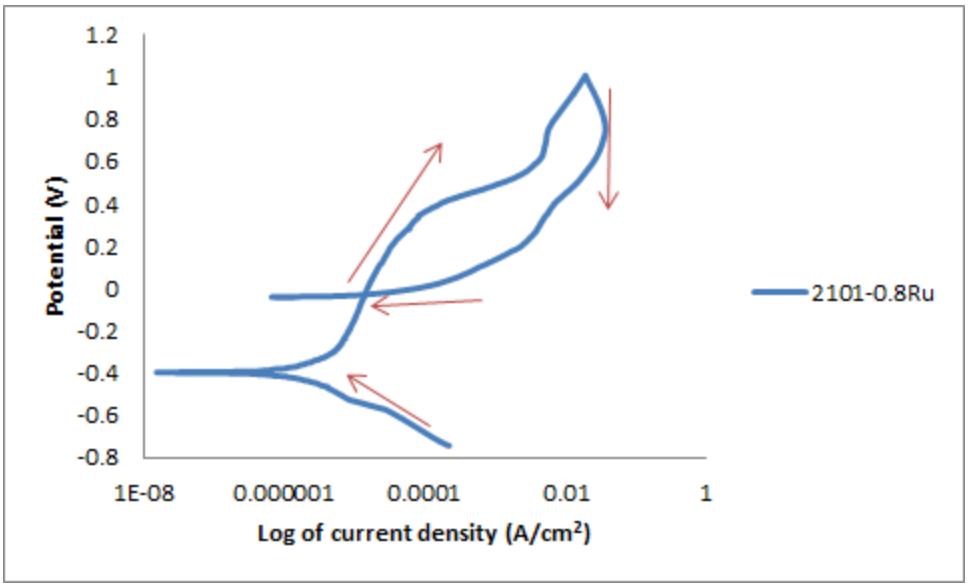

Figure 4.112. Cyclic polarization curve of 2101-0.8 wt% Ru in 3.5M NaCl.

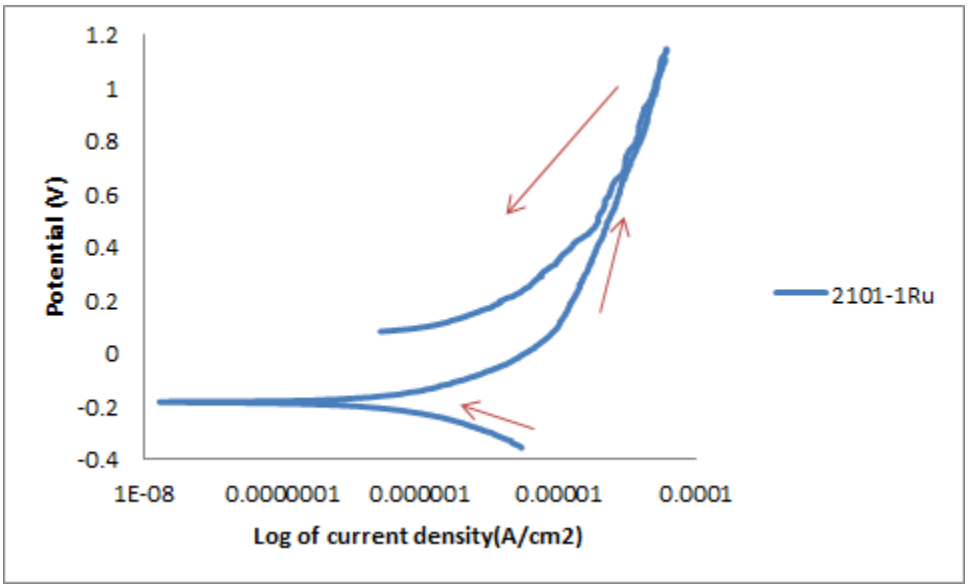

Figure 4.113. Cyclic polarization curve of 2101-1 wt% Ru in 3.5M NaCl.

Table 4.24. Potentiodynamic data for 2101 steel samples with ruthenium in 3.5M NaCl.

Ru addition (wt%)	E_{corr} (mV)	I_{corr} (A/cm^2)	Corrosion rate (mm/y)	β_c (mv/dec)
0.15	-486	4.90E-06	5.73E-02	-143
0.4	-435	2.67E-06	3.12E-02	-145
0.6	-432	2.30E-06	2.69E-02	-154
0.8	-396	1.87E-06	2.19E-02	-198
1.0	-186	9.61E-07	1.12E-02	-203

4.9.7 Potentiodynamic measurements of 2101 with ruthenium in different media

The potentiodynamic curves for 2101-0.15wt% Ru, heat treated at 1080°C for 90 minutes in 1M H_2SO_4 and 1M H_2SO_4 + 1%NaCl are shown in Figure 4.114. The addition of chloride to sulphuric acid increased the corrosion potential of the 2101-0.15 wt% ruthenium sample at 25°C. The 2101-0.15 wt% Ru alloy exposed to sulphuric acid containing chloride produced a critical current density (i_{crit}) slightly higher than in the sulphuric acid solution alone. The passive region was wider in sulphuric acid than in sulphuric acid with chloride solution. The passive current density (i_{pass}) was slightly increased by the presence of chloride. The E_{pass} was lower in the solution containing only sulphuric acid. The calculated corrosion rate was higher for the solution containing chloride than for the solution containing only sulphuric acid. This could be due to its higher critical current density and smaller passive region.

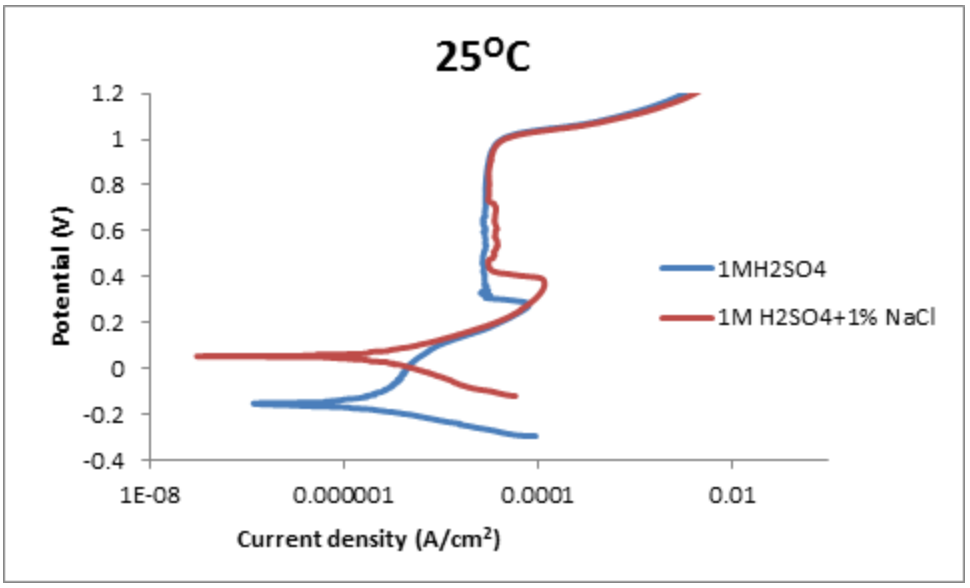

Figure 4.114. Potentiodynamic curves for 2101-0.15 wt% Ru in 1M H_2SO_4 and 1M H_2SO_4 + 1%NaCl at 25°C.

The potentiodynamic curves showing the effects of sulphuric acid and sulphuric acid with chloride solutions on 2101-0.15 wt% Ru at 40°C is presented in Figure 4.115. The critical current density (i_{crit}) and the i_{pass} were higher in sulphuric acid with chloride solution than in the sulphuric acid solution. The passive region was longer in the solution with chloride than for sulphuric acid solution alone. The region of passivity started at ~600 mV, then decreased in current density slightly before it became constant with potential increase.

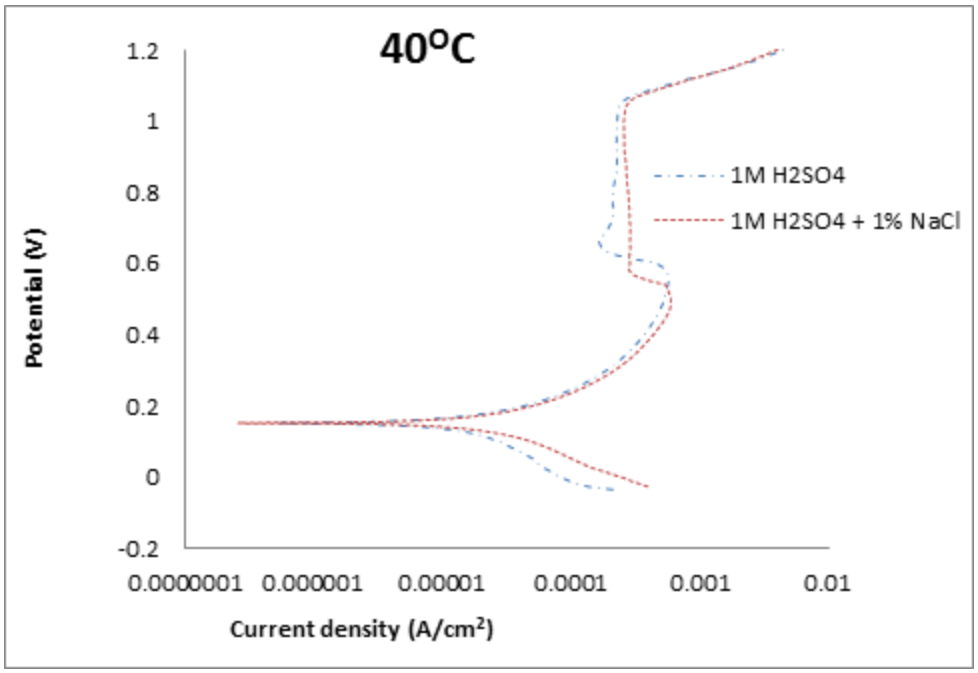

Figure 4.115. Potentiodynamic curves for 2101-0.15 wt% Ru in 1M H_2SO_4 and 1M H_2SO_4 + 1% NaCl at 40°C.

The potentiodynamic curves for 2101-0.15 wt% Ru in 1M H_2SO_4 and 1M H_2SO_4 + 1%NaCl media at 60°C are presented in Figure 4.116. There was a slight shift in the corrosion potential towards a more noble potential in sulphuric acid containing sodium chloride. No active passivation was observed, and the critical current density could not be measured. There was active corrosion in both solutions. The current slightly decreased at ~900 mV, and started to increase with increased potential. There was similarity between the curves indicating common corrosion behaviour.

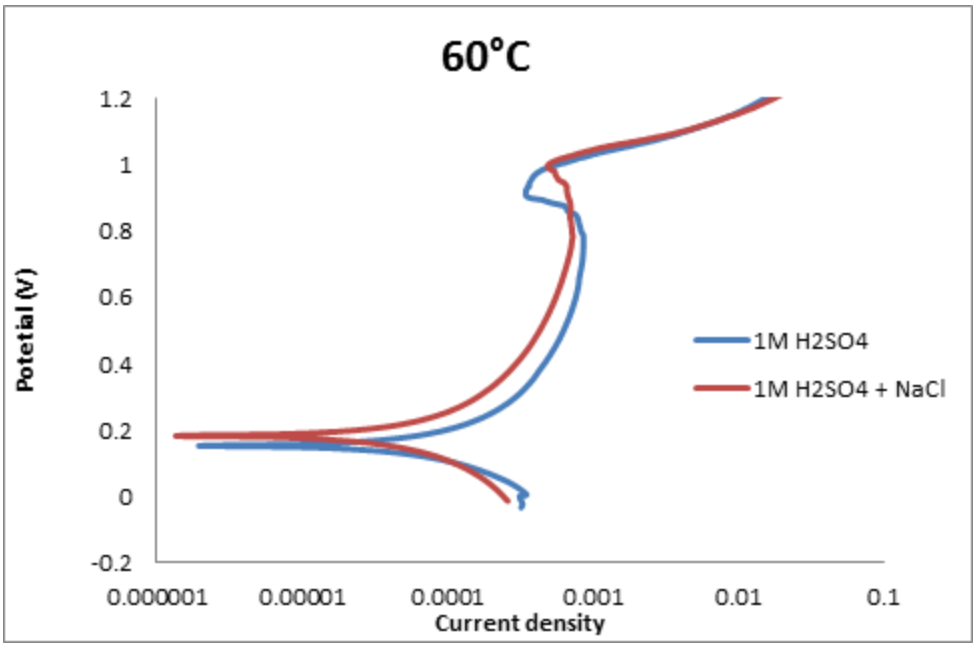

Figure 4.116. Potentiodynamic curves for 2101-0.15 wt% Ru in 1M H_2SO_4 and 1M H_2SO_4 + 1%NaCl at 60°C.

Figure 4.117 shows the potentiodynamic polarization curves for 2101-0.15wt% Ru in 1M H_2SO_4 and 1M H_2SO_4 + 1%NaCl media at 80°C. The corrosion potential of 2101-0.15 wt% Ru was slightly more positive in the presence of sodium chloride, although the curves were very similar, indicating common corrosion behaviour.

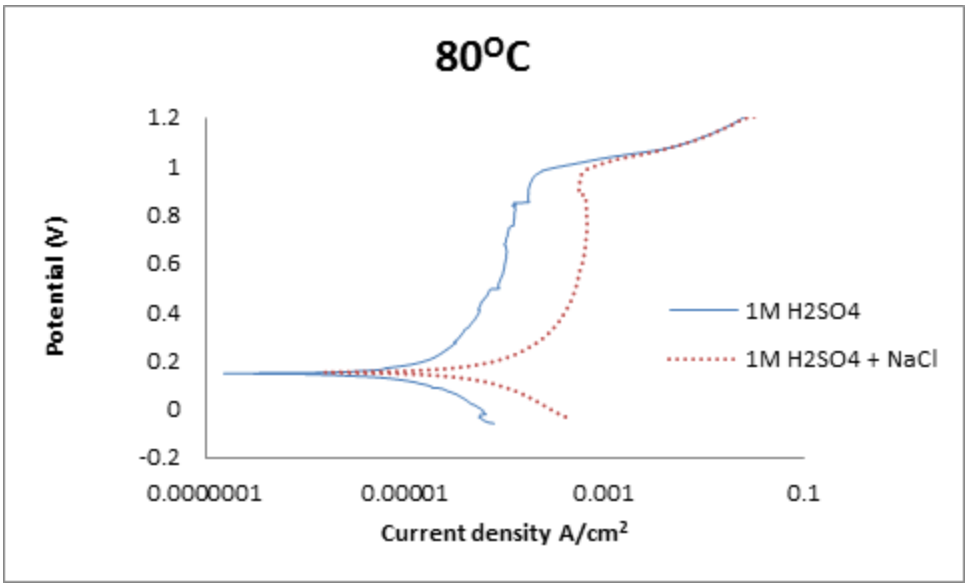

Figure 4.117. Potentiodynamic curves for 2101-0.15 wt% Ru in 1M H_2SO_4 and 1M H_2SO_4 + 1%NaCl at 80°C.

4.9.8 Chronoamperometry results

Chronoamperometry tests were carried out to determine the stability of the passive films and give an additional assessment of the pitting corrosion behaviour of the alloys given by the level of noise generated. Chronoamperometry behaviour was studied for about eight hours in different media at an applied potential of 0.6 V within the passivity regions obtained from the cyclic potentiodynamic polarization measurements. Figures 4.118-4.119 show the chronoamperometry curves of the 2101 DSS in H_2SO_4 at 25°C. The chronoamperometry curves of 2101 with ruthenium alloys in 1M sulphuric acid are shown in Figures 4.120-4.125. The oxidation reaction occurred and the current became constant with increased time, showing that a relatively stable state of passivity has been reached, even though there was slight cyclic behaviour in the current density.

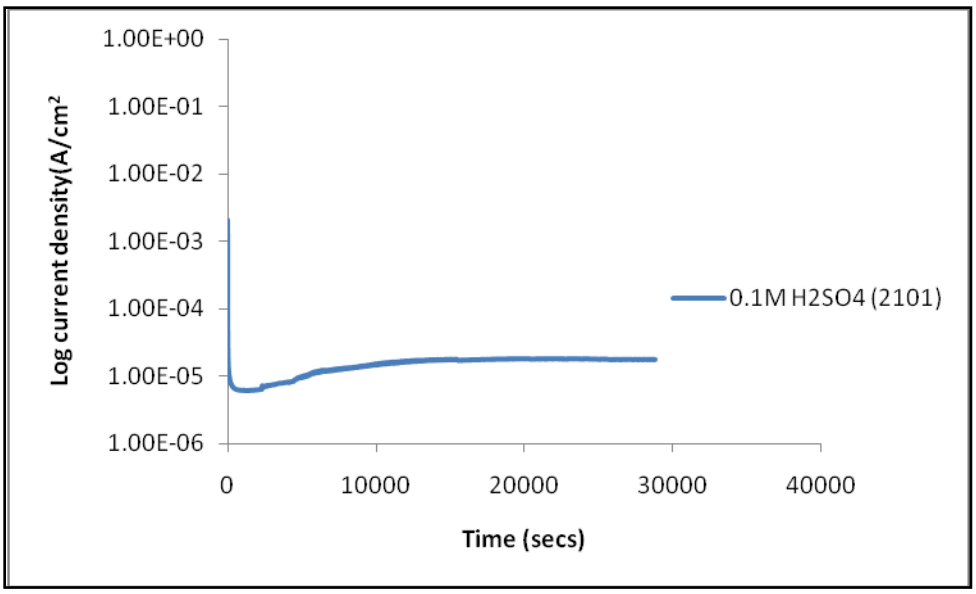

Figure 4.118. Chronoamperometry curve of 2101 in 0.1M H_2SO_4.

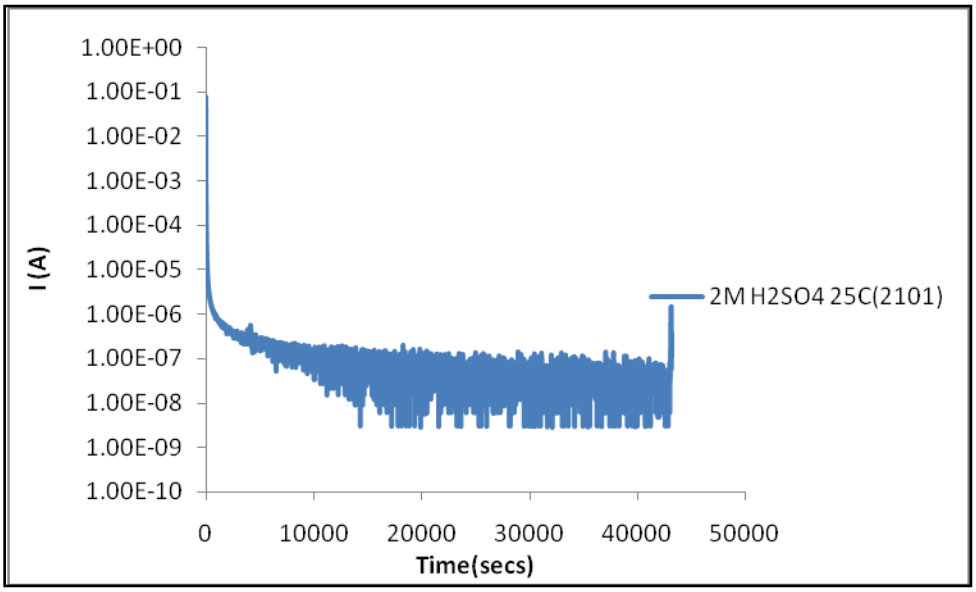

Figure 4.119. Chronoamperometry curve of 2101 in 2M H_2SO_4.

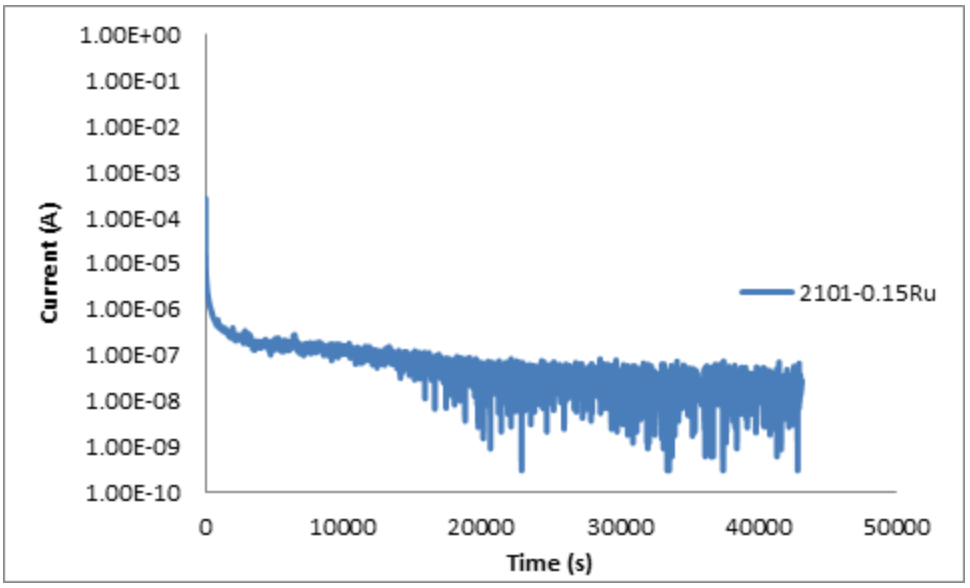

Figure 4.120. Chronoamperometry curve of 2101-0.15 wt% Ru in 1M H_2SO_4.

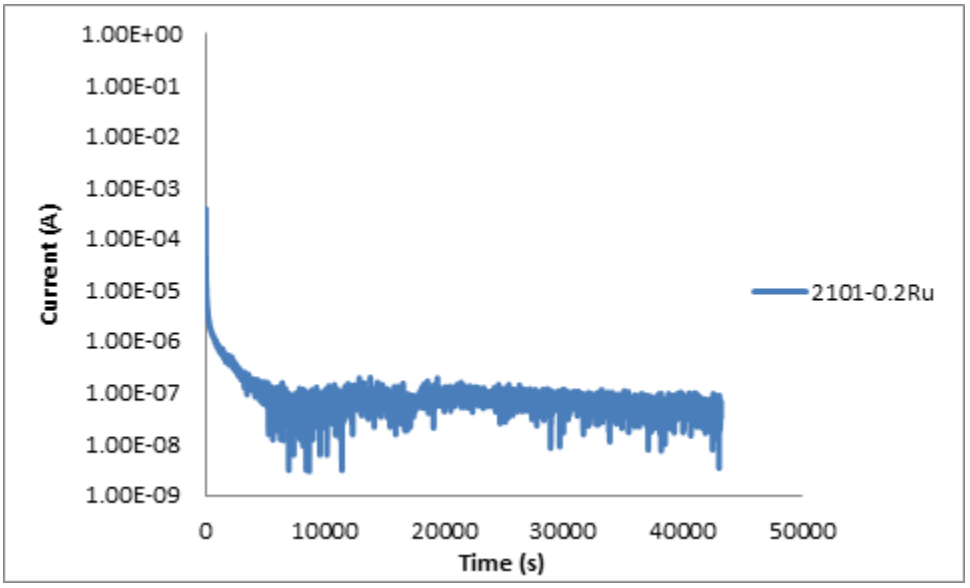

Figure 4.121. Chronoamperometry curve of 2101-0.2 wt% Ru in 1M H_2SO_4.

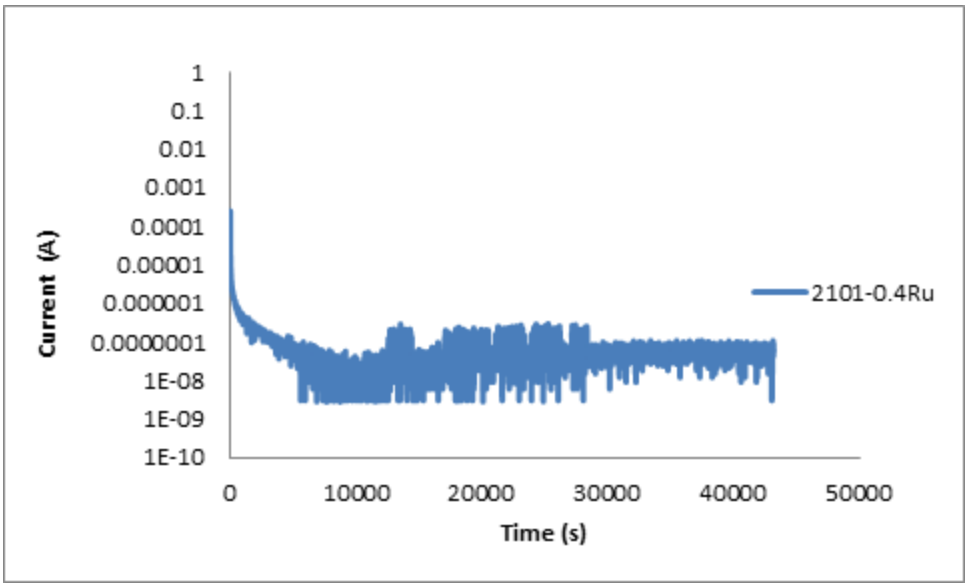

Figure 4.122. Chronoamperometry curve of 2101-0.4 wt% Ru in 1M H_2SO_4.

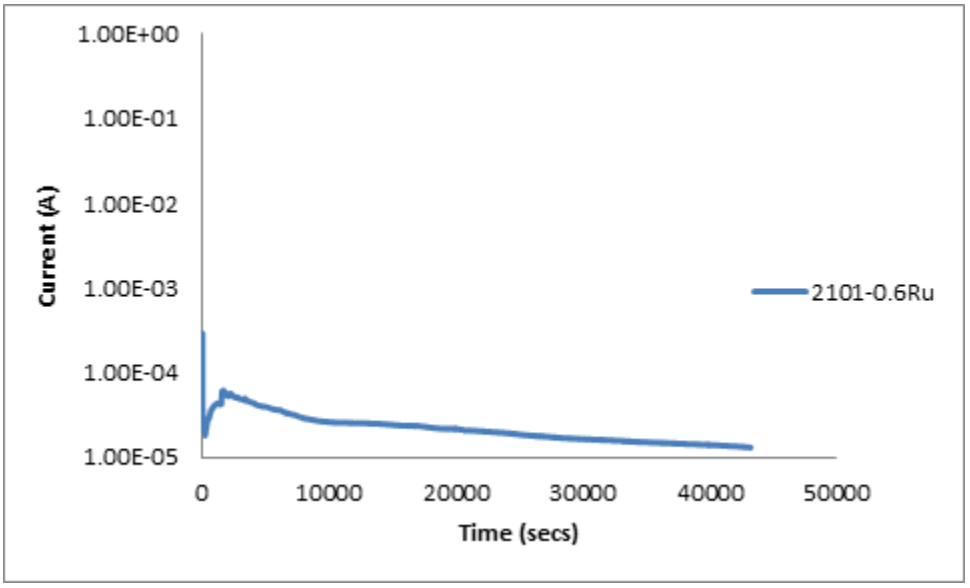

Figure 4.123. Chronoamperometry curve of 2101-0.6 wt% Ru in 1M H_2SO_4.

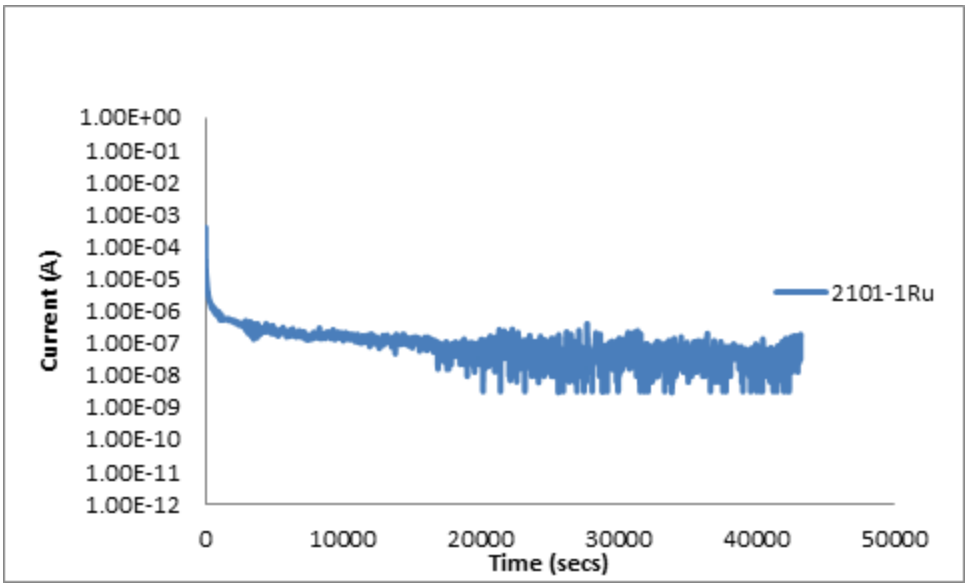

Figure 4.124. Chronoamperometry curve of 2101-1 wt% Ru in 1M H_2SO_4.

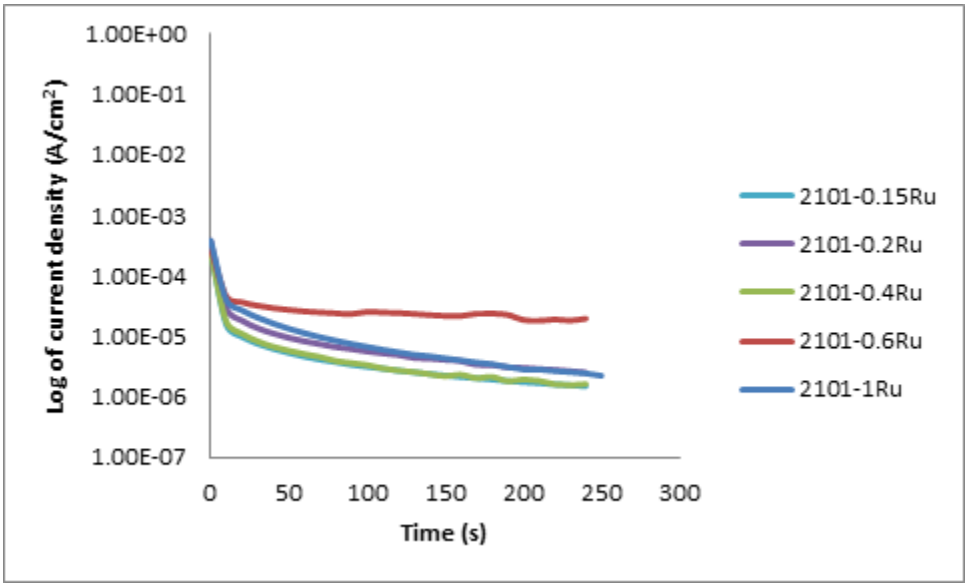

Figure 4.125. Chronoamperometry curves of 2101 with different Ru additions in 1M H_2SO_4.

4.9.9 Post corrosion measurement characterization

The SEM observations on corroded surfaces of 2101 with Ru and the EDX spectra are shown in Figures 4.126-4.140. There was a large area of attack on 2101 (Figure 4.126), both austenite and ferrite phases corroded, and an elongated pit was found on the surface. The EDX analyses revealed a lower content of chromium in the pit (A1) (Figure 4.127). The surface (B1) contained higher chromium contents (Figure 4.128). The individual phases were much smaller than the pit, hence the pit extended over both the austenite and ferrite phases, but it did not give a clear indication to the mechanism of corrosion, except that both phases were affected.

EDX analysis of the corroded surface of 2101-0.15 wt% Ru exposed to 0.5M HCl (Figure 4.129) showed that the unaffected surface A2 (Figure 4.130) contained Fe, Cr Mn and Ni. The corroded surface, area B2 (Figure 4.131), contained Fe, O, S, Cl, Cr and Mn, which are all expected in inclusions in steels. Thus, the inclusions could have been associated with the pit formation.

SEM images and EDX analyses of 2101 sample with 0.4 wt% Ru in 0.5M HCl solution are shown in Figures 4.132-4.134. The surface did not show much attack on the phases, although the austenite particles were standing proud. The EDX analysis did not reveal chlorine.

Figure 4.135 shows the SEM micrograph of 2101-1 wt% Ru after the electrochemical test in 0.5M HCl. Only one pit was observed, and the pit was analysed as well as the surface. The only difference in the composition of area A4 (pit) (Figure 4.136) and area B4, unattacked area, (Figure 4. 137) was the presence of oxygen in the pit. There was very little difference between the phases in terms of attack.

SEM imaging of 2101-0.15 wt% Ru after chroamperometry in 1M H_2SO_4 shows pit initiation at random sites (Figure 4.138). Although the austenite and ferrite phases had the same relief (appeared unattacked, apart from the bad sample preparation), the interface between them had been attacked. The EDX analysis of B5, unattacked ferrite phase (Figure 4.140), reveal Cr, Mn, Ni, and O, while the composition of the pit, A5 (Figure 4.139), revealed Cr Mn, Cl, K, Ca, C, S. The presence of these minor elements could be due to inclusions, which became pit initiation sites.

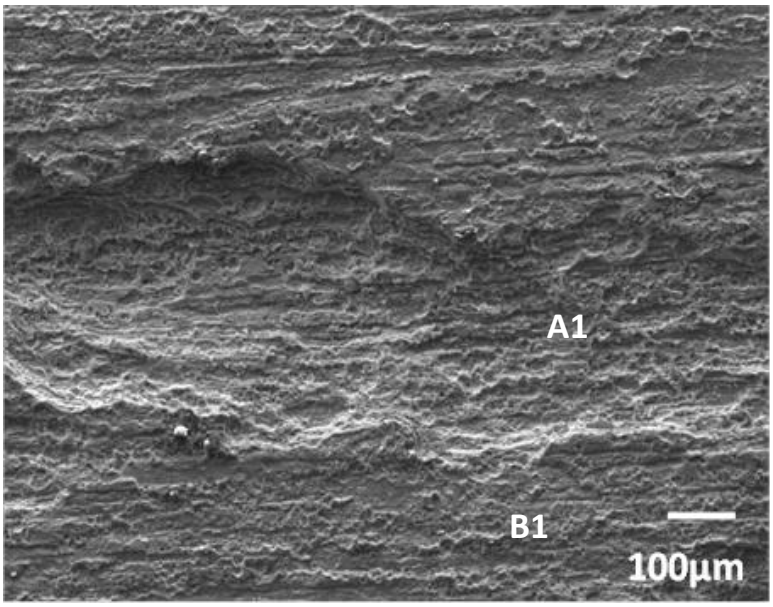

Figure 4.126. SEM secondary electron image of the corroded surface of 2101, after the potentiodynamic test in 0.5M HCl.

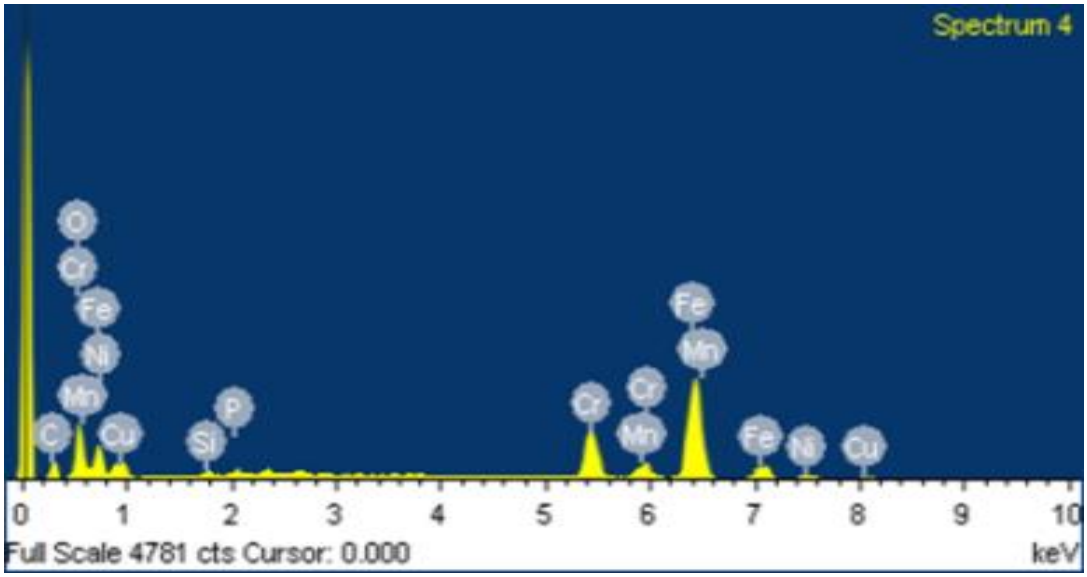

Figure 4.127. EDX spectrum of area A1 in Figure 4.126.

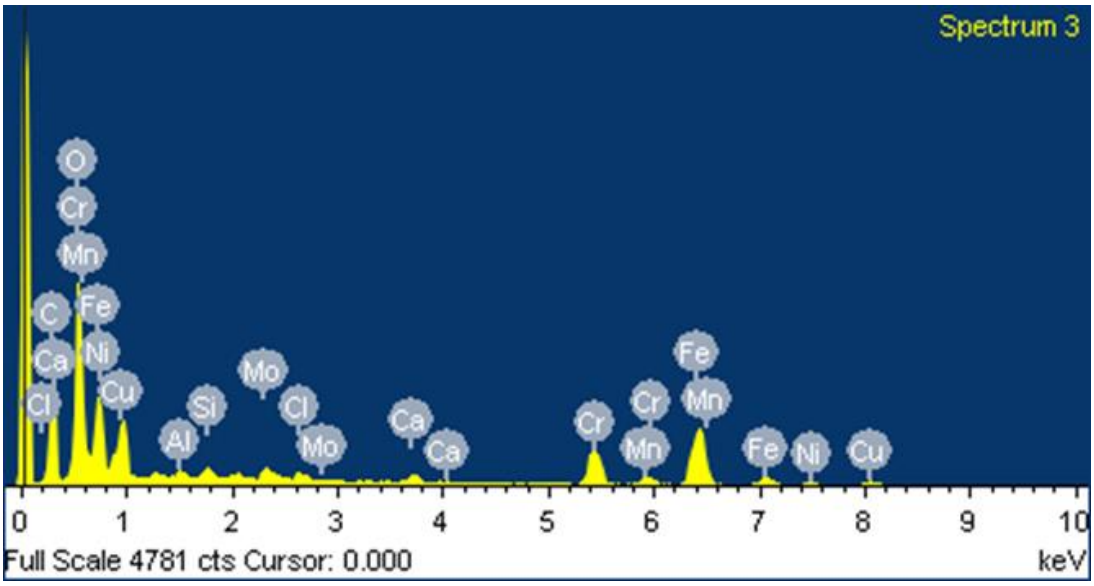

Figure 4.128. EDX spectrum of area B1 in Figure 4.126.

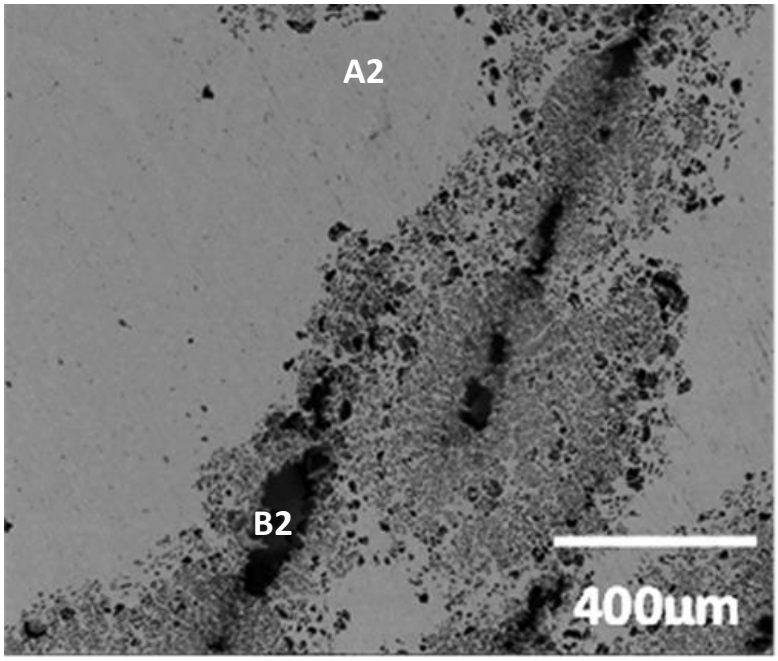

Figure 4.129. SEM secondary electron image of the corroded surface of 2101-0.15wt% Ru, after the potentiodynamic test in 0.5M HCl.

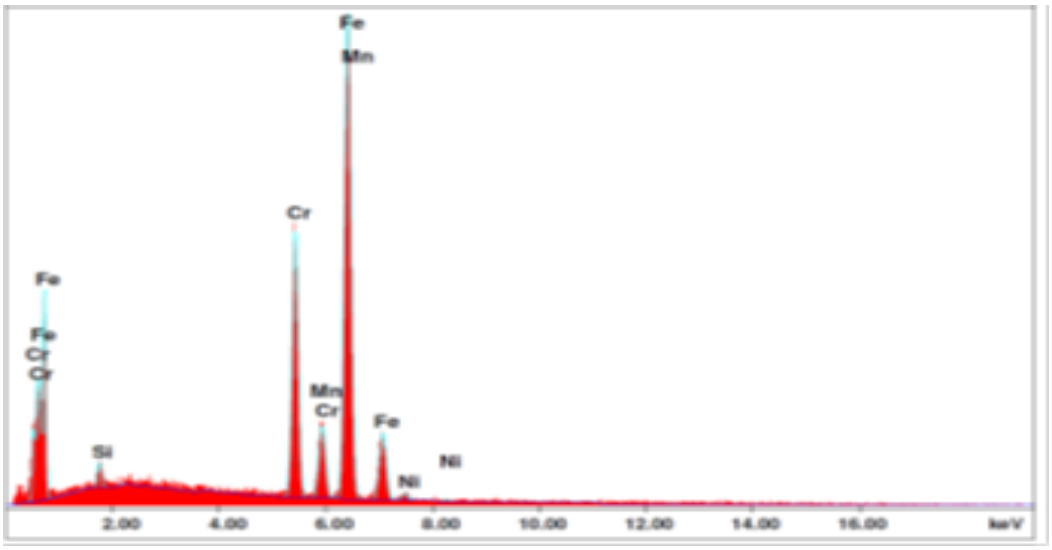

Figure 4.130. EDX spectrum of area A2 in Figure 4.129.

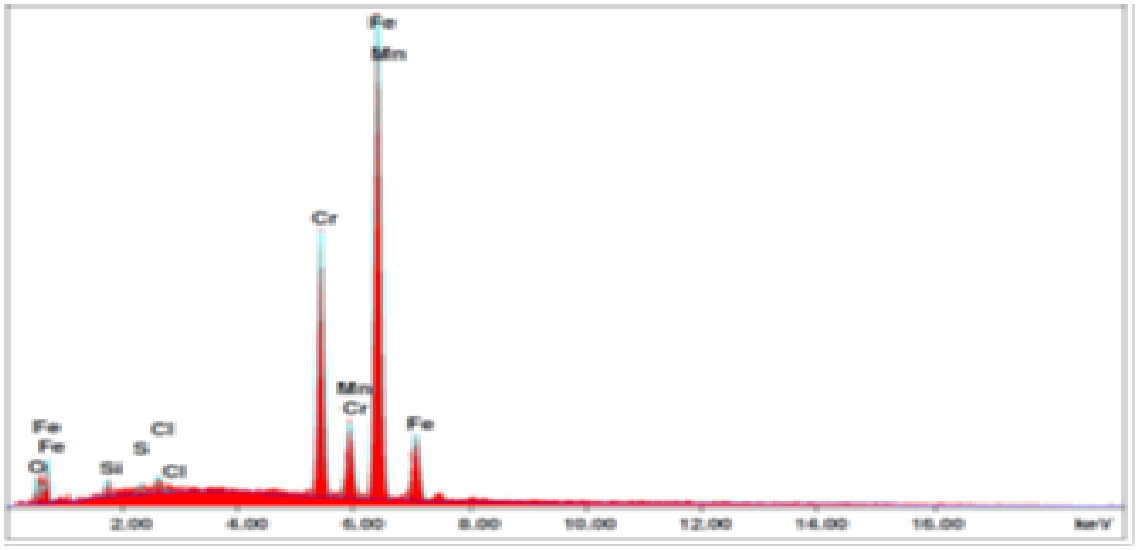

Figure 4.131. EDX spectrum of area B2 in Figure 4.129.

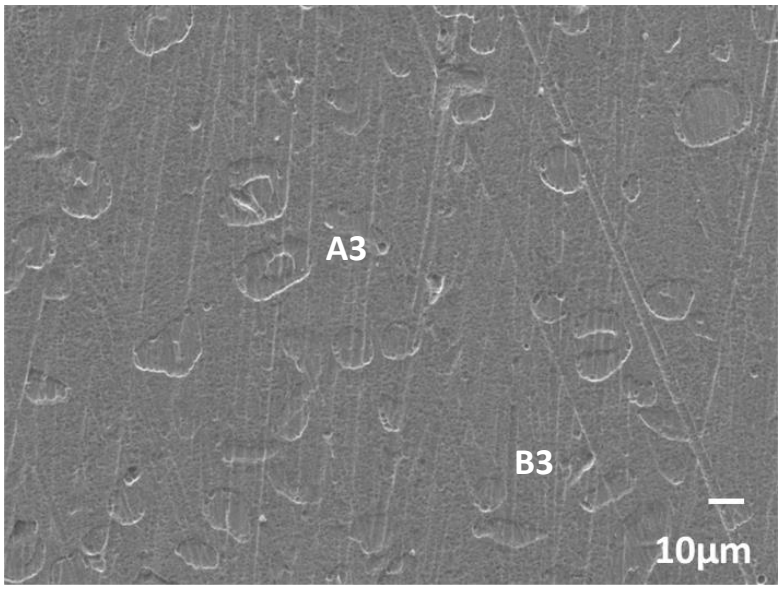

Figure 4.132. SEM secondary electron image of the corroded surface of 2101-0.4 wt% Ru, after the potentiodynamic test in 0.5M HCl, showing austenites regions standing proud.

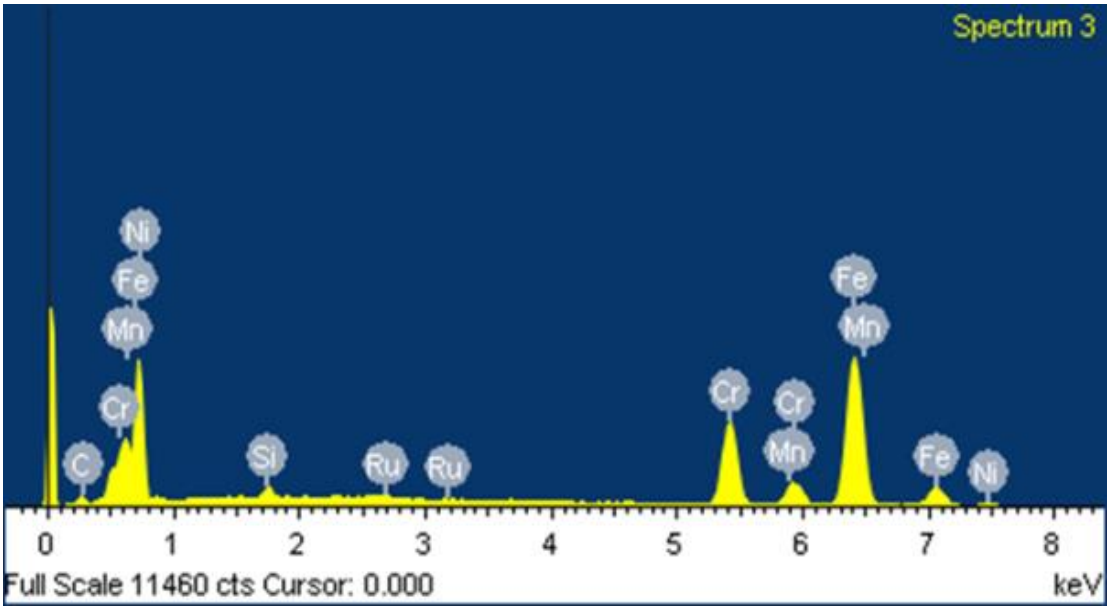

Figure 4.133. EDX spectrum of area A3 in Figure 4.132.

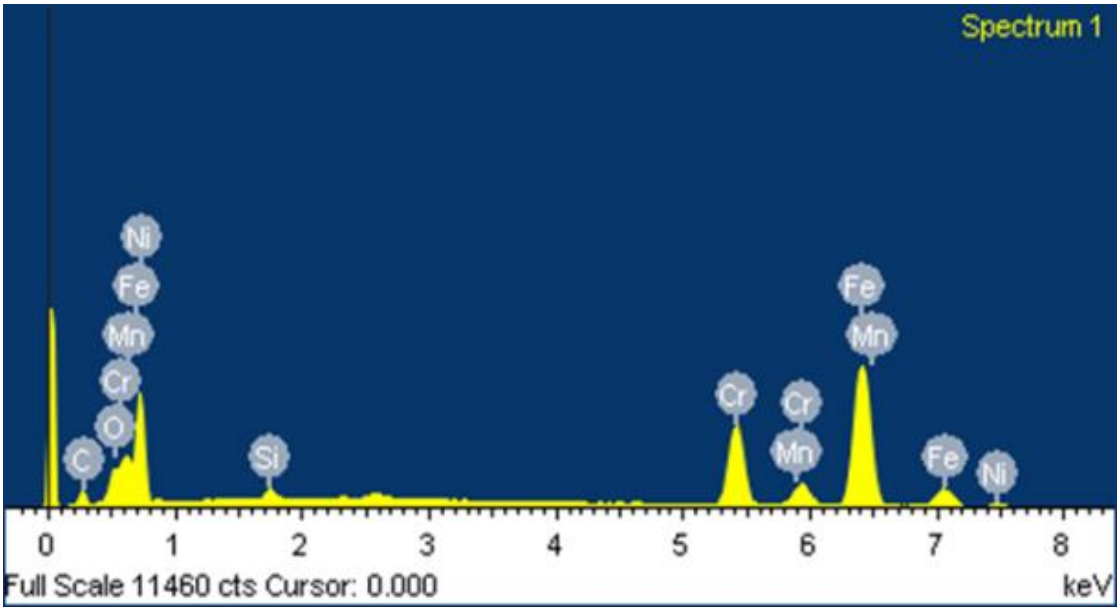

Figure 4.134. EDX spectrum of area B3 in Figure 4.132.

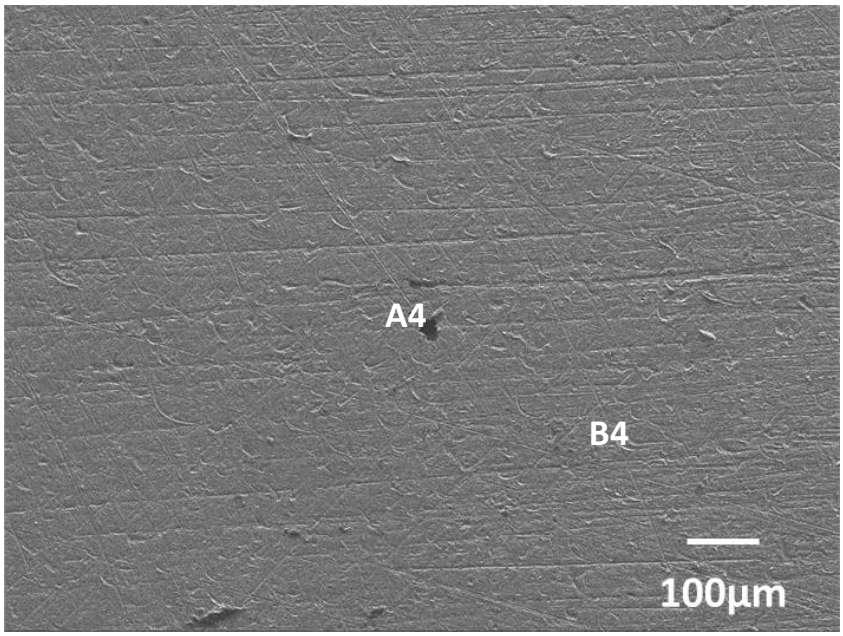

Figure 4.135. SEM secondary electron image of the corroded surface of 2101-1 wt% Ru, after the potentiodynamic test in 0.5M HCl.

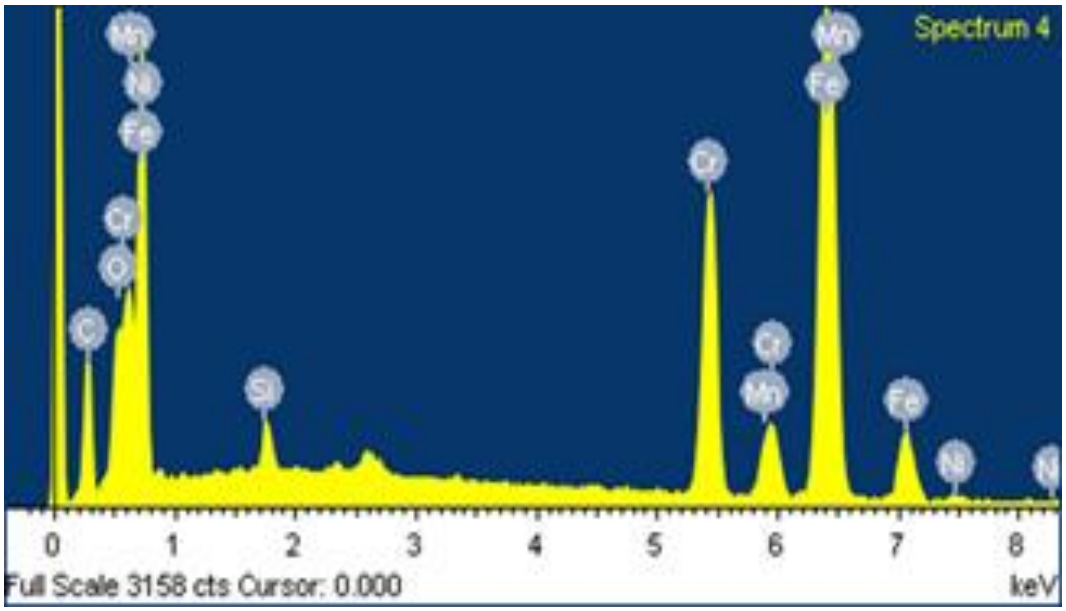

Figure 4.136. EDX spectrum of area A4 in Figure 4.135.

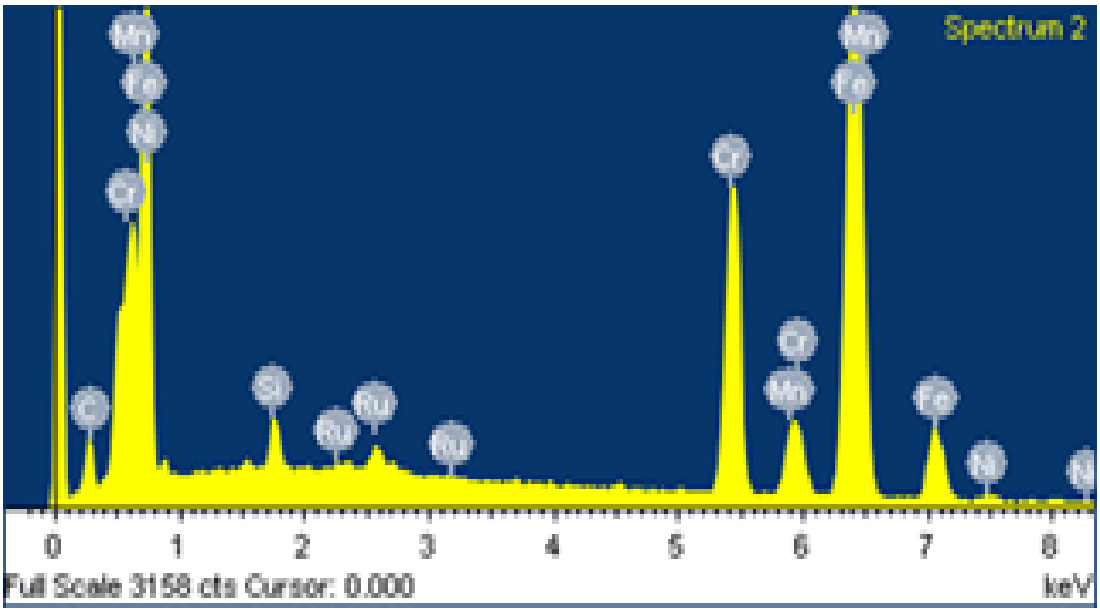

Figure 4.137. EDX spectrum of area B4 in Figure 4.135.

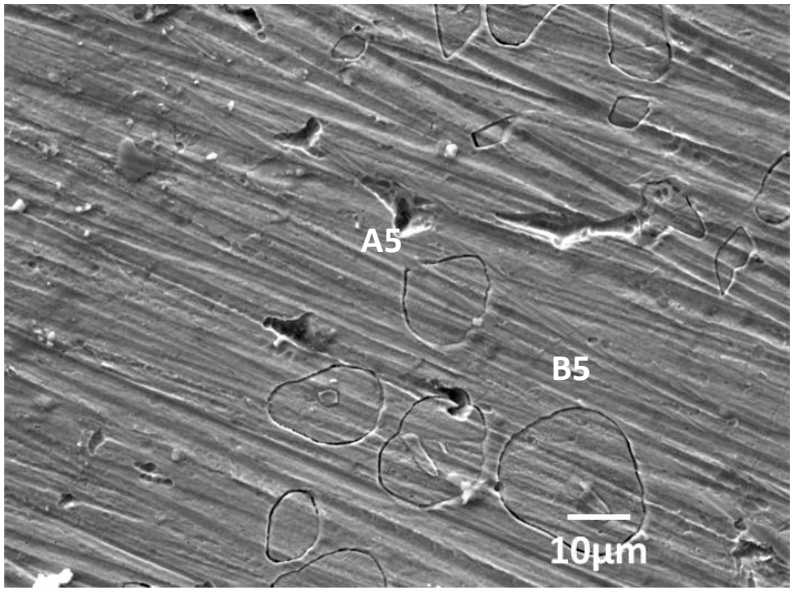

Figure 4.138. SEM secondary electron image of the surface of 2101-0.15 wt% Ru, after the chronoamperometry tests in 1M H_2SO_4.

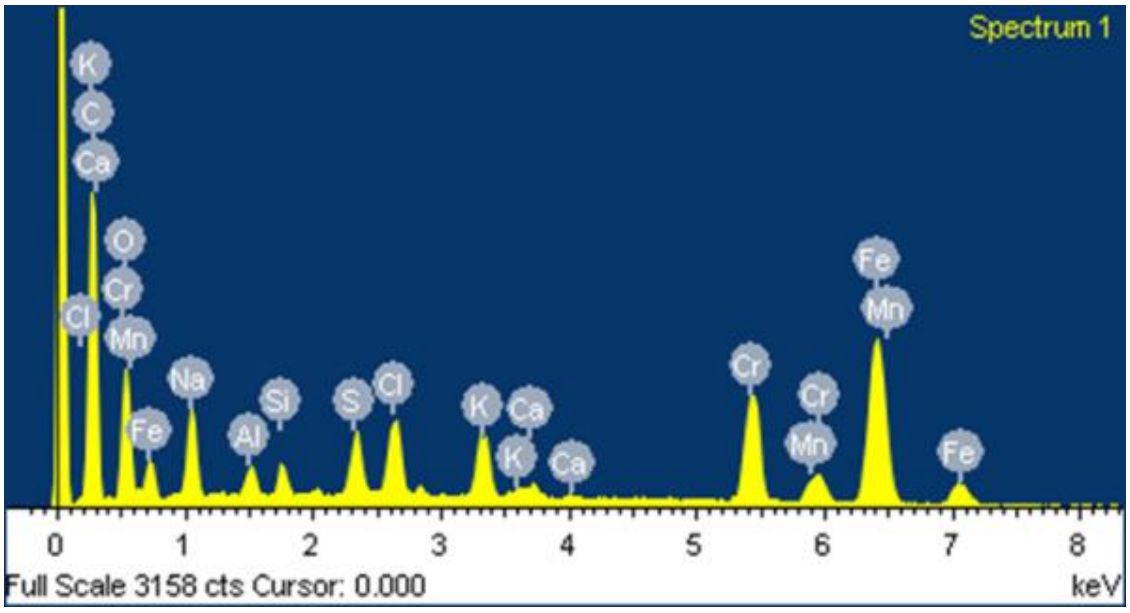

Figure 4.139. EDX spectrum of area A5 in Figure 4.138.

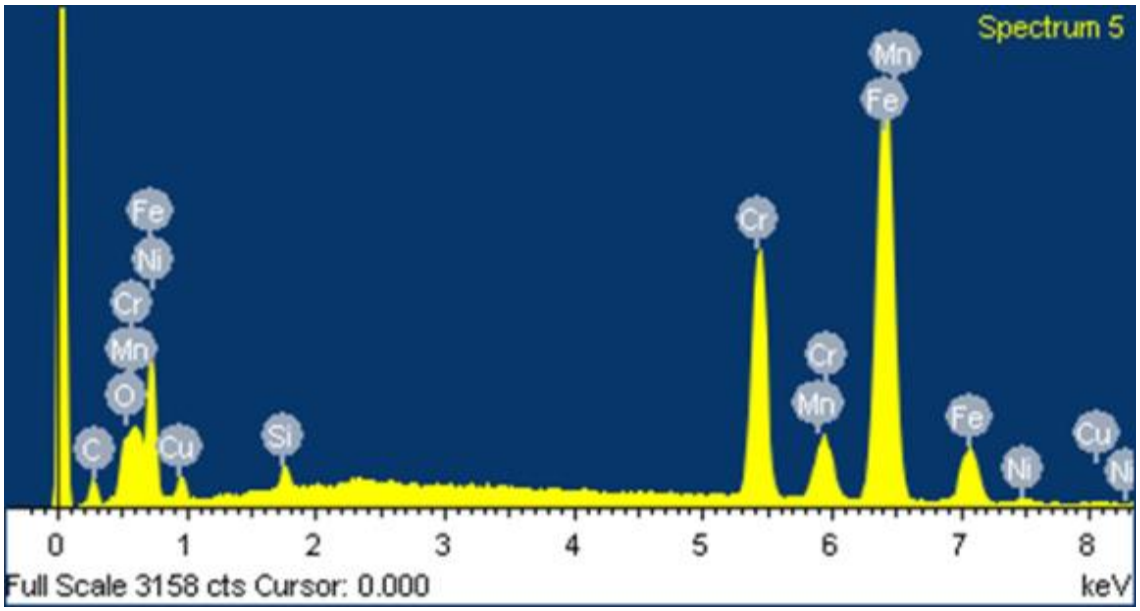

Figure 4.140. EDX spectrum of area B5 in Figure 4.138.

CHAPTER 5

DISCUSSION

5.1 Alloy production, characterization and analysis

The duplex stainless steels were heat treated after casting to adjust the microstructure of the alloys to give the required volume fraction of austenite to ferrite (targeted 50:50).

The purpose of the thermodynamic calculations was to investigate whether the ruthenium partitioned to the ferrite and austenite phases, and to check whether other phases might form. Additionally, Thermo-Calc was used to determine the heat treatment temperatures for the 50:50 ferrite:austenite ratio. The SSOL4 database was mainly used because TCFE5 did not have ruthenium. The results of the 2101 alloy without ruthenium in Figures 4.1 and 4.2 were the same, showing that SSOL4 gave the same result as TCFE5 and so could be used for the other calculations. This was very important, because it showed that the SSOL4 database gave the same answers as the TCFE5 database. The annealing temperature calculated by Thermo-Calc agreed with the temperature of the producers of 2101, which recommended solution solution annealed at 1020-1080°C with rapid cooling [2012Url].

It was observed that up to 0.2 wt% Ru addition, the Thermo-Calc phase proportion diagrams were very nearly the same. The ruthenium addition partitioned almost equally to the two phases (Figures 4.6(c) and 4.6(f)), this was in agreement with the analyses in Table 4.4, even though the technique was not ideal for such low separations. This makes ruthenium beneficial to the two phases, thereby increasing the corrosion resistance of the duplex stainless steel by helping both phases [1997Pot].

Thermo-Calc showed that heat treating the alloys between 1000-1200°C would give a duplex structure for the alloys up to 0.2 wt% Ru (Figures 4.1-4.6). These calculations agreed with the experimental XRD and microscopy results. The partitioning of the other elements in the Thermo-Calc calculations and the EDX analysis were also in good agreement. The EDX analyses showed that chromium partitioned more to ferrite than austenite (Table 4.14), which was in agreement with the average phase compositions for 0.05, 0.1, 0.15 and 0.2 wt% Ru (Tables 4.5-4.8), although for 0.1wt% Ru the amounts were equal. For example, Table 4.8 shows that austenite

had an average of 18 wt% chromium, and there was 22 wt% Cr in ferrite. All the alloys up to 0.2 wt% Ru (Figures 4.1-4.6) showed that the elements were higher in the phases that they promoted (e.g. Cr in ferrite and Ni in austenite), which was expected. Preferential partitioning of elements in duplex stainless steels has been observed by many authors [1996Gar, 1997Pot, 1997Jac, 2009Esc].

The phase proportion diagrams of the 2101 alloy with 2.5 wt% Ru, 5 wt% Ru and 10wt% Ru showed strong deviations from the duplex structure, and the alloys were no longer duplex. The calculations at these ruthenium additions were done to check the correctness of the smaller percentages, since there was so little differences at these smaller percentages. Sigma phase precipitated out at 650°C in 2.5 wt% Ru. It increased with decreasing temperature, and this agreed with the calculations of Tavares [2009Tav] which showed an increase in the sigma fraction as the temperature decreases in 310SS. The sigma precipitated out at 950°C in 310SS.

The micrographs of as-received duplex samples (Figures 4.11-4.14 and Figures 4.27-4.30) revealed that the austenite phases were distributed as islands in the ferrite matrix and were elongated along the rolling direction, showing alternate bands. This is expected for rolled material, and agreed with previous literature [1997Pot, 2008Zha, 2009Zha1, 2009Zha2]. Austenite and ferrite phases were the only phases found in the samples with up to 2.5 wt% ruthenium; no intermetallic phases were observed. Microscopy of 2101-2.5wt% Ru showed a duplex structure, but ruthenium content derived from EDX was 2.0±0.3 wt% Ru and 7.4±0.3 wt% Ru rather than the nominal 2.5wt% Ru and 10wt% Ru as targetted. The differences could be due to the metal loss during alloy manufacturing or poor distribution of the Ru (inhomogeneity). The samples containing 10 wt% Ru had ferrite and hcp phases which were confirmed by XRD.

The EDX analyses of 2101 (Table 4.12) showed the presence of Cr, Ni, Mo, Mg, Al, Si, Ca, Mn and Fe. The ferrite phase had higher amounts of Mg, Si, Ca, Cr and Mo, while austenite had higher amounts of Mn, Fe and Ni, which agreed with previous work [1991Ata, 2009Zha1, 2009Zha2].

XRD analysis of 2205 duplex stainless steel confirmed the two phases austenite and ferrite. The phases analysed by EDX were found to comprise Mg, V, Fe, Si, Mn, Cr, Ni and S. Ferrite had higher amounts of Cr and S, while the austenite had more V, Mn, Fe and Ni, which agreed with previous work [1996Gar 2008Bad].

The metal losses shown in Table 4.2 could be due to rolling oil or other surface contaminants on the surface of the samples, since the metal plates were thin and cut into small chips, therefore giving a large surface area. These large surface areas could have diluted the composition. The losses could also be due to fact that the ruthenium powder was a lot smaller than the chipped pieces of stainless steel, and thus could have been lost during compaction and possibly due to melting.

The hardness tests revealed that additions of ruthenium did not have any detrimental effect on the mechanical properties of the 2101, as shown in Figure 4.62. The 2101 alloy with no ruthenium had a hardness of 230±1 HV, while 2101 with ruthenium varied between 222±4 HV and 240±6 HV. These variations of the hardness were relatively small and could be due to the inhomogeneity of the samples, but overall, the hardness increased with ruthenium content. The hardness value of plain 2101 agreed with the specifications [URLAve].

The austenite grains were coarser at 1080°C than at 1100°C, while the ferrite grains were coarser at 1100°C than at 1080°C, even considering just the 120 minutes annealing time. The 50:50 austenite:ferrite ratios were better achieved at 1080°C than at 1100°C as shown by the the volume fractions (Table 4.16 and 4.17). This agreed with the Thermo-Calc calculations, which predicted that 1080°C was the temperature where the 50:50 proportions were expected. Thermo-Calc also predicted a higher proportion of ferrite than austenite at 1100°C, and this agreed with the volume fractions calculated from the micrographs. The annealing time of 120 minutes produced higher proportions of austenite in all samples (Figure 5.1b). The austenite proportions increased with the annealing time at 1080°C.

The austenite was randomly dispersed in the ferrite matrix for all the samples annealed at 1080°C and 1100°C. Ferrite was occasionally enclosed in austenite particles for samples at 1080°C (Figures 4.35-4.36 and 4.38) and at 1100°C (Figures 4.45-4.46 and 4.48). More austenite was seen at the grain boundaries in the sample with 0.15wt% Ru annealed at 1080°C than for 1100°C (Figures 4.35 and 4.45). Austenite particles were coarser at 1080°C (Figures 4.39-4.41) than at 1100°C (Figures 4.49-452), which could be due to the higher temperature. They were also formed at the grain boundaries at 1080°C and 1100°C (Figures 4.39-4.40 and 4.45-4.52), which is to be expected for precipitation in the solid state.

Overall, the XRD, EDX and microscopy analyses were in good agreement with the Thermo-Calc calculations.

The volume fractions of austenite and ferrite in 2101 with ruthenium were determined by quantitative metallography, using a grid. The austenite volume fractions of the alloys annealed at 1080°C were higher than those annealed at 1100°C, for most of the samples, as shown in Figure 5.1a. The increased volume fraction of ferrite at 1100°C agreed with Thermo-Calc. Figure 5.1b shows that the austenite volume fraction increased with annealing time. The best representative compositions of austenite and ferrite were obtained for the best soaking condition which was determined experimentally to be 120 minutes at 1080°C (Figure 5.1a), agreeing with previous work [2008Zha, 2009Zha1, 2009Zha2]. There was an increase in the volume percentages of austenite as the soaking time increased (Figure 5.1b). The austenite volume fraction reached a peak at 0.4 wt% Ru, although there was only a slight difference between the values, and a greater reduction in austenite at 2.5 wt% Ru. For higher percentages of ruthenium (2.5, 5 and 10 wt% Ru), there were changes in the phases of the duplex stainless steel, reducing the proportions of austenite, to less than a duplex structure. Thus, these compositions would not be suitable for a duplex stainless steel (Figure 5.1a).

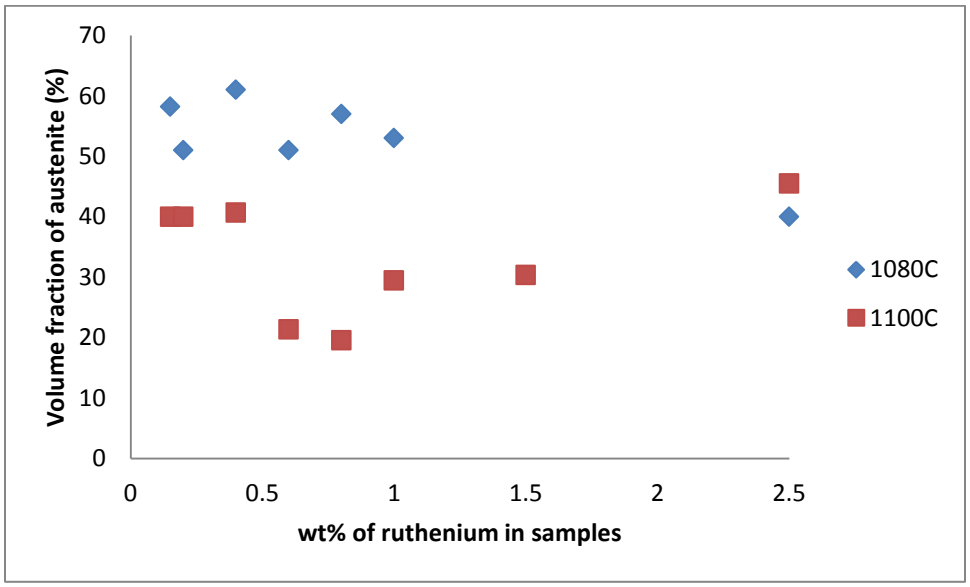

Figure 5.1 (a). Volume fraction of austenite in 2101 alloys with ruthenium additions (wt%) annealed at 1080°C and 1100°C for 120 minutes.

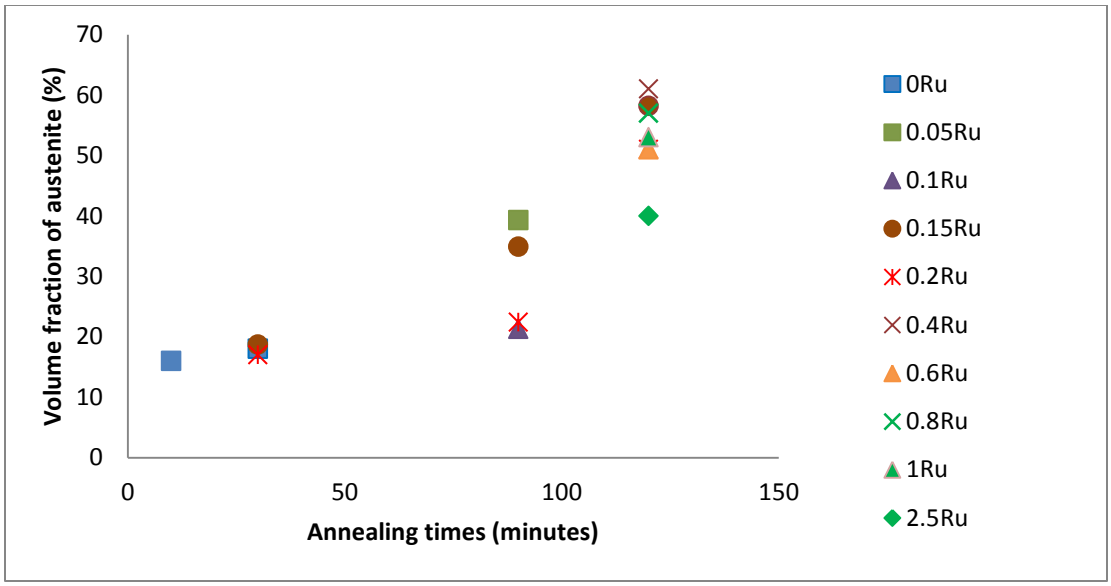

Figure 5.1(b). Volume fraction of austenite for 2101 with different amounts of Ru, annealed at 1080°C for different times.

5.2 Corrosion results

The reason for adding ruthenium to the 2101 alloy was to reduce the overall current densities, and thereby increasing the ease of passivation and corrosion resistance. This was done because many other researchers [1959Ste, 1960Hoa, 1961Gre, 1964Tom, 1970Tom, 1974Tom,1974Str, 1975Tom, 1977Str, 1981Che, 1984Dup, 1989Hig 1990Tjo, 1990Pot, 1991Pot, 1993Pot, 1998Wol, 2008Olu] had found beneficial results after adding PGMs to various various alloys.

The response of these alloys in different environmental conditions was assumed to be controlled by metallurgical factors, including alloy composition, microstucture and partitioning of the elements to the two phases. Firstly, the corrosion behaviour of 2101 was compared with 316, 2205 and 2507 stainless steels. The corrosion results of the cathodically modified 2101 evaluated in sulphuric acid at different temperatures is discussed by looking at the effect of ruthenium on the corrosion characteristics. Similarly, the effect of ruthenium is also discussed for the cyclic potentiodynamic response of these alloys in 3.5M NaCl. From these results, the optimum ruthenium contents for corrosion resistance is discussed in order to compare with the other duplex stainless steel results. The behaviour of the alloys with ruthenium exposed to sulphuric

acid and chloride solutions is compared. According to the corrosion rates, 1wt% Ru was the optimum ruthenium addition.

5.2.1 Comparison of corrosion resistance of 2101 compared to other stainless duplex exposed to acidic and acidic chloride media.

As the potential of a metal in the passive state is made more noble, the passive current density (i_{pass}) remains constant until eventually, the current begins to increase with potential. Such increases in current may be due to localised breakdown of the passivating oxide film by anions, particularly chloride ions [1995Ben]. Overall, the corrosion resistance of 2507 proved to be better than 2205 and 2101 in all the media tested, and this agreed with the manufacturer [URLAve].

The 2101 steel showed a narrow passive range in 1M sulphuric acid when compared to both 2205 and 2507 (Figure 4.63), which could be attributed to a thin surface layer formed since chromium enhances formation of a protective oxide [1992Jon]. The 2101 alloy had the higher i_{pass} in the solutions, but the pseudo-passive region in 40°C and 60°C in 1M sulphuric acidk with 1% sodium chloride were similar to 2205. The width of the passive range and the potentials are sensitive to contaminants such as chloride ions [1979Sed]. The corrosion potential of the stainless steel and thus the dissolution of the material depend on the kinetics of the reaction [2005Kai]. The corrosion resistance of 2205 and 2507 were better than 2101 in 1M sulphuric acid and 1M sulphuric acid and 1% sodium chloride (Figures 4.63-4.70). The corrosion rate of 2101 was higher than the 2205 and 2507 in all the media under study, with a minimum of one order of magnitude difference (Table 4.19). Also, the corrosion resistance of 316 was better than 2101. This agrees with the data of Outokumpu [URLOut]. Nitrogen additions to austenitic and duplex stainless steels improve pitting resistance and retard the kinetics of sigma phase formation. The lower corrosion resistance of 2507 could be attributed to the higher percentage of chromium, nitrogen and nickel in 2507, which resulted in higher pitting resistance equivalent (PREN = %Cr+3.3×%Mo+16×%N) of 42 as compared 35 and 26 for 2205 and 2101 respectively [URLOut,2008 Zha] .

5.2.2 Corrosion behaviour of 2101 duplex stainless steel cathodically modified with ruthenium in sulphuric acid

The polarisation technique was used to investigate the corrosion behaviour of 2101 with different ruthenium contents in 0.5M sulphuric acid at 25°C and 1 molar sulphuric acid at 25°C, 40°C and 60°C, and is presented in Figures 4.74–4.100. The results showed that the alloys passivated rapidly in a solution of 0.5M sulphuric acid, and also that the corrosion rates decreased with ruthenium content (Table 4.21). The corrosion rate of the 2101 alloy without ruthenium was found to be 5.75×10^{-1} mm/y, while for the alloy with 1 wt% ruthenium it was 1.38×10^{-3}mm/y. Similar observations were made by Potgieter [1995Pot] who noted a positive shift in corrosion potential of high chromium duplex stainless steel with ruthenium compared to the alloy without Ru in 10% sulphuric acid. Sheriff *et al*. [2009She] also used open circuit measurements on the effect of minor additions of 0.14%, 0.22% and 0.28% in 2205 in 10% sulphuric acid, and their results also showed that the presence of ruthenium shifted the corrosion potential to more positive values. Myburg *et al.* [1998Myb] observed similar behaviour for the same duplex stainless steel up to 0.3% ruthenium. The work of Olubambi *et al*. [2008Olu] on the addition of ruthenium to Fe-29Cr-2Ni-4Mo super-ferritic stainless steel using polarization measurements in 1M H_2SO_4 showed a shift of the corrosion potential towards more positive values as the ruthenium content increased.

The increase in corrosion potential revealed the tendency of the alloys to resist corrosion. In this study, the shift in the corrosion potential to more positive values with increasing ruthenium contents is shown in Figure 5.2. There was a gradual increase of the corrosion potential up to 0.8 wt% Ru. However, a sudden jump was observed when the ruthenium increased to 1 wt%, although it would have been better to have more data points at higher Ru contents.

The fact that alloys modified with ruthenium and other platinum group metals have more positive corrosion potentials has been well established [1970Bie, 1977Str, 1984Dup, 1995Pot, 1997Pot]. Thus, the increase in the corrosion resistance of the alloys as the ruthenium content increased was expected. This was associated with the differences in active-passive behaviour which agreed with previous work [1961Gre, 1970Bie, 1977Str, 1984Dup, 1995Pot, 1996Pot, 1997Pot].

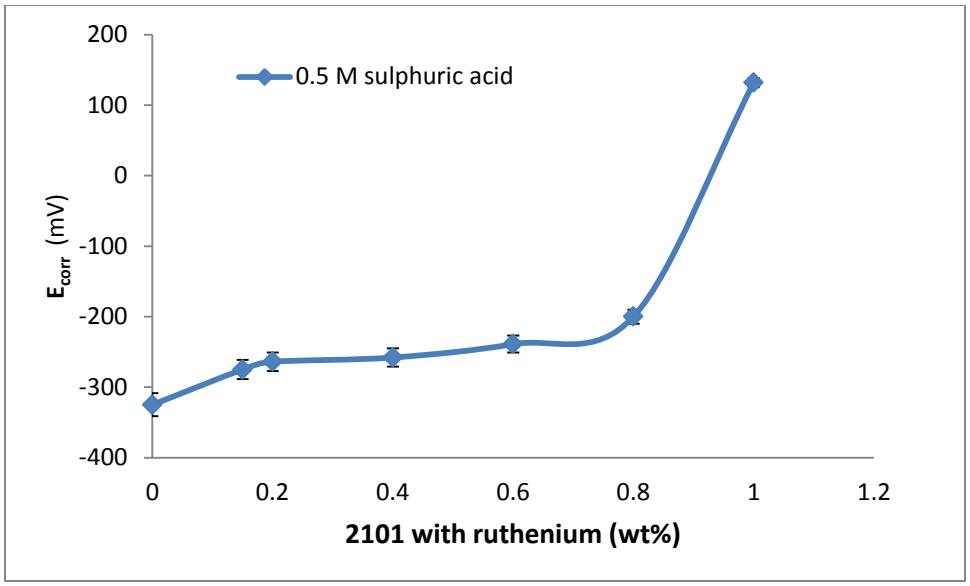

Figure 5.2. Effect of ruthenium contents on Corrosion potential of 2101 steels in 0.5 M sulphuric acid.

Figure 5.3 shows that the i_{pass} was reduced with increasing ruthenium content. Olubambi *et al*. [2008Olu] also observed that in sulphuric acid solution, the i_{pass}, corrosion current and corrosion rates of super-ferritics stainless steel were reduced with increased ruthenium contents. This phenomenon was also observed for Fe-40Cr alloys by Higginson [1989Hig] in 0.5M sulphuric acid. The curve for 2101 with no Ru showed instability in the anodic part, and also the high critical current density showed it was more susceptible to corrosion than the 2101 alloys containing 0.15 and 0.2 wt% Ru (Figure 5.3).

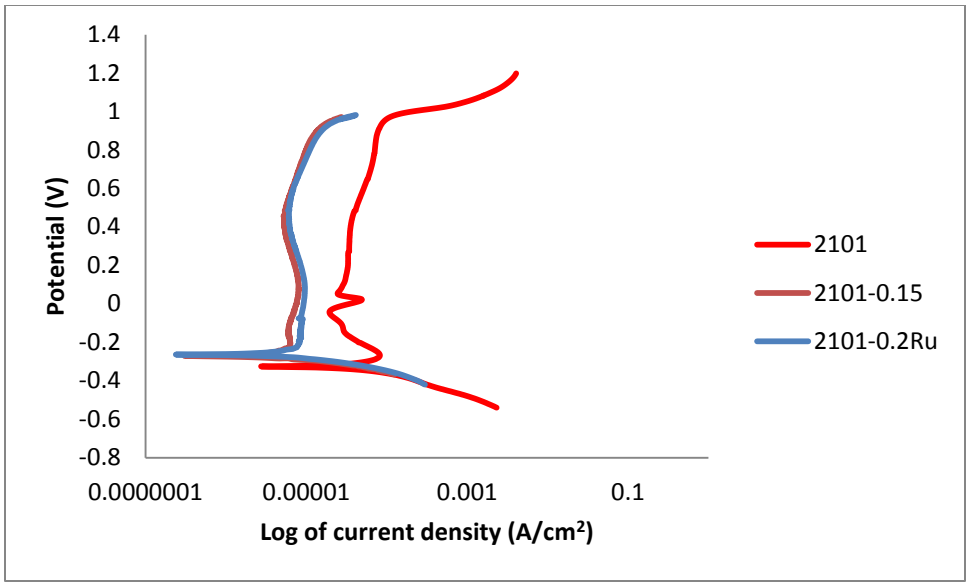

Figure 5.3. Potentiodynamic curves for 2101 with different amounts of Ru in 0.5 M H_2SO_4.

The critical current density was lower for the 2101 alloys with ruthenium than for the 2101 alloy without ruthenium and low critical current indicates increased corrosion resistance [1995Ben]. The reduced corrosion and critical current densities indicated that the ruthenium also inhibited the anodic dissolution of the cathodically modified alloys. There was similarity between the corrosion curves of alloys containing 0.15, 0.2, 0.4, 0.6 and 0.8 wt% Ru where passivation was more pronounced than for 2101 without ruthenium (Figures 5.3 and 5.4). The 1 wt% Ru alloy showed similar passivation, but with a much higher corrosion potential (Figure 5.4). The 2101 alloy showed active-passive transition behaviour, passive films start forming at -300 mV (Figure 5.4). Greene *et al.* [1961Gre] found that when a metal is alloyed with a noble metal, both anodic and cathodic reaction kinetics were affected. The anodic and cathodic reaction kinetics can concurrently increase cathodic exchange current density, while the critical anodic current density is decreased, thereby increasing passivation tendency and the corrosion resistance. This effect was observed in 2101 containing ruthenium in 0.5M H_2SO_4 (Figures 5.3 and 5.4), where there was a modification to both anodic and cathodic parts of the curves. The positive shifts in corrosion potential in alloys containing ruthenium were identified to be a result of diffusion of chromium to the surface of the alloys by other authors [1990Pot, 1997Var, 1995Bar] and also as a result of the ruthenium in the layer on the surface [1992Tjo, 2012Mwa].

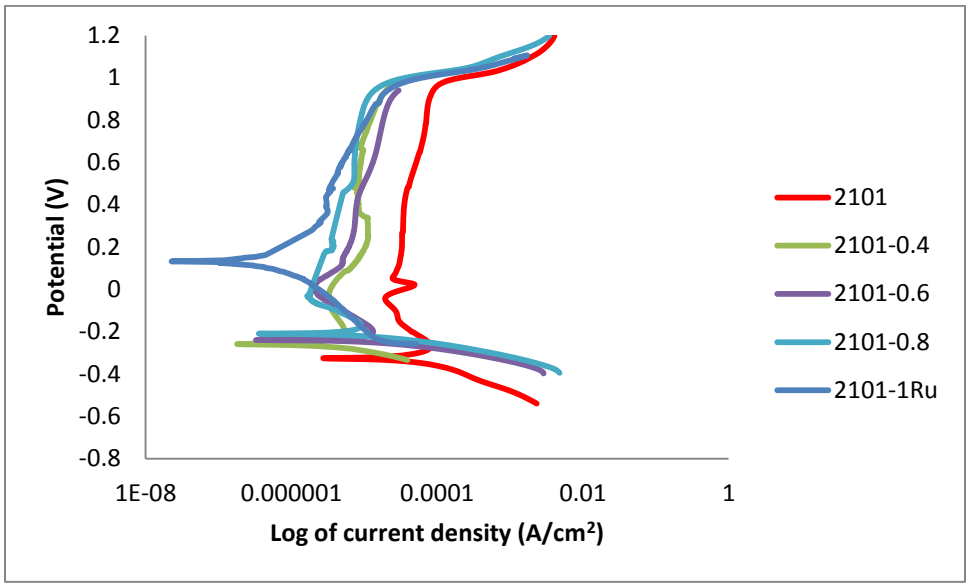

Figure 5.4. Potentiodynamic curves for 2101with different amounts of Ru in 0.5 M H_2SO_4.

It can be seen from Figure 5.5 for 2101 alloys with different Ru contents, heat treated at 1100°C that there was little difference between the curves for 1.5 wt% ruthenium addition and 0.8 wt% ruthenium when exposed to 0.5M sulphuric acid. The critical current density was higher in 2101-1.5 wt% Ru; E_{pit} was observed above 1.0 V (SSE) potential for 0.1, 0.8 and 1.5 wt% Ru alloys. Figure 5.6 presents the potentiodynamic response of 2101 with 0.8 wt% ruthenium heat treated at different temperatures for two hours. Their corrosion potentials were close, but the passive current density was lower for 1080°C. The increase in heat treatment temperature from 1080°C to 1100°C decreased the corrosion resistance (Table 4.21). This could be due to differences in the phase distribution. This agreed with the work of Zhang *et al*. [2009Zha2], which showed that increasing the annealing temperature of 2101 shifted the corrosion potential and pitting potential to more negative values, and the corrosion rates also increased. The passive range of the sample containing 0.1 wt% Ru was wider than that of the alloys containing 0.8 and 1.5 wt% Ru, which was unexpected, and its corrosion potential was more negative. Increasing the annealing temperature and a higher addition of 1.5 wt% Ru did not show great improvements. Hence, addition of 1.5 wt% Ru is uneconomical.

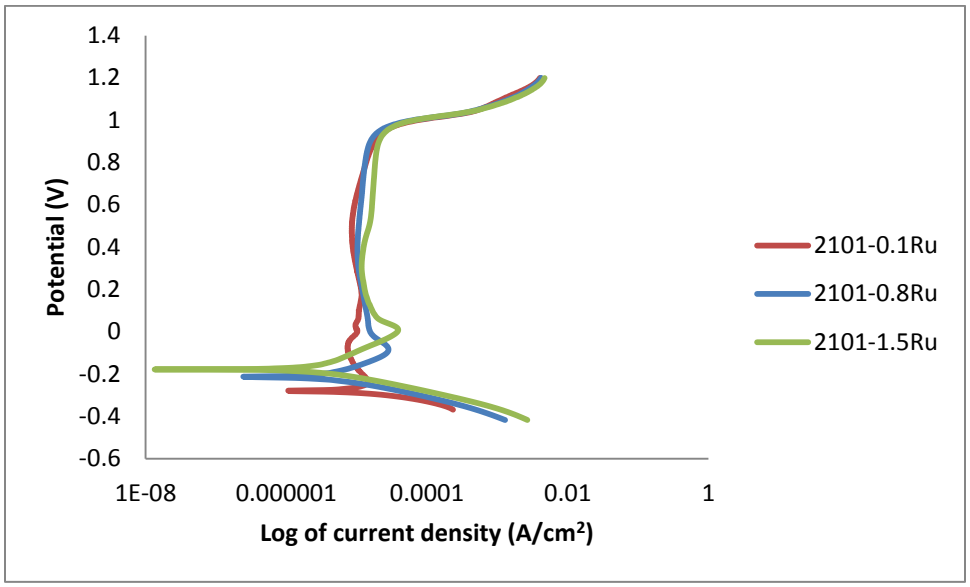

Figure 5.5. Potentiodynamic curves for 2101 with Ru heat treated at 1100°C for 120 minutes in 0.5 M H_2SO_4.

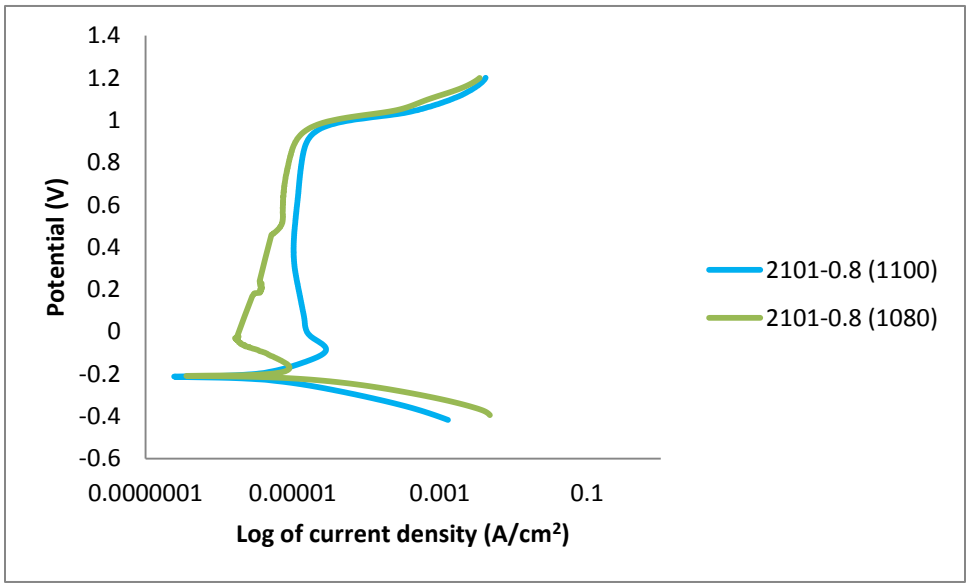

Figure 5.6. Potentiodynamic curves for 2101-0.8 wt% Ru at different heat treament temperatures of 120 minutes in 0.5 M H_2SO_4.

Figures 4.85-4.100 show the polarization behaviours of 2101 with ruthenium at different temperatures exposed to 1M sulphuric acid. The corrosion rate of 2101-1wt% was 2.10×10^{-3} mm/y compared to 1.66×10^{1}mm/y for 2101 without ruthenium (Table 4.22). The observed corrosion rate for alloys without ruthenium was higher than those with Ru, which showed that the alloys with ruthenium in 1M sulphuric acid had a superior corrosion resistance (<0.1 mm/y) which agreed with the manufacturers of 2101 [URLAve]. The low corrosion rates observed in sulphuric acid agree with other workers [1989Hig, 1995Pot, 1997Pot]. Table 4.22 shows that the increase in ruthenium additions resulted in the displacement of the corrosion potentials towards more noble values. The corrosion current decreased with increasing ruthenium contents, and the corrosion rates decreased.

Figure 5.7 shows the cathodic potentiodynamic behaviour of 2101 with different Ru contents in 1M sulphuric acid at 25°C and there was an increase in the corrosion potential up to 1wt% Ru. The shape of the scan of 2101-1 wt% Ru in 0.5M H_2SO_4 was similar to the scan in 1M H_2SO_4. Similarities in the polarisation behaviour of the alloys were observed up to 0.8 wt% Ru. The cathodic curves of 0.8 and 1 wt% Ru were much higher than the others. Figure 5.8 shows the anodic behaviour of 2101 with different Ru contents in 1M sulphuric acid at 25°C. The passive current density decreased with increasing ruthenium contents. The curve of 2101 without ruthenium shows it was more susceptible to corrosion than the 2101 samples with ruthenium.

Potgieter [1990Pot] suggested ruthenium atoms accumulated on the surface of the alloy while the alloy dissolved during the initial stage of the exposure to the acidic solution. He stated that the blocking of the lattice point defects by the ruthenium atoms decreased the corrosion rates from the active sites, and also increased the efficiency for hydrogen evolution and E_{corr} moved towards more positive values.

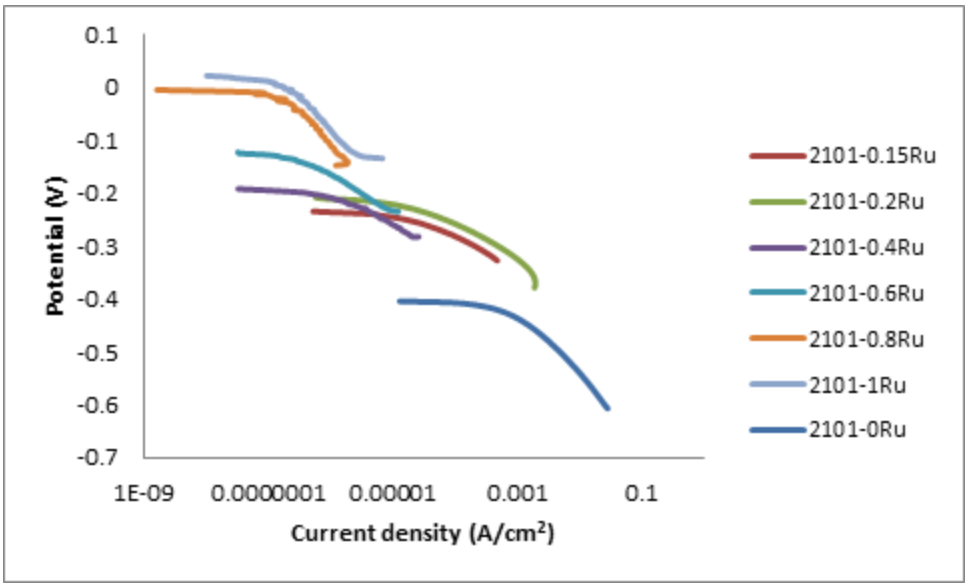

Figure 5.7. Effect of ruthenium addition on the cathodic behaviour of 2101duplex stainless steel in 1M H_2SO_4.

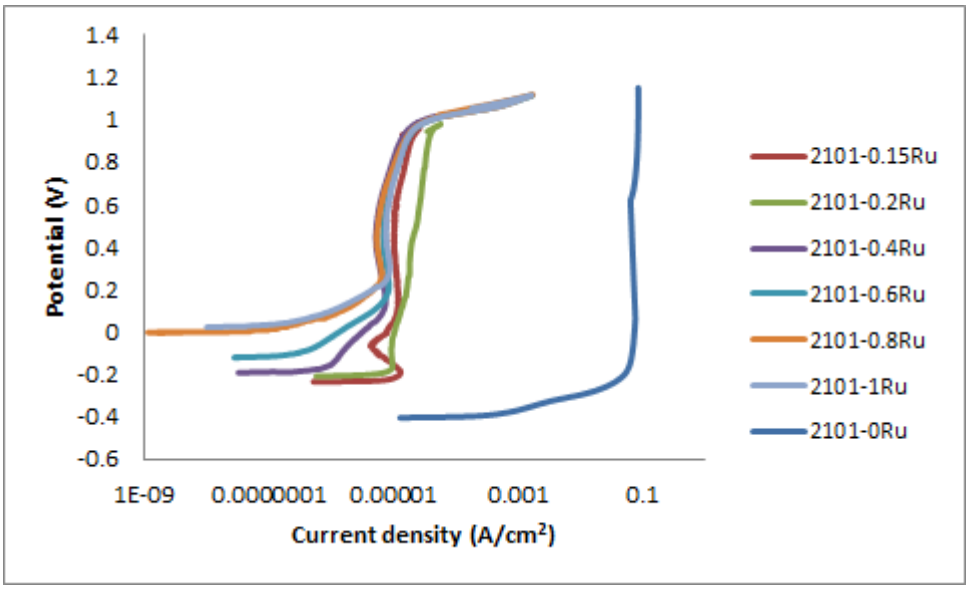

Figure 5.8. Anodic behaviour of 2101 with different ruthenium contents in 1M H_2SO_4 at 25°C.

Since the ruthenium was the only variable, the change in passivation characteristics of the duplex stainless steel must have been due to its presence. The positive shifts in the E_{corr} were due to increasing the effectiveness of the cathodic process, thereby decreasing the rate of the anodic

reactions. Various explanations have been given to the shifting of the corrosion potential of stainless steel by the addition of ruthenium. Tjong *et al.* [1990Tjo] credited it to the presence of ruthenium in the steel which allowed ruthenium to be taken up in the surface scale. This resulted in the formation of a thin film that decreases the uniform corrosion of the DSS alloy in the sulphuric acid. Conversely, other researchers [1998Wol, 2009Olu, 2009She] suggested the presence of Ru in the steel led to possible interaction of ruthenium with Fe, thus allowing free diffusion of Cr to the surface. Even though there was a trend of decreasing corrosion rates with increasing ruthenium, all the corrosion rates were very low for the alloys with ruthenium, compared to the base alloy (Table 4.22).

5.2.3 Influence of temperature on the corrosion behaviour in 1M sulphuric acid

The corrosion behaviour showing the effect of temperature in 1M sulphuric acid are shown in Table 4.22. As temperatures increased, corrosion current density and corrosion rates values increased and corrosion potentials were shifted to more noble values. Increased temperature of the 1M sulphuric acid caused higher corrosion rates and passive current densities for the 2101 alloy with ruthenium, and these were also observed by Potgieter [1996Pot] in high chromium duplex stainless steel and Olubambi *et al.* [2008Olu] in super-ferritic stainless steel.

Increased temperature of the 1M sulphuric acid caused a reduction in passive regions, which is due to the breakdown of the passive layer. All the alloys exhibited passivation at lower temperatures, while the 2101 alloys up to 0.6 wt% Ru showed active-passive transition, and 2101 with 0.8 and 1 wt% Ru exhibited pseudo-passivity at 40°C. At 60°C, only the alloy containing 1 wt% Ru showed strong pseudo-passivity, while there was a weaker effect for 0.6 wt% Ru. At 25°C, 40°C and 60°C, it was observed that the alloy containing the highest ruthenium content (1 wt% Ru) had the lowest corrosion rates. Thus, 1 wt% Ru is the optimum composition to use. Interestingly, Mwamba *et al.* [2012Mwa] found that increasing the PGM content from 0.2 wt% to 1, 1.5 and 2 wt% in Ti-47.5 wt% Al alloys showed no significant improvement to the oxidation resistance. They found that a 1 wt% PGM addition was apparently even deleterious. The optimum PGM addition for their alloys was 0.2 wt%.

5.2.4 Corrosion behaviour of 2101 cathodically modified with ruthenium in 0.5M HCl

The corrosion behaviour of 2101 cathodically modified with ruthenium was investigated in a de-aerated 0.5M HCl solution. The corrosion potentials shifted to more noble values with Ru, which is expected (Figure 5.9). Higginson [1989Hig] found that in Fe-40Cr-0.2Ru in 0.5M HCl, the decrease in the anodic dissolution caused by ruthenium was the major cause of the gradual positive shift in potential that preceded the onset of passivation. These shifts in the corrosion potential in hydrochloric acid were also observed by Potgieter [1996Pot]. More noble values showed the tendency of the alloys to resist corrosion. The corrosion rates in 0.5M HCl were higher than in 0.5M H_2SO_4, which was due to the presence of chloride in the solution and this, was also found by Higginson for Fe-40Cr alloy in 0.5M HCl [1989Hig]. The passivity ranges of the alloys when exposed to 0.5M hydrochloric acid were smaller than when exposed to sulphuric acid. The shift in the corrosion potential (high positive values) of 1 wt% Ru is shown in Figures 5.9 and 5.10. The shape of potentiodynamic curves of alloys containing ruthenium up to 0.8 wt% Ru are similar (Figure 5.10), and similarities in the polarisation behaviour were also observed by Potgieter *et al.* [1996Pot] for alloys containing up to 0.28% Ru addition to Fe-22Cr-9Ni-3Mo alloy.

The critical current density, the corrosion current and the corrosion rates decreased with increased ruthenium content; this demonstrated very clearly that ruthenium inhibits the anodic dissolution processes [1989Hig, 1996Pot, 1997Pot, 2008Olu]. The systematic decrease in the critical current density with increasing ruthenium content up to 0.8 wt% Ru were observed in this present work and is shown in Figure 5.11; 1 wt% Ru was off scale. Ruthenium addition modified both the cathodic and anodic part of the curve in 0.5M HCl, and this agreed with the work of Greene et al. [1961Gre], which stated that the addition of noble metals to alloys improve both the anodic and the cathodic reactions.

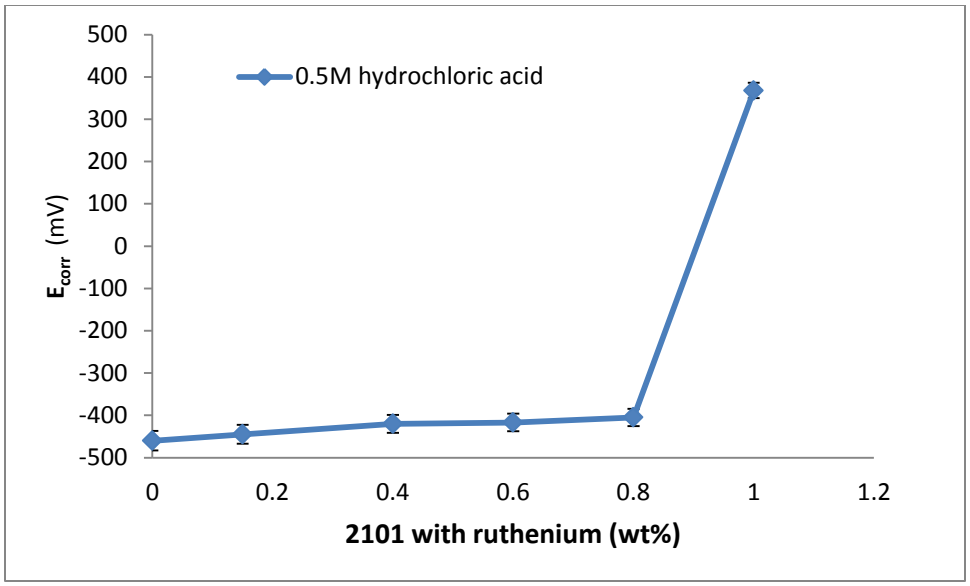

Figure 5.9. Corrosion potential of 2101 with different Ru contents in 0.5M hydrochloric acid.

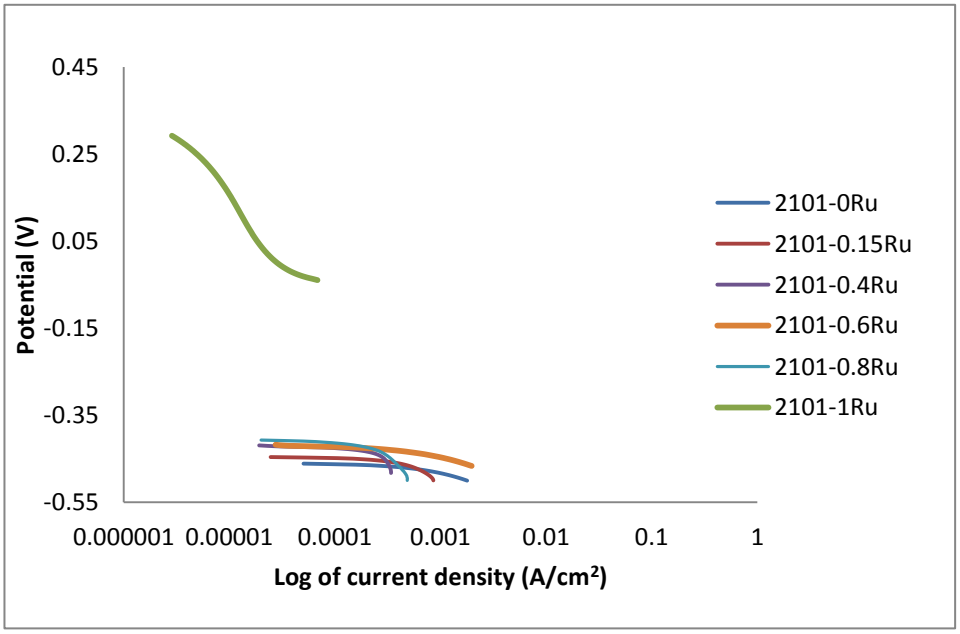

Figure 5.10. Cathodic curves of 2101 with different ruthenium contents in 0.5M HCl.

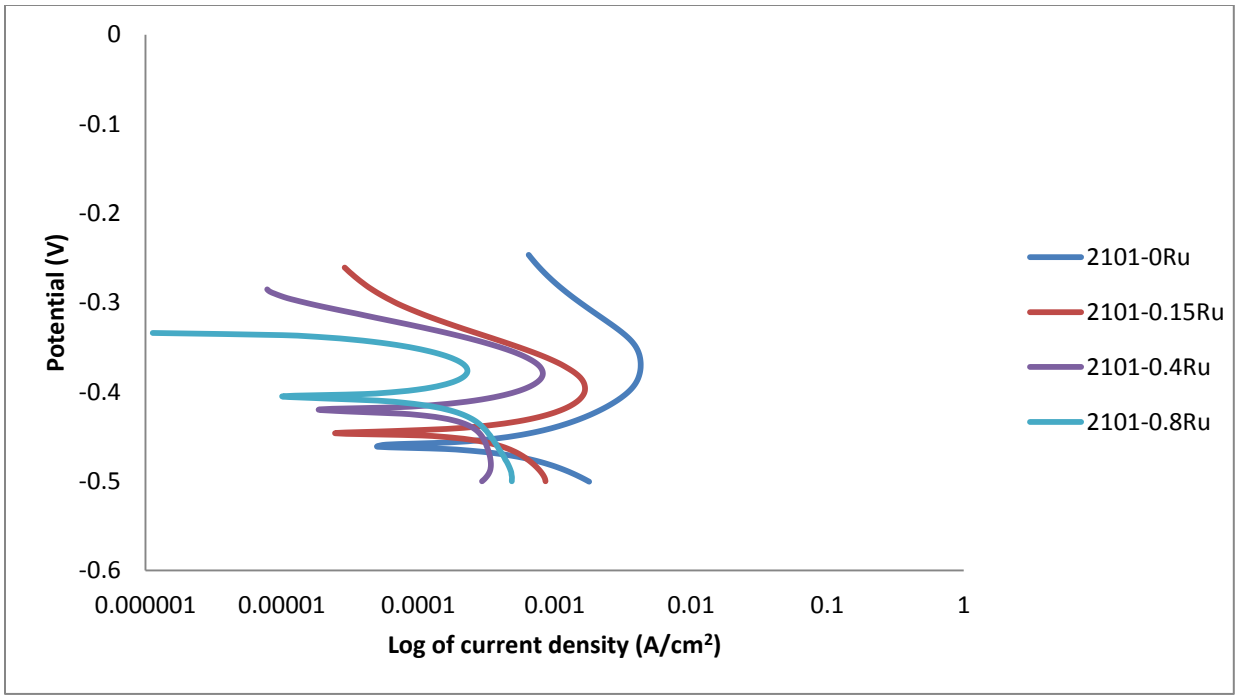

Figure 5.11. Effects of Ru additions to 2101 on the critical current density, icrit, in 0.5M HCl.

5.2.5. Comparison of the alloys in 0.5M HCl and 0.5M H_2SO_4

The corrosion resistance of the alloys was investigated in 0.5 M HCl and was compared to the same molarity of H_2SO_4. The i_{crit} value for 0.5M hydrochloric acid was higher compared to 0.5M sulphuric acid as shown in Figure 5.12. The increases in i_{crit} values were also observed for Fe-40Cr by Higginson [1989Hig] in 0.5M hydrochloric acid compared to 0.5 M sulphuric acid, because chloride ion adsorption affects the rate of surface diffusion of ruthenium, and subsequently affected the surface ruthenium distribution.

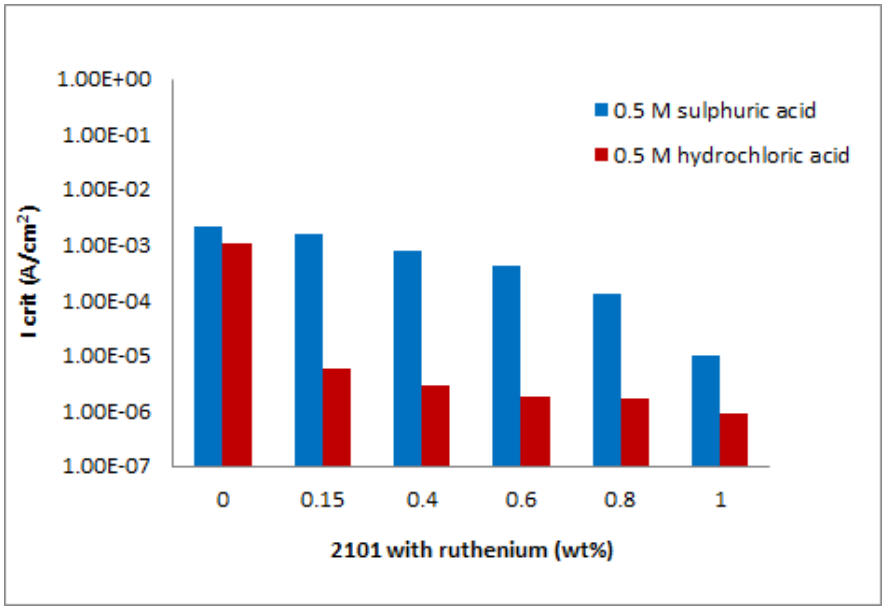

Figure 5.12. Effect of Ru content in 2101 in 0.5M sulphuric and 0.5M hydrochloric acid on the critical current density i_{crit}.

The corrosion rates for the alloy without ruthenium was 5.75×10^{-1}mm/y which is high, while for 2101-0.15wt% Ru it is 4.20×10^{-2} mm/y in H_2SO_4, and in 0.5M HCl 2101 without Ru it was higher than in H_2SO_4. The corrosion rates were reduced by one order of magnitude, for sulphuric acid, while for HCl they were reduced by two orders of magnitude. When exposed to hydrochloric acid, the corrosion potential (E_{corr}) of 2101 moved to more negative values, than when exposed to sulpuric acid. The i_{pass} was lower by one order of magnitude in 0.5M sulphuric acid, than for the alloys in 0.5M hydrochloric acid. This agreed with the work of Olubambi *et al.* [2008Olu].

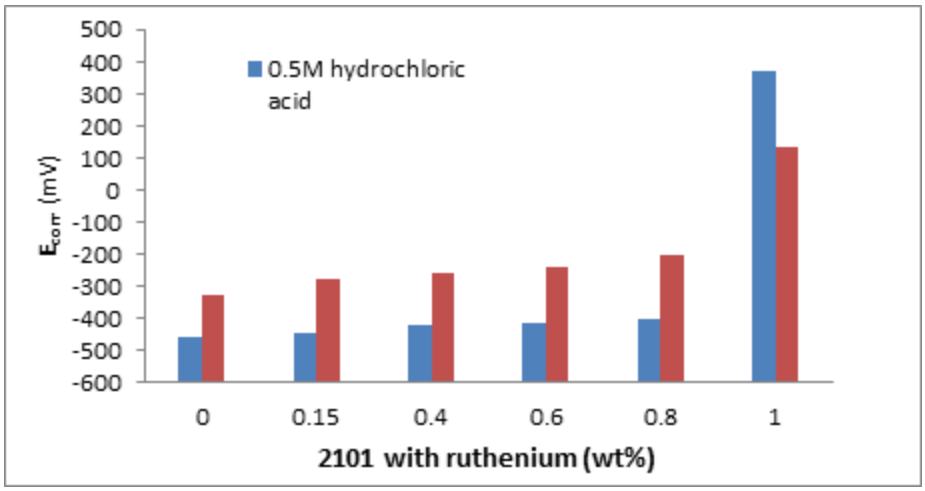

Figure 5.13. Comparison of Ru content in 2101 corrosion potential (Ecorr) in 0.5M sulphuric and hydrochloric acids.

5.2.6 Cyclic potentiodynamic results

Pitting corrosion occurs by the action of aggressive anions on metals and Cl^- is the anionic species most commonly associated with pitting corrosion [1992Jon], hence this is the reason why the pitting tendency of the alloys was tested in 3.5M NaCl. Cyclic tests were also performed in sulphuric acid, but showed no pitting. The addition of ruthenium increased the corrosion potential towards a more positive direction than the alloy without ruthenium. The presence of ruthenium improved the general and pitting corrosion of 2101 in 3.5M sodium chloride, as observed in Figures 4.109 - 4.113. This agreed with Potgieter *et al.* [1990Pot], Varga *et al.* [1997Var], Myburg *et al.* [1998Myb] and Sherif *et al.* [2009She]. They stated that stainless steel with minor additions of ruthenium passivated spontaneously, due to the formation of passive layers which increased corrosion resistance with a shift in corrosion potential of these alloys towards a more positive values.

The appearance of a hysteresis loop between the forward and reverse scans denoted the presence of localized corrosion. Little or no hysteresis in the cyclic curves, as seen in Figures 4.84-4.100, mostly in H_2SO_4, indicated a completely passive alloy, suggesting little risk of pitting corrosion. However, samples of 2101 with ruthenium additions in 3.5M NaCl solution showed large hysteresis curves.

The cathodic reaction for metals and alloys in near neutral oxygenated pH solutions is the oxygen reduction reaction [1979Sed]:

$2H_2O + O_2 + 4e^- \longrightarrow 40H^-$……..5.1

where the anodic reaction of steels at the same condition is the dissolution of iron:

$Fe \longrightarrow Fe^{2+} + 2e^-$. …….5.2

Hydrogen evolution reaction:

$2H^+ + 2e^- \longrightarrow H_2$ …….5.3

In the above reactions (Equations 5.1, 5.2 and 5.3), the different types of cathodic reactions occurring in the solutions were shown. There is further mitigation due to passivity under diffusion control, and this was promoted by the presence of ruthenium. The improved corrosion resistance was evident by the decreased cathodic slope (Figures 4.108-4.113) and corrosion rates, as shown in Table 4.24. Decreased cathodic and anodic slopes are related to the decrease in both anodic and cathodic corrosion reaction rates. The reduction in cathodic slope and the corrosion rates with increasing Ru additions in 3.5M NaCl agreed with Sherif *et al.* [2009She].

Figures 4.110- 4.112 (for 0.4, 0.6 and 0.8 wt% Ru) exhibited larger hystereses, with some current oscillations in the passive range, indicating tendency of the alloys to pit. The position of the reverse scans showed that the film could not repair itself [1992Jon]. Thus, these observations showed detrimental effects on the repassivation of 2101 containing ruthenium in 3.5M NaCl. The result of the alloys in 3.5M NaCl agreed with Sherif *et al.* [2009She].

5.2.7 Chronoamperometric Studies

Pitting corrosion is triggered by the susceptible spots formed on the surface of a metal which could be a crack in the boundary, an inclusion or could arise from flaws on the passive film [1986New, 2005Gal]. Pitting of stainless steel starts from flaws in the oxide film and propagates by the ion transport mechanism thereby, causing the growth of the pit. The pitting will stop once the critical current density is reached. The pit initiation and repassivation processes can be regarded as requiring different critical current densities in order to maintain critical solution composition against a diffusion gradient [1985New, 2005Gal]. As a pit forms, the metal goes

into solution and increases the flow of current, which can be measured by chronoamperometry [2008Sha]. As the number of the active spots on the surface increases, the probability of stable pit formation also increases.

Figures 4.118-4.124 show the chronoamperometry results for 0.15, 0.2, 0.4, 0.6 and 1 wt% ruthenium additions in 1M sulphuric acid solution. For the alloys containing 0.15, 0.2, 0.4 and 1 wt% Ru, the current decreased in the first 100 seconds, and became steady throughout the experiments, showing that there was no pitting. In Figure 4.123 for 2101 sample containing 0.6 wt% Ru in 1m sulphuric acid, the current fluctuation was noticed up to 400 seconds, and afterwards the current became steady. The chronoamperometric tests indicated that the alloys did not undergo pitting corrosion in 1M sulphuric acid (Figures 4.85-4.100), in agreement with the cyclic potentiodynamic tests in 1M sulphuric acid, which also agreed with the chronoamperometric test of 0.28wt% Ru addition to 2205 duplex stainless steel in sulphuric acid solution by Sherif [2012She]. Generally, the occurrence of pitting corrosion is indicated by the increased current of the alloy with time [1975Eva].

The results of the chronoamperometry tests showed that much pitting was not expected. This agreed with the microstructures, because there was not much pitting observed microstructurally on the 2101 alloys with ruthenium after the corrosion tests.

5.2.8 Post corrosion measurement characterization

Corrosion attack was observed on both austenite and ferrite in 2101 without ruthenium exposed to 0.5M HCl, while for the samples with ruthenium, the corrosion attack was not seen in the microstructure. However, for 2101 with 0.4 wt% Ru (Figure 4.132) the austenite particles were standing proud, which was not noticed before the corrosion test.

Corrosion attack was observed to be more on the ferrite phase in duplex stainless steel [1991Fou, 2009Zha]. This preferential pitting behaviour can be explained by the chemical composition of the phases, sample orientations, galvanic effects of the two phases and depletion of chromium from either the ferrite phase or the austenite phase.

The sample without ruthenium showed deterioration of the whole surface (Figure 4.126). The EDX analyses (Figures 4.127 and 4.128) revealed the presence of oxygen, and low chromium peaks were observed, which explains the higher corrosion on the surface.

The initiation of metastable pits was observed in Figure 4.138, where pits were initiated at the grain boundaries. This could be explained by the different chemical composition of the phases, where the unaffected phase was the ferrite, since it contained higher chromium levels.

The addition of ruthenium reduced pit formation. The EDX analyses showed that the un-affected surfaces were rich in chromium (Figures 4.129,132 and 135). The EDX analysis of corroded surface with 2101-1wt% in 0.5M HCl revealed ruthenium on the surfaces, and this agreed with Tjong and Mwaba [1990Tjo]. Ruthenium additions to 2101 increased the pitting resistance, which with increased ruthenium content.

5.2.9 **Comparison of the effect of ruthenium to chromium and stainless steels**

This study was only for the effect of ruthenium on duplex stainless steels, and it would be useful to compare these results with those of other alloys. The effect of ruthenium additions to chromium and different stainless steels were shown in Tables 2.4 and 5.1, where the corrosion current density and corrosion rates were the comparison parameters. The alloys compared are chromium, ferritic and duplex stainless steels, there were limited data for the corrosion rates or corrosion current densities of austenitic stainless steels.

Table 5.1. Summary of corrosion work in this study.

Metal or steel	Ru (wt%)	i_{corr} (A/cm^2)	Corrosion rate (mm/y)	Comment	Comparison
Fe-21Cr-1Ni	0		5.75E-01	0.5M sulphuric acid at 25°C the lowest corrosion rates was found at the highest ruthenium content	Ruthenium addition improved the corrosion rate. Corrosion rate and corrosion current reduced with increased ruthenium contents
	0.15		4.20E-02		
	0.20		4.00E-02		
	0.40		1.13E-02		
	0.60		2.37E-03		
	0.80		1.48E-03		
	1.00		1.38E-03		
Fe-21Cr-1Ni	0		1.66E+01	1M sulphuric acid at 25°C Corrosion rates decreased with increasing ruthenium contents	
	0.15		1.40E-01		
	0.20		1.06E-01		
Fe-21Cr-1Ni	0.40		1.26E-02	1M sulphuric acid at 25°C	
	0.60		4.72E-03		
	0.80		2.53E-03		
	1.00		2.10E-03		
Fe-21Cr-1Ni	0.20	1.90E-3	2.22E+01	1M sulphuric acid at 40°C	

Table 5.2. Summary of corrosion work in this study (continued).

Metal or steel	Ru (wt%)	i_{corr} (A/cm^2)	Corrosion rate (mm/y)	Comment	Comparison
	0.40	6.87E-4	8.03E+00	1M sulphuric acid at 40°C Corrosion current and corrosion rates decreased with increasing ruthenium contents	Corrosion rate and corrosion current reduced with increased ruthenium contents
	0.60	3.19E-4	3.73E+00		
	0.80	3.96E-6	4.63E-02		
	1.00	4.66E-7	5.45E-03		
Fe-21Cr-1Ni	0.20	2.00E-3	2.34E+01	1M sulphuric acid at 60°C Corrosion current decreased with increasing ruthenium contents	
	0.40	3.33E-4	3.89E+00		
	0.60	3.18E-4	3.72E+00		
	0.80	5.83E-5	6.82E-01		
	1.00	8.22E-7	9.61E-03		
Fe-21Cr-1Ni	0		8.88E+03	0.5M HCl at 25°C The lowest corrosion rates was found at the highest ruthenium contents	
	0.15		9.70E+02		
	0.40		5.38E+02		
	0.60		4.33E+02		
	0.80		3.27E+02		
	1.00		1.64E-07		
Fe-21Cr-1Ni	0.15		5.73E-02	3.5M NaCl Corrosion rates decreased with increasing ruthenium contents	
	0.4		3.12E-02		
	0.6		2.69E-02		
	0.8		2.19E-02		
	1.0		1.12E-02		

The additions of ruthenium to chromium, ferritic stainless steels and duplex stainless steels were found to decrease the corrosion rate and corrosion current as the ruthenium contents increased in acidic and chloride environments [1961Gre, 1977Str, 1990Tjo, 1995Pot, 1996Pot, 1998Wol 2009She2]. These effects were also noticed in the study, as shown in Table 5.1.

Table 5.2 shows the comparison of the effect of ruthenium additions to 2101, with the cost of the alloys, weight loss, cost of weight loss and the savings with respect to a 100 m^2 plates exposed to 1 M sulphuric acid. The price increase with ruthenium was very high. However, the weight loss calculated was very much lower for the alloys with ruthenium. This justified the price, as the cost of metal loss through corrosion was lower with the ruthenium additions. The difference in savings was very high for the alloy with 0.15wt% Ru compared to 2101 with no ruthenium, and the difference in savings for higher ruthenium additions was much less. Although the weight loss was lowest for 1 wt% Ru, economically, the best value for money is for the 0.15 wt% Ru addition.

Table 5.2. Comparison of the effect of ruthenium addition on cost and loss of metal in 1 M sulphuric acid.

Ru alloys	Cost ($/Tons)	Weight loss (Tons)	Cost of Weight loss ($/Tons)	Saving ($)
2101-0	3500	7.53E+08	2.63E+12	0.00E+00
2101-0.15	29808	6.04E+06	1.80E+11	2.45E+12
2101-0.2	38577	4.55E+06	1.75E+11	2.46E+12
2101-0.4	73654	5.42E+05	3.99E+10	2.59E+12
2101-0.6	108731	2.04E+05	2.21E+10	2.61E+12
2101-0.8	143808	1.08E+05	1.56E+10	2.62E+12
2101-1	178900	9.05E+04	1.62E+10	2.62E+12

CHAPTER 6

CONCLUSIONS AND RECOMMENDATIONS

Cathodic modification of stainless steels with minor alloying additions of noble metals has proved to be an effective approach to improving their corrosion resistance in many reducing acids. Thus, it is expected that the addition of ruthenium to 2101 duplex stainless steel should improve its corrosion resistance.

The 2101 alloys with different ruthenium additions of up to 10wt% were produced. Thermo-Calc was used to predict the best heat treatment temperature. The samples were characterised with SEM with EDX and XRD. Hardness tests were done on the samples to see the effect of ruthenium on the mechanical properties. Finally, corrosion tests were carried out on the samples in acidic, acidic chloride and chloride environments.

Thermo-Calc calculations showed that:

1. The 2101 duplex stainless steel with ruthenium up to 0.2 wt% Ru had equal amounts of ferrite and austenite at 1080°C and 880°C.
2. The temperature at which the liquid disappeared in 2101-10 wt% Ru was at 1280°C, which was lower than the other 2101 composition with a lower percentage of ruthenium.
3. Ruthenium additions up to 0.2 wt% did not give a significant change to the phase proportion diagram, retaining the duplex structure.
4. A higher percentage of ruthenium (2.5, 5 and 10 wt% Ru) changed the phase proportions of the duplex stainless steel, reducing the proportions of austenite, and thus not having the ~50:50 duplex structure. The 10 wt% Ru was mainly ferrite with some hcp, and no austenite.
5. As the ruthenium content increased, the HCP_A3#2 phases precipitated out at higher temperatures.
6. The 50:50 (austenite:ferrite) ratio was calculated to be at 1080°C for the duplex structure.

Experimental work showed that:

7. The duplex structure targeted was achieved by heat treating 2101 alloy with ruthenium at 1080°C for 2 hours, and times below this gave much less austenite.

8. The increase in ruthenium content up to 2 wt% did not change the microstructure from austenite and ferrite, while for 10 wt% Ru the microstructure changed to ferrite and hcp (51.0±7.5%).

9. Sigma was not found experimentally.

10. The hardness showed that the additions of ruthenium to 2101 was not detrimental to the mechanical properties, and the hardness mostly increased with increasing ruthenium content.

11. The aim of the heat treatment on the alloys was to produce a 50:50 austenite:ferrite ratio. Increasing the annealing time caused increased austenites. Increasing the temperature from 1080°C to 1100°C mostly reduced the austenite at 1100°C. The best heat treatment result were achieved at 1080°C for 120 minutes.

12. Ruthenium additions of up to 1 wt% Ru were beneficial in solutions of 0.5 M HCl, 0.5 M H_2SO_4, 1 M H_2SO_4 and 1 M H_2SO_4 + 1%NaCl.

13. The passive current density was reduced where there was an active to passive transition, and the i_{crit} was reduced with increasing ruthenium contents.

14. Ruthenium additions increased the corrosion potential to more noble values in all the solutions.

15. The corrosion rates decreased with increasing ruthenium additions in 1M sulphuric acid, sulphuric acid with chloride, 0.5 molar sulphuric acid, 0.5M hydrochloric acid and 3.5M NaCl.

16. The 2101 alloys with ruthenium in 1M H_2SO_4 acid were more resistant to pitting corrosion than in 3.5 M NaCl. The hystereses loops of 2101 alloys with ruthenium in 3.5M NaCl were larger than for 1M H_2SO_4, and they decreased with increasing ruthenium additions. After corrosion testing, the microsrtructure did not show much pitting.

17. Addition of 1 wt% Ru caused spontaneous passivation of the samples in all solutions.

18. According to the corrosion rates, 1wt% Ru was the optimum ruthenium addition.

19. The weight loss was lowest for 1 wt% Ru, Although, economically, the best value for money is for the 0.15 wt% Ru addition.

Recommendations are:

- Use WDS for analysing small ruthenium proportions, preferably with TEM.
- Surface analysis should be carried out using XPS to determine the composition after corrosion tests.
- The stress corrosion cracking resistance of the alloys should be studied, because there might be a problem in any application, after forming the alloys.
- The effect of ruthenium additions on the weldability of 2101 should be studied, to ascertain if they are any detrimental effects.

REFERENCES

[1911Mon] P. Monnartz (1911) "Iron-chromium alloys with special consideration of resistance to acids", *Metallurgie (Halle)* 8 (7) 161-176.

[1945Eva] U.R. Evans (1945) "Metallic Corrosion, Passivity and Protection", Edward Arnold and Co., London.

[1950Pug] J.W. Pugh and J.O. Nisbet, Transactions of AIME, Vol. 188, p. 286 (1950).

[1957Ste] M. Stern and A.L. Geary (1957) "Electrochemical Polarization: 1. A theoretical analysis of polarization curves", *Journal of the Electrochemical Society,* 104 (1) 56-63.

[1959Ste] M.J. Stern and H. Wissenberg (1959) "The influence of noble metal alloy additions on the electrochemical and corrosion behaviour of titanium alloys", *Journal of the Electrochemical Society,* 106 (9) 759-764.

[1960Hoa] T.P. Hoar (1960) "Increasing the resistance to titanium to non-oxidising states", *Platinum Metal Review,* 4, 59.

[1961Gre] N.D. Greene, C.R. Bishop and M. Stern (1961) "Corrosion and Electrochemical Behavior of Chromium-Noble Metal Alloys", *Journal of the Electrochemical Society,* 108 (9) 836-841.

[1963Shr] L.L. Shreir (1963) "Corrosion: corrosion of metals and alloys", George Newnes Limited, London, 1, 1.16-1.66.

[1964Tom] N.D. Tomashov (1964) "Passivity and corrosion resistance of metal systems", *Corrosion Science,* 4 (1-4) 315-334.

[1965Lew] M.H. Lewis and B. Hattersley (1965) " Precipitation of M23C6 in austenitic steels", *Acta Metallurgica,* 13 (11) 1159-1168.

[1965Bak] G.T. Bakhvalov and A.V Turkovskaya (1965) "Corrosion and protection of metals", Pergamon Press, Oxford, UK, p. 64.

[1965Wag] C. Wagner (1965) "Passivation and inhibition of metals at elevated temperature", *Corrosion Science,* 5 (11) 751-764.

[1967Tom] N.D. Tomashov (1967) "Development of structural electrochemical theory of the corrosion of metals and alloys", *Protection of Metals*, 3, 3.

[1968Rhi] F.N. Rhines (1968) "Quantitative Microscopy, Eds. R.T. de Hoff and McGraw-Hill, Boot Camp, New York, USA.

[1970Bie] G.J. Biefer (1970) "Effects of polarization and corrosion of type 430 stainless steel", *Canadian Metallurgical Quarterly,* 4 (14) 537-550.

[1970Tom] N.D. Tomashov and L.P. Vershinina (1970). "Kinetics of some electrode processes on a continuosly renewed surface of solid metal", *Electrochim Acta,* 15 (4) 501-517.

[1971 Eng] C.W. Engelhard (1971) "Platinum – Wonder metal of the future", *Chamber of Mines Journal*", 28-31.

[1971Uhl] H.H. Uhlig (1971) "Corrosion and Corrosion Control: An introduction to Corrosion Science and Engineering", 2nd Edition, John Wiley and sons inc. USA.

[1974Str] M.A. Streicher (1974) "Development of pitting-resistant Fe-Cr-Mo alloys", *Corrosion*, 30 (3) 77-91.

[1974Tom] N.D. Tomashov, G.P. Chernova, S.Y Ruscol and G.A Ayuyan, (1974). "The passivation of alloys on titanium bases, *Electrochim Acta*, 19 (4) 159-172.

[1975Eva] U.R. Evans (1975) "The Corrosion and Oxidation of Metals", 2nd Edition, Edward Arnold Limited, London, UK. pp. 37-62.

[1975Tom] N.D. Tomashov and G. Chernova (1975) "New corrosion-resistant alloys based on titanium and high-chromium steels", *Protection of Metals*, 11 (4) 379-84.

[1977Str] M.A. Streicher (1977) "Alloying Stainless Steels with the Platinum Metals", *Platinum Metals Review*, 21, 51-54.

[1977Tom] N.D. Tomashov, G.P. Chernova, V.I. Lakomskii, G.F. Tarkhov, L.A. Chingirinskaya and V.A. Siyshankova (1977) "Corrosion resistance of highly

nitride austenitic stainless steels, alloyed with palladium", *Protection of Metals*, 13 (1) 6-11.

[1978Pic] F.B. Pickering (1978) "Physical metallurgy and design of steels", Applied Science Publishers Ltd, London, UK. pp. 69-72.

[1978Sat] N. Sato (1978) "The passivity of metals and passivating films", *Passivity of Metals*, 39, 29-56.

[1978Sav] E. Savitsky, V. Polyakova, N. Gorina and N. Roshan (1978) "Physical Metallurgy of Platinum Metals", *MIR publishers*, Moscow, Russia.

[1978Sol] H.D. Solomon and T.M. Devine (1978) "Influence of microstructures on the mechanical properties and localised corrosion of a duplex stainless steel", Micon'78 Conference Proceedings, p. 430.

[1979Sed] A.J. Sedricks (1979) "Corrosion of stainless steel", John Wiley and Sons. Inc, USA.

[1979Suu] N. Suutala, T. Takalo and T. Moisio (1979) "Austenitic solidification mode in austenite stainless welds", *Metallurgical Transactions A*, 10A (8) 1173-1181.

[1979Tom] N.D. Tomashov, G.P. Chernova and E.N. Ustinsky (1979) "Corrosion and electrochemical behaviour of ductile chromium alloys", *Platinum Metals Review*, 23, 143-149.

[1980Suu] N. Suutala, T. Takalo and T. Moisio (1980) "Ferritic–austenitic solidification mode in austenitic stainless steel welds", *Metallurgical Transactions A*, 11A, 717-725.

[1980Tom1] N.D. Tomashov (1980) "Corrosion and mechanical properties of very pure high-chromium ferritic steels alloyed with molybdenum and palladium", *Protection of Metals*, 16 (2) 83-89.

[1980Tom2] N.D. Tomashov, G.P. Chernova, V.J. Trevilor, A.N. Ratinsky, N.E. Poryadchenko, E.F. Savranski and E.N. Ustinsky (1980) "Corrosion behaviour of

low alloyed chrome alloys cathodic addition in sulphuric acid solutions", *Protection of Metals,* 16, 208-213.

[1980Tom3] N.D. Tomashov, G.P. Chernova and E.N. Ustinsky (1980) "Self passivation of plastic ruthenium-alloyed chromium in sulphuric acid solution", *Protection of Metals,* 16, 452-455.

[1981Ber] S. Bernhardsson and J. Le Grand (1981) "Special stainless steel for the chemical and petrochemical industry", Sandvik, Sweden, *S-52- 65-ENG*, May 1981.

[1981Che] G.P. Chernova, T.A. Fedoseeva, L.P. Kornieko and N.D. Tomashov (1981) "Increasing the passivation ability and corrosion resistance of chromium steel by surface alloying with palladium", *Surface Technlogy*, 13 (3) 241-256.

[1982Her] G. Herbsleb and P. Schwaab (1982) "Duplex stainless steel", Ed. R.A Lula, ASM Metals Congress, October 25-28 1982 St. Louis, Missouri, ASM, Metals Park, Ohio 1983, pp.693-756.

[1983Cha] J. Chance, W. Coop and K.J. Gradwell (1983) " Structure property relationships in a 25Cr-7Ni-2Mo duplex stainless steel casting alloy", Duplex Stainless Steels Conference Proceedings, Ed. R.A. Lula, American Society of Metals, Metals Park, Ohio, p. 371.

[1983Sol] H.D. Solomon and T.M. Devine (1983) "Duplex stainless steels", pp. 693-756, American Society of Metals, Metals Park, Ohio, USA.

[1984Boy] H.E. Boyer (1984) "Practical Heat Treating", American Society of Metals, 1st Edition, p. 17–33.

[1984DuP] S.C. Du Plessis (1984)."The effect of platinum group metal additions on the corrosion resistance and mechanical properties of a 12% chromium ferritic steel", MSc dissertation, University of the Witwatersrand. Johannesburg, South Africa.

[1984Hig] A. Higginson (Mintek), Private Communication in 1984 to J.H. Potgieter, A.M. Heynes and W. Skinner (1990) "Cathodic modification as a means of improving the corrosion resistance of alloys", *Journal of Applied Electrochemistry*, 20, 711-715.

[1984Tom] N.D. Tomashov, G.P. Chernova and E.N. Ustinsky (1984) "Effect of platinum elements additions on the active dissolution of plastic chromium in sulfuric acid", *Corrosion*, 40 (3) 134-137.

[1985New] R.C. Newman (1985) "The dissolution and passivation kinectics of stainless alloys containing molybdenum-II. Dissolution kinectics in artificial pits. *Corrosion Science*, 25, (5), 341-350.

[1985 Sun] B. Sundman, B. Jansson and J.O. Andersson (1985) "The Thermo-Calc databank system", *CALPHAD*, 9, 153-190.

[1986Gus] P. Gustafsson, and H. Erikksson (1986) "International Conference of Duplex Stainless Steel", The Hague, Netherlands, 26-28 October, 1986, *Nederland Instituut voor Lastechniek*, Paper 9, p. 381.

[1986New] R.C. Newman and M.A.A. Ajjawi (1986) "A micro-electrode study of the nitrate effect on pitting of stainless steel", *Corrosion Science*, 26, (12), 1057-1063.

[1986Ros] C.V. Roscoe and K.J. Gradwell (1986) "International conference on duplex stainless steel", The Hague, Netherlands, 26-28 October 1986, *Nederland, Instituut voor Lastechniek*, Paper 34, p. 126.

[1986Sun] B. Sundman, B. Jansson and J.O. Andersson (1986) "Thermo-Calc, a databank for calculation of phase equilibria and phase diagrams in Computer calculation of phase diagrams", *ASM International*, Materials Park, Ohio, USA.

[1986Tom] N.D. Tomashov, G.P. Chernova, L.A Chingriskaya and E. Nasedkin (1986) "Special features of behaviour of high chrome ferritic stainless steels alloyed with palladium or ruthenium in solution of sulphuric and hydrochloric acid", *Protection of Metals*, 22, 704-710.

[1987Hig] A. Higginson (1987) Ph.D Thesis, University of Manchester, Manchester UK.

[1987How] D. Howart (1987) Mintek, Private Communication in J.H. Potgieter, A.M. Heynes and W. Skinner (1990) "Cathodic modification as a means of improving the corrosion resistance of alloys", *Journal of Applied Electrochemistry*, 20, 711-715.

[1987Str] A.J. Struutt and G.W. Lorimer (1987) "Structure property relationships of Zeron100", *Duplex stainless steels '87, Conference Proceedings,* p. 310.

[1987Sym] E. Symnotis-Barrdahl (1987) "Stainless steel ’87, The Institute of Metals. 14th - 16th September 1987, University of York, Great Britain,

[1987Wri] H.A. Wriedt, N.A. Gokeen and R.H. Nazfiger (1987) "The Fe-N (iron-nitrogen) system", *Bulletin of Alloy Phase Diagrams,* 8, 355-377.

[1988Lar] J.M. Lardon, J. Charles, F. Dupoiron and J.C. Bavay (1988) "Duplex austenitic - ferritic stainless steel, mechanical properties and corrosion resistance”. *Proceedings of the Conference on High Nitrogen Steels,* p. 280.

[1988Raj] T.V. Rajan, C.P. Sharma and A. Sharma (1988) "Heat Treatment Principles and Practice", Prentice–Hall of India, New Delhi, India. p. 175.

[1989Cha] J. Charles, J.P. Audouard, F. Dupoiron, J.M. Lardon, P. Soulignac and D. Catelin (1989) "Duplex stainless steels for marine applications", *NACE Corrosion ’89 Conference Proceedings*, New Orleans, USA, p. 116.

[1989Hig] A. Higginson, R.C. Newman and R.P.M. Procter (1989) "The passivaton of Fe-Cr-Ru alloys in acidic solution", *Corrosion Science,* 29 (11-12) 1293-1318.

[1989Ree] R.P. Reed (1989) "Nitrogen in ausenitic stainless steel”, *Journal of the Mineral, Metal and Materials Society,* March 1989, 41,16-21.

[1989Sav] E.M. Savitsky and A. Prince (1989) "Handbook of Precious Metals", *Hemisphere Publishing Corporation,* Oxford, England.

[1990Cor] M.B. Cortie and J.H. Potgieter (1990) "The effect of temperature and nitrogen content on the partitioning of alloy elements in duplex stainless steel”, *Metallurgical Transactions A,* 22A, 2173–2179.

[1990Pot] J.H. Potgieter, A.M. Heynes and W. Skinner (1990) "Cathodic modification as a means of improving the corrosion resistance of alloys", *Journal of Applied Electrochemistry*, 20, 711-715.

[1990Tjo] S.C. Tjong (1990) "Self passivation of Fe-Cr – PGM alloys in reducing acids studied by electrochemical and electron spectroscopic techniques", *Applied Surface Science*, 44, 301–318.

[1991Ata] S. Atamert and J.E. King (1991) "Elemental partitioning and microstructural developments in duplex stainless steel welds metal", *Acta Metallurgica et Materialia*, 39 (3) 273–285.

[1991Fou] S. Fourier (1991) "The corrosion of duplex stainless steels". PhD thesis, University of the Witwatersrand, Johannesburg, South Africa.

[1991Har] D.C. Harris and L.J. Cabri (1991) "Nomenclature of platinum-group-elements alloys; review and revision", *The Canadian Mineralogist*, 29 (2) 231-237.

[1991Pot] J.H. Potgieter (1991) "Alloys cathodically modified with noble metals", *Journal of Applied Electrochemistry*, 21, 471–482.

[1992Jon] D.A. Jones (1992) "Principles and prevention of corrosion", MacMillan publishing company, Republic of Singapore.

[1992Pot] J.H. Potgieter, L.M. Mathews and P.E. de Visser (1992) "Experimental study of quantitative phase characterisation in duplex stainless steel by potentiostatics etching", *Journal of Materials Science*, 27, 3667.

[1992Tul] M.A.A. Tullmin (1992) "The development of experimental ferritic stainless steels containing 40 percent chromium.". PhD thesis, University of the Witwatersrand, Johannesburg, South Africa.

[1992Sai] S. Saito and K. Kuramasu (1992) "Plasma etching of RuO_2 thin films", *Japanese Journal of Applied Physics*, 31 (1) 135–138.

[1993Des] A. Desestret and J. Charles (1993) "Stainless Steels", Eds. P. Lacombe, B. Baroux and G. Beranger, *Les Editions de Physique*, France, 2006.

[1993Pot] J.H. Potgieter (1993) "Effect of minor ruthenium additions on the corrosion behavior of duplex stainless steels in sulfuric acid", *Suid-Afr, Tydskr. Chem*, 46, 3-4.

[1993Vij] D.P. Vijay, S.B. Desu, and W. Pan (1993) "Reactive ion etching of lead- zirconate titanate (PZT) thin-film capacitors", *Journal of the Electrochemical Society*, 140 (9) 2635–2639.

[1994Fro] J. Frodigh and J. Nicholls (1994) "Mechanical properties of Sandvik duplex stainless steels", *AB Sandvik Steel*, Sweden.

[1994Pan] W. Pan and S.B. Desu (1994) "Reactive ion etching of RuO_2, thin-films using the gas-mixture O_2/CF_3CFH_2". *Journal of Vacuum Science & Technology* B, 12 (6) 3208–3213.

[1995Ben] A. Van Bennekom (1995) " The development of low nickel Cr-Mn-N duplex stainless steels", PhD thesis, University of the Witwatersrand, Johannesburg, South Africa.

[1995Lai] J.K.L. Lai, K.W. Wong and D.J. Li (1995) "The effect of solution treatment on the transformation behaviour of cold rolled duplex stainless steels", *Materials Science and Engineering A*, 203, 356–364.

[1995Les] P.Y. Lesaicherre, S. Yamamichi, K. Takemura, H. Yamaguchi, K. Tokashiki, Y. Miyasaka, M. Yoshida and H. Ono (1995) "A Gbit-scale DRAM stacked capacitor with ECR MOCVD $SrTiO_3$ over RIE patterned RuO_2/TiN storage nodes", *Integrated Ferroelectrics*, 11, 81–100.

[1995Pot] J.H. Potgieter and H.C. Brookes (1995) "Duplex stainless steel with minor additions of ruthenium in sulfuric acid", *NACE International Corrosion–April 1995.*

[1995Usi] U.S. International Trade Commision (1995) "Industry & Trade Summary Stainless Steel Mill Products", *United States International Trade Commission Publication 2880–June 1995.*

[1995Ver] C.F. Vermaak (1995) "The Platinum group metals", Mintek, Randburg, South Africa.

[1996Gar] L.F. Garfas-Mesias, J.M. Sykes and C.D.S. Tuck (1996) "The effect of phase compositions of 25 Cr duplex stainless steel in chloride solutions", *Corrosion Science*, 38 (8) 1319-1330.

[1996Pot] J.H. Potgieter, W.O. Barnard, G. Myburg, K.Varga, P. Baradlai and L. Tomcsanyi (1996) "Corrosion behaviour of duplex stainless steels containing minor ruthenium additions in reducing acid media", *Journal of Applied Electrochemistry*, 26, 1103-1110.

[1997Ben] K.C. Bendall (1997) "Duplex stainless steel in the pulp and paper industry", *Anti-Corrosion Methods and Materials*, 44 (3) 170–174.

[1997Jac] E.M.L.E.M. Jackson (1997) "Kinectics of formation and dissolution in duplex stainless steels", PhD Thesis, University of the Witwatersrand, South Africa.

[1997Lay] N.J. Laycock and R.C. Newman (1997). "Localized dissolution kinetics, salt films and pitting potentials", *Corrosion Science*, 39 (10–11) 1771–1779.

[1997May] E.W. Mayo (1997) "Predicting IGSCC/IGA susceptibility of Ni–Cr–Fe alloys by modelling of grain boundary chromium depletion", *Materials Science Engineering* A, 252, 129–39.

[1997Pot] J.H. Potgieter (1997) "The Efeect of cathodic modification on the corrosion behaviour of duplex stainless steels". PhD thesis, University of the Witwatersrand, Johannesburg, South Africa.

[1997Tys] M. Tystad (1997) "Application of duplex st ainless steel in the offshore industry", 5th World Conference on Duplex Stainless Steels, October 21-23 1997, *Stainless Steel World*, KCL Publishing, D97-208, pp. 95-100.

[1997Wei] P. Wei and S.B. Desu (1997) "Reactive ion etching of RuO_2 films: the role of additive gases in O_2 discharge", *Physica Status Solidi,* A 161 (1) 201–215.

[1997Yam] S. Yamamichi, P.Y. Lesaicherre, H. Yamaguchi, K. Takemura, S. Sone, H. Yabuta, K. Sato, T. Tamura, K. Nakajima, S. Ohnishi, K.Tokashiki, Y. Hayashi, Y. Kato, Y. Miyasaka, M. Yoshida and H.A. Ono (1997) "Stacked capacitor technology with ECR plasma MOCVD (Ba,Sr)TiO_3 and RuO_2/Ru/TiN/$TiSi_x$ storage nodes for Gb-scale AMs", *IEEE Transactions on Electron Devices*, 44 (7) 1076-1083.

[1998Bad] J. Bandaru, T. Sands and L. Tsakalakos (1998) "Simple Ru electrode scheme for ferroelectric (Pb,La)(Zr,Ti)O_3 capacitors directly on silicon", *Journal of Applied Physics,* 84 (2) 1121-1125.

[1998Myb] G. Myburg, K. Varga, W.O. Barnard, P. Baradlai, L. Tomcsanyi, J.H. Potgieter, C.W. Louw and M.J. van Staden (1998) "Surface composition of Ru containing duplex stainless steel after Passivation in non-oxidizing media", *Applied Surface Science,* 136, 29-35.

[1998Wol] I.M. Wolff, L.E. Iorio, T. Rumpf, P.V.T. Scheers and J.H. Potgieter (1998) "Oxidation and corrosion behavior of Fe-Cr and Fe-Cr-Al alloys with minor alloying additions", *Material Science and Engineering,* A241, 264-276.

[1999Aoy] T. Aoyama and K. Eguchi (1999) "Ruthenium films prepared by liquid source chemical vapour deposition using bis-(ethylcyclopentadienyl) ruthenium", *Japanese Journal of Applied Physics,* 38 (10A) 1134-1136.

[1999Far] J.C.M. Farrar, and A.W. Marshall (1999) "Type 300H austenitic stainless steel weld metals for high- temperature service", *Stainless Steel World 99 Conference*, 1999, pp. 147-162.

[1999Fra] R. Francis, G. Byrne, and G.R. Warburton (1999) "Experiences with Zeron 100® superduplex stainless steel in the process industries", *Stainless Steel World 99 Conference*, KCL Publishing, 1999, 613-624.

[1999Lop] N. Lopez, M. Cid and M. Puiggali (1999) "Influence of σ-phase on mechanical properties and corrosion resistance of duplex stainless steel", *Corrosion Science*, 1, 1615–1631.

[1999She] C.H. Shek, D.J. Li, K.W. Wong and J.K.L. Lai (1999) "Creep properties of aged stainless steels containing σ phase", *Materials Science Engineering A,* 266, 30–36.

[1999Tri] E.A. Trillo and L.E. Murr (1999) "Effects of carbon content, deformation, and interfacial energetics on carbide precipitation and corrosion sensitization in 304 stainless steel", *Acta Materialia,* 47, 1, 235–245.

[2000Mun] M.L. Munoz-Saucedo, Y. Watanabe, T. Shoji and H. Takahashi (2000) "Effect of microstructure evolution on fracture toughness in isothermally aged austenitic stainless steels for cryogenic applications", *Cryogenics,* 40 (11) 693–700.

[2000Nil] J.O. Nilssom, P. Kangas, T. Karlsson and A. Wilson (2000) "Mechanical properties, microstructural stability and kinetcs of σ phase formation in a 29Cr–6Ni–2Mo–0.38N superduplex stainless steel", *Metallurgical and Materials Transactions A,* 31A, 35–45.

[2000Tav] S.S.N. Tavares, M.R. Da Silva and J.M. Neto (2000) "Magnetic property changes during embrittlement of a duplex stainless steel", *Journal of Alloys and Compounds,* 313, 168–173.

[2001Dup] L. Duprez, B.C. Decooman and N. Akdut (2001) "Redistribution of the substitutional elements during σ and χ phase formation in a duplex stainless steel", *Steel Research,* 72, 311–316.

[2001Hän] H. Hänninen, J. Romu, R. Ilola, J. Tervo and A. Laitinen (2001) "Effects of processing and manufacturing of high nitrogen – containing stainless steels on their mechanical corrosion and wear properties", *Journal of Materials Processing Technology,* 117, 424-430.

[2001Iiz] T. Iizuka, K. Arita, I. Yamamoto and S. Yamamichi (2001) " $(Ba,Sr)TiO_3$ thin film capacitors with Ru electrodes for application to ULSI processes", *NEC Research and Development,* 42 (1) 64-69.

[2001Imo] International Molybdenum Association (2001) "Practical guidelines for the fabrication of duplex stainless steels", 1st Edn. www. wpsamerica.com (accessed 2009).

[2001Per] R.A. Perren, T.A. Suter, P.J. Uggowitzer, L. Weber, R. Magdowski, H. Bohni and M.O. Speidel (2001) "Corrosion resistance of super duplex stainless steels in chloride ion containing environments: investigations by means of a new microelectrochemical method I. Precipitation-free states'', *Corrosion Science*, 43, 707-726.

[2001Tav] S.S.M Tavares, R.F. de Noronha, M.R. da Silva, J.M. Neto and S. Pairis (2001) "475°C Embrittlement in a duplex stainless steel UNS S31803", *Materials Research*, 4 (4) 237-240.

[2001Van] E. van der Lingen and R.F. Sandenbergh (2001). "The cathodic modification behaviour of ruthenium additions to titanium in hydrochloric acid", *Corrosion Science*, 43, 577-590.

[2003Cam] M. Campos, A. Bautista, D. Caceres, J. Abenojar and J.M. Torralba (2003) "Study of the interfaces between austenite and ferrite grains in P/M duplex stainless steels", *Journal of the European Ceramic Society*, 23, 2813–2819.

[2003Gun] R.N. Gunn (2003) "Duplex Stainless Steels - Microstructure, Properties and Applications", Abington Publishing. Cambridge, UK.

[2003Ols] C.O.A. Olsson and D. Landolt (2003) "Passive films on stainless steels: chemistry, structure and growth", *Electrochimica Acta*, 48, 1093–1104.

[2003Sou] T. Sourmail and H.K.D.H. Bhadesia (2003) "Modelling simultaneous precipitation reactions in austenitic stainless steels", *CALPHAD*, 27, 169-175.

[2004Azu] S. Azuma, T. Kudo, H. Miyuki, M. Yamashita and H. Uchida (2004) "Effect of nickel alloying on crevice corrosion resistance of stainless steels", *Corrosion Science*, 46, 2265–2280.

[2005Gal] J.R. Galvele (2005) "Tafel's law in pitting corrosion and crevice susceptibility", *Corrosion Science*, 47, 3053–3067.

[2005Gru] J.F. Grubb, T. DeBold and J.D. Fritz (2005) "Corrosion of wrought stainless steels", ASM handbook, Ohio, USA, *Corrosion & Materials*, 13B, 54-77.

[2005Hus] E. Hussain and A. Hussain (2005) "Erosion – corrosion of duplex stainless steel under Kuwait marine conditions", *Desalination*, 183, 227–234.

[2005Mar] M. Martins and L.C. Casteletti (2005). "Heat treatment temperature influence on ASTM A890 GR 6A super duplex stainless steel microstructure", *Materials Characterization*, 55, 225-233.

[2005Rus] S.W. Russell and C.D. Lundin (2005). "The development of qualification standards for cast duplex stainless steel", Final Report, submitted to US Department of Energy, Award Number–DE-FC07-00 ID13975.

[2006Ash] H. Ashassi-Sorkhabi and D. Seifzadeh (2006) "The inhibition of steel corrosion in hydrochloric acid solution by juice of *Prunus cerasus*", *International Journal of Electrochemical Science*, 1, 92-98.

[2006AST] ASTM Designation: A923 – 06, Standard Test Methods for detecting Detrimental Intermetallic Phases in Duplex Austenitic/Ferritic Stainless Steel.

[2006Ban] O.A. Bannykh, V.M. Blinov, M.V. Kostina and E.V. Blinov (2006) "Nickel saving in a 0Kh17N12M2-Type (AISI 316) steel due to nitrogen alloying", *Russian Metallurgy (Metally)*, 5, 372-378.

[2006Cui] Z.D. Cui, S.L. Wu, S.L. Zhu and X.J. Yang (2006) "Study on corrosion properties of pipelines in simulated produced water saturated with supercritical CO_2", *Applied Surface Science*, 252, 2368–2374.

[2006Fra] S. Frangini and S. Loreti (2006) "The role of temperature on the corrosion and passivation of type 310S stainless steel in eutectic (Li + K) carbonate melt", *Journal of Power Sources*, 160, 800–804.

[2006Ive] A.K. Iversen (2006) "Stainless steels in bipolar plates – surface resistive properties of corrosion resistant steel grades during current loads", *Corrosion Science*, 48, 1036–1058.

[2006Kho] F.M. Khoshnaw and R.H. Gardi (2006) "Pitting corrosion resistance determination of duplex stainless steel by using critical pitting temperature method", http://www.stainless-steel world.net/duplex/pittingcorrosion.asp (Accessed October 2008).

[2006Mun] A.I. Munoz, J.G. Anton, J.L Guinon and V.P. Herranz (2006) "Effects of solution temperatures on localized corrosion of high nickel content stainless steels and nickel in chromated LiBr solution", *Corrosion Science*, 48, 3349-3374.

[2006Pan] R.K. Pandey (2006) "Failure analysis of styrene reactor tubes", *Engineering Failure Analysis*, 13, 1314–1325.

[2006Vig] V. Vignal, N. Mary, P. Ponthiaux and F. Wenger (2006) "Influence of friction on the local mechanical and electrochemical behaviour of duplex stainless steels", *Wear*, 261 (9) 947–953.

[2007Arm] A.F. Armas, S. Degallaix, G. Degallaix, S. Hereñú, M.C Marinelli and I. Alvarez-Armas (2007) "Beneficial effects induced by high temperature cycling in aged duplex stainless steel", *Key Engineering Materials*, 345/346, 339–342.

[2007Ezu] H.M. Ezuber, A. El-Houd and F. El-Shawesh (2007) "Effects of sigma phase precipitation on seawater pitting of duplex stainless steel", *Desalination*, 207, 268-275.

[2007Ols] Jan Olsson and Snis Malin (2007) "Duplex – A new generation of stainless steels for desalination plants", *Desalination*, 205, 104–113.

[2007Ric] A.D. Richards and A. Rodger (2007) "Synthetic metallomolecules as agents for the control of DNA structure", *Chemical Society Reviews*, 36, 471–483.

[2008Alv] I. Alvarez-Armas (2008) "Duplex stainless steels: brief history and some recent alloys", *Bentham Science*, 1, 51-57.

[2008Arm] A.F. Armas, S. Hereñú, I. Alvarez-Armas, S. Degallaix, A. Condó and F. Lovey (2008) "The influence of temperature on the cyclic behaviour of aged and unaged super duplex stainless steels", *Materials Science Engineering A*, 491, 434–439.

[2008Bad] R. Badji, M. Boubadallah, B. Bacroix, C. Kahloun, K. Bettahar and N. Kherrouba (2008) "Effect of solution treatment temperature on the precipitation kinetic of σ-phase in 2205 duplex stainless steel welds", *Materials Science and Engineering A*, (496), 447- 454.

[2008Bró] J. Brózda and J. Madej (2008) "Cracking of the mixing chamber caused by sigma phase precipitation in austenitic steel welded joints", *Engineering Failure Analysis*, 15, 368–377.

[2008Can] L.C.F. Canale and G.E. Totten (2008) "Steel Heat Treatment Failures due to Quenching", *Failure Analysis of Heat Treated Steel Components,* 1st Edition, ASM, Materials Park, Ohio USA, 255-284.

[2008Inv] I.J. Invernizzi, E. Sivieri and S.P. Trasatti (2008) "Corrosion behaviour of Duplex stainless steels in organic acid aqueous solutions", *Materials Science and Engineering*, 485, 234–242.

[2008Niu] Y. Niu, W.M. Lu, J.T. Pan and K. Zhang (2008) "Accelerated corrosion of five commercial steels under a $ZnCl_2$–KCl deposit in a reducing environment typical of waste gasification at 673–773 K", *Corrosion Science,* 50, 1900–1906.

[2008Olu] P.A. Olubambi, J.H. Potgieter and L.A Cornish (2008) "Corrosion behaviour of super ferritic stainless steels cathodically modified with minor additions of ruthenium in sulphuric and hydrochloric acids", *Materials and Design*, 30 (5) 1451-1457.

[2008Pot] J.H. Potgieter, P.A. Olubambi, C.N. Machio, L. Cornish and M. Sherif El-Sayed (2008) "Influence of nickel additions on the corrosion behaviour of low nitrogen 22%Cr series duplex stainless steels", *Corrosion Science,* 50, 2572–2579.

[2008Rev] R.W. Reve (2008) "Uhlig's Corrosion Handbook second edition", John Willey and Sons, New York, USA.

[2008Sha] A. Shahryari, S. Omanovic and J.A. Szpunar (2008) "Electrochemical formation of highly pitting resistant passive films on a biomedical grade 316LVM stainless steel surface", *Materials Science and Engineering*, 28, 94–106.

[2008Yae] Kina A. Yae, S.S.M. Tavares, J.M. Pardal and J.A. Souza (2008) "Microstructure and intergranular corrosion resistance evaluation of AISI 304 steel for high temperature service", *Material Characterization*, 59, 651–655.

[2008Zha] W. Zhang, L. Jiang, J. Hu and H. Song (2008) "Study of mechanical and corrosion properties of a Fe-21.4Cr-6Mn-1.5Ni-0.24N-0.6Mo duplex stainless steel", *Materials and Engineering* A, 497, 501–504.

[2009Con] O. Conejero, M. Palacios and S. Rivera (2009) "Premature corrosion failure of a 316L stainless steel plate due to the presence of sigma phase", *Engineering Failure Analysis,* 16, 699-704.

[2009Esc] D.M. Escriba, E. Materna-Morris, R.L. Plaut and A.F. Padilha (2009) "Chi-phase precipitation in a duplex stainless steel", *Materials Characterization,* 60, 1214-1219.

[2009Far] G. Fargas, M. Anglada and A. Mateo (2009) "Effect of the annealing temperature on the mechanical properties, formability and corrosion resistance of hot rolled duplex stainless steel", *Journal of Materials Processing Technology*, 209, 1770–1782.

[2009Imo] International Molybdenum Association (2009) Practical guidelines for the fabrication of duplex stainless steels", 2nd Edition. www.imoa.info (accessed 2009).

[2009Mar] M. Martins and L.C. Casteletti (2009) "Microstructural characteristics and corrosion behaviour of a super duplex stainless steel casting", *Material Characterization,* 60,150-155.

[2009Mil] M. Militisky, M. Verhaege, N. de Wispelaere, L. Peguet, J. Z. Ferreira and H. Hänninen (2009) "Corrosion properties of nickel free austenitic stainless steels in 0.5M H_2SO_4 and 0.5M H_2SO_4 plus 0.4M NaCl", *Corrosion Engineering, Science and Technology*, 44, 5, 394-400.

[2009Row] David P. Rowlands (2009) "The secrets of stainless steel", *Stainless Steel Information Series* No*. 7,* South African Stainless Steel Development Association.

[2009She1] E.M. Sherif, J.H. Potgieter, J.D. Comins, L. Cornish, P.A. Olubambi, C.N. Machio, (2009) " Effect of minor additions of ruthenium on the passivation of duplex stainless-steel corrosion in concentrated hydrochloric acid solutions", *Journal of Applied Electrochemistry,* 39, 1385-1392.

[2009She2] E.M. Sherif, J.H. Potgieter, J.D. Comins, L. Cornish, P.A. Olubambi, C.N. Machio, (2009) "The beneficial effect of ruthenium additions on the passivation of duplex stainless steel corrosion in sodium chloride solutions", *Corrosion Science,* 51, 1364–1371.

[2009Tav] S.S.M. Tavares, V. Moura, V.C. da Costa, M.L.R. Ferreira and J.M. Pardal (2009) "The Microstructural changes and corrosion resistance of AISI 310S steel exposed to 600–800°C", *Materials Characterization*, 60 (6) 573-578.

[2009Zha1] W. Zhang, L. Jiang, J. Hu and H. Song, (2009) "Effect of ageing on precipitation and impact energy of 2101 economical duplex stainless steel", *Materials Characterization*, 60, 50–55.

[2009Zha2] L. Zhang, W. Zhang, Y. Jiang, B. Deng, D. Sun and J. Li (2009) "Influence of annealing treatment on the corrosion resistance of lean duplex stainless steel 2101", *Electrochmica Acta*, 54, 5387–5392.

[2010Lia] D. Liang, J.W. Sowards, G.S. Frankel, B.T. Alexandrov and J.C. Lippold (2010) "Corrosion resistance of welds in type 304L stainless made with a nickel-copper-ruthenium welding consumables", *Corrosion Science,* 52, 2439–2451.

[2012Gov] K. Govender, F. Scenini, S. Lyon and A. Sherry (2012) "Influence of Pd and Ru additions on stress corrosion cracking of austenitics stainless steels", *Corrosion Engineering, Science and Technology*, 47 (7) 507-515.

[2012Mwa] I.A. Mwamba, L.A. Cornish and E. van der Lingen (2012) "Microstructural, mechanical, and oxidation property evolution of gamma TiAl alloy with addition

of precious metals", *The Journal of The Southern Institute of Mining and Metallurgy*, 7A, 517-526.

[2012Par] H.H. Pariser and G.C. Pariser (2012) "What's new, stainless scrap", INSG 22st session industry advisory panel, Lisbon. Germany. 23 April, 2012.

[2012Sce] F. Scenini, K. Govender, S. Lyon and A. Sherry (2012) "Stress corrosion cracking of Ru doped 304 stainless steel in high temperature water", *Corrosion Engineering, Science and Technology*, 47 (7) 498-506.

[2012She] El-Sayed M. Sherif (2012) "Corrosion behaviour of duplex stainless steel alloy 2209 in acidic and neutral chloride solution and its passivation by ruthenium as an alloying element", *International Journal of Electrochemical Science*, 7, 2374-2388.

[2012Van] George Van der Voort, Private Communication (AMI 2012).

[URLAve] www.avestapolarit.com, accessed 20th May 2009.

[URLBss] http://www.bssa.org.uk/topics.php, accessed 19 September 2012.

[2012URL] http://events.nace.org/library/corrosion/AnodProtect/passivecurve.asp, assessed 2012.

[URLOda] http://www.odav-online.com/globalmind/precious-metals/ruthenium_-_Most_versatile_of_the_Platinum_Group_Metals.php, accessed 17 July 2012.

[URLOut] http://www.outokumpu.com/en/products/grades/ferritics-stainless steels/pages/ferritics.aspx, accessed July 2010.

[URLSou] thomas-sourmail.net/stainless, assessed 14th November 2012

[URL2013] www.alibaba.com, .accessed June 2013

[URLSpe] www.specialmetals.com, assessed 18th March 2014

[URLOut2] http://www.outokumpu.com/SiteCollectionDocuments/Outokumpu-stainless-steel-handbook.pdf, accessed July 2014.

APPENDIX A

ALLOY SPECIFICATIONS

Chemical composition data for 2101 (www.SandmeyerSteel.com)

Chemical Analysis

Typical Values (Weight %)

Cr	Ni	Mn	Mo	N
21.0 min. - 22.0 max.	1.35 min. - 1.70 max.	4.00 min. - 6.00 max.	0.10 min. - 0.80 max.	0.20 min. - 0.25 max.

C	Si	P	Cu	S	Fe
0.040 max.	1.00 max.	0.040 max.	0.10 min. - 0.80 max.	0.030 max.	Balance*

*Alloy predominates remaining composition. Other elements may be present only in minimal quantities.

Chemical composition data for 2205 (Interlloy Pty Ltd).

Chemical Composition		Min. %	Max. %
	Carbon	0	0.03
	Silicon	0	1.00
	Manganese	0	2.00
	Nickel	4.50	6.50
	Chromium	21.00	23.00
	Molybdenum	2.50	3.50
	Nitrgogen	0.08	0.20
	Phosphorous	0	0.03
	Sulphur	0	0.02

APPENDIX B

REPRODUCIBILITY CURVES

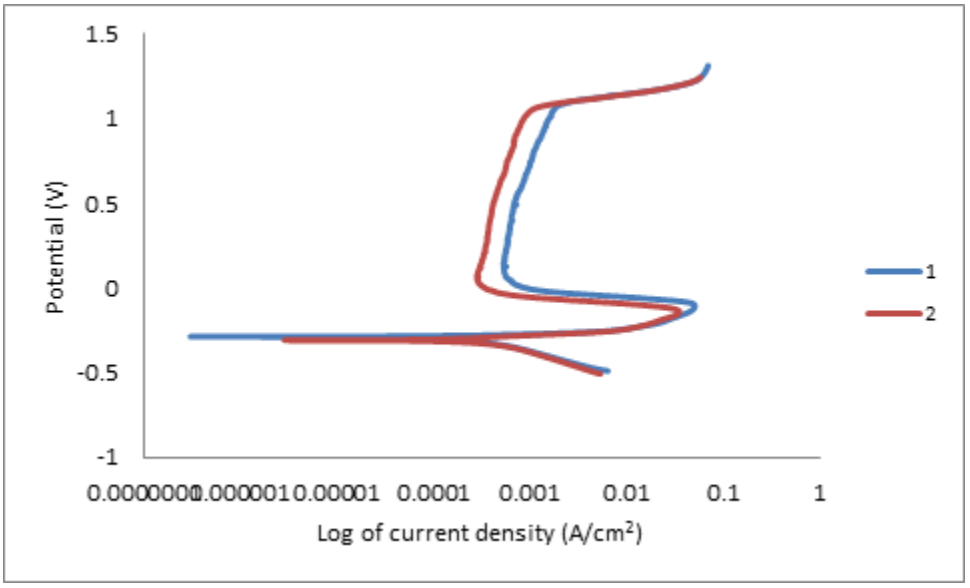

Figure B1. Example of reproducibility of 2507 (1M sulphuric acid at 40°C).

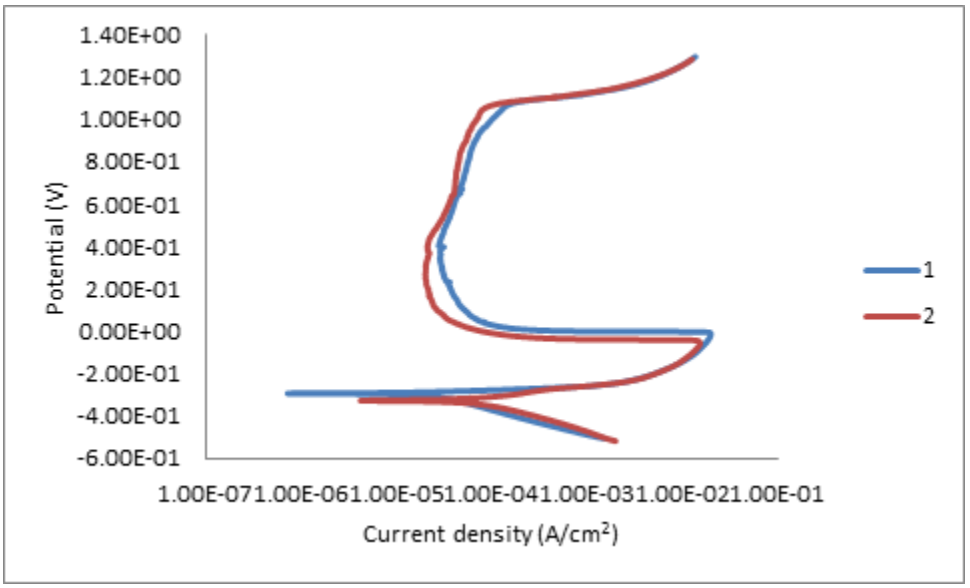

Figure B2. Example of reproducibility of 2205 (1M sulphuric acid at 25°C).

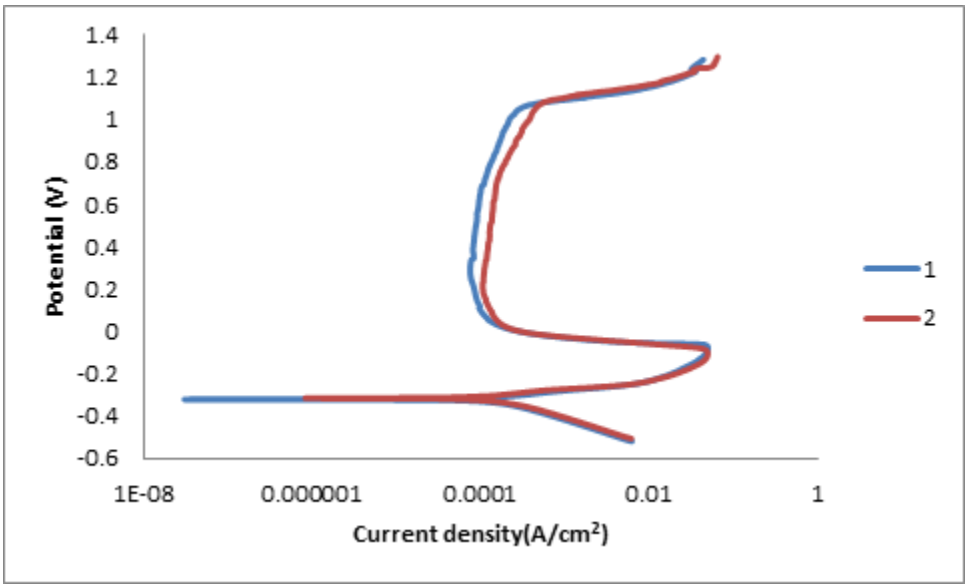

Figure B3. Example of reproducibility of 2205 (1M sulphuric acid at 40°C).

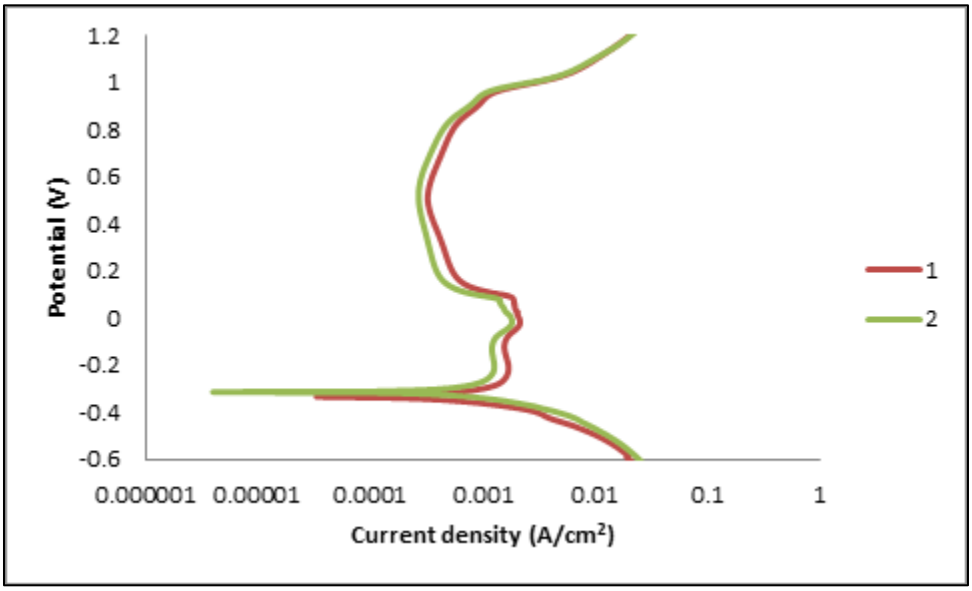

Figure B4. Example of reproducibility of 2101 (1M sulphuric acid with 1% NaCl at 80°C).

APPENDIX C

PUBLICATIONS FROM THIS WORK

Papers published during the course of this work, using this work

O.A. Olaseinde, L.A. Cornish, J.W. van der Merwe and P.A. Olubambi, "Characterization of 2101 lean duplex stainless steel with 0.15wt% ruthenium**",** Proceedings of the Microscopy Society of Southern Africa Conference, Vol. 40, p. 44, Forever resorts, Bela-Bela, South Africa, 26th-29th October 2010. ISSN 0250-0418 : ISBN 0-620-35056-3.

O.A. Olaseinde, L.A. Cornish, J.W. van der Merwe and P.A. Olubambi, "Electrochemical studies of Fe-21Cr-1Ni duplex stainless steel with 0.15 wt% Ru additions at different temperatures", ZrTa2011 New Metals Development Network Conference, Abstracts p. 32, ISBN 978-1-92041023-0, 18-Olaseinde on CD (8 pages), 13th-14th October 2011, Magaliesburg, South Africa.

O.A. Olaseinde, L.A. Cornish, J.W. van der Merwe and P.A. Olubambi, "Electrochemical Behaviour of 2101 DSS with Ruthenium and 316 SS", 18th International Corrosion Congress, Paper 450 on CD (8 pages), Perth, Australia, 20th -24th November 2011.

O.A. Olaseinde, L.A. Cornish, J.W. van der Merwe and P.A. Olubambi, "Effect of Ruthenium Additions on the microstructure of 2101 duplex stainless steel", Proceedings of the Microscopy Society of Southern Africa, Vol. 41, p. 34, Pretoria, South Africa, 6 th-9th December 2011.

O.A. Olaseinde, J.W. van der Merwe, L.A. Cornish, L.H. Chown and P.A. Olubambi, "Electrochemical study of Fe-21Cr-1Ni duplex stainless steels with 0.15wt% ruthenium addition at different temperatures'', The Journal of The Southern African Institute of Mining and Metallurgy. Vol. 7A, pp. 535-538.

O.A. Olaseinde, J.W. van der Merwe, L.A. Cornish, and P.A. Olubambi, "Corrosion behaviour of 2101 duplex stainless steel modified with varying ruthenium additions in hydrochloric and sulphuric acid

solutions'', Ferrous and Base Metal Development Network Conference 2012, Advanced Metal Initiative, The Southern African Institute of Mining and Metallurgy, Symposium Series S73, pp. 115-121, Magaliesburg, South Africa, 15th-17th October 2012.

Presentations from this work

With the exemption of the first presentation, which also had the work of Dr Ukpong, all the research was done for this PhD.

O.A. Olaseinde, A.M. Ukpong, L.A. Cornish, J.W. van der Merwe and P.A. Olubambi, "The effect of minor Ru additions on the phase properties in selected duplex stainless steels", 5th International Conference of the African Materials Research Society, Abuja, Nigeria, 14th–18th December 2009.

O.A. Olaseinde, J.W. van der Merwe, L.A. Cornish, and P.A. Olubambi, "Heat treatment and corrosion behaviour of 2101 duplex stainless steel cathodically modified with ruthenium", 1st African Materials Science Network (AMSEN) Workshop Proceedings, pp. 35-36, Windhoek, Namibia, 27th-29th January 2010.

O.A. Olaseinde, J.W. van der Merwe, L.A. Cornish, and P.A. Olubambi "Heat treatment and corrosion behaviour of 2101 duplex stainless steel cathodically modified with ruthenium", 2nd African Materials Science Network (AMSEN) Workshop Proceedings, pp. 39-40, Nairobi, Kenya, 21st-23rd March 2012.

.

ELECTROCHEMICAL BEHAVIOUR OF 2101, 2101 WITH RUTHENIUM AND 316 SS

O.A. Olaseinde[1,2], J.W. Van der Merwe[1,2], L.A. Cornish[1,2] and P.A. Olubambi[2,3]

[1]School of Chemical & Metallurgical Engineering and DST/NRF Centre of Excellence in Strong Materials, University of the Witwatersrand, South Africa, [2]African Material Science and Engineering Network (Carnegie – RISE Network) and [3]Federal University of Technology of Akure, Akure, Nigeria and Tshwane University of Technology, Pretoria, South Africa.

SUMMARY: Corrosion resistance of stainless steel has been improved by minor additions of platinum group metals. It also improved the ability of the alloy to passivate. It has been shown that 2101 duplex stainless steel has better corrosion resistance than 304 austenitic stainless steel, but less than 316 austenitic stainless steels. Calculations of the alloy using Thermo-Calc showed that minor additions of ruthenium to 2101 duplex stainless steel did not change its dual phase structure and the ruthenium partitioned equally to both phases. The alloy was produced with a nominal composition of 0.15wt% Ru and it was then solution annealed at 1080°C for 90 minutes. The morphology of the alloys was studied using an optical microscope. The electrochemical behaviour of 2101, 2101-Ru duplex stainless steel as well as 316 austenitic stainless steels was studied in sulphuric acid and sulphuric acid with chloride at 25°C. The corrosion rates were calculated and it was shown that minor ruthenium additions improved the corrosion resistance of 2101 duplex stainless steel and it performed better than the 316 austenitic stainless steel in both media. With ruthenium, the passive region increased and a lower passive current density of $2.8x10^{-5}$ A/cm^2 was obtained, compare to $1.0x10^{-4}$A/cm^2 without ruthenium.

Keywords: Duplex stainless steel, Ruthenium.

1. INTRODUCTION

Duplex stainless is characterised by better mechanical and physical properties than austenitic and ferritic stainless steel because it combines the properties of austenite and ferrite. A stainless steel is said to have a duplex structure if it contains ferrite and austenite with a minimum ratio of 70-30%. Lean duplex stainless steel have a small nickel content, e.g 2101LDX. Effects of minor ruthenium additions on duplex stainless steels have been studied [1]. Ruthenium is one of the cheapest PGMs. The 2101 duplex stainless steel is a lean DSS containing 21%Cr and 1%Ni. This paper reports the investigation of electrochemical behaviour of 2101 duplex stainless steel containing minor addition of 0.15wt% ruthenium and 316 austenitic stainless steel. Previous work showed that addition of platinum group metals (PGMs) in minor quantities to duplex stainless steels decrease the anodic dissolution and increase the effectiveness of cathodic processes by reducing the over voltage of hydrogen on them [2-4].

2. EXPERIMENTAL METHODS

The 2101 duplex stainless steel and 316 austenitic stainless steel used for this study was supplied by the Stainless Steel Association of South Africa. The experimental alloy 2101 with nominal weight of 0.15 ruthenium was produced by arc melting. The as-cast samples were solution annealed at 1080°C for 90 minutes and water quenched to obtain a duplex structure, after calculating the phase proportions with Thermo–Calc.

Representative samples were hot mounted in bakelite, ground using SiC papers from 320 to 1000 grit, polished using diamond impregnated clothes. The solution for etching duplex stainless steel was prepared by adding 40g reagent grade sodium hydroxide to 100g distilled water. The specimens were rinsed in hot water and in acetone followed by air drying. The samples were characterized using optical microscopy.

Specimens for electrochemical tests were embedded in resin with an exposed surface area as the working electrode and prepared metallographically as above. The reference electrode was Ag/AgCl and a graphite electrode was used as the counter electrode. The chemicals used were of analytical reagent grade, and solutions of $1MH_2SO_4$ and $1M\ H_2SO_4$ +1% NaCl were prepared as the corrosive environments.

The potentiodynamic responses of the specimens were measured in the solutions using an Autolab potentiostat with GPES 419 software. The experiments were carried out in triplicate. The polarization results showed good reproducibility.

The polarization resistance technique was used and the slope of potential versus current density plot at E_{corr} determined the corrosion rate, CR [5]. The linear polarisation resistance, R_p, was calculated from the overall potential difference ΔV and the change in applied current Δi:

$$R_p = \frac{\Delta V}{\Delta i} \qquad (1)$$

where R_p = polarization resistance

ΔV = change in potential

Δi = change in applied current

The corrosion current density was obtained from the relationship i_{corr}, where $i_{corr} = B / R_p$

where B is the Stern Geary constant, and

$$B = \frac{\beta a . \beta c}{2.3(\beta a + \beta c)}$$

where βa = Anodic Tafel slope

βc = Cathodic Tafel slope

I_{corr} was converted to corrosion rate using Faraday's Law.

3. RESULTS

The calculated phase proportions of as-received 2101 DSS and 2101DSS containing 0.15 weight percent ruthenium are presented in Figures 1-3. Figures 1 and 2 show that there was very little difference between the major phases when Ru was added. The heat treatment temperature was deduced from Figure 2 where there was 50:50 ferrite:austenite. Figure 3 shows how ruthenium was partitioned between the ferrite and austenite phases. Thermo-Calc gives accurate prediction of what to expect at different temperature but it does not specify the holding time. Quantitative analysis calculated by grid for as received 2101 duplex stainless steel show 56.3:43.7 ferrite:austenite, While for the 2101-0.15Ru was 34.9:65.1 ferrite:austenite at soaking time of 90 minutes.

The micrographs of the as-received and the as-cast and heat treated 2101duplex stainless steel containing 0.15 percent ruthenium and 316 austenitics stainless steel are presented in Figures 4 to 7. The micrographs of duplex stainless steel revealed two distinct phases of austenite islands in the ferrite matrix. The optical micrograph in Figure 4 confirmed two phases for the as-received 2101duplex stainless steel,the phases of austenite and ferrite formed alternate band. Figure 5 is the optical micrograph of 316, showing an austenite structure. Figure 6 shows the 2101 sample heat treated at 1080^{0}C, producing a duplex structure with austenite in a matrix of ferrite the austenite formed during the solution annealing. The transformation of ferrite to austenite is characterised by the nucleation of austenite at ferrite-ferrite grain boundaries. The optical micrograph of 2101 containing ruthenium is presented in Figure 7. Two distinct phases were observed, the austenite particles were dispersed in the ferrite matrix. Ruthenium was not detected in the structure, possibly due to its minor content and that it dissolved in austenite and ferrite, as shown in the computational diagram of 2101 with 0.15wt% ruthenium (Figure 3).

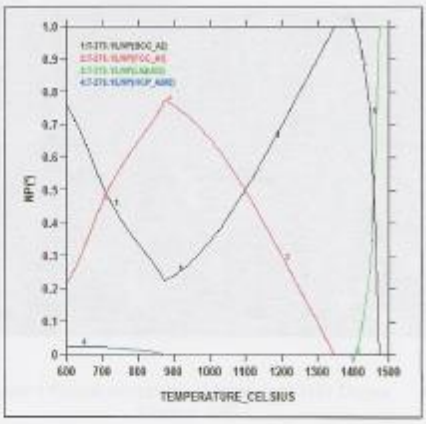

Figure 1 Calculated phase proportions of as-received 2101 LDX.

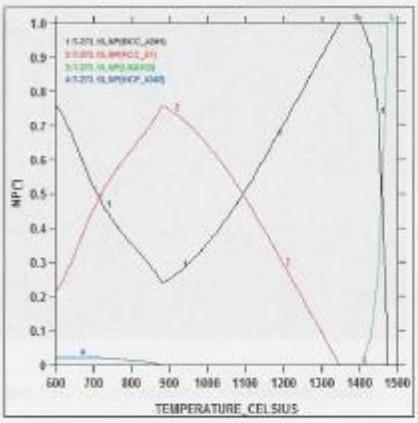

Figure 2 Calculated phase proportions of 2101 - 0.15wt%Ru LDX.

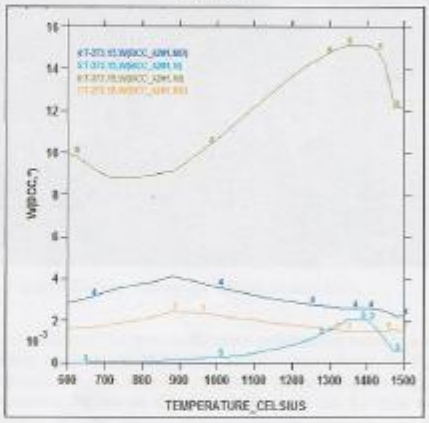

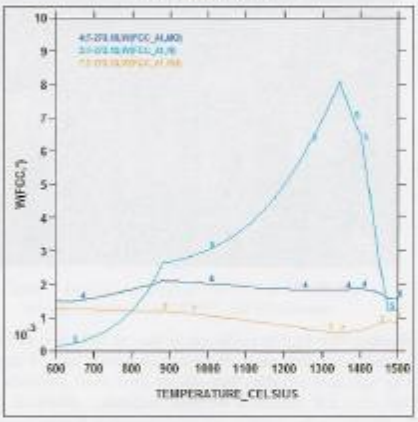

Figure 3 Plots of the compositions of ferrite (BCC_A2) and austenite (FCC_A1) with temperature, for the 2101 stainless steel containing 0.15 wt % Ru, using the SSOL4 database.

Figure 4 Optical micrograph of as-received 2101 Duplex stainless steel.

Figure 5 Optical micrograph of 316 austenitic stainless steel.

Figure 6 Optical micrograph of heat treated 2101.

Figure 7 Optical micrograph of 2101-0.15wt% Ru solution annealed at 1080°C for 90 minutes.

A comparison of the potentiodynamic polarization behaviour of 316 and 2101 as well as the effect of 0.15 wt% ruthenium addition on 2101 in $1MH_2SO_4$ solution were shown in Figure 8. The corrosion potentials were estimated from the polarization curves with the corrosion current densities (I_{cor}) obtained from both anodic and cathodic branches of the polarisation curves, as listed in Table 2. It can be seen that 0.15wt% ruthenium addition increased the polarization resistance of 2101, thereby reducing the corrosion rate. The passive region increased with the addition of ruthenium. The 2101 containing ruthenium had the lowest value of critical current density, i_{crit}, and passive current density, i_{pass}, while the as-received 2101 had the highest values of i_{crit} and i_{pass}. The polarisation curves for 316, 2101 and 2101 containing ruthenium in 1M sulphuric acid and 1% sodium chloride are presented in Figure 9. No noticeable critical current density was observed in the curves of the as-received 2101 and 316. The 2101 containing ruthenium shows a critical current density i_{crit}. The 2101 containing ruthenium shows an active-passive region, while the as-received 2101 does not. This indicated that the ruthenium enhances the formation of passive layer. The results showed that the cathodic regions of the 2101 containing ruthenium moved towards a more positive value.

The Table 2 indicates the dependence of polarisation resistance to corrosion rate. The polarisation resistance in 2101-0.15wt% Ru has the highest R_p (13.601kΩ), resulting in the lowest corrosion rate of $3x10^{-7}$ mm/yr, 2101 duplex stainless steel had the highest i_{pass} ($7.1x10^{-4}$ A/cm^2).

The corrosion rate comparison of the 316, 2101 and 2101 containing ruthenium in 1M sulphuric acid with and without chloride are shown in Figures 10 and 11, and Table 3, and they were calculated from the polarisation curves. For both solutions, the 2101 containing ruthenium had a lower corrosion rate than 316 and as-received 2101. The corrosion rate for the 2101 containing ruthenium in sulfuric acid was lower than the sulfuric acid containing chloride.

Table 1. Compositions of the three stainless steels investigated (wt%)

Samples	Cr	Ni	Cu	Mn	Mo	N	Ru	Fe
2101-0.15wt%Ru	20.76	1.51	0.10	4.81	0.26	0.2	0.15	Bal.
2101	20.76	1.51	0.10	4.81	0.26	0.2	0.00	Bal.
316	16.60	10.03	0.16	1.52	0.26	0.1	0.00	Bal.

Table 2. Electrochemical data of samples in 1M H_2SO_4

Samples	E_{corr} (mV)	i_{pass} (A/cm^2)	R_p (Ω)	CR (mm/yr)
2101-0.15wt%Ru	-157	$2.8x10^{-5}$	13601	$3.0x10^{-2}$
2101	-404	$7.1x10^{-4}$	4.4346	$1.0x10^{-1}$
316	-281	$1.0x10^{-4}$	6.0506	$7.5x10^{-2}$

Table 3. Electrochemical data of samples in 1M H_2SO_4 + 1%NaCl

Samples	E_{corr} (mV)	I_{pass} (A/cm^2)	R_p (Ω)	CR (mm/yr)
2101-0.15wt%Ru	54.32	$3.9x10^{-5}$	143.70	$3.1x10^{-2}$
2101	49.90	$1.7x10^{-4}$	42.20	$1.1x10^{-1}$
316	-255.09	$1.3x10^{-3}$	77.57	$5.9x10^{-1}$

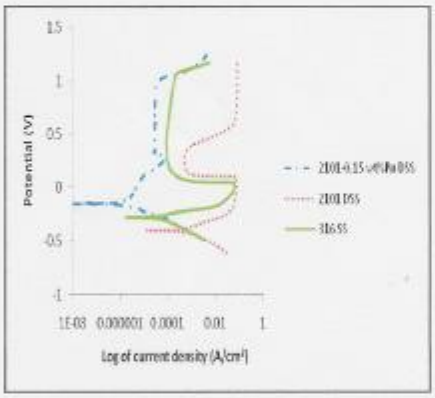

Figure 8 Potentiodynamic polarization curves of stainless steels in 1M H_2SO_4 at 25°C.

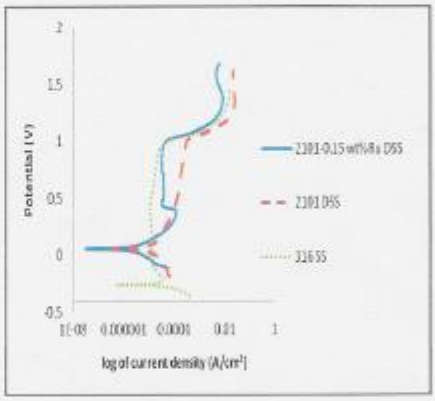

Figure 9 Potentiodynamic polarization curves of stainless steels in 1M H_2SO_4 and1%NaCl at 25°C.

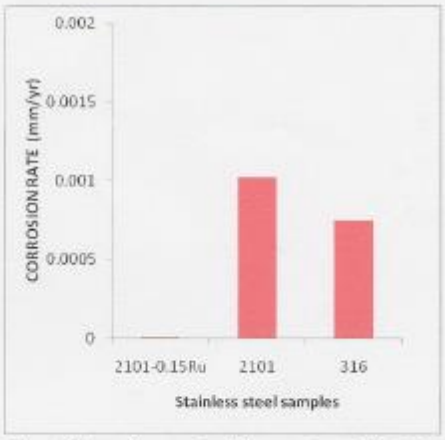

Figure 10 Corrosion rate of stainless steel samples in 1M H_2SO_4 at 25°C.

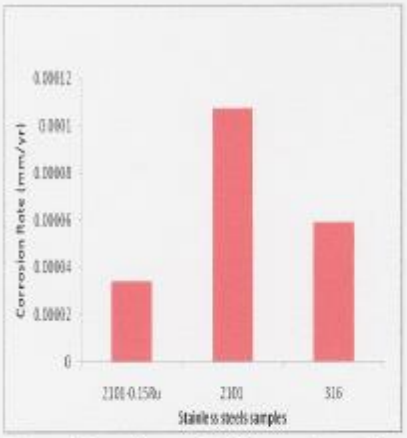

Figure 11 Corrosion rate of stainless steel samples in 1M H_2SO_4 and1%NaCl at 25°C.

4. DISCUSSION

The analysis of 2101 and 2101-0.15wt% Ru revealed the two expected phases, austenite and ferrite. The 316 steel showed a single phase of austenite. There were no observed intermetallic phases. The partitioned of ruthenium equally into the two phases enhances the corrosion properties of 2101 duplex stainless steel, since no phase had more of the beneficial ruthenium. The minor addition of ruthenium to 2101 did not affect the phases present.

The small Ru additions to 2101 base alloys had a significant effect on the corrosion of potential. The values of the corrosion potential (E_{corr}) of 2101-0.15Ru is -0.157V which is more noble than 2101duplex stainless steel which is -0.404V and 316 austenitic stainless steel which is -0.281V. The E_{corr} for 316 is nobler than 2101. As the polarization resistance decreases, the corrosion rate increases. This agrees with the corrosion rates results for 316 having a lower corrosion rate than 2101. Figure 4 shows the large effect of ruthenium addition in the base alloys of 2101. The values of the current density i_{crit} are lower in 2101-0.15 wt% Ru, a lower current density is required to achieve passivity and lower current density is needed to maintain it. i_{pass} of the 2101-0.15 wt% ruthenium is lower than the 2101 without ruthenium. The cathodic region of the 2101-0.15 wt% Ru shifted towards a less negative value. There was also a lowering of passive current density as result of ruthenium addition. The lowering of the cathodic tafel slope by the ruthenium is due to the improved hydrogen evolution efficiency which results in decrease of the hydrogen over potentials which agrees with Wolff [6].

There was a significant change in electrochemical behavior of alloy with ruthenium in 1M sulfuric acid. There was a lowering of the cathodic tafel slope which is enhanced by the ruthenium. The addition of chloride to sulphuric acid increased the corrosion potential of 2101-0.15wt% ruthenium sample. The sulphuric acid containing chloride has an increase in critical current density (i_{crit}) than the sulphuric acid solution alone. The passive region was longer in sulphuric acid than in sulphuric acid with chloride solution. The i_{pass} increased in the sulphuric acid with chloride solution. The as-received 316 did not exhibit a significant active-passive region, and went straight into the passive region. The addition of chloride to sulfuric acid reduced the passive regions in 2101 containing ruthenium. However, 2101containing ruthenium had better corrosion resistance in both 1M sulfuric acid with and without chloride than both 2101 and 316, indicating that the presence of ruthenium increased the alloy's resistance to corrosion in the chloride environment.

5. CONCLUSIONS

Addition of ruthenium to 2101 DSS shifts the cathodic region to a more positive value thereby shifting corrosion potential to a more positive value. There is also a reduction in the current density of 2101 containing ruthenium compared to as-

received 2101 and as-received 316 both sulphuric and sulfuric acid with sodium chloride. The addition of ruthenium to 2101 increased the passive region and caused a decrease in i_{pass}.

6. ACKNOWLEDGMENTS

The authors thank Anglo Platinum, South Africa for the ruthenium, and Mintek, South Africa for the production of the alloy with ruthenium.

7. REFERENCES

1 Potgieter JH, Effect of minor ruthenium additions on the corrosion behaviour of duplex stainless steels in sulfuric acid, Said.-Afrikaanse, Tydskrif vir Natvurwentenstap en Tegnologie Chem. 46 (1993) 3-4.

2 Potgieter JH and Brookes HC, Duplex stainless steel with minor additions of ruthenium in sulfuric acid, Corrosion 51 (1995) 312-320.

3 Sherif EM, Potgieter JH, Comins JD, Cornish L, Olubambi PA and Machio CN, The beneficial effect of ruthenium additions on the passivation of duplex stainless steel corrosion in sodium chloride solutions, Corrosion Science 51 (2009) 1364–1371.

4 Streicher MA, Alloying stainless steels with the platinum metals, Platinum Metals Review 21 (1977) 51-55.

5 Jones DA, Principles and prevention of corrosion, 2nd edition, Macmillan, New York, (1992).

6 Wolff IM, Iorio LE, Rumpf T, Scheers PVT and Potgieter JH, Oxidation and corrosion behaviour of Fe-Cr and Fe-Cr-Al alloys with minor alloying additions, Material Science and Engineering A241 (1998) 264- 276.

Electrochemical studies of Fe-21Cr-1Ni duplex stainless steels with 0.15 wt% ruthenium at different temperatures

by O.A. Olaseinde*†‡, J.W. van der Merwe*†‡, L.A. Cornish*†‡, L.H. Chown*†‡, and P.A. Olubambi‡¢

Transaction Paper

Synopsis

The 2101 lean duplex stainless steel has wide potential application in storage, heat exchangers, and in the oil and gas industries. This work investigates the electrochemical behaviour of 2101 duplex stainless steel with an addition of 0.15 wt% ruthenium, using potentiodynamic techniques in 1M H_2SO_4 at 25°, 40°, 60°, and 80°C. The microstructures of samples were characterized using optical metallography and scanning electron microscopy.

The results showed that the ruthenium addition moved the corrosion potential of alloy 2101 to a more positive potential. All samples containing ruthenium displayed longer passive regions at 25°C and 80°C compared to those without ruthenium. Alloys without ruthenium had higher critical current density (i_{crit}) values when compared to the alloys with ruthenium. Ruthenium additions decreased the passive current densities and inhibited anodic dissolution. At room temperature the corrosion rate of alloys with ruthenium was lower than these without ruthenium.

Keywords
Duplex stainless steels, Fe-21Cr-1Ni, 2101LDX stainless steel, ruthenium addition, corrosion behaviour, passivation, microstructure.

Introduction

Duplex stainless steels, which are also referred to as ferritic-austenitic stainless steels, have the beneficial properties of both ferritic and austenitic steels. They contain high chromium contents and molybdenum. The high strength of the material enables the use of thinner gauges in a variety of applications such as tanks, pressure vessels, piping, and transportation, thus providing cost savings[1]. Lean duplex stainless steel 2101 has been used to build liquid storage tanks[2].

Duplex stainless steels have previously been alloyed with platinum group metals (PGMs), such as palladium and ruthenium[3–5]. It has been reported that small ruthenium additions can significantly improve the corrosion resistance of the duplex stainless steels, displacing their open-circuit corrosion potential towards more positive values in HCl and H_2SO_4 solutions compared to austenitic or ferritic stainless steels[6]. The reduction in corrosion and critical current densities indicates that ruthenium inhibits the anodic dissolution of the cathodically modified alloys[7]. The following criteria must be met for successful cathodic alloying: the base alloy must have a small critical current density; the passivation potential of the alloy must be sufficiently negative to allow the cathodic component that has been introduced to change the corrosion potential; and the transpassive potential of the base alloy must be sufficiently electropositive to allow a wide passive range[7]. These conditions are satisfied in non-oxidizing acids by stainless steel, chromium-based alloys, and titanium based alloys, while the PGMs have the high exchange current density for hydrogen evolution[8].

The addition of ruthenium to duplex stainless steels has been shown to have a beneficial effect on their corrosion resistance[9]. However, there has not been previous research work on the cathodic modification of lean 2101 duplex stainless steel. This work investigates the electrochemical behaviour of 2101 lean duplex stainless steel with 0.15 wt% ruthenium in aqueous sulphuric acid solutions at temperatures from 25–80°C.

Experimental procedure

The experimental 2101 lean duplex stainless steel (2101LDX) was obtained from the Stainless Steel Association of South Africa. The 2101 lean duplex stainless steel containing 0.15 wt% ruthenium (2101LDX+0.15Ru) was produced using an arc melting furnace, then solution-annealed at 1 080°C for 90 minutes

* *School of Chemical & Metallurgical Engineering, University of the Witwatersrand.*
† *DST/NRF Centre of Excellence for Strong Materials, University of the Witwatersrand.*
† *African Materials Science & Engineering Network.*
¢ *Tshwane University of Technology, Pretoria, South Africa & Federal University of Technology, Nigeria.*

 SA ISSN 2225-6253. This paper was first presented at the ZrTa2011 New Metals Development Network Conference, 12–14 October 2011, Mount Grace Country House & Spa, Magaliesburg.

and water-quenched. The specimens for metallographic examination were cut using a Struers® Secotom-10 cutting machine, wet ground on SiC papers, then polished using alumina suspensions of 3 and 1 µm. The duplex structure of the samples was revealed using 40 g NaOH in 100 ml of distilled water, according to ASTM Standard A923-06[10]. The microstructure was examined on a scanning electron microscope (SEM) at the University of Pretoria. EDS (energy-dispersive X-ray spectroscopy) analysis was done to determine the overall alloy and phase compositions, and averages of five different areas in each of the phases and of the overall sample composition were calculated.

Representative samples were cold-mounted in epoxy resin for the corrosion tests. The samples were ground on SiC papers, degreased with ethanol, and washed with distilled water. The size of the areas to be exposed to the corrosive solution were measured.

Solutions of 1M H_2SO_4 were prepared using analytical grade chemicals in distilled water. Electrochemical tests were performed using an Autolab® Potentiostat (computer-controlled PGSTAT20) with the general-purpose electrochemical software (GPES) Version 4.9. Electrochemical studies were conducted using a conventional electrochemical cell, a graphite electrode, a silver/silver chloride reference electrode in saturated potassium chloride (KCl), and a working electrode.

The potentiodynamic polarization responses of the alloys were investigated in naturally aerated 1M H_2SO_4 solution at temperatures of 25, 40, 60, and 80ºC. Polarization curves were measured at a scan rate of 2 mV.s^{-1} starting from -500 mV to 1 500 mV with respect to open-circuit potential. The temperature was measured with a thermometer and maintained by immersing the cell in a water bath. All tests were carried out in triplicate, and good reproducibility was observed.

Results

The secondary electron image (SEI) obtained on the SEM and representative EDS analysis spectra of the phases of 2101 duplex stainless steel are presented in Figure 1. There were two distinct phases: austenite in a matrix of ferrite. The average EDS analyses for the phases are shown in Table I. Austenite had the highest content of nickel and manganese in both 2101LDX and 2101LDX+0.15Ru steels, whereas ferrite had the highest chromium and molybdenum content in 2101LDX. In 2101LDX+0.15Ru, the chromium was higher in ferrite and the molybdenum was the same in both ferrite and austenite. EDS could not be used to determine the ruthenium content because it was below 1 wt% Ru.

Figure 2 shows the SEM micrograph of 2101LDX+0.15Ru with representative EDS spectra of the phases. The austenite phase had the highest nickel content, and the ferrite phase had the highest chromium content.

Figures 3 to 6 show the potentiodynamic polarization responses of 2101LDX and 2101LDX+0.15Ru in naturally aerated 1M H_2SO_4 solution at temperatures of 25, 40, 60, and 80ºC respectively. The electrochemical data is summarized in Table II.

25°C

The addition of ruthenium to 2101 shifted the corrosion potential to a less negative value (Figure 3). The i_{crit} value was

Table I

EDS composition of experimental alloys in wt%. The balance of the composition is iron (Fe)

Alloy	Phases	Cr	Ni	Mn	Mo	O	Si
2101 LDX	Austenite	20.6 ±0.0	2.5±0.2	5.8±0.1	0.0±0.0	0.0±0.0	1.0±0.1
	Ferrite	22.2 ±0.1	1.9±0.1	5.0±0.1	0.3±0.0	0.0±0-0	0.8±0.0
2101LDX+0.15Ru	Austenite	19.1±1.3	2.5±0.6	5.1±0.7	0.2±0.2	2.6±0.3	0.65±0.1
	Ferrite	21.1±0.4	1.8±0.3	4.0±0.5	0.2±0.2	3.1±0.3	0.71±0.1

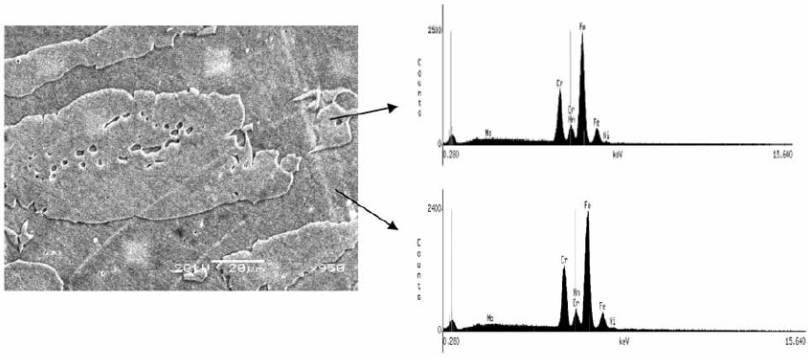

Figure 1—SEM-SEI and EDS analyses of the as-received duplex stainless steel (2101LDX)

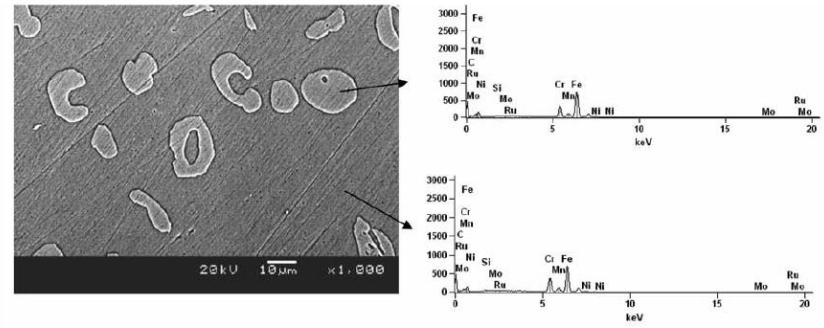

Figure 2—SEM and EDS analyses of 2101LDX+0.15Ru duplex stainless steel (solution-annealed at 1 080°C)

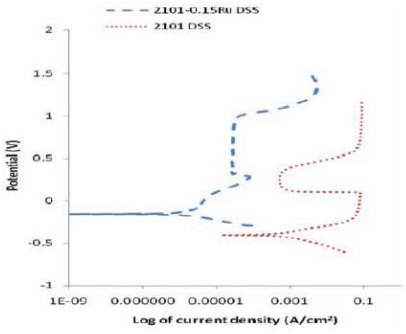

Figure 3—Potentiodynamic curves of duplex stainless steels 2101LDX+0.15Ru and 2101LDX in 1M H_2SO_4 at 25°C

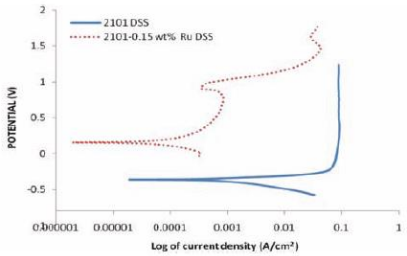

Figure 5—Potentiodynamic curves of duplex stainless steels 2101LDX+0.15Ru and 2101LDX in 1M H_2SO_4 at 60°C

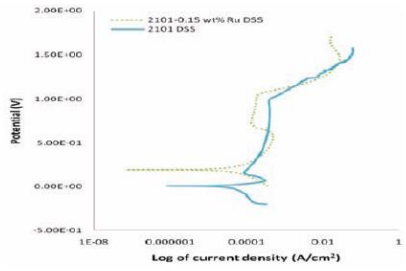

Figure 4—Potentiodynamic curves of duplex stainless steels 2101LDX+0.15Ru and 2101LDX in 1M H_2SO_4 at 40°C

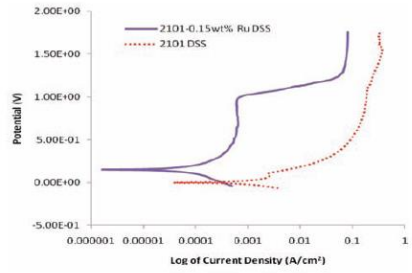

Figure 6—Potentiodynamic curves of duplex stainless steels 2101LDX+0.15Ru and 2101LDX in 1M H_2SO_4 at 80°C

Table II
Electrochemical data for samples in 1M H_2SO_4

Alloy	T (°C)	E_{corr} (V)	i_{crit} (A.cm-2)	Corrosion rate (mm/a)
2101	25	-0.404	4.29 x 10^{-2}	9.80 x 10^{-2}
2101LDX +0.15Ru	25	-0.155	6.79 x 10^{-5}	3.19 x 10^{-5}
2101	40	0.006	5.24 x 10^{-2}	1.66 x 10^{-5}
2101LDX +0.15Ru	40	0.194	5.66 x 10^{-5}	7.2 x 10^{-3}
2101	60	0.141	4.99 x 10^{-2}	1.68 x 10^{-5}
2101LDX +0.15Ru	60	-0.363	2.40 x 10^{-4}	3.61 x 10^{-3}
2101	80	0.0007	2.04 x 10^{-3}	1.29 x 10^{-3}
2101LDX +0.15Ru	80	0.149	2.30 x 10^{-4}	3.61 x 10^{-3}

greatly reduced in 2101LDX+0.15Ru. There was a longer passive region in 2101LDX+0.15Ru.

40°C

Figure 4 shows the effect of 1M sulphuric acid on 2101LDX and 2101LDX+0.15Ru at 40°C. Although the corrosion potential of 2101LDX+0.15Ru moved towards a more positive value, 2101 had a longer passive region than 2101LDX+0.15Ru, thus the corrosion rate of 2101 duplex stainless steel was lower.

60°C

The potentiodynamic polarization curve for 2101LDX and 2101LDX+0.15Ru in 1M sulphuric acid solution at 60°C is shown in Figure 5. The addition of ruthenium shifted the corrosion potential towards a more noble value and the critical current density was also reduced. There was good passivation of the 2101 duplex stainless steel.

80°C

Figure 6 shows the potentiodynamic results of 2101LDX and 2101LDX+0.15Ru in 1M H_2SO_4 at 80°C. The corrosion potential shifted towards a more positive value for samples with ruthenium than samples without ruthenium. For the two samples in the solution at 80°C, no active passivation was observed.

Discussion

The corrosion potential was lower for 2101LDX+0.15Ru in 1M sulphuric acid at 25°C than at other temperatures. The corrosion potentials for 2101LDX+0.15Ru at 40°C, 60°C, and 80°C were very similar. There was an increase in passive current density with temperature from 25°C to 60°C. The passive region became smaller with increase of temperature up to 60°C. No passivity was observed at 80°C.

The anodic behaviour of 2101LDX in 1 M sulphuric acid was very different at 25°C, 40°C, 60°C, and 80°C. At 60°C, 2101LDX had a lower passive current density than at other temperatures. There was active dissolution of 2101LDX sample at 25°C. No passivity was observed at 80°C.

According to the literature[5], addition of ruthenium to stainless steel should move the corrosion potential of the steel towards a more noble potential. This was observed in the present investigation. The addition of ruthenium also lowered the critical current density.

Corrosion rate of the samples increased as the temperature increased from 25°C to 80°C for 2101LDX+0.15Ru. This could be due to the reduction in the passive region with temperature, and also a reduction in passive current density.

Ruthenium was observed to lower the corrosion rates of 2101 duplex stainless steel at room temperature. The samples with ruthenium showed a passive region at the lower temperatures of 25°C and 40°C. Ru and Ni act as blocking agents, which decrease the dissolution rates of Cr and Fe and therefore increase the probability of a stable passive layer forming[7].

Conclusions

- The addition of ruthenium to 2101 duplex stainless steel shifted the corrosion potential to more noble values in the temperature range 20–80°C
- At lower testing temperatures, the addition of ruthenium lowered the critical current density
- Addition of ruthenium decreased the passive current densities of 2101 duplex stainless steel
- The passive current density increased with temperature in 2101LDX+0.15Ru samples
- There was a decrease in the passive region of 2101LDX+0.15Ru as the temperature increased.

References

1. International Molybdenum Association. Practical guidelines for the fabrication of duplex stainless steels. 2nd edn. www.imoa.info. 2009.
2. Outokumpu. www.outokumpu.com accessed May 2011.
3. Streicher, M.A. Alloying stainless steels with the platinum metals. *Platinum Metals Review*, vol. 21, 1977. pp. 51–54.
4. Potgieter, J.H. Alloys cathodically modified with noble metals. *Journal of Applied Electrochemistry*, vol. 21, 1991. pp. 471–482
5. Potgieter, J.H. and Brookes, H.C. Duplex stainless steel with minor additions of ruthenium in sulfuric acid. *Corrosion*, vol. 51, 1995. pp. 312–320.
6. Potgieter, J.H. Effect of minor ruthenium additions on the corrosion behaviour of duplex stainless steels in sulfuric acid. *Suid.-Afrikaanse, Tydskrif vir Natuurwetenstap en Tegnologie*, vol. 46, 1993. pp. 3–4.
7. Myburg, G., Varga, K., Barnard, W.O., Baradlai, P., Tomcsany, I.L., Potgieter, J.H., Louw, C.W., and van Staden M.J. Surface composition of Ru containing duplex stainless steel after passivation in non-oxidizing media. *Applied Surface Science*, vol. 136, 1998. pp. 29–35.
8. Potgieter, J.H., Heynes, A.M., and Skinner, W. Cathodic modification as a means of improving the corrosion resistance of alloys. *Journal of Applied Electrochemistry*, vol. 20, 1990. pp. 711–715.
9. Potgieter J.H., Barnard W.O., Myburg, G., Varga, K., Baradlai, P., and Tomcsany, I.L. Corrosion behaviour of duplex stainless steels containing minor ruthenium additions in reducing acid media. *Journal of Applied Electrochemistry*, vol. 26, 1996. pp. 1103–1110.
10. ASTM Designation: A923-06, Standard Test Methods for detecting Detrimental Intermetallic Phases in Duplex Austenitic/Ferritic Stainless Steel. ◆

EFFECTS OF RUTHENIUM ADDITION ON THE PHASES OF 2101 DUPLEX STAINLESS STEEL

O.A. Olaseinde[1,2,3], L.A. Cornish[1,2,3], J.W. van der Merwe [1,2,3] and P.A. Olubambi[2,4]

[1]School of Chemical & Metallurgical Engineering, University of the Witwatersrand, RSA

[2]African Material Science and Engineering Network (Carnegie – RISE Network)

[3]DST/NRF Centre of Excellence for Strong Materials, University of the Witwatersrand, RSA

[4]Federal University of Technology of Akure, Akure, Nigeria

The effects of minor ruthenium additions on the phases of selected duplex stainless steels were investigated. The samples were prepared metallographically, and electrochemically etched in NaOH, then characterised using high resolution scanning electron microscopy, and spectroscopic analysis was done. The phase proportions of the alloys were calculated using Thermo-Calc with the TCFES5 and SSOL4 databases. Ruthenium contents between 0 and 0.2 wt% were calculated over a 600°C - 1500°C temperature range. The calculated and experimental phase proportions were compared, and good agreement was found. There was very little difference between the phase proportions calculated for the different Ru contents.

INTRODUCTION

Stainless steel is widely used in applications where good corrosion resistance, low maintenance, and low life-cycle costs are required. However, the price volatility of the high nickel content makes this grade of stainless steel prohibitively expensive. Outokumpu addressed this by introducing the lean duplex LDX 2101® stainless steel. Duplex stainless steel have dual phase structures, comprising austenite and ferrite. Several studies [1] show that LDX 2101® stainless steel has superior mechanical and corrosion-resistance properties than 304 austenitic stainless steel, but less than, or almost equal, properties to the 316 austenitic stainless steel. However, it possesses a poor strength-to-corrosion resistance capability compared to the 2205 Code Plus Two® and Outokumpu 2507 super duplex stainless steels [2]. Platinum group metals (PGMs) have been added to stainless steels to give better corrosion resistance properties in non-oxidizing

media [3, 4]. The introduction of an active cathode into the alloy lowers the hydrogen overpotential [5]. Also, addition of sufficient PGMs increases the ability of the alloy to passivate.

This study investigates the effects of minor ruthenium additions on the phases and their proportions of LDX 2101® stainless steel using thermodynamic calculations. The calculated phase proportions of the LDX 2101® stainless steel were compared with the microstructure of an as-received sample of the alloy. In order to identify suitable ranges of ruthenium additions, several calculations were made using different values of ruthenium. The results were then compared, and a suitable ruthenium addition was selected. The calculations were also used to identify the best heat treatment that would give a good duplex austenite/ferrite microstructure. The findings will be the basis of future experimental work, both on making and characterising the alloys, as well as undertaking and comparing corrosion tests.

EXPERIMENTAL PROCEDURE

Samples of the lean duplex LDX 2101® stainless steel were obtained from Outokumpu, and were subjected to standard spectroscopic chemical analysis. The samples were cut into samples of sides 1cm and hot mounted in bakelite. They were ground with silicon carbide papers from 320 down to 1000 grade, and polished with diamond paste until a mirror - like surface were achieved. The surfaces were electrochemically etched in 28.5% NaOH solution that had been prepared by adding 40g of reagent grade NaOH to 100g of distilled water. 1-3 v dc was applied, with a platinum cathode for 5 – 60 s [6]. After etching, the samples were characterised using a high resolution scanning electron microscope (HR-SEM).

Using the analysed values of the chemical compositions, the phase proportions of the alloys were calculated using Thermo-Calc software. Initially, the specialised steel TCFES5 database was used for the thermodynamic calculations of the phase proportions and phase compositions. However, to calculate the effects of the ruthenium additions, the SSOL4 database [7] had to be used because the steel database did not include ruthenium. SSOL4 is a more generalised database and often gives more reliable results out of the ranges of the specialised databases [8]. Calculations were made for different steel compositions where between 0 and 0.2 wt% Ru was substituted for Fe, and the compositions of all the other components was kept the same.

RESULTS

The results from the spectroscopic chemical analysis are given together with the specifications from Outokumpu [9] in Table 1. It can be seen that the as-received sample was within the Outokumpu specifications.

Table 1. Chemical composition (*wt %*) *of as-received sample of LDX 2101 stainless steel compared to the Outokumpu specification [9].*

Element	**Source**	**Cr**	**Ni**	**Mn**	**N**	**Mo**	**Fe**
(wt%)	Chemical analysis	20.76	1.512	4.801	0.205	0.261	Balance
	Outokumpu	21.5	1.5	5.0	0.22	0.3	

Figure 1 shows the microstructure obtained using high-resolution scanning electron microscope. The microstructure shows the expected two phase microstructure of ferrite and austenite, and the NaOH etch behaved as expected, making the austenite phase appear brighter and the ferrite phase darker.

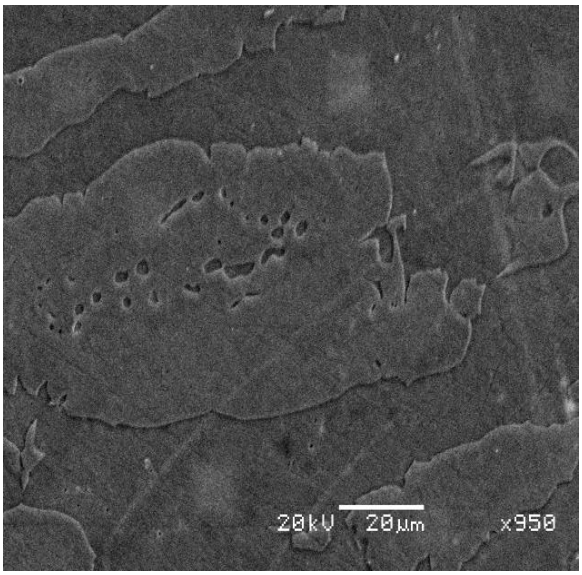

Figure 1. SEM secondary electron image of 2101 LDX showing ferrite (dark) and austenite (light) after etching in 28.5% NaOH.

Using SEM and EDX, the phase compositions were analysed and are given in Table 2, although nitrogen could not be analysed. Only one overall analysis was taken as a rough check.

Table 2. Compositions (*wt %*) *of as-received sample of LDX 2101 stainless steel analysed by EDX.*

Element (wt%)	**Phase**	**Cr**	**Ni**	**Mn**	**Mo**	**Fe**	**Mg**	**Al**	**Si**
	Overall	21.2±0.0	2.25±0.2	5.5 ±0.0	0.25± 0.1	69.6 ±0.3	0.2 ±0.0	0.25± 0.1	0.8 ± 0.0
	Austenite	20.6±0.0	2.5±0.2	5.8±0.1	0.0±0.0	69.9±0.2	0.3±0.1	0.4±0.3	0.8±0.0
	Ferrite	22.2±0.1	1.9±0.1	5.0±0.1	0.3±0.0	69.1±0.0	0.3±0.1	0.3±0.1	1.0±0.1

Figure 2 shows the calculated phase proportions with varying temperature for the 2101 LDX stainless steel, using the compositions listed in Table 2, and for both databases. For each temperature, the proportions of the phases can be read from the y axis. Thus, it can be seen that the ferrite phase solidifies from the liquid and starts to transform to austenite at ~1340°C using the TCFE5 database, and at ~1360°C for SSOL4, until at ~1100°C for both databases, the austenite and ferrite phases are equal in proportion for calculations from both databases. Another phase, hcp, precipitated up to 0.02%, starting at ~860°C.

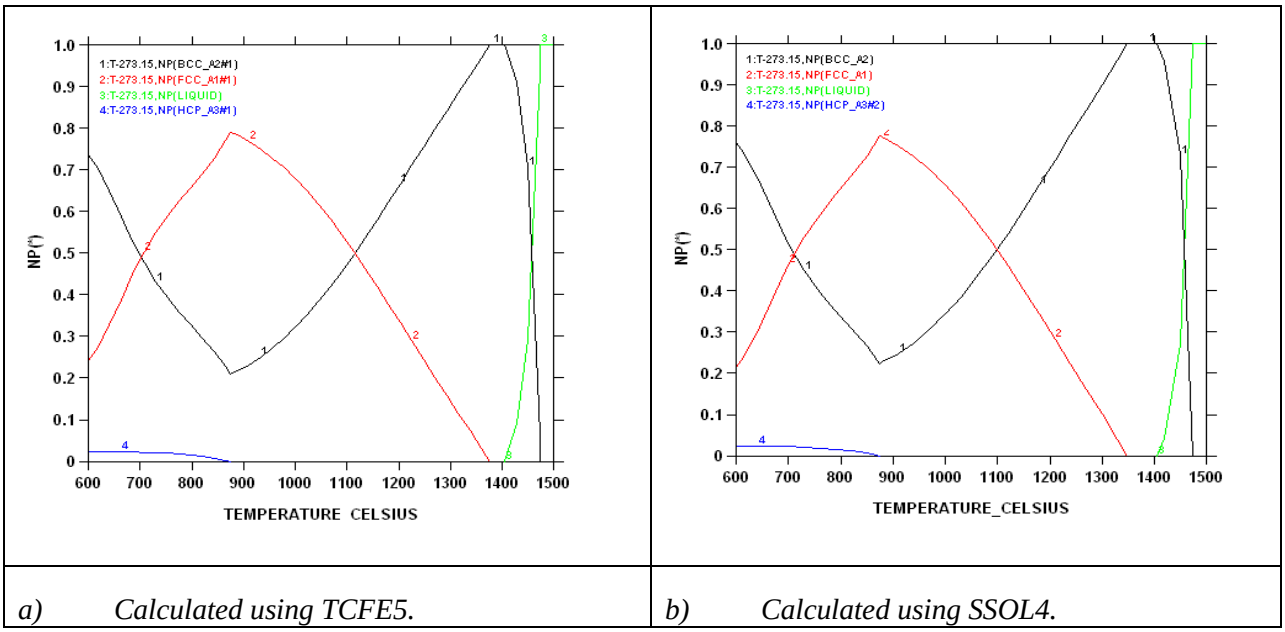

a) Calculated using TCFE5.

b) Calculated using SSOL4.

Figure 2. Calculated phase proportions of as-received 2101 using Thermo-Calc with different databases.

The compositions of the austenite and ferrite phases were calculated, and are shown in Figure 3.

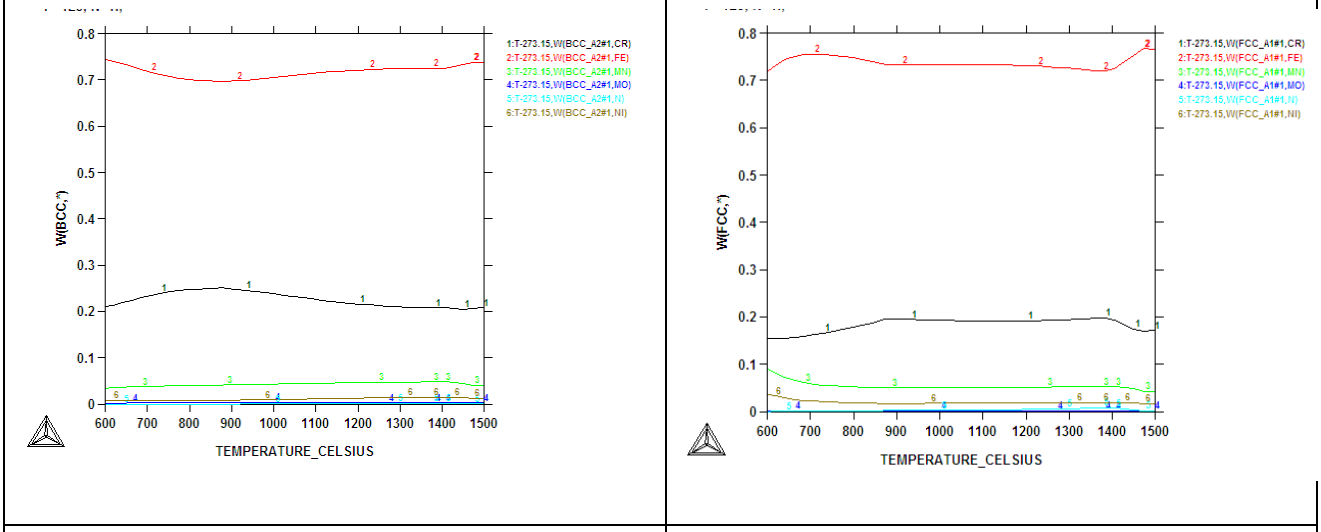

a) Composition of ferrite (BCC) calculated using TCFE5.

b) Composition of austenite (FCC) calculated using TCFE5.

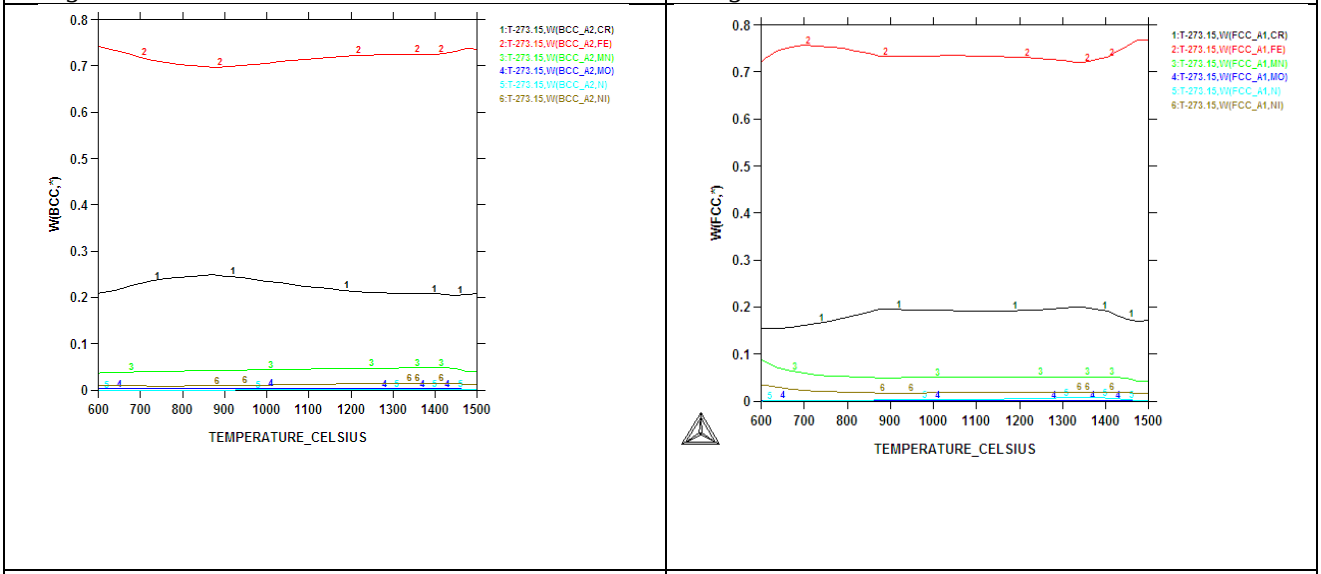

c) Composition of ferrite (BCC) calculated using SSOL4.

d) Composition of austenite (FCC) calculated using SSOL4.

Figure 3. Calculated compositions of the ferrite and austenite phases calculated using the TCFE5 and SSOL databases.

Since the results in Figure 3 were comparable, the next stage was to calculate the composition diagrams for the planned alloys using SSOL4, now that it had been shown to be representative of the stainless steel alloys. The results are shown in Figure 4 for the 0.1 wt% and 0.2 wt % Ru compositions, and both are very similar to Figure 1. There was very little difference between the phase proportions calculated for the

different Ru contents; this is not surprising since the amounts added were small. As a check that the Thermo-Calc program was calculating the effects of Ru additions correctly, a larger amount was calculated as a check, even though this amount was not going to be used in practice. Figure 4 shows the addition of 10 wt% Ru, and as it was completely different from the lower Ru content calculations, it is taken as proof that the program was working correctly, since higher Ru contents stabilised the bcc ferrite phase.

2

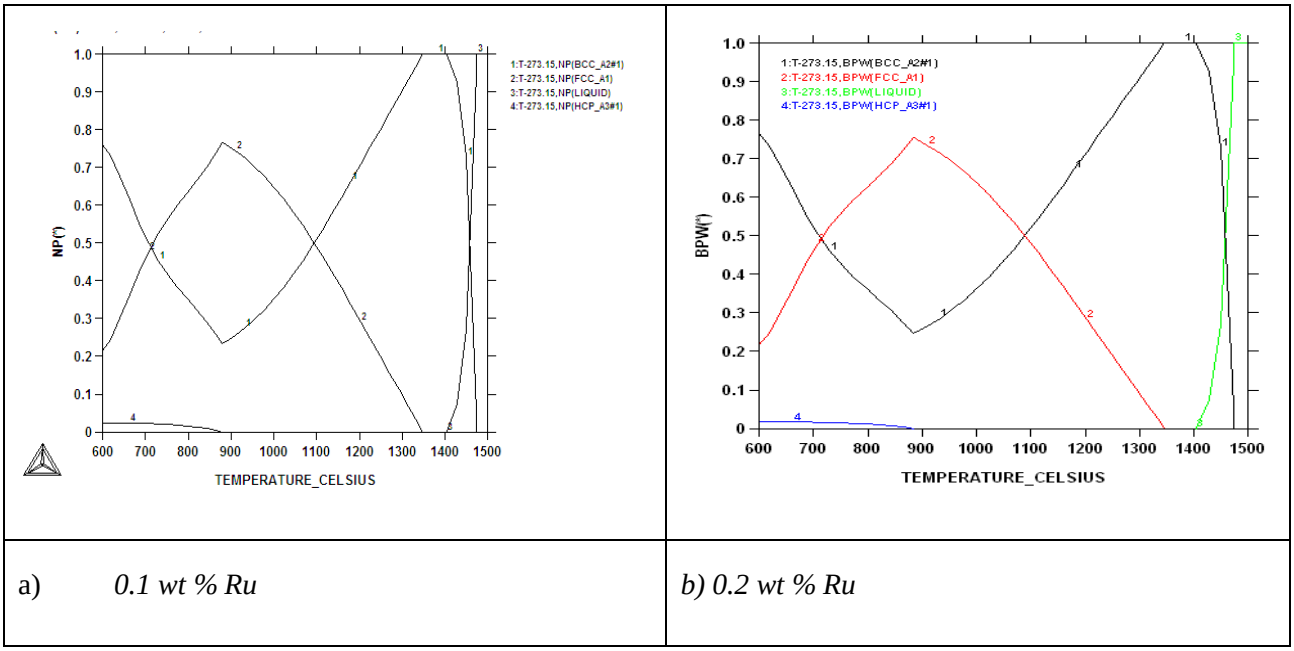

a) *0.1 wt % Ru*

b) 0.2 wt % Ru

Figure 5. Calculated phase proportions of as-received 2101 using Thermo-Calc with different databases.

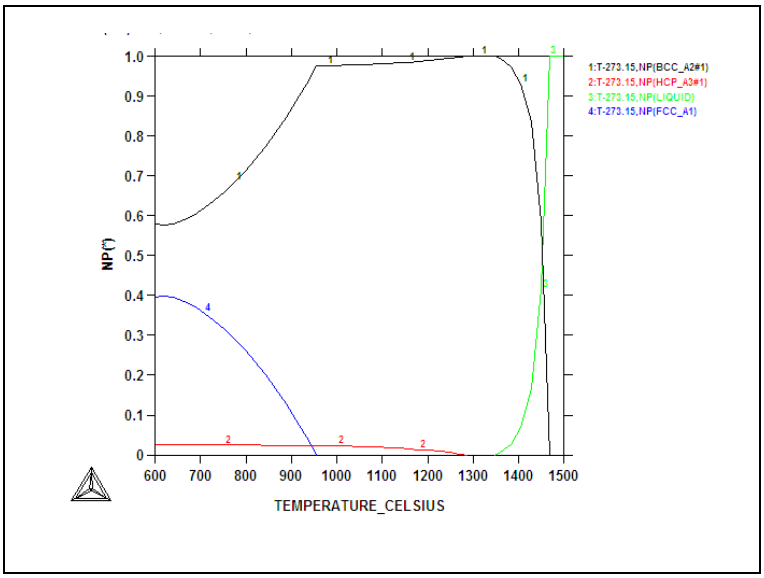

Figure 4. Calculated phase proportions of as-received 2101 with 10 wt% using SSOL4.

The compositions of the ferrite and austenite phases were calculated for the 0.2 wt% Ru composition are shown in Figure 5, where a) and c) show the major components, and b) and d) show the minor components in an expanded plots for ferrite and austenite respectively. The calculations for the other Ru compositions showed that the Ru content in both austenite (FCC) and ferrite (BCC) have the same trend for the different ruthenium additions, and that as the Ru content was increased, the amounts in both phases increased.

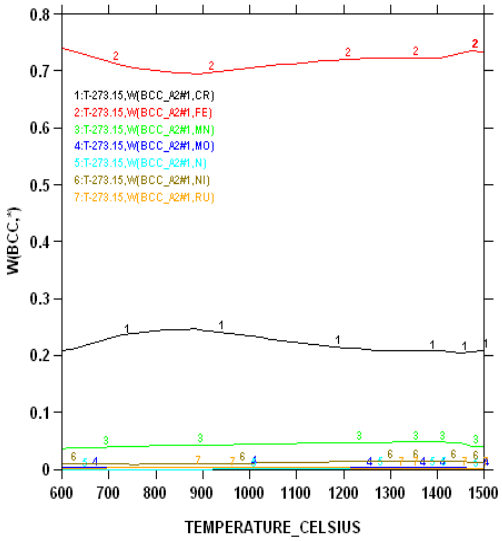

a) Calculated composition of ferrite with temperature in 0.2 wt% Ru composition using SSOL4 for the major components.

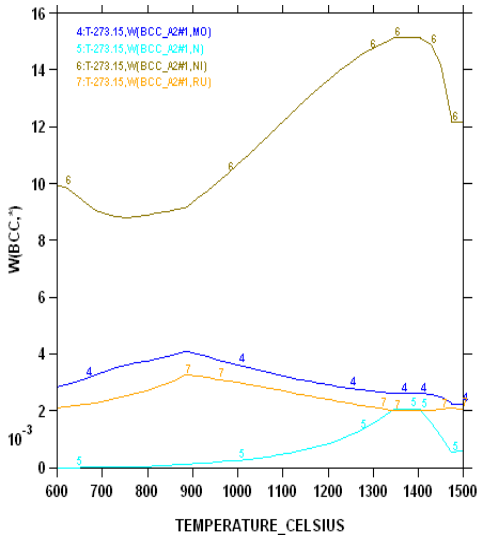

b) *Calculated composition of ferrite with temperature in 0.2 wt% Ru composition using SSOL4 for the minor components.*

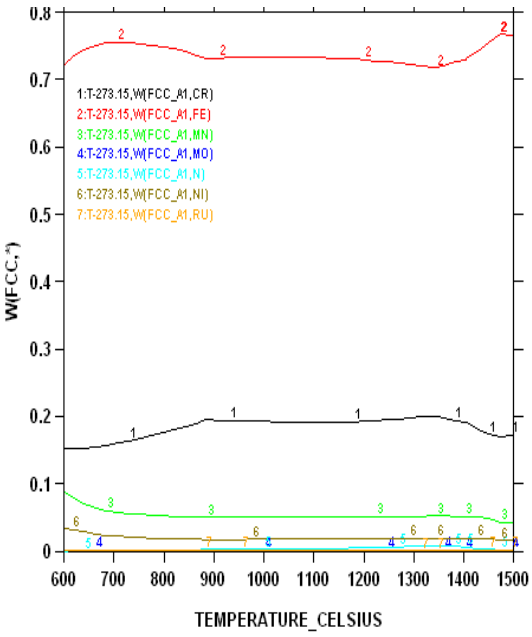

c) *Calculated composition of austenite with temperature in 0.2 wt% Ru composition using SSOL4 for the major components.*

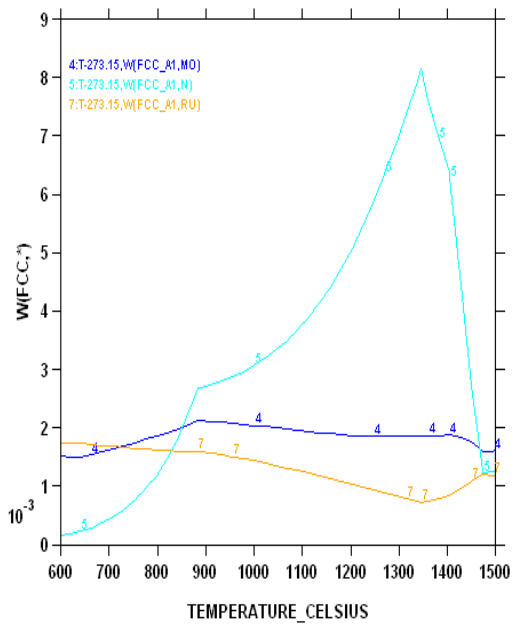

d) *Calculated composition of austenite with temperature in 0.2 wt% Ru composition using SSOL4 for the minor components.*

Figure 6. Calculations of the compositions of ferrite and austenite with temperature for the 0.2 wt% Ru composition using SSOL4.

DISCUSSION

Chemical analysis of the as-received 2101 LDX alloy had similar compositions for all the elements, except that for all measured elements, the amounts were slightly less, although still in the correct proportions. After metallographic preparation, the as-received 2101 LDX had the expected ferrite-austenite microstructure, with discrete austenite within ferrite. As well as etching the ferrite phase dark and the austenite lighter, the NaOH is usually used to detect intermetallic phases in the ferrite, and none were found. However, when the trends of the phase analyses were compared with Zhang et al. [10], all were in agreement, This was true, even taking the errors into account. The Thermo-Calc results showed better agreement with Zhang et al. [10] rather than with the current EDX analyses, although the compositions are fairly close for both phases. The EDX values showed higher Ni content (~2.4 wt %) than either the Outokumpu specification [9] or the chemical analysis done on the same material. This is possibly an indication that the material was inhomogeneous. However, studying the elements present in small quantities, Al, Mn and Ni partitioned more to austenite than ferrite, while Si, Ca, Cr and Mo partitioned more to ferrite, which is in agreement with the results of Zhang et. al., [11] and Atamert and King [12]. Also Mg partitioned more out in the two phases.

Using computer calculation of the phases and their compositions is an accepted way of shortening the alloy design process, although it is necessary to verify the results against actual experimental results. The results in Figure 2 were encouraging because they showed good agreement between calculations of the 2101 LDX compositions from the two different databases. This is important, because only SSOL4 could be used for to calculations involving Ru additions. Ideally the specialised steels database, TCFE5, should have been employed for all the calculations, but since it does not contain ruthenium, the more generalised database had to be used. Calculations for the phases from same composition of duplex stainless steel showed that either database could be used (Figure 3). Both databases showed that the ~50:50 phase distribution was at ~1100°C, thus this would be a good heat treatment temperature.

Due to the high expense of the ruthenium additions, only small amounts were planned, since improved corrosion resistance has been reported with minor additions [11-12]. However, when the very similar results for the low Ru compositions were calculated, there was concern that ruthenium was not being calculated properly. As a check, a higher Ru content was calculated (even outside the required amounts), and it was found that there was a significant difference, as shown in Figure 4. The targeted duplex structure was disrupted for calculations showing higher Ru additions than. Since this calculation demonstrated that Ru was being calculated, more work was done on the planned lower compositions.

Both the component phases over a temperature range and the varying compositions of those phases were calculated (Figure 5). There was very little effect on the component phase proportions and stabilities, and calculation of the phase compositions showed that the Ru was partitioning to both phases, almost equally (Figure 6). The likely reason why there is no noticeable shift in the calculated diagram is because ruthenium partitions to both FCC austenite and BCC ferrite phases thereby roughly balancing the Ru content in both phases. This should be advantageous for the corrosion results, since the ruthenium is balanced between both phases. If the Ru was partitioning to one phase rather than the other, this would mean that the phase with Ru would have better corrosion resistance than the phase without Ru, and so there would be a galvanic effect. Thus, the calculations show that from a partitioning consideration, Ru additions should be beneficial because the partitioning is about the same in each phase.

The calculations to date have showed that Ru additions could be very beneficial since it partitions almost equally to both component phases, ferrite and austenite. Small amounts of ruthenium have proved beneficial for steels [3-4], as well as titanium alloys [13] and WC-Co hardmetals [14], and this near equal distribution suggest that the Ru addition will be equally beneficial to the 2101 LDX stainless steels.

CONCLUSIONS

Predictions using Thermo-Calc have shown that small amounts of ruthenium can be added to duplex stainless steels without changing the structure, up to about 0.2 wt%*. A potential heat treatment temperature of ~1100°C has been identified on the basis of the ~50:50 distribution of the phases there. The ruthenium partitions fairly equally between the ferrite and austenite which will be beneficial to the corrosion resistance of the steels since Ru will protect both phases.

ACKNOWLEDEMENTS

Anglo Platinum,South Africa for the ruthenium.

REFERENCES

1. W. Zhang, L. Jiang, J. Hu and H. Song, *Materials Science and Engineering*, A497, 501-504 (2008).

2. J. Olsson and S. Malin, *Desalination*, 205, 104-113 (2007).

3. J. H. Potgieter, A.M. Heynes and W. Skinner, *Journal of Applied Electrochemistry*, 20, 711-715 (1990).

4. J.H. Potgieter, A. van Bennekom and P. Ellis, *ISIJ International*, 35, 197-* (1995).

5. I.M. Wolf, L.E. Iorio, T.Rumpf, P.V.T. Scheers and J. H. Potgieter, *Materials Science and Engineering*, A241, 264-276 (1998).

6. ASTM Designation: A293 – 06, Standard Test Methods for Detecting Detrimental Intermetallic Phases in Duplex Austenic/Ferritic Stainless Steel.

7. A. T. Dinsdale, CAPHAD, 15(4), 317-415 (1991).

8. J. Kerr, S.M. Wessman and L.A. Cornish, *Journal of Mining and Metallurgy*, 37 (1-2), 1-12 (2001).

9. Otukumpu: www.outokumpu.com accessed 6th October 2009.

10. L. Zhang, W. Zhang, Y. Jiang, B. Deng, D. Sun and J. Li, *Electrochimica Acta*, **54** (23), 5387-5392 (2009).

11. S. Atamert and J.E. King, *Acta Metal. Mater., 39* (3), 273-285 (1991).

12. W. Zhang, L. Jiang, J. Hu and H. Song H., *Materials Characterization*, 60, 50-55 (2009).

13. E. van der Lingen and R.F. Sandenbergh, *Journal of Corrosion Science*, 43, 577-* (2001).

12. I. Wolff, T.L. Shing, S. Luyckx and I.T. Northrop, EURO PM99: European Conference on Advances in Hard Materials Production, Turin, Italy, 8th-10th November 1999.

CHARACTERIZATION OF 2101 LEAN DUPLEX STAINLESS STEEL WITH 0.15 wt% RUTHENIUM

O.A. Olaseinde[1,2] , L.A. Cornish[1,2], J.W. van der Merwe [1,2] and P.A. Olubambi[2,3]

[1]School of Chemical & Metallurgical Engineering, and DST/NRF Centre of Excellence in Strong Materials, University of the Witwatersrand; [2]African Material Science and Engineering Network (Carnegie – RISE Network); [3]Federal University of Technology of Akure, Akure, Nigeria

Duplex stainless steels are a special class of steels that are usually used in many industrial environments where good corrosion resistance is required. They comprise about 50% austenite (γ) and ferrite (α) in their microstructure. Cathodic modification of stainless steel with minor alloying additions of noble metals has proved to be an effective approach for improving their corrosion resistance in many reducing environments[1]. Studies on the addition of platinum group metals (PGMs) on stainless steel and other alloys have already been investigated[2]. The PGMs can improve corrosion resistance of stainless steel which results from their comparatively larger exchange current density and low over potential for hydrogen evolution, which can easily facilitate the cathodic reaction[3]. However, their addition to LDX 2101 has not been investigated. This work investigates the microstructure of LDX 2101 with 0.15wt% Ru addition before and after heat treatment.

An LDX 2101 alloy with 0.15wt% ruthenium was manufactured by arc melting, then cut into two. One half was studied in the as–cast condition the other heat treated using solution annealing at 1080°C, soaked for 30 minutes, then water quenched. After metallographic preparation, the sample's surface was immersed in 40% NaOH, and electrochemically etched at 3V for 8–10 seconds, with a platinum electrode, according to ASTM A293-06. After etching, the samples were examined using backscattered electrons in a scanning electron microscope (SEM), with energy dispersive X-ray spectroscopy, EDX. The incident beam was 20kV, and each phase and overall composition was calculated using an average of more than five measurements.

The as-cast sample showed grains of ferrite (Fig. 1) and the heat treated sample had austenite precipitated on grain boundaries and within the grains, but the amount was far less than the expected 50 vol.% expected. EDX analyses showed that chromium partitioned to the ferrite, whereas Ni and Mn partitioned to austenite, agreeing with Zhang[4]. All the other elements were distributed evenly between the two phases, including Ru. The equal distribution of Ru agreed with Thermo-Calc calculations[5].

The two phases, ferrite and austenite, expected from heat treated duplex stainless steel were achieved, but austenite had a far smaller proportion than expected. This is due to the sample not being heat treated for long enough. The recommended time is 90 minutes at per 25mm 1020-1100°C[6] thickness and it was wrongly thought that with smaller sample, this time could be reduced. It could be seen that austenite formed very easily on the grain boundaries, since this are good nucleation sites. Ruthenium partitioned equally to the two phases, which should be beneficial for corrosion resistance.

References

1. Stern, J. et al. (1959). J Electrochem. Soc.106, 751.
2. Tomashov, N. D. (1964) Corr. Sci. 4 (1-4), 315.
3. Potgieter, J. H. et al. (1990). J. of Appl. Electrochem. 20, 711.
4. Zhang L et al. (2009). Mat. Sci. and Eng. A497, 501.
5. Olaseinde O.A. et al. (2009). 5thAMRS Conf., Abuja, Nigeria, 14th –18th December.
6. CS2205 Technical Data, Columbus Stainless steels.

Table 1. Chemical composition of selected elements in heat treated LDX 2101with Ru as analysed by EDX (wt%)

Bal (Fe)	Cr	Ni	Mn	Mo	Ru
Overall	20.9 ±0.2	0.7 ±0.0	4.2 ±0.5	0.1 ±0.0	0.2 ±0.2
γ	19.1 ±1.3	2.5 ±0.6	5.1 ±0.7	0.1 ±0.2	0.1 ±0.2
α	21.1 ±0.4	1.8 ±0.3	4.0 ±0.5	0.2 ±0.2	0.1 ±0.1

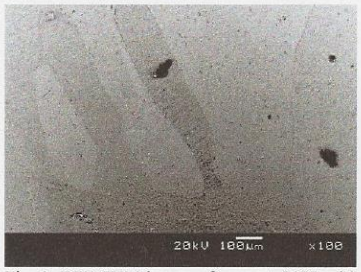

Fig. 1. BSE-SEM image of as-cast 2101 with 0.15 wt% Ru, showing ferrite grains.

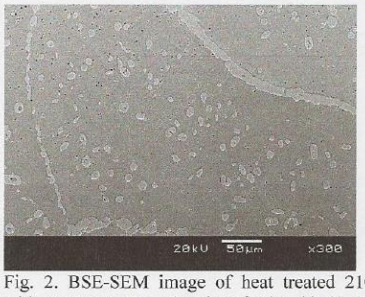

Fig. 2. BSE-SEM image of heat treated 2101 with 0.15wt% Ru, showing ferrite (dark) and austenite (light).

*Corresponding author: adenikeseinde@yahoo.com

CORROSION BEHAVIOUR OF 2101 DUPLEX STAINLESS STEEL MODIFIED WITH VARYING RUTHENIUM ADDITIONS IN HYDROCHLORIC AND SULPHURIC ACID SOLUTIONS

O.A. Olaseinde	School of Chemical & Metallurgical Engineering, University of the Witwatersrand, South Africa,
	DST/NRF Centre of Excellence for Strong Materials, University of the Witwatersrand,
	African Material Science and Engineering Network (A Carnegie – RISE Network),
L.A. Cornish	School of Chemical & Metallurgical Engineering, University of the Witwatersrand, South Africa,
	DST/NRF Centre of Excellence for Strong Materials, University of the Witwatersrand,
	African Material Science and Engineering Network (A Carnegie – RISE Network),
J.W. van der Merwe	School of Chemical & Metallurgical Engineering, University of the Witwatersrand, South Africa,
	DST/NRF Centre of Excellence for Strong Materials, University of the Witwatersrand,
	African Material Science and Engineering Network (A Carnegie – RISE Network),
P.A. Olubambi	African Material Science and Engineering Network (A Carnegie – RISE Network),
	Federal University of Technology of Akure, Nigeria and Tshwane University of Technology, Pretoria, South Africa

Abstract

The addition of minor quantities of platinum group metals (PGMs), and some noble metals, to ferritic and duplex stainless steels increases their corrosion resistance, without changing their microstructures. They also improve the ability of the alloy to passivate. The 2101 lean duplex stainless steels containing 0.15, 0.4 and 0.8 wt% ruthenium were produced using a button arc melting furnace, then solution annealed at 1080°C for 120 minutes and water quenched. The morphology of the alloys was studied using a scanning electron microscope. Polarization curves were measured in naturally aerated solutions of hydrochloric and sulphuric acids at 25°C. The corrosion rates were calculated.

Scanning electron microscopy confirmed two phases, austenite and ferrite, for all alloys. The polarization curves shapes were used to understand the electrochemical behaviour of the alloys. The corrosion rates in the passive range were very low. The curves displayed Tafel-like behaviour, and exhibited an active-passive transition in 0.5M sulphuric acid and 0.5M hydrochloric acid. The evolution of gaseous oxygen with some metal dissolution was observed at potential of 0.88V with reference to silver/silver chloride 3M KCl reference electrode for all alloys in 0.5M sulphuric acid. The pitting potentials occurred at more active potentials in 0.5M hydrochloric acid than 0.5M sulphuric acid. The corrosion rates of 0.15 wt% Ru in hydrochloric acid was higher

than 8.6×10^{-4} mm/yr and 4.8×10^{-6} mm/yr in sulphuric acid. The 0.4 wt% Ru alloy had corrosion rates of 4.8×10^{-4} mm/yr in HCl and 2.2×10^{-6} mm/yr in H_2SO_4. Similarly, the alloy with 0.8 wt% Ru in HCl corroded at 2.9×10^{-4} mm/yr and 1.9×10^{-6} mm/yr in H_2SO_4.

Increasing ruthenium contents decreased the corrosion rate in the acid solutions: the critical current density decreased, corrosion potential increased and the passive current density decreased.

INTRODUCTION

Duplex stainless steels (DSSs) contain a high content of chromium and nitrogen and sometimes molybdenum. The approximately equal volume fractions of ferrite and austenite are achieved by the simultaneous control of chemical composition and the annealing temperature and holding time[1]. They have good resistance to pitting and uniform corrosion, and the microstructure contributes to the high strength and high resistance to corrosion cracking. Duplex stainless steel is about twice as strong as regular austenitic or ferritic stainless steel, although they are more susceptible to the precipitation of embrittling phases than austenitic steels[2]. They have better toughness and ductility than ferritic grades, even though they do not have the high values of austenitic grades. Compared to austenitic stainless steels, DSSs are less expensive because of lower nickel contents. The combination of lower nickel content and reduction of thickness of duplex stainless steel can lead to significant weight savings compared to austenitic stainless steel. Duplex stainless steels have higher yield strength and toughness, lower coefficient of thermal expansion and higher thermal conductivities than austenitic stainless steels due to good ductility[3]. They possesses low fatigue properties, and the impact energy decreases gradually with ageing temperature[4]. Chromium and molybdenum partitions to ferrite[5,6]. Duplex stainless steels are susceptible to spinodal decomposition of the ferrite phase to Cr-rich and Fe-rich phases between 300°C-500°C. The composition of duplex stainless steel has an effect on its mechanical, corrosion properties and maintaining the austenite-ferrite phase. Elements like chromium stabilise the ferrite phase while nickel is an austenite promoter and improver of pitting resistance[7,4]. The corrosion resistance of duplex stainless steel depends mostly on its composition[8]. Increasing nickel content in duplex stainless steel lowered its depassivation pH in acidic media[9]. Many useful properties of duplex stainless steel depend strongly on the austenite-ferrite ratio.

Cathodic modification is an electrochemical means of improving the corrosion resistance of alloys, particularly stainless steels and titanium-based alloys. In 1911 Monartz[10] reported that the rapid corrosion of iron-chromium alloys can be prevented by the winding of a platinum wire around the sample used in the corrosion test or by alloying of the steel with platinum. Passivity can be induced in a base metal or an alloy by the addition of a noble metal with a high cathodic exchange current density, provided that the passive region of the base alloys extends to potentials that are more negative to the reduction potentials. Platinum group metals (PGMs) caused the spontaneous passivation of titanium in boiling dilute sulphuric acid and hydrochloric acid[11]. Cathodic modification with noble metals and PGMs gives excellent corrosion resistance in ferritic stainless steels. The addition of ruthenium to Fe-29Cr-14Ni-3Mo (wt%) increased the efficiency of hydrogen evolution, changing the cathodic reaction kinetics and inhibited anodic dissolution of the alloy by decreasing the critical and passive current densities[12]. Surface compositions of ruthenium-containing duplex stainless steels after passivation in non-oxidizing media were investigated[13]. Increasing ruthenium content decreased the pitting and anodic dissolution of DSS through increasing surface and polarization resistance[14].

Various investigations have been carried out on the cathodic modification of duplex stainless steel but less on lean duplex stainless steel. This paper describes the metallography and corrosion resistance of 2101 lean duplex stainless steel cathodically modified with 0.15 wt% Ru, 0.4 wt% Ru and 0.8 wt% Ru in 0.5M sulphuric acid and 0.5M hydrochloric acid.

1. Experimental Procedure

The alloys were melted in a button arc furnace, under an argon atmosphere, using titanium as an oxygen scavenger. The cast alloys were solution annealed at 1080°C for 2 hours and water quenched.

Specimens for microstructure examinations were cut into square samples of sides 10mm, and hot mounted in bakelite. Samples were mechanically ground with silicon carbide papers from 320, 600, 800 and 1000 grades, and polished with 3µm down to 1µm diamond pastes to obtain a mirror-like surface. The surfaces were rinsed in distilled water and degreased with acetone. The surfaces were immersed in 40% NaOH without allowing the surface to dry, and were electrochemically etched at a potential of 3V for between 8–10 seconds, with a platinum electrode, according to the ASTM standards[15]. After etching, each sample was examined using optical microscopy and scanning electron microscopy.

Corrosion tests were carried out in an electrochemical cell consisting of a 500 ml Pyrex glass conical flask suitable for a conventional three-electrode system, comprising the sample, a silver/silver chloride 3M KCl reference electrode, and graphite counter electrode. The cover of the cell had five holes for the reference electrode, working electrode, counter electrode, temperature measurement and aeration/de-aeration.

The samples were cold mounted in epoxy resin after an electrical connection was provided by attaching a conductive wire to the rear side using an aluminium conducting tape, then prepared metallographically as above. The areas exposed to corrosion studies were measured.

Solutions were prepared using chemicals of analytical grade and distilled water. All electrochemical measurements were made at 25°C±1°C using an Auto lab potentiostat (PGSTAT20 computer controlled) with NOVA software Version 1.7. The temperature was measured with a thermometer and maintained with a water-bath. All tests were carried out in triplicate; the tests with good reproducibility were recorded. The potentiodynamic polarisation responses of the alloys were investigated in naturally aerated solutions. Polarization curves were obtained at a scan rate of 1mV/s, from -500mV to 1200mV with respect to open circuit potential (OCP). Samples were polished, and rinsed with ethanol to remove the products that might have formed on the surface before further measurements.

3 Results and discussion

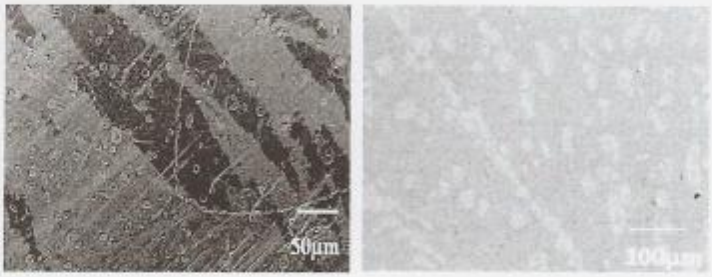

(a) (b)

(c) (d)

Figure 1-SEM–BSE images of 2101 duplex stainless steel solution annealed at 1080°C for 2 h containing nominal: a) 0 wt% Ru, b) 0.15 wt% Ru, c) 0.4 wt% Ru and d) 0.8 wt% Ru, ferrite is dark and austenite is light.

3.1 Microstructure observation

Typical micrographs of the two-phase microstructures of the four investigated alloys are shown in Figure 1. The austenite particles were randomly dispersed in the ferrite matrix, with some at the grain boundaries. No other phases were seen.

3.2 Electrochemical behaviour

Figure 2 shows the polarization curves obtained in 0.5M hydrochloric acid solution. There was an active-passive transition over the samples' entire anodic polarization ranges. Alloy 2101 containing 0wt% Ru showed the least uniform corrosion resistance, while the alloy with 0.8 wt% Ru had the best resistance to uniform corrosion. The polarization curves were similar, but the extent of the passive regions increased with ruthenium content. The smallest passive range was exhibited by alloy containing 0.15 wt% Ru. The results for the corrosion current, corrosion current densities and corrosion rates derived from the electrochemical tests for the samples in different solutions are shown in Table 1. As the amount of ruthenium increased, the values of corrosion currents, corrosion current densities and corrosion rates decreased. The values of corrosion potential shifted to more positive values. The increase in corrosion resistance of alloys as the ruthenium content increased was directly attributed to the ruthenium in the alloy[7,10,12]. Potgieter[16] reported that the cathodic modification shifts the corrosion potential towards more noble values. Olubambi *et al.*[7] postulated that ruthenium increases the passivation region through the replacement and substitution of chromium and molybdenum after their selective dissolution.

Polarization curves for alloys containing 0.15, 0.4 and 0.8 wt% Ru in 0.5M sulphuric acid are shown in Figure 3. Addition of ruthenium to 2101 duplex stainless steel inhibited corrosion, as the ruthenium contents increased. The values of corrosion current, E_{corr}, and corrosion rates were determined from polarization measurements and are given in Table 1. The anodic and cathodic reactions were reduced by the increased presence of ruthenium. Potgieter *et al.*[17] deduced the positive shift in the E_{corr} to be due to increasing the effectiveness of cathodic processes.

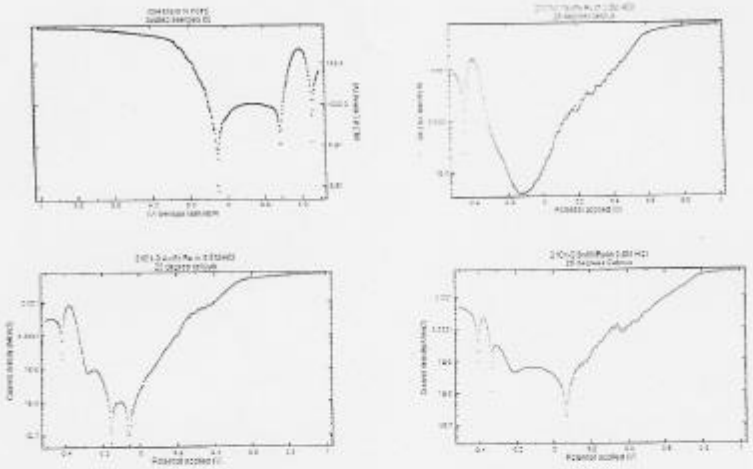

Figure 2-Polarization diagrams for the 2101 duplex steels with different weight percent of ruthenium in 0.5M HCl.

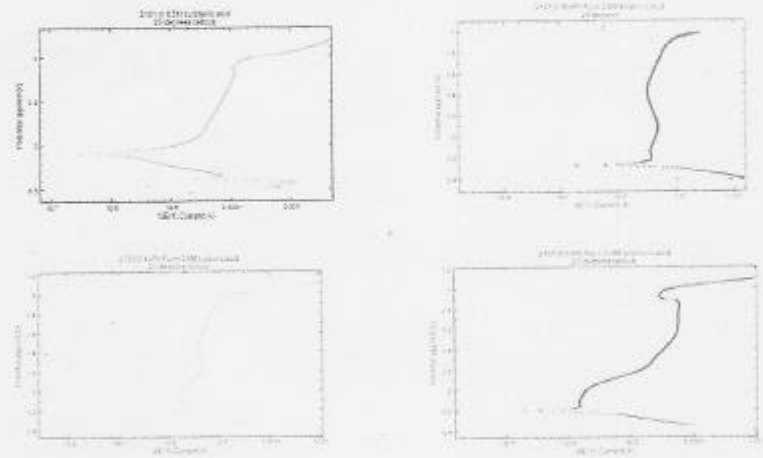

Figure 3-Polarization diagrams for the 2101 duplex steels with different weight percent of ruthenium in 0.5M H_2SO_4.

Table 1. corrosion data obtained from the electrochemical tests.

Corrosion media	Ru addition (wt%)	I_{crit} (A/cm^2)	E_{corr} (mv)	I_{corr} (A/cm^2)	Corrosion rate (mm/yr)
0.5M HCl	0	2.2E-03	-460	7.6E-01	8.8E-02
	0.15	1.6E-03	-445	8.3E-02	8.6E-04
	0.4	7.9E-04	-420	4.6E-02	4.8E-04
	0.8	2.3E-04	-405	2.8E-02	2.9E-04
0.5M H_2SO_4	0	1.1E-03	-451	1.6E-04	1.8E-00
	0.15	3.5E-06	-275	4.6E-04	1.2E-06
	0.4	2.9E-06	-258	2.1E-04	2.2E-06
	0.8	1.6E-06	-200	1.8E-04	1.9E-06

4. Conclusions

The effect of the addition of 0.15, 0.4 and 0.8 wt% ruthenium on the corrosion behaviour of 2101 duplex stainless steel was studied with linear potentiodynamic polarization techniques.

Increasing ruthenium content improved the corrosion resistance of the alloys, due to the cathodic modification effects resulting from its large exchange current density

Polarization measurements indicated that ruthenium passivated the alloy against uniform and pitting corrosion through the corrosion currents and corrosion rates, as well as by shifting the corrosion potential to more positive values.

Acknowledgements

The authors wish to acknowledge Carnegie and IAS, the National Research Foundation, Mintek, and Anglo-Platinum for their support.

References

1. S.C. Tjong, (1990) "Self passivation of Fe-Cr – PGM alloys in reducing acids studied by electro chemical and electron spectroscopic techniques", *Applied Surface Science*, 44, 301–318.
2. W. Zhang, L. Jiang, J. Hu and H. Song, (2009) "Effect of ageing on precipitation and impact energy of 2101 economical duplex stainless steel", *Materials Characterization*, 60, 50–55.
3. J.M. Lardon, J. Charles, F. Dupoiron and J.C. Bavay, (1988) "Duplex austenitic - ferritic stainless steel, mechanical properties and corrosion resistance". *Proceedings of the Conference on High Nitrogen Steels*, 280.
4. S.S.N. Tavares, M.R. Da Silva and J.M. Neto, (2000) "Magnetic property changes during embrittlement of a duplex stainless steel", *Journal of Alloy and Compounds*, 313, 168–173.
5. M.B. Cortie and J.H. Potgieter, (1990) "The effect of temperature and nitrogen content on the partitioning of alloy elements in duplex stainless steel", *Metallurgical Transactions A*, 22A, 2173–2179.
6. S. Azuma, T. kudo, H. Miyuki, M. Yamashita and H. Uchida (2004) "Effect of nickel alloying on crevice corrosion resistance of stainless steels", *Corrosion Science*, 46, 2265–2280.
7. P.A. Olubambi, J.H. Potgieter and L. Cornish, (2008) "Corrosion behaviour of super ferritic stainless steels cathodically modified with minor additions of ruthenium in sulphuric and hydrochloric acids", *Materials and Design*. 30, 5, 1451-1457.
8. International Molybdenum Association. (2009). Practical guidelines for the fabrication of duplex stainless steels", 2nd Edn. www.imoa.info (assessed 2009).
9. N.D. Tomashov, G.P. Chernova, V.I. Lakomskii, G.F. Tarkhov, L.A. Chingirinskaya and V.A. Siyshankova, (1977) *Protection of Metals*, 13, 1, 6-11.
10. P. Monnartz, (1911) "Iron-chromium alloys with special consideration of resistance to acids", Metallurgie (Halle) 1911, 8, 7, 161-176.
11. M. Stern and A.L. Geary, (1957) "Electrochemical Polarization: 1. A theoretical analysis of polarization curves", *Journal of the Electrochemical society*, 104, 1, 56-63.
12. J.H. Potgieter and H.C Brookes, (1995) "Duplex stainless steel with minor additions of ruthenium in sulfuric acid". *NACE International Corrosion*–April 1995.
13. G. Myburg, K. Varga, W.O. Barnard, P. Baradlai, L. Tomcs´anyi, J.H. Potgieter, C.W. Louw and M.J. van Staden, (1998) "Surface composition of Ru containing duplex stainless steel after Passivation in non-oxidizing media", *Applied Surface Science*, 136. 29–35.
14. El-Sayed. M. Sherif, J.H. Potgieter, J.D. Comins, L. Cornish, P.A. Olubambi and C.N. Machio, (2009) "The beneficial effect of ruthenium additions on the passivation of duplex stainless steel corrosion in sodium chloride solutions", *Corrosion Science*, 51, 1364–1371.
15. ASTM Designation: A923–06, Standard Test Methods for detecting Detrimental Intermetallic Phases in Duplex Austenitic/Ferritic Stainless Steel.
16. J.H. Potgieter, (1991) "Alloys cathodically modified with noble metals, *Journal of Applied Electrochemistry*, 21, 471–482.
17. J.H. Potgieter, (1993) "Effect of minor ruthenium additions on the corrosion behavior of duplex stainless steels in sulfuric acid", *Suid-Afr, Tydskr. Chem*, 46, 3-4.
18. O.A. Olaseinde, A.M. Ukpong, L.A.Cornish, J.W.Van der Merwe and P.A. Olubambi (2009). "Studies of the effect of minor Ru addition on the phases in selected duplex stainless steels",5th *African Materials Research Society Conference*, Abuja, Nigeria, 14th–18th December 2009.

HEAT TREATMENT AND CORROSION BEHAVIOUR OF 2101 DUPLEX STAINLESS STEEL CATHODICALLY MODIFIED WITH RUTHENIUM

O.A. Olaseinde[1,2,3], J.W. Van der Merwe[1,2,3], L.A. Cornish[1,2,3] and P.A. Olubambi[2,4]

[1] School of Chemical & Metallurgical Engineering, University of the Witwatersrand, RSA,
[2] African Material Science and Engineering Network (AMSEN), a Carnegie–IAS RISE Network,
[3] DST/NRF Centre of Excellence in Strong Materials, University of the Witwatersrand, RSA,
[4] Federal University of Technology of Akure, Akure, Nigeria

INTRODUCTION

Duplex stainless steels are a special class of steels that are usually used in many industrial environments [1]. The 2101 duplex stainless steel is a lean newly-developed stainless steel which has lower chromium and nickel contents. Owing to the rationale of effectiveness and cost of 2101 in replacing 316 and 304, studies have shown that 2101 has an increased corrosion resistance than 304, but has not been able to effectively surpass that of 316. Cathodic modification of stainless steel with minor alloying additions of noble metals has proved to be an effective approach for improving their corrosion resistance in many reducing environments, and a number of studies on the successful addition of noble metals on stainless steel and other alloys have already been investigated by several authors [2,3].

EXPERIMENTAL PROCEDURE

Samples of the lean duplex LDX 2101® stainless steel were obtained from Outokumpu. The samples were cut into samples of sides 1cm and hot mounted in bakelite. They were ground with silicon carbide papers from 320 down to 1000 grade, and polished with diamond paste until mirror-like surfaces were achieved. The surfaces were electrochemically etched in 28.5% NaOH. After etching, the samples were characterised using a high resolution scanning electron microscope (HR-SEM) equipped with EDX.

For Electrochemical analysis, samples were prepared by attaching an insulated copper wire to one face of the sample using aluminium conducting tape, and cold mounted in resin. The surfaces of the samples were ground with silicon carbide papers from 320 down to 1000 grade, washed with distilled water, degreased with acetone and dried in air. Electrochemical corrosion behaviour of the samples was investigated using potentiodynamic polarisation measurements in 1 M and 2M sulphuric acid solutions at room temperature (25 ± 1°C) with an Autolab (PGSTAT20 computer controlled) potentiostat using the general purpose electrochemical software (GPES) version 4.9. The phases and phase compositions of LDX 2101® were calculated from the Thermo–Calc program.

RESULTS AND DISCUSSION

The calculated phase proportions were compared with the microstructure of as- received LDX 2101®, the calculations were used to identify the best heat treatment temperature that would give a good duplex ferrite / austenite microstructure. The predicted heat treatment temperature of 1080°C agrees with Outokumpu temperature of 1020 - 1080°C for heat treatment [4]. Table 1 shows the partitioning of the elements between austenite and ferrite; the alloying elements stabilising each phase were more concentrated in that phase. Figure 1 shows the austenite and ferrite phases for 2001and 2507DSS, with the ferrite dark and austenite light, no other phases were present while Figure 2 is the SEM micrograph of 2205 and 2101 which shows two distinct phases of austenite and ferrite and no intermetallic phases.

The Thermo–Calc calculations were used to predict the heat treatment temperatures for different minor Ru additions to 2101LDX. It was discovered that there was no noticeable shift in the calculated diagram because ruthenium partitions to both FCC austenite and BCC ferrite phases nearly equally, thereby roughly balancing the Ru content in both phases [5]. Figures 5 and 6 show the phase proportions of as received 2101 and 2101 with 0.2 wt% Ru calculated with the TCFES and SSOL4 databases.

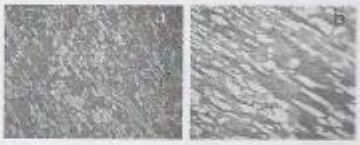

Figure 1. Optical micrograph of duplex stainless steels with ferrite (dark) austenite (light): (a) 2001, and (b) 2507.

Figure 2. SEM secondary electron image of duplex stainless steels with ferrite (dark) austenite (light): (a) 2205, and (b) 2101.

Figures 6 and 7 show the polarisation curves of 316 and 2101 in sulphuric acid. The values of the corrosion potentials of 2101 in 1M and 2M concentrations were more negative than for 316. Thus, 316 had the higher corrosion resistance, which agrees with literature [5].

CONCLUSION

The alloying elements stabilising each phase were more concentrated in the phases. SS 316 had higher corrosion resistance than 2101 in 1M and 2M sulphuric acid. The next stage in this work is the characterisation and corrosion behaviour of 2101with minor Ru additions.

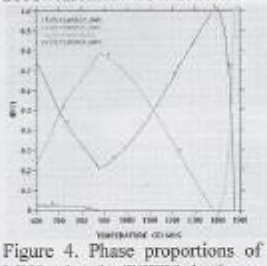

Figure 4. Phase proportions of as-received 2101 LDX using the TCFES database.

References

1. Herbsleb, G. and Schwaab, P. (1983) ASM Metals Congress, 693-756.
2. Tomashov, N.D. (1964) Corrosion Science, 4, 1-4, 315-334.
3. Tomashov, N.D. and Chernova, G. (1975) Protection of Metals, 11,4, 379-84.
4. Http//www.outokumpu.de/29143.epibrw assesed2010)
5. Olaseinde, O.A., Ukpong, A.M., Cornish, L.A, Van der Merwe, J.W. and Olubambi, P.A , 5th African Materials Research Society Conference, Abuja, Nigeria, 14th – 18th December 2009.
6. Zhang, W., Jiang, L., Hu, J. and Song, H. (2008) Mat. & Eng. A, A497, 501 – 504.

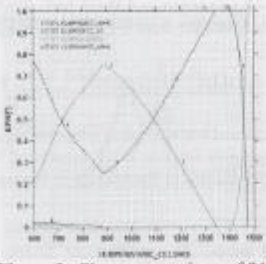

Figure 5. Phase proportions of 2101 LDX with 0.2 wt% Ru using the SSOL4 database.

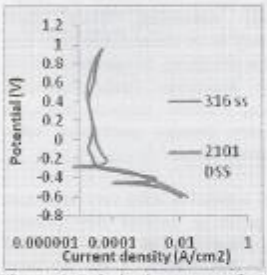

Figure 6. Polarisation curves for the 2101DSS and 316 stainless steels alloys in 1M sulphuric acid solution.

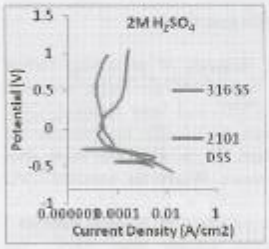

Figure 7. Polarisation curves for the 2101DSS and 316 stainless steels alloys in 2M sulphuric acid solution.

DSS	Phase	Fe	Cr	Ni	Mn	Mg	Si	Mo
2101	Ferrite	69.1±0	22.2±0.1	1.9±0.1	5.0±0.1	0.3±0.1	1.0±0.1	0.3±0
	Austenite	69.9 ±0.3	20.6±0	2.5±0.2	5.8± 0.1	0.2±0.2	0±0	0±0
2001	Ferrite	71.5±08	20.4±14	1.9±0.3	4.4±0.4	0±0	1.1±0.5	0±0
	Austenite	72.1±0.6	20.1±1.08	2.0±0.4	4.6±0.1	0±0	0.7±0.1	0±0
2507	Ferrite	59.0±4.3	26.0±1.5	5.8±0.3	0±0	0.0±0.1	0.50±0.1	4.1±0.4
	Austenite	61.7±0.3	24.8±0.4	8.55±0.07	0.9±0	0.1±0.1	0.4±0	2.8±0.1
2205	Ferrite	66.9±0.6	25.3±0.4	4.2 ± 0.3	1.7±0.2	0.0±0.1	0.3±0.1	0±0
	Austenite	67.9±0.6	20.6±0.4	7.4 ±0.3	3.04±0.42	0.0±0.0	0.3±0.1	0±0

Table 1. Compositions (wt%) of as-received samples analysed by EDX.

EFFECT OF RUTHENIUM ADDITIONS ON THE MICROSTRUCTURE OF 2101 DUPLEX STAINLESS STEEL

O.A. Olaseinde[1,2,3], L.A. Cornish[1,2,3], J.W. van der Merwe[1,2,3] and P.A. Olubambi[3,4]

[1]School of Chemical & Metallurgical Eng., WITS, [2]DST/NRF Centre of Excellence for Strong Materials, WITS, [3]African Mater. Science and Eng. Network (Carnegie – RISE Network), [4]FederalUniversity of Technology of Akure, Akure, Nigeria

Stainless steel is widely used in applications where good corrosion resistance, low maintenance, and low life-cycle costs are required. Duplex stainless steel (DSS) has dual phase structures, comprising austenite and ferrite. Lean duplex 2101 stainless steel has lower nickel content than the conventional duplex stainless steels. It has superior mechanical and corrosion-resistance properties than 304 austenitic stainless steel, but less than, or almost equal, properties to the 316 austenitic stainless steel. Cathodic modification of stainless steel with minor alloying additions of noble metals has proved to be an effective approach for improving their corrosion resistance in many reducing environments, and a number of successful studies on the addition of noble metals on stainless steel and other alloys have already been investigated by several authors[1,2]. Minor ruthenium additions do not affect the microstructure of duplex stainless steel but improve its corrosion resistance[1,2]. Thermo-Calc calculations were used as comparisons against experimental measurements[3]. The aim of this work was to study the effect of additions of nominal 0.2 and 2.5wt% ruthenium on the microstructure of 2101 duplex stainless steel.

The composition diagrams were calculated with Thermo-Calc to provide the optimum heat treatment temperature. The samples were produced by melting samples with 0.2 and 2.5wt% Ru in an arc furnace. The 2101 samples with ruthenium were heat treated at 1080°C, where Thermo-Calc showed 50:50 α:γ proportion (Fig. 1). Samples were prepared for metallographic examination. 0.2wt% was etched with 40g Sodium hydroxide in 100ml water. Marble's reagent was used to reveal the structure of 2101-2.5wt% Ru. Optical microscopy and XRD were used to examine the samples and confirmation of phases respectively.

Figure 1 gives the composition diagram of 2101, showing the phase percentages with temperature. The calculation results for up to 0.2wt% Ru were similar to 2101.

The microstructure of 2101-0.2wt% Ru (Fig. 2) shows the austenite phase as discrete particles, randomly dispersed in the ferrite matrix. The austenite was finer along the grain boundaries and formed nearby continuous precipitation. Here the austenite formed during the solution annealing. The transformation of ferrite to austenite is characterised by the nucleation of austenite at ferrite-ferrite grain boundaries. XRD detected only the two phases of austenite and ferrite, but any ruthenium solid solution would be in too small a proportion to be detected.

The optical micrograph of 2101-2.5 wt% Ru (Fig. 3) etched with Marble's etchant. Two phases were observed, the matrix was ferrite, with irregular austenite dispersed throughout the microstructure. XRD confirmed only ferrite and austenite phases.

Addition of 0.2 and 2.5 wt% ruthenium did not reveal a significant change in the structure of 2101 duplex stainless steel. However it increases its corrosion resistance

References

1. Potgieter, J.H. (1993) S.-Afr. Tydskr. Chem. 46, 3-4.
2. Sherif, E.M. *et al.*(2009) Corros. Sci. 51, 1364–1371.
3. Tavares, S.S.M. *et al.*(2009) Mater. Charac. 60, 573-578.

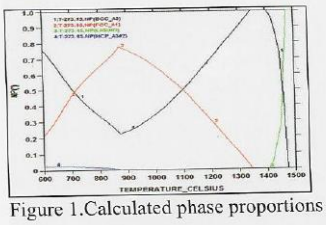

Figure 1.Calculated phase proportions of 2101.

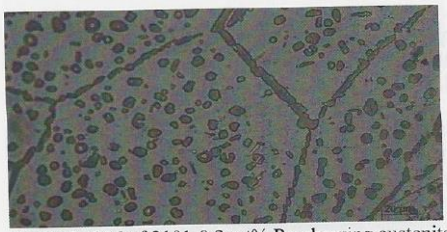

Figure 2. OM of 2101-0.2 wt% Ru showing austenite in a ferrite matrix.

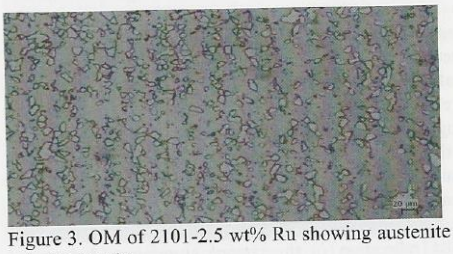

Figure 3. OM of 2101-2.5 wt% Ru showing austenite in a ferrite matrix.

Corresponding author: *adenikeseinde@yahoo.com*

Appendix 3

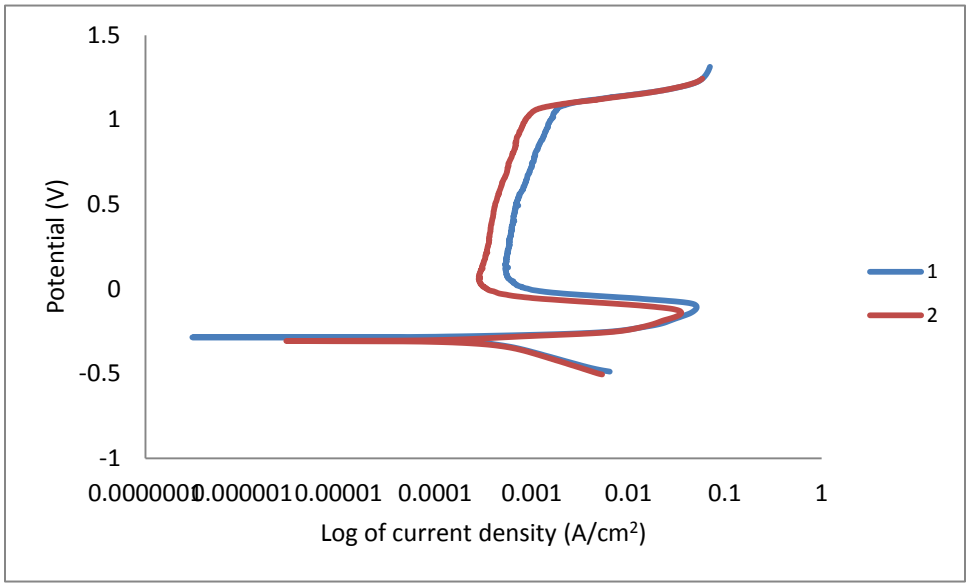

Figure 1.0 An example of reproducibility of 2507 (1M sulphuric acid at 40°C)

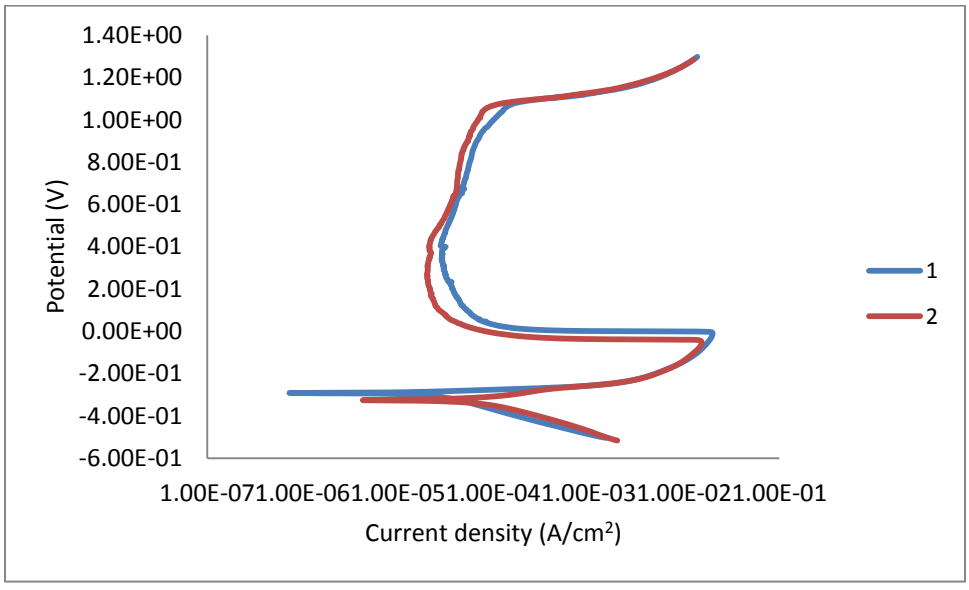

Figure 2.0 An example of the reproducibility of 2205 (1M sulphuric acid at 25°C)

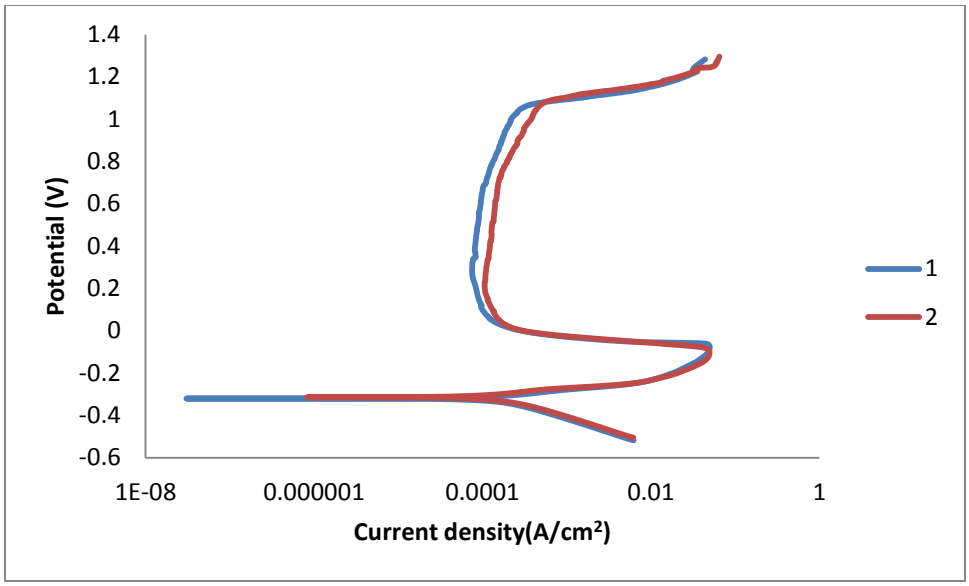

Figure3.0. An example of the reproducibility of 2205 (1M sulphuric acid at 40°C)

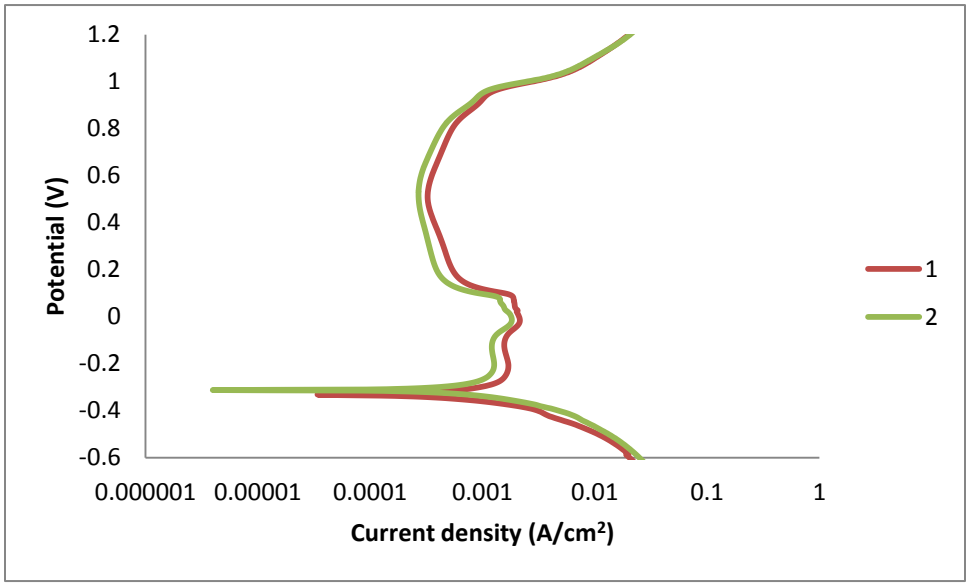

Figure 3.0 An example of. the reproducibility of 2101 (1M sulphuric acid +1% NaCl at 80°C)